NASA Contractor Report 3338

Solid State SPS Microwave Generation and Transmission Study

Volume I - Phase II Final Report

Owen E. Maynard

CONTRACT NAS8-33157
NOVEMBER 1980

NASA

NASA Contractor Report 3338

Solid State SPS Microwave Generation and Transmission Study

Volume I - Phase II Final Report

Owen E. Maynard
Raytheon Company
Wayland, Massachusetts

Prepared for
Marshall Space Flight Center
under Contract NAS8-33157

National Aeronautics
and Space Administration

**Scientific and Technical
Information Branch**

1980

Preceding Page Blank

TABLE OF CONTENTS

SECTION		PAGE
1.	INTRODUCTION AND BACKGROUND	1-1
2.	RESULTS OF INVESTIGATION	2-1
2.1	Issues/Considerations	2-3
2.2	Specific Task	
2.2.1	Definition and Math Modeling of Basic Solid State Microwave Devices	2-3
2.2.2	Initial Conceptual Subsystem and System Design	2-5
2.2.3	Sidelobe Control and System Selection	2-5
2.2.4	Assessment of Selected System Concept	2-5
2.2.5	Parametric Solid State MPTS Data Relevant to SPS Concept	2-6
2.3	Summary of Study	2-8
2.3.1	Background and Assumptions	2-8
2.3.2	The MSFC Sandwich Concept as a Baseline	2-12
2.3.3	Technical Approach	2-13
2.3.4	Architecture and Options	2-14
2.3.4.1	System Level Concepts and Options	2-14
2.3.4.2	Antenna Partitioning	2-16
2.3.4.3	Subarray	2-17
2.3.4.4	Multifunction Sandwich Design Integration and Partitioning Layout	2-19
2.3.5	Weight Estimation	2-24
2.3.6	Use of Data	2-27
2.3.6.1	Example Calculations for Uniform Power Distribution Cases	2-30
2.3.6.2	Example Calculations for Single Step Taper Cases	2-40
2.3.6.3	Example Calculations for Multiple Step Taper Cases	2-70
2.3.7	Technical Issues Resolution and Status	2-76
2.3.8	Recommendations for Further Investigations	2-81
3.	PRELIMINARY PARAMETRIC STUDIES	3-1
3.1	Frequency Considerations	3-12
3.2	Ionospheric and Sidelobe Power Density Considerations	3-14
3.3	Array Efficiency Considerations	3-15
3.4	Waste Heat Dissipation Form Factor Considerations	3-15
3.5	Element Spacing Considerations	3-15
3.6	Spacetenna and Rectenna Size Considerations	3-16
3.7	Sidelobe Control	3-16
3.7.1	Single Step Edge Tapers	3-17
3.8	Baseline for Preliminary Analysis	3-17
3.9	Selected System Concept Assessment With Respect to Sidelobe Control and Maximum Power Density Potential	3-22
3.10	Power Delivery and Associated Cost Estimation	3-28

TABLE OF CONTENTS -- Continued

SECTION		PAGE
4.	RF ELEMENT SELECTION	4-1
5.	MICROWAVE DEVICES AND CIRCUITS	5-1
5.1	Microwave Device Performance	5-1
5.2	Simplified Amplifier Circuit	5-5
5.3	Active Element Transmitter	5-8
5.4	Harmonic Noise Generation, Suppression and Transmission Characteristics	5-8
5.5	Active Element Pilot Receiver	5-11
5.6	Present State of the Art Versus SPS Amplifiers	5-11
6.	POWER BALANCE, THERMAL MODELING AND EXPECTED LIFE	6-1
6.1	Power Balance and Partitioning	6-1
6.2	Amplifier Thermal Model	6-5
6.3	Amplifier Expected Life Relationships Due to Thermal Considerations	6-10
6.3.1	Background	6-10
6.3.2	Amplifier Reliability	6-10
6.3.3	Failure Rate Versus Junction Temperature	6-12
6.3.4	Form Factor and Negative Values of P_{SM}	6-16
7.	CHARGED PARTICLE RADIATION EFFECTS	7-1
8.	BASIC PARAMETRIC RELATIONSHIPS AND RESULTING DATA	8-1
8.1	Power Source Characteristics Which Interact With Parameters On the Microwave Side of the Sandwich	8-2
8.2	Microwave and DC Power Demand Characteristics Which Interact With Waste Heat Dissipation and Other Power Supply Parameters of the Photovoltaic Array	8-4
8.3	Calculation of ΔP_B and P_A as a Function of the Efficiency Chain, P_{DC} Supply, P_{DC} Demand and Other Microwave System Parameters	8-13
8.4	Parametric Data Summary	
8.4.1	Introduction and Data Format	
8.4.2	Baseline Sensitivity to Daily Variations in Incident Solar Heat Load on the Microwave Side	8-21
8.4.3	Baseline Sensitivity to Waste Heat Radiator Form Factor	8-24
8.4.4	Baseline Sensitivity to Emissivity and Absorptivity	8-26
8.4.5	Baseline Sensitivity to Amplifier Efficiency	8-29
8.4.6	Baseline Sensitivity to Material for Thermal Conductor	8-32
8.4.7	Baseline Sensitivity to Junction Temperature	8-35
8.4.7.1	Design Performance for the Autonomous Case	8-38
8.4.7.2	Design Performance for the Non-Autonomous Case ($P_{SM} = 0$)	8-40
8.4.7.3	Summary, Comparison and Assessment	8-43
8.4.8	Baseline Sensitivity to Solar Cell Temperature	8-46

TABLE OF CONTENTS -- Continued

SECTION		PAGE
9.	ASSESSMENT OF PRELIMINARY DESIGN INVESTIGATIONS AND PARAMETRIC DATA	9-1
9.1	DC Power Distribution Systems	9-2
9.2	Spacetenna General Architecture (Example)	9-4
9.3	Multiple Step Taper	9-8

LIST OF ILLUSTRATIONS

FIGURE		PAGE
2.3.1-1	Raytheon's Participation in Solar Power Satellite Program Related Work - System Studies and Technologies	2-9
2.3.4-1	Subarray Layout (Transmit Elements, Receive Elements & Amplifiers)	2-18
2.3.4-2	Multi-Function Sandwich and Architectural Partitioning Layout	2-20
2.3.5-1	Subarray Layout - Typical Corner and Section	2-26
2.3.6.2-1	Single Stepped Taper Aperture Efficiencies and Sidelobe Margins Relative to Uniform	2-41
3-1	Spacetenna Diameter and Power Density Versus Edge Taper	3-4
3-2	Cross Plot from Figure 3-1	
3-3	Spacetenna Diameter Versus Active Element Power Output for Uniform Illumination	3-6
3-4	Ratio of Synchronous Orbit Range to $2D_T^2/\lambda$	3-7
3-5	SPS Beam Geometry, Tapered Illumination (5W/Element)	3-8
3-6	SPS Beam Geometry, Uniform Illumination (5W/Element)	3-9
3-7	Rectenna Size Versus Beam Efficiency - Tapered Illumination	3-10
3-8	Rectenna Size Versus Beam Efficiency - Uniform Illumination	3-11
3-9	SPS Number of Elements Versus D/a Ratio	3-13
3.8-1	Preliminary Estimates of Power Transmission and Conversion Efficiency Chain	3-19
3.8-2	Solid State MPTS Spacetenna Subarray Circuit Diagram	3-21
3.8-3	Spacetenna - Dipole Concept	3-23
3.9-1	Sidelobe Comparison of Uniform Power Distribution With Two Examples of Single Step Edge Taper	3-24
3.10-1	DC Power Delivered to Grid Versus Module Power Per Element	3-29
3.10-2	Solar Power Satellite System and Subsystem Costs	3-35
3.10-3	Solar Power Satellite Cost Figure of Merit	3-36
4-1	Solid State MPTS Spacetenna Subarray Circuit Diagram	4-2
4-2	Spacetenna - Dipole Concept	4-4
4-3	Solid State MPTS Spacetenna - Slot Concept	4-5
4-4	Microstrip Patch Radiator	4-7
5.2-1	Simplified Amplifier Circuit Model	5-6
5.2-2	Simulated Microwave Power Amplifier Waveforms	5-7
5.3-1	Transmitter Active Element Block Diagram and Requirements	5-9
5.5-1	Pilot Receiver Active Element Block Diagram and Requirements	5-12
6.1-1	Preliminary Thermal Power Balance	6-2
6.2-1	Amplifier Thermal Model	6-6
6.2-2	Current and Projected Technology and Goals for Absorptivity and Emissivity	6-9
6.3-1	Accelerated Life Data and Projections for Solid State SPS MPTS Study	6-11
6.3-2	Failure Rate Vs Years at Temperature Based on Raytheon A_L Gate Projections	6-13
6.3-3	Daily Cycle of Normally Incident Solar Flux on Microwave Side of Sandwich	6-14
6.3-4	Accelerated Life Data and Projections for Solid State SPS MPTS Study	6-15

LIST OF ILLUSTRATIONS -- Continued

FIGURE		PAGE
8.2-1	Daily Cycle of Normally Incident Solar Flux on Microwave Side of Sandwich	8-6
8.2-2	Accelerated Life Data and Projections for Solid State SPS MPTS Study	8-7
8.4-1	Selected Microwave Baseline Parametrics for T_S = 200°C and P_{SE} = 822 W/m^2	8-20
8.4-2	DC Power Demand/Supply - Format Summary	8-22
8.4-3	Baseline Sensitivity to Daily Variations of P_{SE}	8-23
8.4-4	Baseline Sensitivity to Waste Heat Radiator Form Factor	8-25
8.4-5	Baseline Sensitivity to Emissivity	8-27
8.4-6	Baseline Sensitivity to Absorptivity	8-28
8.4-7	Baseline Sensitivity to Amplifier Efficiency	8-30
8.4-8	Baseline Sensitivity to Waste Heat Conductor Material	8-33
8.4-9	Baseline Sensitivity to Junction Temperature	8-36
8.4-10	Failure Rate Vs Years at Temperature Based on Raytheon A_L Gate Projections	8-37
8.4-11	Effective Energy Performance Improvement Above Autonomous Baseline	8-39
8.4-12	Effective Energy Performance Improvement Above P_{SM} = 0 Baseline	8-42
8.4-13	Effective Energy Performance Improvement Above Baseline Vs Junction Temperature	8-44
8.4-14	Baseline Sensitivity to Solar Array Temperature	8-47
9.2-1	First Approximation of Multi-Step Taper Architecture	9-5
9.2-2	Power Flow for First Approximation to Multi-Step Taper Concept	9-6
9.3-1	Transmit Antenna Illumination Multiple Step Taper	9-9
9.3-2	Transmit Antenna Illumination Taper Smoothed Gaussian	9-10

LIST OF TABLES

TABLE		PAGE
2.1-1	Summary and Conclusions - Solid State Sandwich Concept Issues and Resolution Summary	2-4
2.3.5-1	Weight Summary for Solid State MPTS Full Subarray	2-25
2.3.6-1	SPS Microwave Power Transmission System & Other SPS Interactive Data for Initial Concept Comparison & Assessment	2-28
2.3.6-2	Initial Concepts Summary Data for Comparative Assessment	2-31
2.3.6-3	Microwave & Associated Thermal Related Parameters - Worksheet	2-32
2.3.6.3-1	Multiple Step -10 dB Taper Data Sheet	2-74
3-1	Solid State MPTS Parameters and Constraints	3-2
3-2	Solar Power Satellite Antenna Analysis	3-3
3-3	Key Formulas (Assumes Far Field Analysis)	3-3
3.7-1	Sidelobe Suppression Considerations	3-18
3.10-1	SPS Solid State MPTS Cost Estimating Relationships	3-30
3.10-2	SPS Solid State MPTS Costs (ROM)	3-33
3.10-3	SPS Solid State MPTS Costs (Normalized ROM)	3-34
3.11-1	Conclusions	3-37
4-1	Radiator Implementation Comparison	4-3
5.1-1	Candidate Device Technologies	5-1
5.1-2	Microwave Power Amplifier Circuit	5-3
5.1-3	Definition of Microwave Terms	5-3
5.1-4	Microwave Device Characteristics	5-4
5.2-1	Microwave Power Amplifier	5-8
5.4-1	Transmitter Noise Goals	5-10
5.4-2	Transmitter Harmonics	5-10
6.1-1	Definition of Thermally Related Terms	6-4
8.3-1	Microwave and Associated Thermal Related Parameters - Worksheet	8-18
8.4-1	Device and Energy Loss Relationship to Junction Temperature	8-35
8.4-2	Average Energy Per Element Related to Junction Temperature and Autonomous P_{RF}	8-38
8.4-3	Effective Energy Performance Improvement Percentage Above Baseline (Autonomous Case)	8-40
8.4-4	Average Energy Per Element Related to Junction Temperature Non-Autonomous ($P_{SM} = 0$)	8-41
8.4-5	Effective Energy Performance Improvement Percentage for $P_{SM} = 0$ Above the $P_{SM} = 0$ Baseline	8-41
8.4-6	Effective Energy Performance Improvement Percentage for $P_{SM} = 0$ Above the Autonomous Baseline	8-43
9.3-1	Summary of Results	

SECTION 1
INTRODUCTION AND BACKGROUND

Investigations of Microwave Power Transmission System (MPTS) concepts by Raytheon in the past have not addressed solid state approaches due primarily to the problem of trying to achieve long life (30 years) in an application where high power density and limited waste heat dissipation capabilities are inherent.

Solid state amplifier efficiencies for the current technology are too low (50% to 70% range) requiring 50 to 30% of the DC power to be radiated as waste heat while keeping junction temperatures within acceptable limits. Recent projections of solid state amplifiers have indicated that the efficiency may be as high as 80%, requiring 20% of the DC power to be radiated as waste heat, reducing the problem by a factor close to 2.

Solid state amplifiers operate at low voltage, 10 V to 20 V, compared to 20 kV to 40 kV for tubes and the DC power transmission and conditioning system weights, complexities and cost for known overall system concepts were of major concern for kV power distribution systems and incredible for low voltage systems. The solid state sandwich concept, where the DC power distribution is a simple grid interface with the static microwave portion of the sandwich, is such that investigation of the solid state approach became of considerable interest.

Results have been encouraging and the concept is considered to warrant further and more in-depth investigation. The critical outstanding issues include the need for demonstration of the high efficiency for the amplifiers. When this is accomplished, the issues and considerations discussed herein become important.

SECTION 2
RESULTS OF INVESTIGATION

Raytheon's investigation has included the following tasks:

1. Definition and Math Modeling of Basic Solid State Microwave Devices
2. Initial Conceptual Subsystem and System Design
3. Sidelobe Control and System Selection
4. Assessment of Selected System Concept
5. Parametric Solid State MPTS Data Relevant to SPS Concept

An efficiency goal for the DC to RF amplifiers of 80% has been established. Although this has not been demonstrated it is considered to be a realistic goal and is therefore the basis for the investigation. Parametric data for 75% and 85% are included.

Conceptual subsystem and system design investigations gave the following results for the autonomous sandwich concept having uniform RF power distribution. Updating after assessment resulted in the numbers shown in brackets [ ]. This was due primarily to an assumed solar cell temperature increase from T_S = 200°C to T_S = 250°C, a microwave junction temperature increase from 114°C to 118°C and a clearer understanding of the thermal models.

(a) 1.95 km diameter transmitting antenna having uniform power density of 500 W/m^2 (RF) [1.82 km and 690 W/m^2]

(b) 4.5 km beam diameter or minor axis rectenna having maximum power density of 23 mW/cm^2 at center of main lobe reducing to 1 mW/cm^2 at edge of the rectenna [4.8 km and 23 mW/cm^2]

(c) Free space sidelobes < 0.1 mW/cm^2 for 2nd and further out sidelobes

(d) First sidelobe above 0.1 mW/cm^2 out to the fenced minor axis of 9.2 km [9.8 km]

(e) Subarray size 32 x 32 elements 3.2 m x 3.2 m

(f) Microwave subsystem for spacetenna weight of ~3 kg/m^2

(g) DC to DC efficiency of 0.51

(h) Total transmitted power of $\frac{\pi \times 1.95^2}{4} \times 500 \times 10^6 = 1.493 \times 10^9$ W RF [1.8×10^9 W RF]

(i) DC power into antenna = $\frac{1.493 \times 10^9}{.99 \times .99 \times .8 \times .96 \times .98} = \frac{1.493 \times 10^9}{.738}$

$= 2.02 \times 10^9$ W DC [2.44×10^9 W DC]

(j) Power out of rectenna to power grid = $1.80 \times 10^9 \times .98 \times .825 \times .89 \times .97$

$= 1.26 \times 10^9$ W DC [1.26×10^9 W DC]

(k) Antenna concept uses an amplifier/transmitting antenna element (narrow bandwidth) with element printed on tape 1/4 λ from ground plane. Receiving antenna elements are wide bandwidth and are orthogonal to the transmit elements to minimize adverse coupling.

(l) Waste heat is passively radiated to deep space from pyrographite conductors to radiators having $\varepsilon = 0.8$ and $\alpha = 0.05$ thermal control coatings. Waste heat (568 W/m^2) from the photovoltaic array is assumed to add to the heat load on the microwave side. Temperature of the solar array was assumed to be $T_S = 200°C$. [568 W/m^2 and $T_S = 250°C$]

(m) Single step taper at the transmitting antenna was investigated to determine sensitivity for reduction of 2nd sidelobe. Significant reduction is achievable with single step.

(n) Further parametric investigations indicate that the RF power per element may be increased from 5 W/element to [6.9], thus permitting a significant reduction in spacetenna diameter for the same power density on the ground. This increase is due in part to an increase in junction temperature, $T_J = 114°C$ to [$T_J = 118°C$], to achieve an optimum total energy output over a 30-year period. This is discussed further in Section 8.4.

(o) Further detailed investigation of the concept is warranted.

2.1 ISSUES/CONSIDERATIONS

The issues and considerations along with their resolution and status, shown in Table 2.1-1, have evolved during the investigation. Each of them is summarized on charts that may be used as visual aids for presentation purposes. These charts are included in the report as Appendix D. Although a considerable amount of work has been done since these charts were formulated, the basic resolution and status in each case has not changed significantly.

The first area that requires more emphasis than was initially thought to be important is that of semi-autonomous and non-autonomous concepts employing uniform power distribution and single step tapers. These require an in-depth investigation into DC power transport and techniques for near optimum solar illumination of the system.

The second area that warrants further investigation is that of the hybrid concept employing tubes in the central high power density region and solid state in the outboard low power density region of single step taper configurations.

2.2 SPECIFIC TASK RESULTS

2.2.1 Definition and Math Modeling of Basic Solid State Microwave Devices

Results of the investigation into definition and math modeling of basic solid state microwave devices are included in Sections 5, 6, 7 and 8 with the associated parameters defined in the appropriate section.

Section 5 presents results on microwave device performance with the key parameter being a projection of 80% for the amplifier efficiency. The active element transmitter and pilot receiver each are conceived to include all the elements required to achieve the requirements of gain, efficiency, harmonic suppression, noise filtering and matching at the RF antenna element end, the RF drive for the transmitter, the input to the phase conjugating electronics from the receiver and the DC power interface. The selected device technology is Gallium Arsenide MESFET and it is recommended to be implemented in flip chip configuration for minimum temperature rise between the junction and the waste heat radiator.

Section 6 presents results of power balance and partitioning investigations for waste heat dissipation purposes and provides the basic inputs for thermal modeling and expected life considerations.

Table 2.1-1 Summary and Conclusions - Solid State Sandwich Concept Issues and Resolution Summary

ISSUES/CONSIDERATIONS	RESOLUTION/STATUS
LOW VOLTAGE DISTRIBUTION	FURTHER REFINEMENT REQUIRED TO MINIMIZE WEIGHT AND CONTROL THERMAL LEAKAGE
HARMONIC AND NOISE SUPPRESSION	FREQUENCY ALLOCATION NEEDS AT HARMONICS SHOULD BE CONSIDERED OR CONSIDER SPREAD SPECTRUM AND ACTIVE SUPPRESSION
SUBARRAY SIZE	3M X 3M MAY BE CLOSE TO OPTIMUM, FURTHER STUDY OF IMPLEMENTATION REQUIRED
MONOLITHIC TECHNOLOGY	MONOLITHIC APPROACHES APPLY AND REQUIRE TECHNOLOGY DEVELOPMENT FOR MINIMIZATION OF COST AND WEIGHT
LIFETIME	LIFETIME AFFECTED BY JUNCTION TEMPERATURE LIMITS AND CHARGED PARTICLE RADIATION REQUIRING TECHNOLOGY DEVELOPMENT IN BOTH AREAS
MUTUAL COUPLING	IMPLEMENTATION BY PRINTED DIPOLES SPACED FROM GROUND PLANE WITH BALUN IN CIRCUITRY AND CLOSE ELEMENT SPACING TO MINIMIZE DETRIMENTAL MUTUAL COUPLING EFFECTS
INPUT TO OUTPUT ISOLATION	ORTHOGONAL DIPOLES, OFFSET FREQUENCIES AND FILTERING PROVIDE SATISFACTORY ISOLATION OF TRANSMIT FROM RECEIVE SIGNALS
CHARGED PARTICLE RADIATION EFFECTS	GaAs IS CURRENTLY BEST TECHNOLOGY (REQUIRES MORE ADVANCEMENT IN "MECHANISMS" OF FAILURE)
TOPOLOGICAL CONSIDERATIONS	REQUIRED FUNCTIONS CAN BE IMPLEMENTED IN SANDWICH CONCEPT. FURTHER DETAILS AT SUBARRAY BOUNDARIES REQUIRED.
SIDELOBE SUPPRESSION	SINGLE STEP EDGE TAPER MAY BE REQUIRED.

Section 7 discusses charged particle radiation effects.

The basic parametric relationships and resulting data for the microwave system as it interacts with the photovoltaic system are presented in Section 8.

Section 9 presents the results of a preliminary assessment which initiated further investigations reported in Appendices B and C, which in turn influenced Section 2 in particular.

2.2.2 Initial Conceptual Subsystem and System Design

Section 3 summarizes the preliminary parametric studies leading to the baseline for preliminary analysis purposes. It includes ionospheric and sidelobe power density considerations primarily as constraints. It also includes power delivery and associated cost estimations for preliminary comparative assessment purposes. As will be observed, the baseline is continually challenged in the assessment of Section 9 and in Section 2.3.6, wherein making use of the data and studying the results in considerable depth it became clear that the baseline had served its purpose and other concepts do appear to warrant in-depth investigation.

2.2.3 Sidelobe Control and System Selection

Section 3 begins the investigation of sidelobe control, however two appendices were prepared to document more thoroughly the microwave power transmission antenna analyses. Appendix B treats the more general cases of antenna concepts including uniform power distribution and multiple step approximations to truncated Gaussian distributions over a range of tapers. Appendix C was prepared to report on in-depth investigations into single step taper concepts when the assessment of Section 9 began to indicate that they may have more potential than had been indicated in earlier studies. Section 2.3.6.2 uses the data from Appendix C and elsewhere to more clearly indicate the potential of the single step taper concept to deal with a range of sidelobe control requirements in an optimum manner.

2.2.4 Assessment of Selected System Concept

The uniform power density case selected for initial conceptual subsystem and system design had its DC power provided autonomously from the photovoltaic array on the deep space side of the spacetenna/solar cell sandwich. As discussed at length in Sections 8 and 9, it is believed that the constraint imposed on both the microwave and photovoltaic portions for autonomous operation may be unduly penalizing solid state concepts in general.

If solar illumination can be tailored and the photovoltaics can be configured to generate the power more independently and if relatively efficient and effective DC power transfer systems can be developed, the overall concept may benefit. This comes about largely due to the fact that waste heat dissipation is largely a function of temperature to the fourth power times the area from which that temperature can cause the waste heat to be radiated. When the photovoltaics which can operate at a high temperature are constrained to interface thermally with the microwave system whose amplifier junctions must operate at a significantly lower temperature, there is a limitation on T^4. Similarly, when a microwave system is loaded with waste heat from the photovoltaics there is a limitation on the temperature rise to the critical junctions. This limitation on junction temperature rise limits the waste heat allowable at the junction which in turn limits its RF generation capability and the RF power density is thereby constrained.

In the assessment of penalties for the sidelobe control concepts and the assessment of the autonomous uniform power distribution, comparisons were made of both optimized single step taper concepts and multiple step taper concepts at the specific power level. Specific power is here defined to be the power delivered to the ground divided by the several areas known to drive the system cost. In particular, $P_G/A_T + A_{PVA}$, which is delivered ground power divided by the sum of the areas of the transmitting antenna and the area of the photovoltaics, provides a first approximation to the effectiveness of a particular concept for comparison to other concepts. This along with other specific power relations are compared in Section 2.3.6 for ten concepts. From this assessment it appears that single step taper concepts which include DC power transport allow the photovoltaics and the microwave systems to perform closer to their individually maximum temperatures, thus improving the specific power factors significantly. Furthermore, it appears that a hybrid approach using tubes in the central high power density region and solid state amplifiers in the outboard lower power density region is worthy of further investigation.

2.2.5 Parametric Solid State MPTS Data Relevant to SPS Concept

The parametric data relating to the RF power densities and how the different elements of the sandwich concept interact are summarized in Section 8. An assessment of sensitivity for each parameter is included and a series of issues for autonomous, semi-autonomous and non-autonomous concepts are identified.

The parametric data at the microwave power transmission system level including system sizing and sidelobe power density considerations are included primarily in Appendices B and C.

Section 2.3.6 makes use of the parametric data in formulating 10 concepts for comparative purposes.

2.3 SUMMARY OF STUDY

This section summarizes the study in terms of

(a) Background and Assumptions
(b) The MSFC Sandwich Concept as a Baseline
(c) Technical Approach
(d) Architecture and Options
(e) Weight Estimation
(f) Use of Data
(g) Technical Issues Resolution and Status
(h) Recommendations for Further Investigations.

2.3.1 Background and Assumptions

Prior to the initiation of this Solid State SPS Microwave Generation and Transmission System Study, Raytheon had performed a series of investigations into the application of microwave power transmission to the Solar Power Satellite. These studies were based exclusively on tubes such as the Klystron, Amplitron and Magnetron. The NASA Marshall Space Flight Center concept for solar illumination of the photovoltaics of the sandwich concept and the trend toward higher potential efficiency for solid state amplifiers than had been anticipated created the motivation and need to investigate solid state microwave power transmission systems. Much of the data from prior investigations is relevant to solid state approaches and for this reason Figure 2.3.1-1 is included here to put this data is perspective.

It should also be noted that some of the concepts and data from this current solid state microwave power transmission system study are applicable to approaches using tubes.

The technical work reported here was performed in the April 1979 to February 1980 time period and was based on the following assumptions and technical considerations as established with the NASA Program Manager, W. Finnell. These assumptions and technical considerations were treated as guidelines in that imaginative approaches were not inhibited by any particular specification.

A. Amplifier Efficiency and Stages

The range of interest for efficiency of the amplifier stage section is assumed to be 75% to 85%. It is understood that it is the intention of NASA to initiate

	DESCRIPTIVE TITLE	PRIOR TO 1970	PERIOD OF PERFORMANCE 70 71 72 73 74 75 76 77 78 79 80 81	CUSTOMER	PRIME	SUB	RELATED REPORT NUMBER
1	Microwave Powered Helicopter	1964		USAF	Raytheon		RADC-TR-65-188
2	Orbit-to-Orbit Power Transmission	1969		NASA-MSFC	Raytheon		PT-4601
3	MPTS in Satellite Solar Power Station			In-House			ER72-4038
4	Feasibility Study of SPS			NASA-LeRC	Arthur D. Little	Raytheon Grumman Spectrolab	NASA CR-2357
5	Microwave Power Transmission System Studies			NASA-LeRC	Raytheon	Shared Applic's & Grumman	NASA CR-134886
6	Reception-Conversion Subsystem (RXCV) for Microwave Power Transmission System			NASA	JPL	Raytheon	ER75-4386
7	RF to DC Collector/Converter Technology Development			NASA-LeRC	Raytheon		NASA CR-135194
8	Design and Fabrication of Crossed Field Amplifier			NASA-LeRC	Raytheon		NASA CR-159410
9	Areas of Investigation Relationships to Development Approaches			In-House			
10	Space Station System Analysis Study			NASA-MSFC NASA-JSC	GAC MDAC	Raytheon Raytheon	
11	Space Based Solar Power Conversion and Delivery System Study			NASA-MSFC	ECON	Raytheon	ECON 77-145-1 S/C ECON-0003
12	Satellite Power System Development Plan Summary			In-House			
13	DOD Applications & DARPA Advanced Technology Development (Relevant Space Based Investigations)			SAMSO RADC	TRW/GAC Raytheon	Raytheon	
14	SPS System Evaluation Phase III - Rectenna Technology Study			NASA-JSC	Boeing	G.E. Raytheon	D180-24635-1 PT-5155
15	SPS & Alternate Technology Comparisons			ANL	UE&C Inc.	Consultant	UE&C-ANL-79031
16	Crossed Field Directional Amplifiers For Use in the Solar Power Satellite			In-House			
17	SPS Pilot Beam & Communication Link Study			NASA-MSFC	Raytheon		NAS8-33157
18	SPS Pilot Beam Ionospheric Effects Discussion of Critical Issues			In-House			Draft 6/79
19	Solid State SPS Microwave Generation and Transmission Study			NASA-MSFC	Raytheon		
20	Magnetron Tube Assessment			NASA-MSFC	Raytheon		

Figure 2.3.1-1 Raytheon's Participation in Solar Power Satellite Program Related Work - System Studies and Technologies

in-depth investigations, possibly including technology development, to narrow this range of uncertainty. Incorporation of results of such investigations are beyond the scope of this supplemental agreement. Module efficiency is here defined to be:

$$\frac{\text{RF Power Out of Stage}}{\text{RF Power In + DC Power In}}$$

B. RF Input Power

The RF power in is assumed to be in the range of 10 to 20 dB down from the RF power out and the RF power in is to be supplied from a local subarray phase control subsystem to be designed as a part of the antenna array.

C. DC Power In

The DC power into the RF portion of the module is assumed to come from solar cells on the backside. The voltage range of interest is assumed to be 15 V to 60 V and the length of the conductor will be configuration dependent. Configurations where all the DC power comes from the solar cell area immediately behind the module will have minimum length conductors. Configurations where the DC power is fed in from solar cells located remote from the RF module will have large length conductors. Raytheon will establish and state the assumptions for DC power distribution that are used to estimate associated weights and costs.

D. Waste Heat and Maximum RF Power Considerations

It is assumed that waste heat from the RF portion will be radiated passively toward the earth with a system configuration such that the radiation area sees the earth and deep space continuously from geosynchronous altitude, and sees the sun periodically. Waste heat radiator areas will be configuration dependent and a range of surface characteristics will be established and mutually agreed to in the course of Task 1 to estimate the radiator temperatures. The range of transmitted RF power densities of interest will be estimated based on solar power concentration ratios of 4, 5 and 6 with the associated efficiencies reported in a February 1979 briefing by MSFC to NASA/DOE.

E. Antenna Element and Subarray

Approaches to the RF radiating antenna element concepts will be investigated with the objective being to establish a near-optimum concept which exhibits low losses, is implementable in a low cost format and makes provision for effective waste heat radiation areas. Element spacing will be established based on system

performance considerations which minimize the losses at the subarray level as well as considerations of grating lobes.

F. Antenna Array

The transmitting antenna array will be comprised of a large number of constant phase subarrays controlled by a retrodirective concept similar to those of previous SPS MPTS system investigations conducted by Raytheon. The sizing of the associated pilot beam system and the reference phase distribution system along with the associated losses will be estimated by Raytheon.

G. Configurations to Control Sidelobes

RF power taper and phase taper (where appropriate) will be the primary techniques to control sidelobes. RF power taper will be considered to be implementable in at least two ways:

(a) Vary the area of solar cells powering the RF module in the sandwich. This will result in uniform RF antenna elements and subarrays facing the earth with steps down in RF power level to as much as 10 dB, similar to those of previous investigations. The RF elements are assumed to be powered by progressively lower power amplifiers or fewer stages as you proceed to the lower RF power density regions. In the gaps on the solar cell side, the areas between the solar cells will be simple reflectors constructed to minimize cost of that segment of the sandwich.

(b) Keep the solar cells contiguous over the backside of the array and feed DC power in from the outboard segments of cells to increase the DC power to the RF modules near the center and decrease the DC power to the RF modules progressively as you move outboard. Where the DC conductors become excessively large to the point where they interfere with a low cost format, use approach (a) above to the degree necessary to define a workable hybrid approach.

H. Microwave Power Beam

The investigation will be bounded by considering (a) a limit on the maximum RF power density at the earth of 23 mW/cm^2 with no sidelobe or grating lobe limits, and (b) the same as above with the additional constraint that sidelobes will be limited to 0.1 mW/cm^2. Associated losses, transmitting antenna and rectenna sizes will be established. Overall sensitivity to the 23 mW/cm^2 and the 0.1 mW/cm^2

limits will be established. The transmitting antenna aperture will be much larger due to the lower maximum RF power density associated with solid state as compared to tubes. New effects such as those due to the extension of the near field region toward the earth as aperture increases will be assessed.

2.3.2 The MSFC Sandwich Concept as a Baseline

The MSFC sandwich concept assumed as a baseline is that reported in the February 1979 briefing by MSFC to NASA/DOE. Variations on this baseline have been reported in several presentations by NASA contractors and certain details from North American Rockwell presentations and private communications have been used in such areas as photovoltaic power generation characteristics as a function of the several temperatures and waste heat dissipation considerations. In-depth design integration of the sandwich concept to interface the microwave portion with the photovoltaic portion has not been performed and warrants further detailed study and technology development.

The MSFC overall concept continued to support the microwave system concepts where uniform photovoltaic power distribution was involved. Microwave systems which are optimized to operate at close-to-critical temperatures semi-autonomously with photovoltaics such as to achieve fully effective use of the aperture require a modification to the MSFC baseline.

As indicated in Sections 8 and 9 and particularly Section 2, stepped taper concepts are of considerable interest where sidelobe control is otherwise limiting the power density at the main lobe. Optimum solar illumination for stepped taper cases is high effective concentration ratio C_E outside the spacetenna aperture with continuously decreasing C_E as radius decreases and with freedom to radiate waste heat from the spacetenna on both sides over an open aperture behind the spacetenna over the high RF power density central region. Concepts such as deletion of a circular region from the solar concentrating reflectors and possibly distorting the remaining reflector into an approximation to a stressed shallow cone and shaping, possibly conical, the outboard photovoltaics to achieve such illuminations should be investigated. Such investigations have not been conducted in this study, however it has been assumed that solar illuminations of this type can be achieved.

2.3.3 Technical Approach

The technical approach was to formulate a preliminary conceptual design based on the assumptions and technical considerations of Section 2.3.1. This was done to form a data base and obtain the experience required to develop the rationale for more effective assumptions, requirements, constraints, etc.

The generation of more detailed design data pertaining to the baseline and filling in certain areas of the data base was the next step.

Assessment of the baseline by comparing it with other concepts and recommending concepts that address potentially critical issues was essentially the last step. Section 2 was prepared last in an attempt to assure that the data was "usable." This caused other sections to be improved and supplemented by appendices to provide a complete set of parametric data and tools to use it. Section 2 also provides the most directly comparable set of data for concepts believed to be worth pursuing further.

2.3.4 Architecture and Options

Provisions in the parametric data of Sections 3 and 8 support solid state microwave power transmission systems analyses for six classes of architecture and options that may be of interest in projected SPS system investigations.

2.3.4.1 System Level Concepts and Options

The following options provide for system concept flexibilities that may be employed to suppress sidelobes. They also provide for approaches that minimize or preclude the penalties associated with sidelobe suppression.

(a) Uniformly distributed microwave power density with autonomous photovoltaic DC power supply. Spacetenna operating at critical junction temperature.

(b) Uniformly distributed microwave power density with DC power imported from dedicated region around periphery of spacetenna. Spacetenna operating at critical junction temperature.

(c) Same as (a) but with single step taper. All subarrays are autonomous with no radial flow of DC power. Central region operating at critical junction temperatures.

(d) Single step taper with DC power transported. Inboard regions utilize all power available for import from the outboard step. Both regions are at critical junction temperatures.

(e) Multiple step taper. All regions are at critical junction temperatures. Inboard regions have $P_{SM} = 0$ and import all power. Outboard regions have $P_{SM} = 0$ and provide power up to their critical junction temperature limits. They import or export power as required or available. Additional power is imported from a dedicated photovoltaic ring around the periphery as required.

(f) Hybrid; tubes in high power central region of single step taper. Solid state in the outboard lower power density region.

The architecture at the total spacetenna level comprises constant RF phase and power density 3.2 m x 3.2 m subarrays which may be grouped into 12.8 m x 12.8 m or greater power and or structural modules. Power and/or structural modules of

about 12.8 m x 12.8 m size will be essentially identical across the spacetenna aperture for Option (a) and will receive their DC power from the photovoltaics on the sandwich face on the opposite side of the spacetenna from the earth. Option (a) has received primary attention in the Raytheon work reported here.

The architecture for Option (b) from the microwave point of view may be identical to that for (a) with the following differences in waste heat dissipation and DC power distribution. Waste heat may be dissipated from both sides of the ground plane. DC power must be imported and converted to low voltage at the power module level and distributed by the necessarily heavier bus bar network to the using equipment; primarily the amplifiers. To achieve maximum microwave power density performance, the solar power system must not shield the free space waste heat radiation from either side of the ground plane. The degree to which such shielding on one side exists will limit the maximum RF performance to a value comparable to the situation where P_{SM} (waste heat from photovoltaics) is zero and the RF power density will be as estimated by the relationships given in Section 8.

In the case of Option (c), the region of the step where RF power density is reduced will not be operating up to the limits imposed by critical junction temperature if each transmit dipole has a dedicated amplifier. Splitting RF power to multiple dipoles would reduce the number of amplifiers in the outboard stepped region. The effective concentration ratio would also be less in the outboard region.

Option (d) makes use of the otherwise non-thermally critical outboard stepped region to generate more DC power (up to thermal limits) than is consumed locally. The appropriate DC power distribution concepts discussed in Section 9.1 would be employed to transport the surplus power inboard. The power generation requirement in the central region would be thereby reduced. The RF power density could therefore be increased and the maximum average power density will increase until regions are operating at critical temperatures.

Option (e), although complex, provides the potential for maximum sidelobe suppression and maintenance of high beam efficiency. The SPS concept that permits near optimum solar flux illumination of solar cells to support this option may also be complex, however investigations should be conducted to conceive such approaches and to understand their full potential.

Option (f), unless imaginatively and productively pursued, may be too complex or in some other respects incredible. Advantages that tubes may have over solid state will probably be greatest where high power densities are required and tubes can provide due to the inherent higher critical temperatures for tubes. Advantages that solid state may have over tubes will probably be greatest where power densities can be sufficiently low to permit the achieving of low junction temperatures and associated long life. Costs in terms of dollars per watt have been shown to decrease as average and maximum power density increases. Sidelobes have been shown to decrease as power density in the outboard region of the spacetenna decreases with respect to that of the inboard regions. Investigations of this option to date suggest that such an approach should be investigated in depth in future system concepts.

2.3.4.2 Antenna Partitioning

The spacetenna is partitioned from five points of view:

(a) Structurally replaceable sections 12.8 m x 12.8 m assumed.

(b) DC power isolatable sections 12.8 m x 12.8 m assumed.

(c) Uniform RF power density section 12.8 m x 12.8 m assumed.

(d) Constant RF phase over region 3.2 m x 3.2 m.

(e) Transmit antenna element spacing.

Transmit antenna elements are distributed on a 10 cm x 10 cm grid and there is one amplifier per transmit element where amplifier junction temperature limits the RF power density. The lower the power per junction the lower will be the temperature rise, however partitioning an amplifier into four dispersed and paralleled junctions as an example is not considered viable from the total active element point of view. Splitting power from one amplifier to four transmit elements is viable, however the junction temperature rise above that of the ground plane will be $\simeq$ 4 times the rise associated with a single amplifier for each transmit element.

Power splitting of RF drive power to 32 dipole power amplifiers dictates $>$ 15.05 dB gain. Splitting to 64 dipoles would dictate 18.06 dB gain. 15 dB has been selected for the baseline, which results in the following:

32 elements/drive amplifier

32 drive amplifiers/central amplifier

∴ 32 x 32 = 1024 elements/central amplifier which controls phase

∴ subarray is 32 x 10 = 320 cm square, i.e., 3.2 m x 3.2 m

2.3.4.3 Subarray

A preliminary layout of a 3.2 x 3.2 meter subarray is shown in Figure 2.3.4-1. A narrative description of the subarray is provided in thirteen parts.

A. The subarray has four quadrants with the highest level of detail provided for the negative quadrant.

B. Four regions in each quadrant include Drive Amplifiers (DAs) with provisions for two sets of four switchable backup (SB) locations that drive, through a single point, each of two sets of 32 non-redundant Dipole Amplifiers (DPA).

C. A single amplifier and in particular its junction is mounted to a cold plate/radiator. This junction is one of the thermally critical 1024 non-redundant parallel configured Field Effects Transistors (FET).

D. One to four Switchably Redundant (SR) Drive Amplifiers (DA) are mounted on cold plates interspersed between the Dipole Amplifiers (DPA).

E. There are 32 sets of drive amplifiers (128 drive amplifiers) per subarray with 32 amplifiers active at a time.

F. Dipole mounting tapes are arranged above the ground plane. They must have minimum width to minimize blockage of waste heat from the amplifiers. The tapes must be continuous to the edges of the subarray and must be tied to neighboring subarray tapes, with edge members around the subarray to maintain the dipole to ground plane spacing. Alternate approaches include compression posts and tension ties forming a truss network to support the dipoles above the ground plane.

G. The waste heat thermal conductor and radiator is assumed to be effectively 8 cm in diameter without obstruction to radiation of waste heat.

H. Transmit dipoles are mounted on each vertical element of a 10 x 10 cm grid, except on the right-hand edge. The right-hand edge dipoles are provided by the right-hand neighboring subarray.

SUBARRAY LAYOUT (TRANSMIT ELEMENTS, RECEIVE ELEMENTS & AMPLIFIERS)

Ⓜ CENTRAL CONTROL & DRIVE REGION

Ⓐ NEGATIVE QUADRANT OF SUBARRAY

Ⓓ 1 TO 4 AMPLIFIERS ON COLD PLATE INTERSPERSED BETWEEN DIPOLE AMPLIFIERS PROVIDE DRIVE POWER (ASSUMED ANT. 4 1:1) 32 SETS OF TRANSMIT DIPOLE AMPLIFIERS

Ⓔ DRIVE AMPLIFIER SET (32 SETS / SUBARRAY, UP TO 128 AMPLIFIERS)

Ⓒ SINGLE AMPLIFIER JUNCTION ON COLD PLATE RADIATOR PROVIDE RF ENT. POWER TO EACH TRANSMIT DIPOLE.

Ⓕ TAPES NOT TO SCALE ≃ 1.2 CM WIDE.

Ⓖ ≃ 8 CM DIA EFFECTIVE WASTE HEAT RADIATOR FOR EACH TRANSMIT DIPOLE AMPLIFIER JUNCTION

Ⓙ RECEIVE DIPOLES IN NON-INTERFERENCE AREAS ON GRID. SPECIFICALLY NOT (a) ON EDGES OF SUBARRAY (b) WHERE OTHER ELECTRONICS & WASTE HEAT RADIATORS TAKE PRECEDENCE i FIRST STAGE AMPLIFIERS ii DRIVER AMPLIFIERS ii CONTROL ELECTRONICS; PHASE, COMMAND & DRIVER

Ⓗ TRANSMIT DIPOLES ON ALL VERTICAL GRID LINES EXCEPT RIGHT HAND EDGE → (32 X 32 = 1024 TRANSMIT DIPOLES/SUBARRAY)

Ⓛ 10 CM × 10 CM

Ⓝ SUBARRAY 3.2 M × 3.2 M. 1024 TRANSMIT DIPOLES 1024 " AMPLIFIERS 256 RECEIVE DIPOLES 32 DRIVER AMPLIFIER SETS. PROVISION FOR CENTRAL ELECTRONICS INCLUDING 12 AMPLIFIERS.

Ⓚ

1" = 10 CM

Figure 2.3.4-1 Subarray Layout (Transmit Elements, Receive Elements & Amplifiers)

J. Receive dipoles are mounted orthogonally to the transmit dipoles. They are centered at the grid points. They are located such as to not unduly compromise the dissipation of waste heat and to not create undue other electrical or mechanical complexities.

K. The right-hand neighboring subarray tape with transmit dipoles is shown to overlap the subject subarray, necessitating the development of unique fabrication and assembly techniques around the periphery.

L. The subarray grid is on 10 cm x 10 cm centers.

M. The control and drive functions are allocated areas distributed between the transmit amplifiers so as to not create overheating of junctions. Techniques for distribution of the electronics for control and drive must be worked out. Such functions are projected to be developed by other programs so that they will be small and lighweight, however the constraint to distribute the equipment so as not to create undue blockage constitutes an architectural problem unique to the SPS application.

N. The subarray is 3.2 x 3.2 meters. It incorporates 1024 transmit dipoles, 1024 transmit amplifiers, 256 receive dipoles, 32 driver amplifier sets and provisions for distributed central electronics including 12 amplifiers.

2.3.4.4 Multifunction Sandwich Design Integration and Partitioning Layout

Layouts of each of the several functional parts of the autonomous subarray sandwich are shown in Figure 2.3.4-2. The nature of the interactions of the several functional design requirements for an autonomous subarray is brought out by discussing the several layers in some detail.

I. Photovoltaic Solar Array

The photovoltaic solar array is shown to be made up of:

A. 40 cm (18 cells) string of approximately 2.04 cm solar cells at .656 x 1.1 V/cell, giving 13 V (end of life) per cell and 13.7 V start of life. This is not intended to constitute a definitive photovoltaic array design, however it is intended to indicate the nature of a somewhat typical layout.

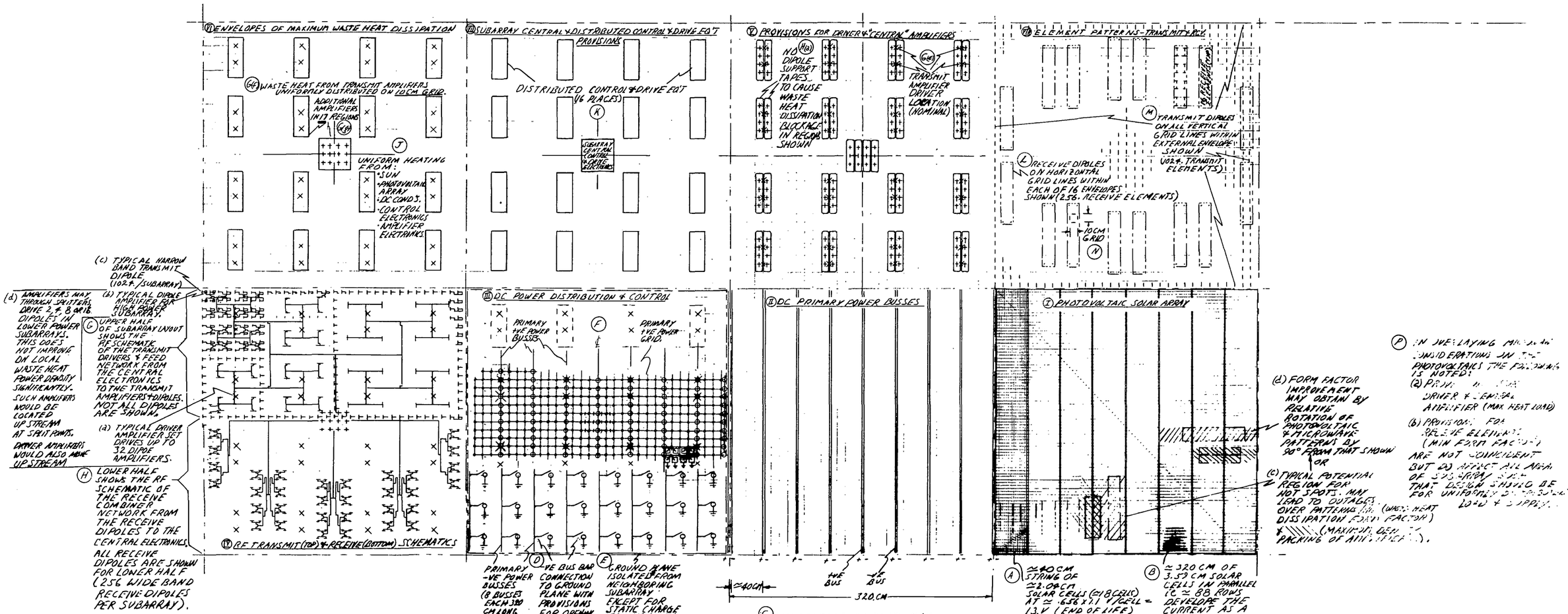

Figure 2.3.4-2 Multi-Function Sandwich and Architectural Partitioning Layout

B. There are approximately 320 cm of 3.59 cm solar cells in parallel, i.e., 88 rows which develop the current as a function of effective concentration ratio C_E, temperature and efficiency.

As will be discussed later, the regions of the microwave side of the sandwich that create mutual interference, particularly in the thermal category, are distributed throughout the photovoltaic array.

II. DC Primary Power Busses

DC primary power busses resulting from I are on 40 cm centers with negative and positive busses being close together.

C. Low voltage DC power may be introduced periodically across the bus bars. Where the photovoltaics are continuous there will be a uniform introduction of supply power. It is noted that where DC power is brought in from other regions it would be introduced periodically on these bus bars. This would be the situation for the non-autonomous approaches.

III. DC Power Distribution and Control

D. There are 8 negative busses each 320 cm long for a total of 2560 cm/subarray. The bus bars are assumed to be a fundamental part of the photovoltaic array and the negative bus bars are connected to the ground plane through an array of 64 power switches.

E. The ground plane is assumed to be electrically isolated from the neighboring subarray ground plane for the autonomous case. There must, however, be incorporated static charge equalization circuitry. Such interconnections detailed requirements and design should be included in design integration investigations.

F. The primary positive busses are similarly a part of the photovoltaic array. They are connected on 10 cm centers to a 10 cm x 10 cm positive power grid. Typically the amplifiers are mounted on the ground plane (negative) and have positive connections to the 10 x 10 cm grid.

IV. RF Schematics

G. The RF transmit schematic is detailed in the top half of the lower left hand sketch. Such detail includes the drivers and feed network from the

central electronics to the transmit amplifiers and dipoles. A typical driver amplifier is shown to drive up to 32 dipole amplifiers. Typical dipole amplifiers are shown in the open region of the dipole 10 x 10 cm grid. Narrow-band transmit dipoles are indicated typically to receive RF power from the amplifiers. It is further indicated that a single amplifier may be configured to drive more than one dipole, however its waste heat dissipation would be concentrated in a local region and result in higher junction temperatures than if each dipole had a dedicated amplifier.

H. The lower half of the sketch details the schematic for the receive dipoles and combiners. Each of the dipoles and combiners are detailed to show where they are located within the subarray. There are provisions for 256 wideband receive dipoles per subarray.

V. Provisions for Driver and Central Amplifiers

It is noted that the architecture is to be such as to not have dipole support tapes over the drive amplifiers as well as over the amplifiers located in the central control electronics region.

VI. Envelopes of Maximum Waste Heat Dissipation

The envelopes of maximum waste heat dissipation are shown to be distributed throughout the subarray. These are the regions requiring in-depth design integration and technology development to assure that junction temperatures do not rise to the point where failures of the non-redundant transmit dipole amplifier junctions will occur prematurely.

J. The elements of uniform heating that must be considered are indicated.

VII. Subarray Central and Distributed Control and Drive Equipment Provisions

K. Provisions for the control and drive electronics are shown to be distributed to minimize heat concentration and to minimize shielding of waste heat dissipation paths.

VIII. Element Patterns - Transmit and Receive

L. The element location pattern of receive dipoles is shown to be on selected intersections of the 10 x 10 cm grid lines. They are constrained to be within the 16 envelopes shown. These envelopes do not overlap the provisions for driver and central amplifiers discussed under Item V.

M. The element location pattern of transmit dipoles is shown to be on all vertical grid lines within the envelope shown. The right-hand column of transmit dipoles is provided by the neighboring subarray. There are 1024 transmit elements that completely populate the 10 x 10 cm grid.

Summary of Photovoltaic Solar Array Potentially Critical Regions

P. In overlaying microwave considerations on the photovoltaics, it is noted that provisions for (a) driver and central amplifiers which maximize heat load (W/m^2) and (b) receive elements contributing to low values of waste heat dissipation form factor are not coincident but do affect all areas of the autonomous subarray. It is indicated that the simple concept of leaving off the solar cells over potential thermally critical regions immediately leads to depletion of more than a proportional area of solar cells. It is also indicated that a relative rotation by 90° of the photovoltaic solar array layup may be advantageous.

In any case, design integration for fully autonomous and dedicated subarrays requires in-depth investigation in the areas of thermal control, thermal leakage, DC power distribution, isolation and protection. The concept of distributed central control and drive electronics must also be included in detailed design integration investigations.

2.3.5 Weight Estimation

Table 2.3.5-1 summarizes the weight estimate for a baseline 3.2 m x 3.2 m subarray. This was derived from a detailed analysis of a typical corner and section of a subarray early in the preliminary design phase as shown in Figure 2.3.5-1. 3 to 4 kg/m^2 is considered to be a good first approximation to the specific weight of the RF, DC distribution and waste heat dissipation portions of an autonomous subarray sandwich. Weight estimates for the photovoltaics and associated bus bars are not included. The specific weights in terms of kg/m^2 and kg/kW as summarized at the bottom of Table 2.3.5-1 are for the autonomous baseline case only.

Weight estimates may be derived for other values of parameters such as fewer receive elements by modifying the appropriate "factor" column and using the given "specific weights". The area of greatest uncertainty is that of the photovoltaic waste heat conductors. This along with the DC conductor weights must be the subject of in-depth study and technology development as a part of the design integration process to assure control of the waste heat leakage from the photovoltaic side to the microwave side.

Table 2.3.5-1

WEIGHT SUMMARY FOR SOLID STATE MPTS FULL SUBARRAY

32 X 32 TRANSMIT ELEMENTS AND AMPLIFIERS AT 10 CM SPACING . . 3.2M X 3.2M = 10.24 M^2

TRANSMIT ELEMENTS AND AMPLIFIERS = 32 X 32 = 1024

RECEIVE ELEMENTS = 1024 - (32 + 2 + 128) = 862

DRIVER RADIATORS = 32

DRIVER AMPLIFIERS = 32 + 32 S.B. = 64

FIRST STAGE RADIATORS = 2

FIRST STAGE AMPLIFIERS = 4

RECEIVE ELEMENTS LEFT OUT AT EDGES = 32 X 4 = 128

DC POWER PER CELL = 8 TO ~10 W, RF POWER PER CELL = 6 TO ~7.5 W/CELL

ITEM	SPECIFIC WEIGHT	FACTOR	WEIGHT (GRAMS) ITEM	SUBTOTAL	SUBARRAY
AMPLIFIER	3.32 GM/AMP	1024 + 64+4 = 1092	3,625		
AMPLIFIER WASTE HEAT COND.	5.29 GM/RADIATOR	1024 + 32 + 2 = 1058	5,597		
AMPLIFIER WASTE HEAT TCC	1.59 GM/RADIATOR	1058	1,682	10,904	
PHOTOVOLTAIC WASTE HEAT COND.	7- 16.32 GM/CELL	1024	7,168 TO 16,712	7,598 TO 17,142	
PHOTOVOLTAIC WASTE HEAT TCC	0.42 GM/CELL	1024	430		
DC CONDUCTORS & GROUND PLANE	0.0687 GM/CELL	1024	71	71	
DIPOLES AND ASSOCIATED MICROWAVE					
DIPOLES - TRANSMIT	.11 GM/ELEMENT	1024	113		
DIPOLES - RECEIVE	.16 GM/ELEMENT	862	138		
CONDUCTORS (50 CM/CELL)	5.0 GM/CELL	1024	5,120	5,371	
STRUCTURAL SPACERS	0.2 GM/CELL	1024	205		
CONTIGUOUS LAYERS	4.8 GM/CELL	1024	4,951		
DIPOLE SUPPORT TAPES	.178 GM/CELL	1024	182	5,338	
SUBARRAY EDGE MEMBER	0.3 GM/CM	4 X 320=1280	384		
PHASE CONTROL ELECTRONICS	250 GRAMS	1	250		
COMMAND CONTROL ELECTRONICS	250 GRAMS	1	250		
DRIVER CONTROL ELECTRONICS	250 GRAMS	1	250	1,134	
					30,416 TO 39,960

A = 10.24 M^2

P_T = 6 X 1024 = 6,144W, i.e., 600 W/m^2, TO 7.5 X 1024 = 7,680W, i.e. 750 W/m^2

SPECIFIC WEIGHTS: $\frac{30,416}{10.24}$ = 2.97 kg/m^2 TO $\frac{39,960}{10.24}$ = 3.90 kg/m^2

AND $\frac{30,416}{6,144}$ = 4.95 kg/kW TO $\frac{39,960}{7,680}$ = 5.21 kg/kW

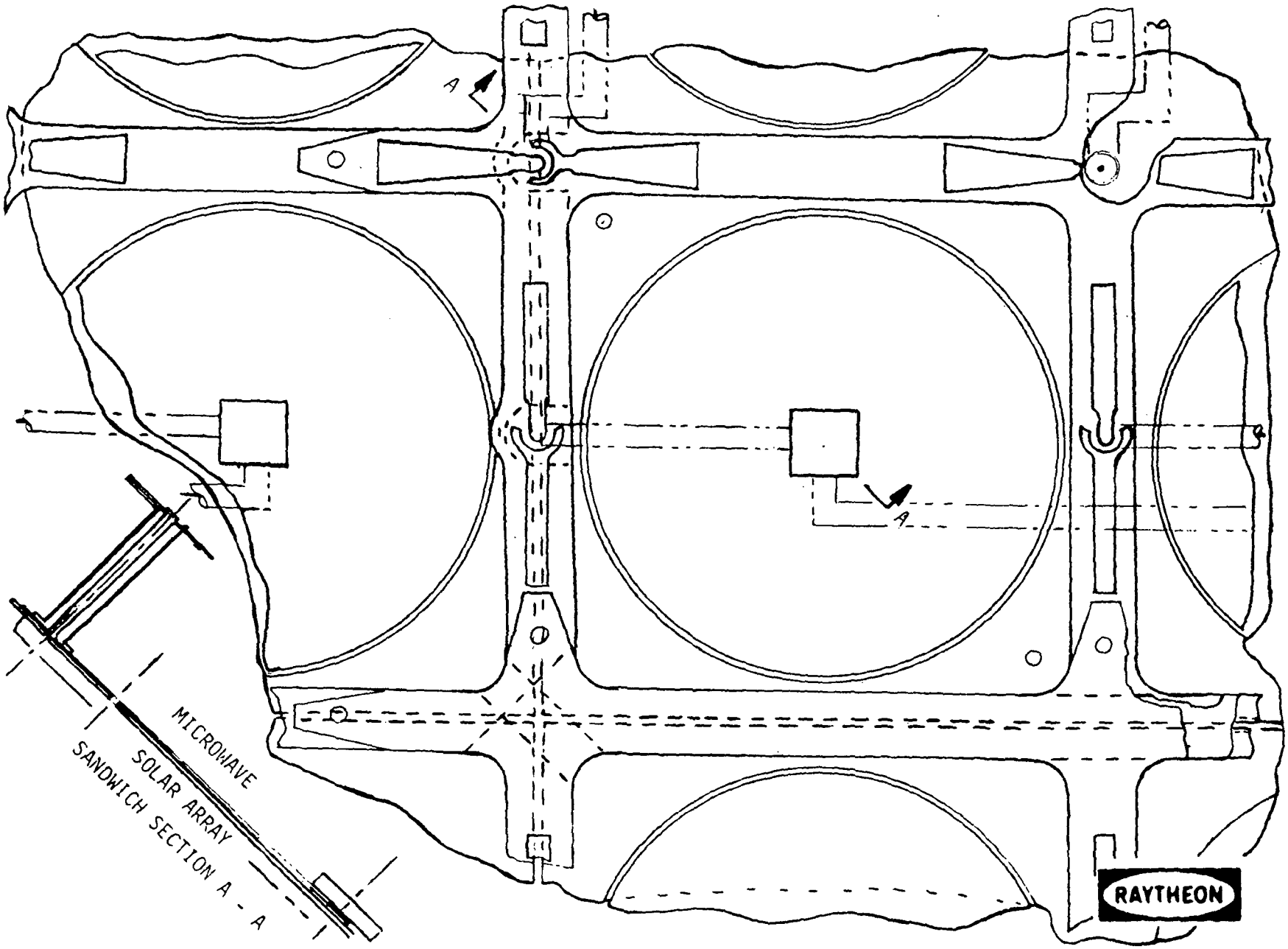

Figure 2.3.5-1 Subarray Layout - Typical Corner and Section

2.3.6 Use of Data

This section illustrates the use of the data established in other sections of the report. It is anticipated that many new concepts will become of interest in the near future and the approaches as well as the data developed in this study will become useful in such activities.

In order to maximize the transfer of knowledge gained by Raytheon in the study to possible users of the report, the details of calculations are included for clarity.

Ten concepts that are considered of interest have been analyzed at a consistent level of detail that initial comparisons and assessments can be made and the more interesting concepts can be selected for further investigation. Details of the supporting calculations are presented in the following subsections, however it is considered useful to summarize the results at the outset.

Parameters

The values for 25 key parameters are presented in Table 2.3.6-1 for each of the 10 concepts. The key parameters begin with P_G (GW of power delivered to the ground grid).

The system size in terms of D_T (Spacetenna Diameter), D_S (Spacetenna and Solar Array Diameter), D_R (Rectenna Diameter), D_F (Fenced Region Diameter) and D_{NCSL} (Diameter to the Next Possibly Critical Sidelobe) is shown on a directly comparative basis.

Specific power in terms of delivered ground power per unit area as well as per solid state amplifier and element of each of costly portions of the system is presented on a comparative basis. The costs per unit area or other divisor will be different, however even without getting into cost it is clear that certain concepts are more advantageous than others.

The key thermal and RF parameters are included again on a comparative basis.

The parameters that are common to all concepts are identified in the top right-hand corner.

Table 2.3.6-1 SPS Microwave Power Transmission System & Other SPS Interactive Data For Initial Concepts Comparison & Assessment

	CONFIGURATION	UNIFORM POWER DISTRIBUTION			SINGLE STEP TAPER						MULTIPLE STEPS -10 DB GAUSSIAN	
	CRITERIA	FIRST SIDELOBE PROTECTED			FIRST SIDELOBE SUPPRESSION			MAX SIDELOBE SUPPRESSION				
	CASE CODE	U-A-SS	U-D-SS	U-D-T	SST-FSS-A	SST-FSS-SA	SST-FSS-NAH	SST-MSS- A	SST-MSS-SA	SST-MSS-NAH	MS-10dB	
	AMPLIFIER	SOLID STATE		TUBES	SOLID STATE		HYBRID	SOLID STATE		HYBRID	SOLID STATE	
	MICROWAVE/ PHOTOVOLTAICS INTEGRATION	AUTONOMOUS	SEGREGATED (DEDICATED	SEGREGATED (DEDICATED	AUTONOMOUS	SEMI AUTONOMOUS	NON AUTONOMOUS (HYBRID)	AUTONOMOUS	SEMI AUTONOMOUS	NON AUTONOMOUS (HYBRID)	SEMI AUTONOMOUS	
	PARAMETERS											
SYSTEM SIZE	P_G (GW)	1.26	2.35	7.42	.906	1.68	5.34	.833	1.55	4.91	1.78	Power delivered to Ground Grid
	D_T (Km)	1.82	1.33	.75	2.34	1.72	1.28	2.42	1.78	.997	1.74	Diameter of Spacetenna
	D_S (Km)	1.82	2.58	3.87	2.34	2.12	3.56	2.42	2.03	3.50	2.05	Diameter of Satellite (First Approximation)
	D_R (Km)	4.8	6.5	11.6	4.69	6.4	11.4	4.69	6.40	11.39	5.84	Diameter of Rectenna
	D_F (Km)	9.8	13.4	23.8	5.57	7.6	13.5	5.52	7.53	13.40	6.87	Diameter of Fenced Region (>.1 mw/cm^2)
	D_{NCSL} (km)	13.0	17.8	31.6	NAI	NAI	NAI	NAI	NAI	NAI	NAI	Diameter at next critical sidelobe where the configuration is limited with respect to potential for margins.
SPECIFIC POWER	P_G/A_T+A_{PVA} (W/M^2)	241.	451.	629.	142.	348	538.	126.	324.	512.	332	Delivered power/ Microwave + Photovoltaic
	P_G/A_R (W/M^2)	69.5	72.8	70.4	52.4	52.4	52.4	48.2	48.2	48.2	66.1	Delivered power/ Area of Rectenna.
	P_G/A_F (W/M^2)	16.7	16.6	16.6	37.2	36.0	37.2	34.8	34.8	34.8	40.1	Delivered power/ Area out to Fence.
	P_G/A_{NCSL} (W/m^2)	9.5	9.5	9.5	NAI	(NAI) NOT AT ISSUE		NAI	NAI	NAI	NAI	Delivered Power/ Area out to next possibly critical sidelobe.
	P_G/A_T (W/M^2)	482.	1684.	16,751.	211.	729.	7,329.	181.	625.	6,284.	750.	Delivered power/ Area of spacetenna.
	P_G/A_{PVA} (W/M^2)	482.	616.	654.	431.	666.	580.	414.	673.	557.	596.	Delivered power/ Area of "assumed" photovoltaics.
	P_G/N^O Amplifiers (W/Amp)	4.8	16.8	NDC (NOT DIRECTLY COMPARABLE)	4.30	7.29	NDC	4.14	6.25	NDC	8.6	Effective Ground power per Amplifier on orbit
	P_G/N^O Elements (W/El)	4.8	16.8		2.11	7.29	NDC	1.81	6.25	NDC	8.6	Effective Ground power per Element on orbit
	T_J (^{O}C)	118.	130.		118.	130.	130	118.	130.	130.	130.	Junction Temp of Last Stage Amplifiers.
THERMAL & RF PARAMETERS	Sp(30th year)%	96.	90.		96.	90.	90.	96.	90.	90.	90.	Survival Probability After 30 years.
	% Energy (30 years)	96.25	91.1		96.25	91.1	91.1	96.25	91.1	91.1	91.1	% of P_Gx30 (GW YEARS) After 30 years.
	ΔT_E C^O/Step	0.	0.		Large	68.6	Large (-ve)	Large	68.6	Large(-ve)	9.5	Temp. Gradient between steps.
	Dissipation Form Factor	1.	1.75		1.	1.71&.95	1.43	1.	1.7&.95	1.43	1.71to.95	Waste Heat dissipation form factor on microwave side of sandwich.
	% DC Transported	0.	100.		0.	63.7	100.	0.	55.3	100.	56.	Percentage of dc power to be transported (Not direct feeding as in case of autonomous sandwich
	C_E for T_S=250^{O}C	6.04	8.56	8.56	6.04	0& 6.47 & 8.56	8.56	6.04	0& 6.47 & 8.56	8.56	0, 5.22 to 6.58 & 8.56	Effective Concentration Ratio
	$P_{RF}(1)$ (W/m^2)	690.	2,412.	24,000.	690.	2386.	24,000	690.	2386.	24,000.	2386. in 10 steps to 303. with 934 average.	Transmitted RF power Density
	$P_{RF}(2)$ (W/m^2)	NA	NA	NA	62.1	215.	2160	62.1	215.	2160.		
	$P_{SM}(1)$ (W/m^2)	568.	0	0	568.	0	NA	568.	0	NA	P_{SM} = 0 to 931	Waste Heat from Photovoltaics.
	$P_{SM}(2)$ (W/m^2)	NA	NA	NA	Large (-ve)	859.	NA	Large(-ve)	859.	NA	with 504 Average	

η_{AMP} = 0.80 (Solid State)
η_{AMP} = 0.85 (Tubes for Reference)
α = 0.05
ε = 0.80
P_{SE} = 812 W/m^2 in Autonomous and Semi-Autonomous Regions
= 1200 W/M^2 in regions dedicated to microwave & free to radiate both ways.
T_S = 250^{O}C (Assumed for baseline).

Concepts

The ten concepts begin, on the left, with uniform power distribution cases which for almost every parameter are most advantageous. It should be noted that tubes are included in each category to indicate the "capability of the competition" and as we progress across the table to indicate where hybrid (tubes and solid state in one configuration) concepts become of interest. The disadvantages of uniform power distribution appear to be in the size of the fenced area at the ground and in the area to the second sidelobe that may become critical if allowable power densities are decreased much below 0.1 mW/cm^2. The disadvantages of complete autonomy are clear in terms of specific power for essentially all divisors. The advantage of complete autonomy is that there is zero DC power transport and it lends itself well to the simple uniform solar power illumination concept. Whether this advantage is worth a factor of essentially 2 in specific power is doubtful at least to the point where DC power transport penalties should be analyzed in considerable detail and other solar power illumination concepts should be conceived.

In the uniform power distribution case, the first sidelobe above 0.1 mW/cm^2 is protected, i.e., it is enveloped by the protective fence. The case code U-A-SS means Uniform, Autonomous and completely Solid State. The next case is U-D-SS meaning Uniform RF where the array is dedicated to RF and the photovoltaics also have their own dedicated region which means that all the DC power must be transported over a considerable distance ≈ 1 km and supplied to the solid state devices at low voltage. The third case is that of the tubes which also require the transport of their power from a remote region.

The Single Step Taper cases are responsive to two levels of criteria. The first one is simply suppressing the first sidelobe to 0.1 mW/cm^2, thus minimizing the fenced area. We observed that we pay a significant penalty in specific power except that associated with the fenced area and surprisingly there is an advantage with respect to photovoltaic area for the semi-autonomous concept. This is primarily due to about 64% of the photovoltaic power generation being unconstrained by the low temperature limits of the solid state microwave equipment. The second set of single step tapers are responsive to a criteria where the goal is to provide the maximum possible margin at the sidelobe for two projected possibilities: (a) the allowable may in the future be reduced below 0.1 mW/cm^2 and (b) the allowable at the peak of the beam may increase above 23 mW/cm^2, in which case the size

of the rectenna would reduce and the total power per system would increase with significant economic advantages.

The Multiple Step -10 dB Gaussian concept gives slightly higher specific power than the semi-autonomous single step first sidelobe suppression concept in terms of rectenna area, the fence area and the spacetenna area, however it gives lower specific power in terms of the photovoltaic array. We note that the ΔT_E steps for the -10 dB Gaussian case are only about 10C°, whereas in the semi-autonomous case it is about 69C°. This could be significant when the design integration issues to provide for the requisite thermal isolation become more clearly understood.

Such comparisons can be discussed indefinitely, so it is perhaps most relevant to study the most cost effective cases as summarized in Table 2.3.6-2. Here the completely autonomous cases have been left off due to their universally low specific power factors and interest is focused on the hybrid concepts. It is recommended that these hybrid concepts be investigated in further detail and compared with comparable tube concepts.

The following subsections will present the specific calculations for each of the concepts discussed above. Table 2.3.6-3 is the primary work sheet for calculating the RF, DC and thermal parameters for cases of interest. It is formatted similar to those included in Section 8. Appendices B and C provide the basic system relationships for spacetenna and rectenna sizing.

2.3.6.1 Example Calculations for Uniform Power Distribution Cases

The parameters for three uniform power distribution concepts are calculated. Based on calculations recorded on the data sheet of Table 2.3.6-3 for the solid state cases and on the microwave system equations of Appendix C, two solid state concepts were analyzed. The first concept is the autonomous case with the solar array temperature being T_S = 250°C and the junction temperatures being 118°C. The second uniform solid state case is for a microwave system segregated from the photovoltaic system. The general calculations for the photovoltaic DC power supply are included. The third concept is that of high power tubes for reference purposes.

Table 2.3.6-2 Initial Concepts Summary Data for Comparative Assessment

( ) Normalized to First Sidelobe Suppressed -23.6 dB Code

CASES / PARAMETER	SPACETENNA RF POWER DISTRIBUTION CASES							
	UNIFORM		SINGLE STEP TAPER				MULTIPLE (10 STEP)	
	FIRST SIDELOBE PROTECTED		FIRST SIDELOBE SUPPRESSED $D_2/D_1 = 1.509$		MAXIMUM SIDELOBE SUPPRESSION $D_2/D_1 = 1.620$		-10 dB GAUSSIAN	
	TUBE "REFERENCE"	SOLID STATE SEGREGATED	SOLID STATE SEMI AUTONOMOUS	HYBRID	SOLID STATE SEMI AUTONOMOUS	HYBRID	SOLID STATE SEMI AUTONOMOUS	
Delivered Ground Power	7.42 (1.39)	2.35 (0.44)	1.68 (0.31)	5.34 (1.0)	1.55 (0.29)	4.91 (0.92)	1.78 (0.33)	GW
$\frac{P_G}{\text{Spacetenna Area}}$	16571.0 (2.29)	1684.0 (.23)	729.0 (.10)	7329.0 (1.0)	625.0 (.09)	6284.0 (.86)	750.0 (.10)	W/m^2
$\frac{P_G}{\text{Rectenna Area}}$	70.4 (1.34)	72.8 (1.39)	52.4 (1.0)	52.4 (1.0)	48.2 (.92)	48.2 (.92)	66.1 (1.26)	W/m^2
$\frac{P_G}{\text{Fenced Area}}$	16.6 (.45)	16.6 (.45)	36.0 (.97)	37.0 (1.0)	34.8 (.94)	34.8 (.94)	40.1 (1.08)	
$\frac{P_G}{\text{Photovoltaic Area}}$	654.0 (1.13)	616.0 (1.06)	666.0 (1.15)	580.0 (1.0)	673.0 (1.16)	557.0 (.96)	596.0 (1.03)	W/m^2
% DC Transported	100	100	63.7	100	55.3	100	56	%

Table 2.3.6-3 Microwave & Associated Thermal Related Parameters - Worksheet
(values not shown are taken to be those above).

PYROGRAPHITE RADIATOR THERMAL CONDUCTORS

	PARAMETRIC / RELATIONSHIPS / CASE	① T_{EFF} °C	② ϵ	③ F	④ ϵF	⑤ P_{SE}	⑥ α	⑦ $P_{SE\alpha}$	⑧ P_{SM}	⑨ η_{AMP}	⑩ $1-\eta_{AMP}$	⑪ $3RT^4_{AMP}$	⑫	⑬	⑭	⑮	⑯	⑰ P_R/A_C	⑱ ΔP_R	⑲	⑳ P_{DC}	㉑	㉒ P_{RF}	㉓ ΔT_C for R.C.R.	㉔ T_S(°C)	㉕ $P_{RF}/569$	㉖ $P_{DC}/772$	DC AVAILABLE (LOCAL) P_{DCS} for T_S=200°C = .28×⑧ +651.95	P_{DCS} for T_S=250°C = .2311×⑧ +803.83	C_E = 3.6094 +.00153 R_M for T_S=200 *T_S:1898 + .00149 R_M for T_S=250
		㉔-492/1.8 = ㉓			②×③	WATTS/M²		⑤×⑥	㉔-⑯-⑦ WATTS/M²		1.-⑨	3RT⁴×⑨	.0578 ⑪/⑩	1.+⑫	(48①+492) = ⑬ °R; ⑬/555 = ⑭; ⑭⁴×.5457×10⁻⁸ = ⑮; ⑮×④×⑧ = ⑯	⑯×.5457 = ⑰; ⑰⁴×10⁻⁸ = ⑱; ⑱×④×⑧ = ⑲	⑲-⑧-⑦ WATTS/M² = ⑳	⑳/㉑ WATTS/CELL	㉒×⑰ WATTS/M²	.980×⑯	⑰/⑯ WATTS/M²	.9608×②/④	㉔×⑰ WATTS/M²	㉕ C°	①+㉓ °C	㉔/569	㉖/772			
DESIGN BASELINE		96.	0.8	1.0	0.80	822.	0.15	123.3	527.8	0.80	0.20	1.1931	0.0592	1.3392	664.8	853.6	202.5	151.3	51.	0.196	772.	3.763	567.	18.	114.	1.0	1.0	799.7		
FROM PRELIMINARY DESIGN AND ASSESSMENT	" " AUTONOMOUS*	85.4							5200						663.7	852.5	208.2	156.3	52.86		797.6*		588.2	18.6	114.02	1.034	1.033	797.6*	924.00	4.41*
	α=.05, P_{SM}=0 T_S = 130 °C	53.7		1.75	1.4	1200.	0.05	60	0.						588.7	917.8	857.8	641.	216.78		3270.		2412.	76.3	130.0			0	0	
FOR AUTONOMY*	" P_{SM}=+ve @ T_S = 118°C	98.7		1.0	0.8	822			620.8						669.7	878.6	216.6	161.9	54.75		826.*		609.	19.3	113.			825.8*		4.57*
		96.2							588.4						665.1	859.8	245.2	183.3	61.99		935.*		690.	21.8	118.				935.20*	6.04*
		68.6							32.4						616.5	626.8	535.4	415.0	140.35		2117.		1562.	49.4	118.				811.32	
		112.0							903.3						693.7	1011.3	66.9	50.	16.91		253.		188.	5.9	118.				1012.58	
		70.4							63.6						618.7	640.	535.3	400.	135.28		2040.		1505.	47.6	118.				818.53	
FOR -10dB GAUSSIN		54.6		1.71	1.37	1200	0.05	60	0						590.2	908.6	849.5	634.1	214.45		3239.		2386	75.5	130.			0	0	
		62.9		1.39	1.11										605.2	815.0	755.0	564.2	190.81		2879.		2123	67.1	130.			0	0	
		72.8		1.07	.855										623.0	703.0	643.0	480.5	162.57		2451.		1808	57.2	130.			0	0	
		79.7		.95	.76	822		41.1	73.9						635.5	676.5	565.1	422.3	142.82		2155		1589	50.3	130.				820.9	5.30
		91.9		.96	.768				313.2						657.4	782.2	428.4	320.5	108.39		1635.		1206	38.1	130.				876.2	5.66
		101.4		.97	.776				514.3						674.5	873.9	321.5	240.2	81.24		1226.		904	28.5	130.				922.7	5.96
		115.7		.98	.784				827.3						700.3	1029.1	163.7	120.1	40.62		613.		452	14.3	130.				995.1	6.42
	Autonomous Step Taper (Outboard Region No DC Transport)	LOW		1.75	1.4	1200		60	2831.						NEAR 2732		39.2	27.3			14%.6		110.4	3.5	LOW					
	Single Step (Outboard)	117.9		.95	.76	822	0.05	41.1	843.5						704.2	1020	135.8	101.5	34.3		517.9		382.	12.1	130				998.8	6.45
		123.2		.95	.76	822		41.1	959.3						713.8	1077.	76.37	57.066	19.3		291.2		214.7	6.79	130				1025.5	6.62
	General	124.05		.95	.76	822		41.1	978.1						715.3	1086.	66.91	50.	16.9		255.1		188.15	5.95	130.				1029.9	6.65
FOR MULTIPLE-STEP -10dB GAUSSIAN ILLUMINATION	ΔT_S +4.6	54.55		1.71	1.37	1200	0.05	60.	0						590.2	907.4	848.5	634.1	214.45		3235.		2386	75.45	130			0	–	
	+9.0	59.1		1.53	1.22	"	"	"	0						598.4	857.3	797.3	595.8	201.50		3040.		2242	70.80	130			0	–	
	+9.5	68.08		1.21	.97	"	"	"	0						614.5	756.3	686.3	520.3	175.97		2655.		1958	61.92	130			0	–	
	+7.1	77.60		.95	.76	822	"	41.1	19						631.7	698.2	589.2	440.3	148.91		2246.		1657	52.40	130			808.2	5.22	
	+6.4	84.71		.96	.768	"	"	"	170.3						644.5	720.6	509.2	380.6	128.70		1942.		1432	45.29	130			843.2	5.44	
	+6.9	91.13		.97	.776	"	"	"	306.3						656.0	784.5	437.1	326.6	110.46		1666.		1229	38.86	130			874.6	5.65	
	+6.4	98.06		.97	.776	"	"	"	445.8						668.5	846.1	359.2	268.4	90.77		1369.		1010	31.94	130			906.9	5.85	
	+7.2	104.48		.97	.776	"	"	"	558.0						680.1	906.1	287.0	214.5	72.54		1094.		807	25.52	130			937.4	6.02	
	+8.8	111.63		.97	.776	822	0.05	41.1	729.0						692.9	976.7	206.6	154.4	52.22		788.		581	18.37	130			972.3	6.28	
		120.42		.98	.784	"	"	"	931.1						708.8	1080.	107.8	80.5	27.23		411.		303	9.58	130			1019.0	6.58	
	Avr. 7.3	100.48		.98	.784	"	"	"	504.2						672.9	877.	332.0	248.	83.90		1266.		933.5	29.52	130		Averages→	920.3	5.94	
																												↓ 908.8	↓ 5.86	
		61.69		1.434	1.147	1200	"	60.	0						603.0	838.1	768.14	574.	194.		2929.		2160.	68.31	130					

UNIFORM POWER DISTRIBUTION (UPD) DESIGN BASELINE AUTONOMOUS (T_S = 250°C)

P_{RF} = 690 W/m^2

C_E = 6.04

P_{DC} = 935 W/m^2 (Supply = Demand)

F = 1 (Waste Heat Rad. Form Factor)

α = .05

ε = .80

P_{SE} = 822 W/m^2

P_{SM} = 568.4 W/m^2

T_E = 96.2°C

ΔT = 21.8°C (PG Radiators)

T_J = 118°C

ΔP_B = 61.99 W/m^2

η_{-DC} = .99

η_{+DC} = .99

η_{AMP} = .80

η_{FILT} = .96

η_{ANT} = .98

η_{DC-RF} = .7377

η_{AT} = .98

η_{EC} = .825

η_R = .89

η_G = .97

η_{RF-G} = .6980

η_{DC-G} = 0.515

η_{AR} = 1 where η_{DC-RF} includes η_{ANT}

P_{di} is calculated at ground level, i.e., includes atmospheric loss

$P_T = P_o A_T F(-4)$ and F = Power Taper Factor = 1 for Uniform Power Distribution

$$D_T = 2\left(\frac{P_{di}}{P_o \eta_{AR} \eta_{AT}}\right)^{.25} \sqrt{\frac{\lambda_o R_o}{\pi}}$$ and for $P_{di} = 230\ W/m^2$, $P_o = P_{RF} = 690\ W/m^2$, $\eta_{AR} = 1$, $\eta_{AT} = .98$,

$\lambda_o = 0.121$ m, $R_o = 37 \times 10^6$ m

$$D_T = 2\left(\frac{230}{690 \times 1 \times .98}\right)^{.25} \sqrt{\frac{.121 \times 37 \times 10^6}{\pi}} = 1{,}823 \text{ m}$$

$\therefore A_T = \frac{\pi\ 1823^2}{4} = 2.61 \times 10^6\ m^2$, N° Active Elements = 261×10^6

$P_T = 690 \times 2.61 \times 10^6 = 1.801$ GW

$P_G = P_T \times .6980 = 1.257$ GW

$$D_G = \left(\frac{P_o \eta_{AR} \eta_{AT}}{P_{di}}\right)^{1/4} \sqrt{\lambda_o R_o \pi}\ U = \left(\frac{690 \times 1 \times .98}{230}\right)^{1/4} \sqrt{.12 \times 37 \times 10^6 \pi}\ U = 4.911 \times 10^3\ U$$

From Figure B-4, for the rectenna at 1 mW/m^2, B = 0 $\therefore U_R = 0.97$.

for the fence at the first sidelobe at 0.1 mW/cm^2 $\therefore U_F = 2.0$

peak of second sidelobe at .0958 mW/cm^2 (free space) $\therefore U_{SLL} = 2.65$

$D_{GR} = 4.8$ km $\therefore A_R = 18.1 \times 10^6\ m^2$, $A_R/A_T = 6.93$ | $P_G/A_T + A_{PVA} = \frac{1.257}{.00261 + .00261} = 240.8\ W/m^2$

$D_{GF} = 9.8$ km $\therefore A_F = 75.4 \times 10^6\ m^2$ | $P_G/A_R = 69.45\ W/m^2$, $P_G/A_F = 16.67\ W/m^2$, $P_G/A_{SSL} = 9.45\ W/m^2$,

$D_{GSSL} = 13.0$ km $\therefore A_{SSL} = 133 \times 10^6\ m^2$ | $P_G/A_T = 481.6\ W/m^2$, $P_G/A_{PVA} = 481.6\ W/m^2$

FOR UPD NON-AUTONOMOUS (SEGREGATED) CASE, T_S = 250°C

P_{RF} = 2412 W/m^2

P_{DC} = 3270 W/m^2 (Demand)

F = 1.75 (Double Sided Waste Heat Radiator)

P_{SE} = 1200 W/m^2

P_{SM} = 0

T_E = 53.7°C

ΔT = 76.3°C

T_J = 130°C

ΔP_B = 216.78

All others same as autonomous case.

$$D_T = 2\left(\frac{230}{2412 \times 1 \times .98}\right)^{.25}\sqrt{\frac{.121 \times 37 \times 10^6}{\pi}} = 1333 \text{ m}$$

A_T = 1.397 x 10^6 m^2, N^o Active Elements = 140 x 10^6

P_T = 2412 x 1.397 x 10^6 = 3.370 GW

P_G = 3.370 x .6980 = 2.352 GW

$$D_G = \left(\frac{2412}{690}\right)^{1/4} \times 4.911 \times 10^3 \text{ U} = 6.715 \times 10^3 \text{ U}$$

D_{GR} = 6.51 km $\therefore$ A_R = 32.3 x 10^6 m^2, A_R/A_T = 23.1

D_{GF} = 13.43 km $\therefore$ A_F = 141.7 x 10^6 m^2

D_{GSSL} = 17.79 km $\therefore$ A_{SSL} = 248.6 x 10^6 m^2

P_G/A_R = 72.8 W/m^2, P_G/A_F = 16.6 W/m^2, P_G/A_{SSL} = 9.46 W/m^2

P_G/A_T = 1684 W/m^2

$$P_G/A_T + A_{PVA} = \frac{2.352}{.001397 + .003819} = 450.92\ m^2$$

DC Power To Be Imported:

$$\frac{P_{DC}\ \text{Demand} \times A_T}{.9368 \times .963} = \frac{3270 \times 1.397 \times 10^6}{902} = \underline{\underline{5.064\ GW}}$$

At $T_S = 250°C$, $T_E = 200°C$

$P_{SE} = 822$

$\alpha = .05$

$\varepsilon = 0.8$

$F = 1$

$P_{SM} = 2260\ W/m^2$

$P_{DC} = 1326\ W/m^2$

$C_E = 8.56$

$\therefore\ A_{PVA} = (5.064/1326) \times 10^9 = 3.819 \times 10^6\ m^2$

$P_G/A_{PVA} = 615.9\ W/m^2$ [D_o (Equiv.) = 2577 m]

Photovoltaic DC Power Supply Estimates for Dedicated Photovoltaic Array

$T_S = 250°C$

$T_E = 200°C$

$P_{RF} = 0$

$P_A = 0$

$P_{SE} = 822$

$\alpha = .05$

$\varepsilon = 0.8$

		Microwave Worksheet Column Numbers
$F = 1.0$	$\varepsilon F = 0.8$	(4)
$P_{SE}\alpha = 41.1$		(7)
$(1.8 \times 200 + 492) = 852$		(14)
$852^4 \times 0.5459 \times 0.8 \times 10^{-8} = 2301$		(15)

$P_{RF} = 0 \therefore P_A = 0 \therefore (16) = 0 = (16)$

$P_{SM} = (15) - (16) - (7) = 2301 - 0 - 41.1$

$= 2260 \text{ W/m}^2$ (8)

$P_{DC} = .2311 \times (8) + 803.83 = 1326 \text{ W/m}^2$

$C_E = 5.1888 + .0014917\ P_{SM} = 8.56$

For $P_{DC}\ A_{PVA} = 5.064$ GW

$$A_{PVA} = \frac{5.064 \times 10^9}{1326} = 3.819 \times 10^6 \text{ m}^2$$

For D_i = internal diameter = D_T = 1333 m

D_o = outside diameter

$$\frac{\pi}{4}(D_o^2 - D_i^2) = 3.819 \times 10^6 \text{ m}^2$$

$$\therefore D_o = \sqrt{3.819 \times 10^6 \times \frac{4}{\pi} + 1333^2} = 2577 \text{ m}$$

CASE U-D-T (UNIFORM POWER DISTRIBUTION USING TUBES)

$P_{RF} = 2400\ W/m^2$

$\eta_{AMP} = 0.85$ and $\eta_{RF-G(U)} = 0.698$

$P_{DC}(\text{Demand}) = 30{,}650\ W/m^2$

$D_{TU} = 750.796\ m$

$P_{TU} = 10.625 \times 10^9\ W$

$U = D_{TU} \frac{\pi}{\lambda} \sin\theta = \frac{D_G}{74 \times 10^6} \times \frac{D_{TU}\,\pi}{.121}$

$D_G = \frac{2.850 \times 10^6}{D_{TU}} U$

$U_R = 3.05 \quad \therefore \quad D_G = \frac{2.85 \times 10^6}{750.796} U = 3796\,U$

$D_{GR} = 3796\ U_R = 3796 \times 3.05 = 11{,}578\ m$

$U_F = 6.28$

$D_F = 23{,}840\ m$

$U_{SSL} = 8.33$

$D_{SS} = 31{,}620\ m$

$A_R = 105.282 \times 10^6\ m^2$

$A_F = 446.37 \times 10^6\ m^2$

$A_{SSL} = 785 \times 10^6\ m^2$

$A_{TU} = .442725 \times 10^6\ m^2$

$P_{GU} = 24000 \times .442725 \times 10^6 \times .698 = 7.416 \times 10^9\ W$

Photovoltaic Array Required:

$P_{DC}(\text{Demand})\ A_T = 30650 \times .442725 \times 10^6 = 13.5695 \times 10^9\ W$

Taking the additional efficiency penalty for power transport of 0.902 increases the DC power requirement to $13.5695/.902 = 15.044 \times 10^9$ W.

For a photovoltaic array (PVA) operating at P_{DC} = 1326 W/m^2,

$$A_{PVA} = \frac{15.044 \times 10^9}{1326} = 11.345 \times 10^6 \ m^2$$

For inside diameter = 750.796 m,

$$\frac{\pi}{4} (D_o^2 - 750.796^2) = 11.345 \times 10^6$$

$$\therefore \ D_o = 14.445 + .56369 \times 10^3 = 3874 \ m$$

$$P_{GU}/A_T + A_{PVA} = \frac{7.416}{.0004427 + .011345} = 629.13 \ W/m^2$$

$$P_G/A_R = 7.416/.105282 = 70.43 \ W/m^2$$

$$P_G/A_F = 7.416/.44637 = 16.614 \ W/m^2$$

$$P_G/A_{SSL} = 7.415/.785 = 9.447 \ W/m^2$$

$$P_G/A_{TU} = 7.415/.000442725 = 16,751 \ W/m^2$$

$$P_G/A_{PVA} = 7.415/.001345 = 653.68 \ W/m^2$$

P_G/N^o 40 kW Power Modules = 7.415/.0002656 = 27,918 W/module

P_G/N^o Slots = 7.415/.0442725 = 167.5 W/slot

2.3.6.2 Example Calculations for Single Step Taper Cases

Figure 2.3.6.2-1 shows the results of an assessment of a series of single step taper investigations recorded in Appendix C. This figure shows that an optimum (with respect to efficiency η_{TA}) power taper exists to implement a requirement for the first sidelobe to be reduced below that of the uniform power distribution case.

In the uniform case, the first sidelobe is -17.4 dB from the peak of the main beam. If the peak of the main lobe is 23 mW/cm^2, then the peak of the first sidelobe will be 0.39 mW/cm^2. This may in the future be shown to be an acceptable level for an unprotected region. For the purposes of this investigation, however, it is assumed that a fenced/protected region will be required to envelope those free space sidelobes above 0.1 mW/cm^2. Such a fence would therefore envelope a region beyond the peak of the first sidelobe.

It is of interest to know what the penalties would be to suppress the first sidelobe (a) to the point where it is at the -23.6 dB level, thus reducing the protected region to that of the main lobe, (b) to a minimum value that would be responsive to more stringent sidelobe limits, (c) to any value in between and (d) to a value relative to the main lobe such that if main lobe allowable power density increases to a value like 3 dB above 23, i.e., 46 mW/cm^2, there would be an approach to reduce the sidelobes down to the 0.1 mW/cm^2 level.

The first approximation to the penalties as indicated on Figure 2.3.6.2-1 is as follows:

(1) To reduce the first sidelobe and eliminate its fence requirement means another 10.6% penalty in η_{TA} has to be accounted for, i.e., $\eta_{TA} = 0.894$ and $\eta_U \eta_{TA} = 0.825 \times 0.894 = .73755$ would replace the rectenna energy collection efficiency in the efficiency chain. The 0.51 value for the total chain would reduce to 0.456, i.e., a 5.4% loss of energy.

(2) Reducing the first and other near-in sidelobes to the optimum minimum results in the need to account for an additional 3.4% penalty in η_{TA}, i.e., $\eta_{TA} = 0.86$ and $\eta_U \eta_{TA} = 0.825 \times 0.86 = .7095$ would replace the rectenna energy collection efficiency in the efficiency chain. The 0.51 value for the total chain would reduce to 0.4386, i.e., a 7.14% loss of energy which is an additional 1.78% loss.

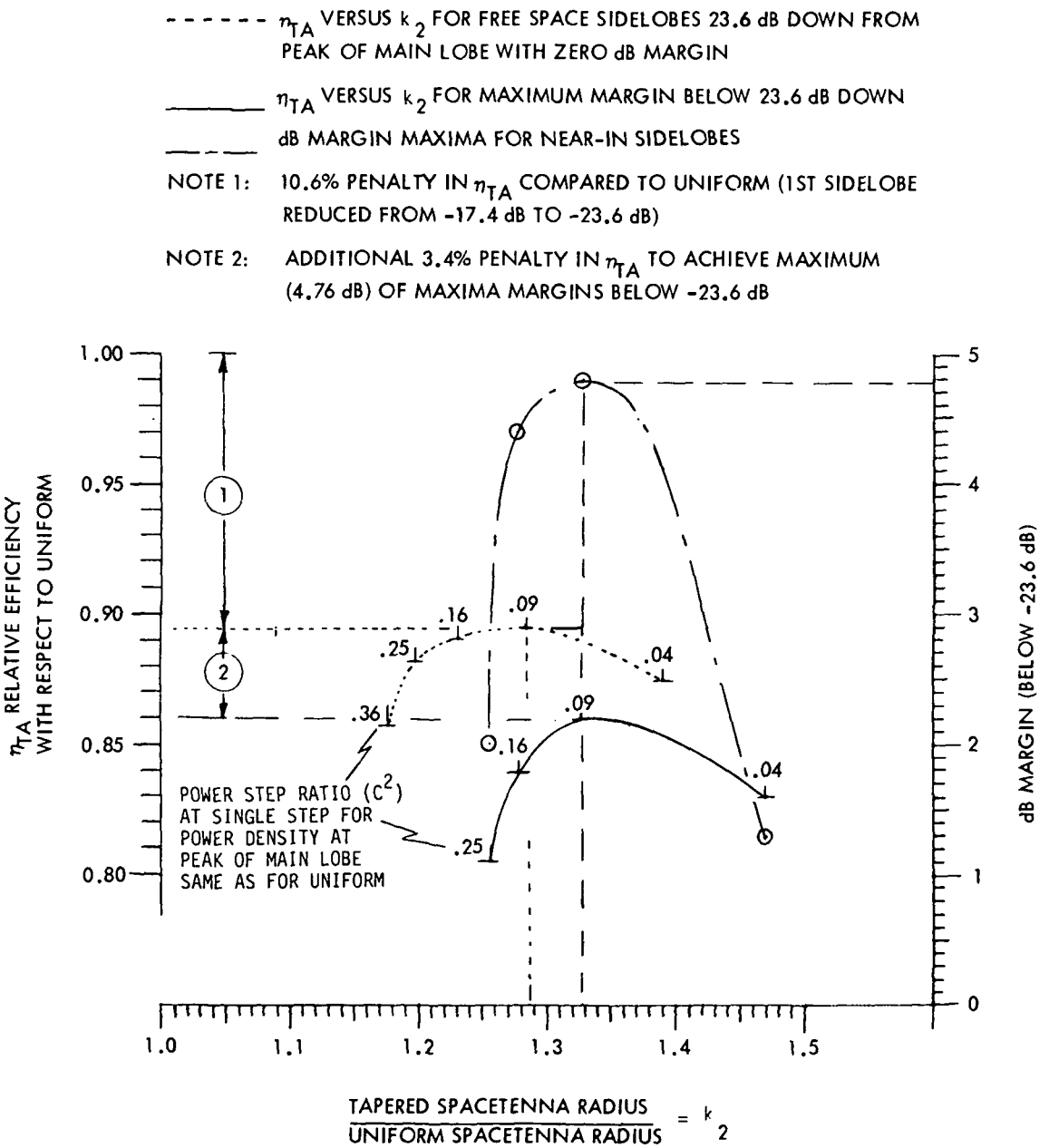

Figure 2.3.6.2-1 Single Stepped Taper Aperture Efficiencies and Sidelobe Margins Relative to Uniform

The following cases and calculations are provided to approximate the penalties more closely and to illustrate how the parametric data may be used to investigate a great range of assumptions.

CASE (SST-MSS) SINGLE STEP TAPER MAX SIDELOBE SUPPRESSION

Voltage Step C = 0.3

Power Step C^2 = 0.09

Sidelobe Suppression is 23.6 + 5 = 28.6 dB

P_{DI} = 23 mW/cm^2

$\therefore$ P_D (sidelobes) $\leq$ 0.0317 mW/cm^2

Note: If P_D sidelobe were acceptable at 0.1 mW/cm^2 and the free space value were achieved and the ionospheric limit were completely relieved, $P_{DI} = \frac{0.1}{0.0317} \times 23 = 72.5$ mW/cm^2. This could indeed lead to advantageous economics.[12]

Continuing with

P_{DI} = 23 mW/cm^2

k_2 = 1.3285 from Figure 2.3.6.2-1

U_R = 3.0 (at -13.6 dB, i.e., 1.0 mW/cm^2)

U_F = 3.53 (at -23.6 dB, i.e., 0.1 mW/cm^2)

U_R and U_F are measured on Figure C-3 of Appendix C. Such measurements show U_R = 3 and U_F = 3.53 over range of k_2 values.

$$k_1 = \left[\frac{1 - k_2^2 C}{1 - C} \right]^{1/2} = \left[\frac{1 - 1.3285^2 \times 0.3}{1 - 0.3} \right]^{1/2}$$ from Equation (C-1) of Appendix C

= 0.81987

The diameter of the higher power density region is 0.81987 x the diameter (D_U) of a uniform power distribution case operating at the same power density on orbit for the same P_{DI} at the ground. See Section 2.3.6.2 for the uniform case calculations. Similarly the outside diameter of the lower power density region is 1.3285 times that of the uniform case. The outside diameter of the high power density

region is referred to as D_1 and the outside of the low power density region is referred to as D_2.

$$D_2/D_1 = 1.3285/0.81987 = 1.6204$$

$$D_{TU} = 2\left(\frac{P_{DI}}{P_o\ \eta_{AR}\ \eta_{AT}}\right)^{.25}\sqrt{\frac{\lambda_o\ R_o}{\pi}}$$

where

$P_o = P_{RF1}$ = RF power density in the high power central region referred to as Region (1).

P_{DI} = 23 mW/cm^2
= 230 W/m^2 for this equation.

λ_o = 0.121 meters = wavelength of P_{RF}

R_o = 37×10^6 m = spacetenna-to-ground distance

η_{AR} = 1, i.e., the uniform distribution value

η_{AT} = 0.98 = efficiency due to the atmosphere so that P_{DI} is really at ground level

$$D_{TU} = 9344.9/(P_{RF1})^{.25} \text{ meters}$$

$$D_2 = 1.3285\ D_{TU} = 12415/(P_{RF1})^{.25}$$

$$D_1 = 0.81987\ D_{TU} = 7662/(P_{RF1})^{.25}$$

$P_{TU} = P_{RF1}\ A_{TU}\ F$ = Total power transmitted from the uniform aperture.

where

$F = 1$

$$A_{TU} = \frac{\pi\ D_{TU}^2}{4} = \frac{68.586 \times 10^6}{(P_{RF1})^{.5}}$$

$$P_{TU} = 68.586 \times 10^6\sqrt{P_{RF1}}$$

$$P_{TT} = P_{RF1} \frac{\pi\ 7662^2}{4\sqrt{P_{RF1}}} + P_{RF2} \frac{\pi}{4}\left(\frac{12415^2}{\sqrt{P_{RF1}}} - \frac{7662^2}{\sqrt{P_{RF1}}}\right)$$

$$= \sqrt{P_{RF1}}\ 46.1078 \times 10^6 + \frac{P_{RF2}}{\sqrt{P_{RF1}}} \times 74.9474 \times 10^6$$

$$\frac{P_{TT}}{P_{TU}} = \frac{\sqrt{P_{RF1}}\ 46.1078 \times 10^6 + \frac{P_{RF2}}{\sqrt{P_{RF1}}} \times 74.9474 \times 10^6}{68.586 \times 10^6\ \sqrt{P_{RF1}}}$$

$$= 0.672263 + \frac{P_{RF2}}{P_{RF1}} \times 1.09275$$

where

$$\frac{P_{RF2}}{P_{RF1}} = C^2 = 0.09$$

$\therefore\ P_{TT}/P_{TU} = .77061$

$$P_{TT} = \sqrt{P_{RF1}} \times 52.853 \times 10^6\ W$$

SST-MSS-A (AUTONOMOUS)

The first sub-case is that of each section being autonomous, i.e., P_{DC} Demand = P_{DC} Supply in each region and there is no DC power transport.

P_{RF1} = 690 W/m^2 (the same as the previously discussed uniform autonomous case)

$P_{RF2} = 0.09 \times 690 = 62.1\ W/m^2$

Autonomy in Region (1) is assumed to be constrained on the RF side of the sandwich to the parameters below down to η_{DC-RF}. η_{AT} through η_{DC-G} will be used in subsequent analyses. The efficiencies are consistent with the efficiency chain of Figure 3.8-1. The determination of the other parameters is performed on the work sheet Table 2.3.6-1.

P_{DC} (Demand) = 935 W/m^2

F = 1 (waste heat dissipation form factor)

α = 0.05

ϵ = 0.80

P_{SE} = 822 W/m^2

P_{SM} = 568.4 W/m^2

T_E = 96.2°C

ΔT = 21.8C° (pyrographite thermal conductors)

T_J = 118°C

ΔP_B = 61.99 W/m^2

η_{-DC} = 0.99 η_{AT} = 0.98

η_{+DC} = 0.99 η_{EC} = 0.825 x η_{TA}

η_{AMP} = 0.80 η_R = 0.89

η_{FILT} = 0.96 η_G = 0.97

η_{ANT} = 0.98

η_{DC-RF} = 0.7377 η_{RF-G} = 0.6980 η_{TA}

η_{DC-G} = 0.515 η_{TA} for "no DC transport" cases.

Autonomy in Region (1) is assumed to be constrained on the photovoltaic side of the sandwich to make P_{DC} (Supply) equal to P_{DC} (Demand). Furthermore, the photovoltaics are assumed to operate at C_E = 6.04, and a T_S of 250°C. These, of course, are not optimized and the relationships of P_{DC} (Supply) to P_{SM} is the driving constraint. For design integration activities this section of the calculations would change as the actual heat transfer relationships become known and the photovoltaic characterisitcs are definitized.

Autonomy in Region (1) with the above conditions requires that:

P_{DC} (Demand) = -2.031 P_{SM} + 2089.5

$$P_{DC}\ (\text{Supply}) = +0.2311\ P_{SM} + 803.83$$

$$\therefore\ P_{SM} = 568.4 \text{ and } P_{DC} = 935\ W/m^2$$

Autonomy in the outboard region requires that:

$$P_{DC}\ (\text{Demand}) = C^2\ P_{DC}\ (\text{Demand}) \text{ for Region (1)}$$

$$= .09 \times 935 = 84.15\ W/m^2$$

$$P_{DC}\ (\text{Potential Supply}) = 935\ W/m^2$$

Since 91% of the potential DC supply is not required, the area of solar cells could simply be reduced to 9% of that of the spacetenna in the outboard region. It is noted that Region (2) is not operating at full efficiency in terms of maximum allowable temperatures.

If the P_{DC} (Supply) reduction is relatively uniform over a subarray, then P_{SM} average would be as follows:

$$P_{SM}\ (\text{Region 2}) = \frac{84.15 - 803.83}{0.2311} = -3113\ W/m^2$$

This is inconsistent with the $T_S = 250°C$ in that heat would not flow passively from the cooler microwave side to the hotter photovoltaic side of the sandwich except in regions where the solar cells are replaced by high ε and low α thermal control coatings. The heat transfer subject will not be gone into further here; however, for the purposes of comparative assessment, the reduction in solar cell area will be credited and the temperatures of the ground plane as well as the junctions will be noted as being low. It will also be assumed that one amplifier will drive $1/C^2 \simeq 11$ dipoles in the outboard region, thus reducing the number of amplifiers.

This is known to be an uninteresting case, however the data will be developed for quantitative comparison purposes and to support the development of trend data.

$$D_{TU} = \frac{9344.9}{(690)^{.25}} = 1823\ m$$

$$D_2 = 1.3285 \times 1823 = 2422\ m$$

$$D_1 = 0.81987 \times 1823 = 1495 \text{ m}$$

$$P_{TU} = 68.586 \times 10^6 \quad 690 = 1.802 \times 10^9 \text{ GW}$$

$$P_{TT} = .77061 \times 1.802 \times 10^9 = 1.388 \times 10^9 \text{ GW}$$

U_{Space} = 3.0 for 13.62 dB down from the peak (23 mW/cm^2) of the main lobe which is 1 mW/cm^2 or the edge of the free space rectenna.

Similarly,

U_{Space} = 3.53 for the fence at 23.62 dB down or 0.1 mW/cm^2

$$U = \frac{2\pi a}{\lambda} \sin\theta = D_{TU} \frac{\pi}{\lambda} \sin\theta = 25.964\, D_{TU} \sin\theta$$

where a is the transmit aperture radius for the uniform case, i.e., 2a = 1823 m and λ = 0.121 m.

$$\therefore U = \frac{1823\ \pi}{0.121} \sin\theta = 47332 \sin\theta$$

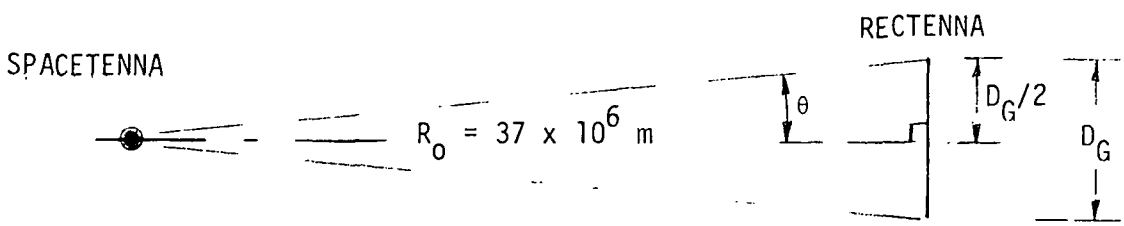

$$\frac{D_G}{74 \times 10^6} D_{TU} \times 25.964 = U \quad \therefore D_G = \frac{2.850 \times 10^6}{D_{TU}} U$$

Diameter to the edge of the rectenna, i.e., at the 1 mW/cm^2 free space power density level, is related to U_R as follows:

$$U_R = 3.0 = 47332 \sin\theta_R = \frac{D_{GR}/2}{37 \times 10^6} \times 47332$$

$$\therefore \quad D_{GR} = \frac{3.0 \times 37 \times 10^6 \times 2}{47332}$$

$$= 1563.4\ U_R$$

$$= 4.690 \text{ km}$$

Similarly,

$$U_F = 3.53$$

$$\therefore \quad D_{GF} = 5.52 \text{ km}$$

$$A_R = \frac{\pi\ 4.69^2}{4} \times 10^6 = 17.28 \times 10^6 \text{ m}^2$$

$$A_F = \frac{\pi\ 5.52^2}{4} \times 10^6 = 23.93 \times 10^6 \text{ m}^2$$

Areas and number of components on orbit will be as follows:

$$A_T = \frac{\pi\ 2422^2}{4} = 4.607 \times 10^6 \text{ m}^2$$

$$A_{T(1)} = \frac{\pi\ 1495^2}{4} = 1.755 \times 10^6 \text{ m}^2$$

$$A_{T(2)} = A_T - A_{T1} = 2.852 \times 10^6 \text{ m}^2$$

$$N^o \text{ Antenna Elements} = 460.7 \times 10^6$$

$$N^o \text{ Amplifiers} = \left(\frac{1.755}{.01} + \frac{2.852}{11 \times .01}\right) \times 10^6 = 201.4 \times 10^6$$

$$\text{Area of Photovoltaics} = (1.755 \times 0.09 \times 2.852) \times 10^6$$

$$A_{PVA} = 2.01 \times 10^6 \text{ m}^2$$

The power delivered to the ground grid will be as follows:

For this case $\eta_{TA} = 0.86$

$$\eta_{RF\text{-}GT} = 0.698 \times 0.86 = 0.600$$

$$P_{GT} = P_{TT} \times \eta_{RF\text{-}G(T)} = P_{TT} \times 0.600$$

$$= 1.388 \times 0.600 \times 10^9$$

$$= 0.8328 \times 10^9 \text{ W}$$

$$(P_G/A_T + A_{PVA})_T = \frac{0.8328}{.006617} = 125.86 \text{ W/m}^2$$

$$(P_G/A_R)_T = \frac{0.8328}{.01728} = 48.19$$

$$(P_G/A_F)_T = \frac{0.8328}{.02393} = 34.81$$

$$(P_G/A_{SSL})_T = \text{(not an issue)}$$

$$(P_G/A_T)_T = \frac{0.8328}{.004607} = 180.77$$

$$(P_G/A_{PVA})_T = \frac{0.8328}{.00201} = 414.33$$

$$(P_G/N^o \text{ Amplifiers})_T = \frac{0.8328}{.2014} = 4.135$$

$$P_G/N^o \text{ Elements})_T = \frac{0.8328}{.4607} = 1.808$$

SST-MSS-SA (SEMI-AUTONOMOUS)

This is the case where there is a single step taper with both regions of solid state operating at critical temperatures and transporting DC power from the outboard to the inboard region. The inboard region is assumed to get all its DC power from (a) the outboard and (b) a further outboard dedicated region.

$$\text{Inboard Area/Outboard Area} = A_{T1}/A_{T2} = \frac{k_1^2}{k_2^2 - k_1^2} = \frac{0.81987^2}{1.3285^2 - 0.81987^2}$$

$$= 0.615147$$

Spacetenna System Parameters:

$C = 0.3$

$C^2 = 0.09$

Sidelobe Suppression = 28.6 dB

$P_{DI} = 23\ mW/cm^2$

$\therefore\ P_{DSL} \leq 0.0317\ mW/cm^2$

$k_2 = 1.3285$

$U_R = 3.0$

$U_F = 3.53$

$k_1 = 0.81987$

$D_2/D_1 = 1.6204$

$D_{TU} = 9344.9/(P_{RF1})^{.25}$

Region (1) Parameters:

$P_o = P_{RF1} = 2386\ W/m^2$

P_{DC1}(Demand) $= 3239\ W/m^2$

$T_J = 130°C$

$T_E = 54.6°C$

$\eta_{AMP} = 0.8$

$\alpha = 0.05$

$\varepsilon = 0.80$ } $F = 1.71$

$P_{SE} = 1200\ W/m^2$

$P_{SM} = 0$

} RF and thermal parameters consistent with a maximum value of P_{RFI} for a region dedicated to RF.

Spacetenna and Ground Parameters:

$P_{DI} = 230\ W/m^2$

$\lambda_o = 0.121$ meters

$R_o = 37 \times 10^6$ m

$\eta_{AR} = 1$

$\eta_{AT} = 0.98$

$$D_{TU} = \frac{9344.9}{(2386)^{.25}} = 1337 \text{ m}$$

$D_2 = 1.3285 \times 1337 = 1776$ m

$D_1 = 0.81987 \times 1337 = 1097$ m

$P_{TU} = 68.586 \times 10^6 \sqrt{2386}$

$= 3.350 \times 10^9$ W

$P_{TT} = 2386 \times 52.85 \times 10^6$ W

$= 2.582 \times 10^9$ W

$$U = \frac{D_{TU}\, \pi \sin\theta}{\lambda} = \frac{1337\, \pi}{.121} \sin\theta$$

$$= 34713 \sin\theta = \frac{D_G/2}{37 \times 10^6} \times 34713$$

$$D_G = \frac{74 \times 10^6}{34713} U = 2132\ U$$

$D_{GR} = 2132 \times 3 = 6396$ m

$D_{GF} = 2132 \times 3.53 = 7526$ m

$A_R = 32.13 \times 10^6\ m^2$

$A_F = 44.48 \times 10^6\ m^2$

Areas and Numbers of Components On Orbit:

$$A_T = \frac{\pi\ 1776^2}{4} = 2.4773 \times 10^6\ m^2$$

$$A_{T1} = \frac{\pi\ 1097^2}{4} = .9452 \times 10^6\ m^2$$

$$A_{T2} = 1.5321 \times 10^6\ m^2$$

N^o Antenna Elements = 247.73×10^6

N^o Amplifiers = 247.73×10^6

Area of Photovoltaics on the Spacetenna $\Delta_2\ A_{PVA} = 1.5321 \times 10^6\ m^2$

Region (2) Parameters:

$$P_{RF2} = C^2\ P_{RF1}$$

$$= .09 \times 2386$$

$$= 214.74\ W/m^2$$

P_{DC2}(Demand) = 291.2 W/m^2

P_{DC2}(Supply) = 1025.5 W/m^2

T_S = 250°C

T_J = 130°C

T_E = 123.2°C

η_{AMP} = 0.8

F = 0.95

ε = 0.8

α = 0.05

P_{SE} = 822 W/m^2

P_{SM} = 859.3

Additional Photovoltaic Array Required:

The additional photovoltaic array required to supply the power for the central region that is not available from the outboard region of the spacetenna is as follows:

Power required for the inboard region is:

$$P_{DC1}(\text{Demand})\ A_{T1} = 3239 \times .9452 \times 10^6 = 3.062\ \text{GW}$$

For the outboard region it is:

$$P_{DC2}(\text{Demand})\ A_{T2} = 291.2 \times 1.5321 \times 10^6 = 0.4461\ \text{GW}$$

Power available from the inboard region is zero and power supply in the outboard region is

$$P_{DC2}(\text{Supply})\ A_{T2} = 1025.5 \times 1.5321 \times 10^6 = 1.5712\ \text{GW}$$

Total power to be transported:

$$= P_{DC1}(\text{Demand})\ A_{T1} + P_{DC2}(\text{Demand})\ A_{T2} - P_{DC2}(\text{Supply})\ A_{T2}$$

$$= (3.062 + 0.4461 - 1.5712)\ \text{GW}$$

$$= 1.9369\ \text{GW, i.e., } 55.3\%$$

Taking an additional efficiency penalty for this power of 0.9368 x .963 = 90.2% increases the value to 1.9369/.902 = 2.137 GW.

The outboard region provides 1.5712 - .4461 = 1.1251 GW.

The rest is to be provided by a dedicated photovoltaic array, i.e., 2.147 - 1.1251 = 1.0219 GW.

For a photovoltaic array (PVA) operating at $P_{DC} = 1326\ W/m^2$,

$$\Delta_3\ A_{PVA} = \frac{1.0219 \times 10^9}{1326} = 0.77066 \times 10^6\ m^2$$

For an inside diameter of $D_2 = 1776$ m, the outside diameter would be:

$$\frac{\pi}{4}\left(D_o^2 - 1776^2\right) = 0.77066 \times 10^6$$

$$\therefore\ D_o = \sqrt{.981239 + 3.154176} = 2.034\ \text{km}$$

Total $A_{PVA} = (1.5321 + .77066) \times 10^6 = 2.302 \times 10^6\ m^2$

The power delivered to the ground grid will be as follows:

$\eta_{RF\text{-}G(T)} = 0.6980\ \eta_{TA} = 0.6980 \times 0.86 = 0.600$

$P_{GT} = P_{TT}\ \eta_{RF\text{-}G(T)} = 2.582 \times 10^9 \times 0.6$

$= 1.55 \times 10^9\ W$

$(P_G/A_T + A_{PVA})_T = \dfrac{1.549}{.0024773 + .002302} = 324\ W/m^2$

$P_G/A_R = \dfrac{1.549}{.03213} = 48.2\ W/m^2$

$P_G/A_F = 1.549/.04448 = 34.8\ W/m^2$

P_G/A_{SSL} = not an issue

$P_G/A_T = 1.549/.0023773 = 625.3\ W/m^2$

$P_G/A_{PVA} = 1.549/.002302 = 672.9\ W/m^2$

P_G/N^o Amplifiers = 1.549/.24773 = 6.25 W/Amplifier

P_G/N^o Elements = 1.549/.24773 = 6.25 W/Element

SST-MSS-NAH (NON AUTONOMOUS AND HYBRID)

This is the case where there is a single step taper with both regions operating at critical temperatures. The inboard region is assumed to be implemented with tubes and the outboard region is assumed to be implemented with solid state. DC power is transported to both regions from a dedicated photovoltaic array.

The amplifier efficiency for the tubes is assumed to be $\eta_{AMP(1)} = 0.85$ and $P_{RF(1)} = 24{,}000\ W/m^2$ is assumed in this case to begin to investigate the implications of such a concept.

In Region (2) the parameters are as follows:

$P_{RF2} = 24{,}000 \times C^2 = 24{,}000 \times .09$
$= 2160\ W/m^2$

$P_{DC2}(\text{Demand}) = 2929\ W/m^2$

$T_J = 130°C$

$T_E = 61.69°C$

$F = 1.434$ (i.e., it is less than the 1.71 assumed in previous cases in anticipation of more blockage from the DC distribution system)

$\alpha = 0.05$

$\varepsilon = 0.80$

$P_{SE} = 1200\ W/m^2$

$P_{SM} = 0$

$P_{DC2}(\text{Demand}) = 2929\ W/m^2$

Spacetenna System Parameters:

$C = 0.3$

$C^2 = 0.09$

Sidelobe Suppression = 28.6 dB

$P_{DI} = 23\ mW/cm^2$

$\therefore P_{DSL} \leq 0.0317\ mW/cm^2$

$k_2 = 1.3285$

$U_R = 3.0$

$U_F = 3.53$

$k_1 = 0.81987$

$D_2/D_1 = 1.6204$

$D_{TU} = 9344.9/(P_{RF1})^{.25}$

Region (1) Parameters:

$P_o = P_{RF1} = 24{,}000\ W/m^2$

Temperatures and other thermal parameters are those associated with tubes and slotted waveguide subarrays.

$\eta_{AMP} = 0.85$

All other elements of the chain including filtering are assumed to be the same as for solid state.

$P_{DC1}(\text{Demand}) = P_{RF1}/.99 \times .99 \times \eta_{AMP} \times .96 \times .98$

$= P_{RF1}/.783 = 24{,}000/.783 = 30{,}650\ W/m^2$

Spacetenna and Ground Parameters:

$P_{DI} = 230\ W/m^2$

$\lambda_o = 0.121\ m$

$R_o = 37 \times 10^6\ m$

$\eta_{AR} = 1.0$

$\eta_{AT} = 0.98$

$D_{TU} = \dfrac{9344.9}{(24000)^{.25}} = 750.796\ m$

$D_2 = 1.3285 \times D_{TU} = 997.43\ m$

$D_1 = 0.81987 \times D_{TU} = 615.55\ m$

$$P_{TU} = 68.586 \times 10^6 \quad 24{,}000 = 10.625 \times 10^9 \text{ W}$$

$$P_{TT} = \sqrt{24000} \times 52.853 \times 10^6 \text{ W}$$

$$= 8.187 \times 10^9 \text{ W}$$

$$U = \frac{D_{TU}\, \pi \sin \theta}{\lambda} = \frac{750.796\, \pi}{.121} \sin \theta$$

$$= 19493 \sin \theta = \frac{D_G/2}{37 \times 10^6} \times 19493$$

$$D_{GR} = 3796 \times U_R = 3796 \times 3 = 11389 \text{ m}$$

$$D_{GF} = 3796 \times U_F = 3796 \times 3.53 = 13400 \text{ m}$$

$$A_R = 101.873 \times 10^6 \text{ m}^2$$

$$A_F = 141.026 \times 10^6 \text{ m}^2$$

Areas and Numbers of Components On Orbit:

$$A_{TU} = 0.442725 \times 10^6 \text{ m}^2$$

$$A_T = 0.781366 \times 10^6 \text{ m}^2$$

$$A_{T1} = 0.297589 \times 10^6 \text{ m}^2$$

$$A_{T2} = 0.483777 \times 10^6 \text{ m}^2$$

N^o Antenna Elements in Region (2) = 48.38×10^6

N^o Slots in Region (1) ≈ 29.76×10^6

N^o (Elements + Slots) ≈ 78.14×10^6

N^o Amplifiers in Region (2) = 48.38×10^6

N^o 40 kW Power Modules in Region (1) = $.179 \times 10^6$

Photovoltaic Array Required:

All power is supplied by a dedicated photovoltaic array.

Power required for the inboard region is:

$$P_{DC1}(\text{Demand})\ A_{T1} = 30650 \times .297589 \times 10^6 = 9.121 \times 10^9\ \text{W}$$

For the outboard region it is:

$$P_{DC2}(\text{Demand})\ A_{T2} = 2929 \times .483777 \times 10^6 = 1.417 \times 10^9\ \text{W}$$

Total power to be supplied and transported:

$$\Sigma\ P_{DC}A\ (\text{Demand}) = 10.538 \times 10^9\ \text{W}$$

Taking the additional efficiency penalty for power transport of .902 increases the DC power requirement to $10.538/.902 = 11.68 \times 10^9$ W.

For a photovoltaic array (PVA) operating at $P_{DC} = 1326\ W/m^2$,

$$A_{PVA} = \frac{11.68 \times 10^9}{1326} = 8.811 \times 10^6\ m^2$$

For an inside diameter of $D_2 = 997.43$ m the outside diameter would be as follows:

$$\frac{\pi}{4}(D_o^2 - 997.43^2) = 8.811 \times 10^6$$

$$\therefore\ D_o = \sqrt{11.218 + .9949} = 3.495\ \text{km}$$

The power delivered to the ground grid would be as follows:

$$\eta_{RF\text{-}G(T)} = 0.6980\ \eta_{TA} = .698 \times .86 = 0.600$$

$$P_{GT} = P_{TT}\ \eta_{RF\text{-}G(T)} = 8.187 \times 10^9 \times .6$$

$$= 4.91 \times 10^9\ \text{W}$$

$$(P_{GT}/A_T + A_{PVA}) = \frac{4.91}{.000781 + .008811} = 511.88\ W/m^2$$

$$P_G/A_R = 4.91/.101873 = 48.20\ W/m^2$$

P_G/A_F = 4.91/.141026 = 34.82 W/m^2

P_G/A_{SSL} = not an issue

P_G/A_T = 4.91/.000781366 = 6284 W/m^2

P_G/A_{PVA} = 4.91/.00881 = 557.3 W/m^2

P_G/N^O Amplifiers (2) = 4.91/.04838 = 101.48 W/Amplifier

P_G/N^O 40 kW Power Modules (1) = 4.91/.000179 = 27430 W/40 kW Module

P_G/N^O Elements (2) = 4.91/.04838 = 101.49 W/Element

P_G/N^O Slots (1) = 4.91/.02976 = 164.99 W/Slot

P_G/N^O (Elements + Slots) = 4.91/.07814 = 64.84 W/Element (effective)

CASE (SST-FSS) SINGLE STEP TAPER FIRST SIDELOBE SUPPRESSION

Voltage Step C = 0.3

Power Step C^2 = 0.09

Sidelobe Suppression is -23.6 dB with zero margin.

P_{DI} = 23 mW/cm^2

$\therefore$ P_D (First Sidelobe) = 0.1 mW/cm^2

k_2 = 1.283 from Figure 2.3.6.2-1

U_R = 3.0

U_F = 3.56

$$k_1 = \left[\frac{1 - 1.283^2 \times .3}{1 - 0.3} \right]^{1/2} = 0.85$$

$D_1 = 0.85\ D_U$

$D_2 = 1.283\ D_U$

$D_{TU} = 9344.9/(P_{RF1})^{.25}$

$D_1 = 7943.165/(P_{RF1})^{.25}$

$D_2 = 11989.5/(P_{RF1})^{.25}$

$P_{TU} = 68.586 \times 10^6 \times \sqrt{P_{RF1}}$

$$P_{TT} = P_{RF1} \frac{\pi\ 7943.165^2}{4\sqrt{P_{RF1}}} + P_{RF2} \frac{\pi}{4} \left(\frac{11989.5^2}{\sqrt{P_{RF1}}} - \frac{7943.165^2}{\sqrt{P_{RF1}}} \right)$$

$$P_{TT}/P_{TU} = \frac{49.5538 \times 10^6 + \frac{P_{RF2}}{P_{RF1}}\ 63.345691 \times 10^6}{68.586 \times 10^6} = .722506 + C^2\ .923595$$

$$= .805629$$

$P_{TT} = \sqrt{P_{RF1}} \times 55.2549 \times 10^6$ W

CASE SST-FSS-A

This case is the same as SST-MSS-A in terms of microwave thermal and DC demand/m^2 within the Regions (1) and (2).

The diameters of the apertures as well as the total power and efficiencies (η_{TA} = 0.894) are different.

$P_{RF1} = 690\ W/m^2$

$P_{RF2} = 62.1\ W/m^2$

$D_{TU} = 1823\ m$

$D_2 = 1.283 \times 1823$

$D_1 = 0.85 \times 1823 = 1549.55\ m$

$P_{TU} = 68.586 \times 10^6 \times \sqrt{690} = 1.802 \times 10^9\ W$

$P_{TT} = .805629\ P_{TU} = 1.4514 \times 10^9\ W$

$D_G = \frac{2.850 \times 10^6}{D_{TU}} U = \frac{2.850}{1823} \times 10^6 \times 3$

$D_{GR} = 4.690\ km$

$D_{GF} = 5.57\ km$

$A_R = 17.28 \times 10^6\ m$

$A_F = 24.34 \times 10^6\ m$

$A_T = \frac{\pi\ 2338.91^2}{4} = 4.29652 \times 10^6\ m^2$

$A_{T(1)} = \frac{\pi \times 1549.55^2}{4} = 1.88582 \times 10^6\ m^2$

$A_{T(2)} = A_T - A_{T1} = 2.4107 \times 10^6 \text{ m}^2$

N^O Antenna Elements $= 429.65 \times 10^6$

N^O Amplifiers $= \left(\frac{1.88582}{0.1} + \frac{2.4107}{11 \times .01} \right) \times 10^6 = 210.497 \times 10^6$

Area of Photovoltaics $= (1.88582 + 0.09 \times 2.4107) \times 10^6$

$A_{PVA} = 2.10278 \times 10^6 \text{ m}^2$

The power delivered to the ground grid will be as follows:

For this case $\eta_{TA} = .894$

$\eta_{RF\text{-}G(T)} = 0.08 \times .894 = 0.624$

$P_{GT} = P_{TT} \times \eta_{RF\text{-}G(T)} = P_{TT} \times .624$

$= 1.4514 \times .624 \times 10^9 = .90567 \times 10^9 \text{ W}$

$P_G/A_T + A_{PVA} = .90567/(.004297 + .002103) = 141.5 \text{ W/m}^2$

$P_G/A_R = .90567/.01728 = 52.41 \text{ W/m}^2$

$P_G/A_F = .90567/.02434 = 37.21 \text{ W/m}^2$

P_G/A_{SSL} = (not an issue)

$P_G/A_T = .90567/.0042965 = 210.7925 \text{ W/m}^2$

$P_G/A_{PVA} = .90567/.00210278 = 430.72 \text{ W/m}^2$

P_G/N^O Amplifiers $= .90567/.210497 = 4.3025$ W/Amplifier

P_G/N^O Elements $= .90567/.42965 = 2.1079$ W/Element

CASE SST-FSS-SA

Parameters are the same as SST-MSS-SA except as follows.

$k_1 = 0.85$

$k_2 = 1.283$

$D_1 = .85\ D_U$

$D_2 = 1.283\ D_U$

$P_{RF1} = 2386\ W/m^2$

$n_{TA} \approx 89.4\%$

$P_{RF2} = .3^2 \times 2386 = 214.74\ W/m^2$

Sidelobe Suppression = 23.6 dB

$\therefore P_{DSL} = .1\ mW/cm^2$

$U_R = 3$

$U_F = 3.56$

$D_{TU} \approx 9344.9/(2386)^{.25} = 1337\ m$

$D_1 = .85 \times 1337 = 1136.45\ m$

$D_2 = 1.283 \times 1337 = 1715.4\ m$

$P_{TU} \approx 3.35 \times 10^9\ W$

$P_{TT} \approx \sqrt{2386} \times 55.2549 \times 10^6\ W$

$$D_G = \frac{2.85 \times 10^6}{D_{TU}} U = 2132\ U$$

$$D_{GR} = 6396\ m$$

$$D_{GF} = 7590\ m$$

$$A_R = 32.13 \times 10^6\ m^2$$

$$A_F = 46.803 \times 10^6\ m^2$$

$$A_T = \frac{\pi\ 1715.4^2}{4} = 2.31111 \times 10^6\ m^2$$

$$A_{T(1)} = \frac{\pi\ 1136.45^2}{4} = 1.01436 \times 10^6\ m^2$$

$$A_{T(2)} = 1.29675 \times 10^6\ m^2$$

$$\Delta_2\ A_{PVA} = 1.29675 \times 10^6\ m^2$$

Photovoltaic Array Required:

Power required for the inboard region is:

$$P_{DC1}(\text{Demand})\ A_{T1} = 3239 \times 1.01436 \times 10^6 = 3.2855 \times 10^9\ W$$

For the outboard region it is:

$$P_{DC2}(\text{Demand})\ A_{T2} = 291.2 \times 1.29675 \times 10^6 = .37761 \times 10^9\ W$$

Power available from the inboard region is zero and power supply in the outboard region is:

$$P_{DC2}(\text{Supply})\ A_{T2} = 1025.5 \times 1.29675 \times 10^6 = 1.32982 \times 10^9\ W$$

Total power to be transported

$$= P_{DC1}(\text{Demand})\ A_{T1} + P_{DC2}(\text{Demand})\ A_{T2} - P_{DC2}(\text{Supply})\ A_{T2}$$

$$= (3.2855 + .37761 - 1.32982)\ GW = 2.33329\ GW, \text{ i.e., } 63.7\%$$

Taking an additional efficiency penalty for this power of .902 increases the value to $2.33329/.902 = 2.5868 \times 10^9$ W.

The outboard region provides $1.32982 - .37761 = .9522 \times 10^9$ W.

The rest is to be provided by a dedicated photovoltaic array, i.e., $2.5868 - .9522 = 1.6346 \times 10^9$ W.

At $P_{DC} = 1326\ W/m^2$

$$\Delta_3 A_{PVA} = \frac{1.6346 \times 10^9}{1326} = 1.23273 \times 10^6\ m^2$$

For an inside diameter of 1715.4 m, the outside diameter would be:

$$\frac{\pi}{4}(D_o^2 - 1715.4^2) = 1.23273 \times 10^6$$

$$D_o^2 = 1.56956 + 2.942597$$

$$D_o = 2.1241838$$

$$\text{Total } A_{PVA} = (1.29675 + 1.23273) \times 10^6 = 2.52948 \times 10^6\ m^2$$

Power delivered to the ground grid would be as follows:

$$\eta_{RF\text{-}G(T)} = 0.6980\ \eta_{TA} = 0.698 \times .894 = .624$$

$$P_{TT} = P_{RF1} \times 55.2549 \times 10^6\ W$$

$$= 2386 \times 55.2549 \times 10^6\ W$$

$$= 2.699 \times 10^9\ W$$

$$P_{GT} = P_{TT}\ \eta_{RF\text{-}G(T)} = 2.6987 \times .624 \times 10^9 = 1.684 \times 10^9\ W$$

$$P_G/A_T + A_{PVA} = \frac{1.684}{.00231111 + .00252948} = 347.90\ W/m^2$$

$$P_G/A_R = 1.684/.03213 = 52.41\ W/m^2$$

P_G/A_F = 1.684/.046803 = 35.98 W/m^2

P_G/A_{SSL} = (not an issue)

P_G/A_T = 1.684/.00231111 = 728.66 W/m^2

P_G/A_{PVA} = 1.684/.00252948 = 665.77 W/m^2

P_G/N^o Amplifiers = 1.684/.231111 = 7.287 W/Amplifier

P_G/N^o Elements = 1.684/.231111 = 7.287 W/Element

CASE SST-FSS-NAH

Parameters are the same as SST-MSS-NAH except as follows:

k_1 = 0.85

k_2 = 1.283

D_1 = .85 D_J

P_{RF1} = 24000 W/m^2

η_{TA} = 89.4%

P_{RF2} = $.3^2$ x 24000 = 2160 W/m^2

Sidelobe Suppression is 23.6 dB.

$\therefore P_{DSL}$ = 0.1 mW/cm^2

U_R = 3.0

U_1 = 3.56

η_{AMP} = 0.85

P_{DC2}(Demand) = 2929 W/m^2

P_{DC1}(Demand) = 30650 W/m^2

$D_{TU} = 750.796$ m

$D_2 = 1.283 \times 750.796 = 963.27$

$D_1 = .85 \times 750.796 = 638.177$

$P_{TU} = 68.586 \times 10^6 \times \sqrt{24000} = 10.625 \times 10^9$

$P_{TT} = .805629\ P_{TU} = 8.560 \times 10^9$

$D_G = \frac{2.85 \times 10^6}{D_{TU}}\ U$

$D_{GR} = \frac{2.85 \times 10^6}{750.796} \times 3 = 11{,}388$ m

$D_{GF} = 3795.97 \times 3.56 = 13{,}514$ m

$A_R = 101.855 \times 10^6\ m^2$

$A_F = 143.435 \times 10^6\ m^2$

Areas and Numbers of Components on Orbit:

$A_{TU} = \frac{\pi \times 750.776^2}{4} = .442725 \times 10^6\ m^2$

$A_T = \frac{\pi \times 963.27^2}{4} = .728762 \times 10^6\ m^2$

$A_{T1} = \frac{\pi}{4}\ 638.177^2 = .319869 \times 10^6\ m^2$

$A_{T2} = .408893 \times 10^6\ m^2$

N^o Antenna Elements in Region (2) $= 40.889 \times 10^6$

N^o Slots in Region (1) $\simeq 31.987 \times 10^6$

N^o (Elements + Slots) $\simeq 72.876 \times 10^6$

N^o Amplifiers in Region (2) = 40.8893×10^6

N^o 40 kW Power Modules in Region (1) = $\frac{24000}{40000} \times .319869 \times 10^6 = .192 \times 10^6$

Photovoltaic Array Required:

All power is supplied by a dedicated photovoltaic array.

Power required for the inboard region is:

$P_{DC1}(\text{Demand})\ A_{T1} = 30650 \times .319869 \times 10^6 = 9.804 \times 10^9$ W

For the outboard region it is:

$P_{DC2}(\text{Demand})\ A_{T2} = 2929 \times .408893 \times 10^6 = 1.198 \times 10^9$ W

Total power to be supplied and transported:

$\Sigma\ P_{DC}(\text{Demand}) = 11.002 \times 10^9$ W

Taking the additional efficiency penalty for power transport of 0.902 increases the DC power requirement to $11.002/.902 = 12.197 \times 10^9$ W.

For a photovoltaic array (PVA) operating at $P_{DC} = 1326$ W/m^W:

$$A_{PVA} = \frac{12.197}{1326} \times 10^9 = 9.199 \times 10^6 \text{ m}^2$$

For an inside diameter of $D_2 = 963.27$ m, the outside diameter would be as follows:

$$\frac{\pi}{4}(D_o^2 - 963.27^2) = 9.199 \times 10^6$$

$$\therefore\ D_o = \sqrt{11.712 + .9279} = 3.555 \text{ km}$$

The power delivered to the ground grid would be as follows:

$$\eta_{RF\text{-}G(T)} = 0.6980\ \eta_{TA} = 0.698 \times .894 = 0.624$$

$$P_{GT} = P_{TT}\,\eta_{RF\text{-}G(T)} = 8.560 \times .624 \times 10^9 = 5.341 \times 10^9 \text{ W}$$

$$\underline{P_{GT} = 5.341 \times 10^9 \text{ W}}$$

$$P_{GT}/A_T + A_{PVA} = \frac{5.341}{.0007288 + .009199} = 537.98 \text{ W/m}^2$$

$$P_G/A_R = 5.341/.101855 = 52.44 \text{ W/m}^2$$

$$P_G/A_F = 5.341/.143435 = 37.24 \text{ W/m}^2$$

$$P_G/A_{SSL} = \text{(not an issue)}$$

$$P_G/A_T = 5.341/.000728762 = 7329 \text{ W/m}^2$$

$$P_G/A_{PVA} = 5.341/.009199 = 580 \text{ W/m}^2$$

P_G/N^o Amplifiers (2) = 5.341/.040889 = 130.6 W/Amplifier

P_G/N^o 40 kW Power Modules (1) = 5.341/.000192 = 27,818 W/Module

P_G/N^o Elements = 5.341/.040889 = 130.6 W/Element

P_G/N^o Slots (1) = 5.341/.031987 = 166.97 W/Slot

P_G/N^o (Elements + Slots) = 5.341/.072876 = 73.29 W/(E + S)

2.3.6.3 Example Calculations for Multiple Step Taper Cases

From Figure B-4 of Appendix B, it is evident that a Gaussian illumination taper at the spacetenna has the potential to reduce the free space power density at the first sidelobe effectively. For a power density P_{di} = 23 mW/cm^2 at the peak of the main lobe, a power density of < 1 mW/cm^2 is achieved for edge tapers in the -9 to -10 dB range.

From Figure B-7 of Appendix B, it is evident that the Gaussian illumination also results in high beam efficiency, i.e., 95% as compared to 82.5% for uniform illumination and 68.6% for a single step taper that is optimized for low sidelobes.

A -10 dB edge taper has been selected as an illustrative example of the potential and issues associated with multiple step taper cases.

The development of the relationships among the parameters is given in Appendix B.

The diameter of the spacetenna is given by

$$D_T = 2\left(\frac{P_{di}}{P_o\, \eta_{AR}\, \eta_{AT}}\right)^{.25} \sqrt{\lambda_o\, R_o} \sqrt{\frac{.115B}{\pi(1 - 10^{-B/20})}}$$

where

P_{di} = 230 W/m^2

P_o = 2,386 W/m^2, which is estimated to be the practical potential upper limit for the RF power density from a solid state active element. This is referred to as P_{RF} watts per element or P_{RF}/A_C = watts/m^2 at the active element cell level.

Both P_{di} and P_o should be the subject of in-depth technology development and significant changes, plus or minus, in both of them should be anticipated.

η_{AR} = 1 (a value of η_{ANT} = 0.98 is incorporated in the estimate of P_{RF}).

η_{AT} = 0.98 (The power density, P_{di}, therefore is really at the earth's surface rather than in the ionosphere.)

λ_o = 0.121 m

R_o = 37 x 10^6 m

B = 10 (dB).

$$D_T = 2\left(\frac{230}{2386 \times 1 \times .98}\right)^{.25} \sqrt{.121 \times 37 \times 10^6} \sqrt{\frac{.115 \times 10}{\pi(1 - 10^{-10/20}}}$$

$$= 1738 \text{ meters}$$

$$D_G = \left(\frac{P_o \eta_{AR} \eta_{AT}}{P_{di}}\right)^{.25} \sqrt{\frac{\lambda_o R_o \pi (1 - 10^{-B/20})}{0.115B}} \; U$$

$$= \left(\frac{2386 \times 1 \times .98}{230}\right)^{.25} \sqrt{\frac{.121 \times 37 \times 10^6 \times \pi (1 - 10^{-10/20})}{0.115 \times 10}}$$

$$= 5163.68 \; U$$

From Figure B-4 of Appendix B,

U_F = 1.33 for the 0.1 mW/cm^2 level on the main lobe.

U_R = 1.13 for the 1.0 mW/cm^2 level on the main lobe at the edge of the rectenna.

U_{FSL} = 1.75 in the region of the first sidelobe which would be < 0.1 mW/cm^2 in free space.

The diameters are as follows:

$D_R = 1.13 \times 5163.68 = 5.835$ km

$D_F = 1.33 \times 5163.68 = 6.868$ km

$D_{FSL} = 1.75 \times 5163.68 = 9.036$ km

The relevant areas at the ground (normal to boresite) are:

$A_R = 26.74 \times 10^6 \; m^2$

$A_F = 37.04 \times 10^6 \; m^2$

$A_{FSL} = 64.13 \times 10^6 \; m^2$

The transmitted RF power is

$$P_T = \frac{P_o A_t (1 - 10^{-B/10})}{0.23 B}$$

where

$$A_t = \frac{\pi D_T^2}{4} = \frac{\pi 1738^2}{4} = 2.3724 \times 10^6 \text{ m}^2$$

$$P_T = \frac{2386 \times 2.3724 \times 10^6}{.23 \times 10} (1 - 10^{-10/10}) = 2.2150 \text{ GW}$$

The power to the ground grid is $P_G = P_T \eta_{AT} \eta_{EC} \eta_R \eta_G = P_T \eta_{RF-G}$, where η_{EC} for the -10 dB step Gaussian case is 0.95, as indicated on Figure B-7 of Appendix B, and other efficiencies are consistent with those of the efficiency chain in Section 3. It should be noted that the efficiency loss for the transport of DC power included in the DC power estimate is assumed to be the same as that for the NASA reference concept as shown in the efficiency chain exclusive of the slip rings. $\eta_{DC} = 0.9368 \times 0.963 = .902$ only for that portion that is transferred from one region to another and will be included upstream of P_T along with η_{-DC}, η_{+DC}, η_{AMP}, η_{FILT} and η_{ANT}.

$$\eta_{RF-G} = 0.98 \times 0.95 \times 0.89 \times 0.97 = 0.8037$$

$$\therefore \quad P_G = 2.2150 \times 0.8037 = 1.7803 \text{ GW}$$

MULTIPLE STEP REPRESENTATION OF -10 DB GAUSSIAN ILLUMINATION

$$P = P_o e^{-2Kr^2}$$

where

$$K = \frac{0.115\ B}{R_t^2}$$

for B = 10

$$R_t = D_T/2 = 1738/2 = 869 \text{ m}$$

$$\therefore K = \frac{0.115 \times 10}{869^2} = 1.52285 \times 10^{-6}$$

$$P_o = 2386 \text{ W/m}^2$$

$$P = 2386\ e^{-3.04570\ r^2 \times 10^{-6}}$$

From earlier studies reported in Section 6 of NASA CR-134886, a multiple step representation of the Gaussian illumination should be in the range of 5 to 10 steps. The RF subarrays are 3.2 x 3.2 m and a convenient power module would be 4 x 3.2 x 4 x 3.2 = 12.8 x 12.8 m. With one power module centered at the center line of the spacetenna, convenient steps would occur at r = 83.2, 185.6, 313.6, 377.6, 441.6, 492.8, 572.4, 662.0, 751.6 and 869. The last plateau may be tailored for edge effects.

The multiple step data sheet, Table 2.3.6.3-1, summarizes the pertinent parameters at the region, spacetenna and spacetenna + dedicated photovoltaic region levels. The dedicated photovoltaic region parameters are not firm or optimized, however the assumptions are consistent with those utilized in the uniform and single step cases. In this context they are considered relevant for preliminary concept assessment purposes.

Table 2.3.6.3-1 Multiple Step -10 dB Taper Data Sheet

SPACETENNA GEOMETRY			RF & DC PERFORMANCE REQTS.				P_{DC} (MW)				THERMAL PARAMETERS							
R (m)	REGION	AREA ($10^6 m^2$)	P_{RF} (w/m^2)	P_T ($10^6 w$)	P_{DC} DEMAND (w/m^2)	P_{DC} DEMAND ($10^6 w$)	P_{DC} SUPPLY (w/m^2)	LOCAL ($10^6 w$)	LOCAL -DEMAND ($10^6 w$)	FROM OTHER S.T. REGIONS ($10^6 w$)	FROM DEDICATED PVA REGION ($10^6 w$)	DISSIP'N FORM FACTOR	P_{SE} w/m^2	P_{SM} w/m^2	P_M/A_C w/m^2	T_E °C	ΔT_J C°	ΔT_E C°	C_E (Assumed)
0.0																			
	(1)	.021747	2.386.	57.888	3235.	70.35	0.	0.	- 70.35		70.35	.71	1200	0	634.	54.6	25.5		—
83.2																		+4.6	
	(2)	.086472	2242.	193.870	3040.	262.87	0.	0.	- 262.87		262.87	1.53	1200	0	596.	59.1	70.9		—
185.6																		+9.0	
	(3)	.200740	1958.	393.049	2655.	532.96	0.	0.	- 532.96		532.96	1.21	1200	0	520.	68.1	61.9		—
313.6																		+9.5	
	(4)	.138974	1657.	230.280	2246.	312.14	888.2	112.32	- 199.82		199.82	.85	822	19.	440.	77.6	52.4		5.22
377.6																		+7.1	
	(5)	.164710	1432.	235.865	1942.	319.87	843.2	138.88	- 180.99	144.99	36.00	.96	822	170.	381.	84.7	45.3		5.44
441.6																		+6.4	
	(6)	.149369	1229.	183.525	1666.	248.85	874.6	130.64	- 118.21	118.21		.97	822	306.	327.	91.1	38.9		5.65
492.8																		+6.9	
	(7)	.267304	1010.	269.977	1369.	365.94	906.9	242.42	- 123.52	123.52		.97	822	446.	268.	98.1	31.9		5.85
572.4																		+6.7	
	(8)	.186115	807.	150.195	1094.	203.61	937.4	174.46	- 29.15	29.15		.97	822	538.	214.	104.5	25.5		6.02
622.0																		+7.2	
	(9)	.559261	581.	324.931	788.	440.70	972.3	543.77	+ 103.07			.97	822	729.	154.	111.6	18.4		6.28
751.6																		+5.8	
	(10)	.597714	303.	181.107	411.	245.66	1019.0	609.07	+ 363.41			.98	822	931.	80.	120.4	9.6		5.58
869.0										50.61*	119.73*								
	Σ	2.372406	933.54	2214.735	1266 =	3002.95		1951.56	-1051.39	466.48	1221.73							At R ie between regions	
	④ to ⑩	ΔA_{PVA} = 2.063447.			3002.95 / 2.372406														

* Losses in transported power due to $\eta_{DC} = 0.9368 \times 0.963 = 0.902$

$T_J = 130°C$, $\epsilon = 0.8$, $\alpha = 0.05$, $\eta_{AMP} = 0.8$, Microwave & DC (At .01 m^2 Cell level) Efficiency $\eta_{DC-RF} = 0.7377$

GAs Amplifier Junctions, Pyrographite Waste Heat Radiator Thermal Conductors, $\Delta T_J = 0.119\ P_{RF}$ Watts/Junction, One Non Redundant Amplifier Junction (Not in series with other non redundant $T_J = 130°C$ junctions) per Element

For a dedicated Photovoltaic Array (PVA) operating at 1326 w/m^2
Assumed F=1, $P_{SM} = 2260\ w/m^2$, $P_{DC} = 1326\ w/m^2$ + $C_E = 8.56$
$\therefore \Delta A_{PVA}$ (Dedicated) = 1221.73 / 1326. = $0.9214 \times 10^6 m^2$ $\therefore \Sigma A_{PVA} = 2.063447 + 0.921 + = 2.9848 \times 10^6 m^2$
R_I = Inside Radius $\simeq$ 869 m $\therefore R_O$ = Outside Radius = 1024. m

Summarizing the significant ground power/area and N^o relationships:

$$(P_G/A_T + A_{PVA})_{MT} = \frac{1.7803}{.002372} + .0029848 = 332\ W/m^2$$

$$(P_G/A_R)_{MT} = 1.7803/.02674 = 66.6\ W/m^2$$

$$(P_G/A_F)_{MT} = 1.7803/.03704 = 40.1$$

$$(P_G/A_{SSL})_{MT} = \text{(probably not an issue)}\ 1.7803/.06413 = 27.8\ W/m^2$$

$$(P_G/A_T)_{MT} = 1.7803/.0023724 = 750\ W/m^2$$

$$(P_G/A_{PVA})_{MT} = 1.7803/.0029848 = 596\ W/m^2$$

$$(P_G/N^o\ \text{Amplifiers})_{MT} = 1.7803/.2063447 = 8.6\ W/Amp$$

$$(P_G/N^o\ \text{Elements})_{MT} = 1.7803/.2063447 = 8.6\ W/Element$$

2.3.7 Technical Issues Resolution and Status

The approach to establishing the technical issues is:

(a) Review the technology risk rating and ranking presented in Section 11 of the tube oriented Microwave Power Transmission System Studies, Volume IV, NASA Report CR-134886 to establish the risks that are common to the tube and solid state approaches.

(b) Identify the new or different risk areas unique to the solid state approach.

(c) Discuss the new or different risk areas in terms of what constitutes the risk and what steps may be taken to resolve them.

The objective of the discussion of the following items is to attempt to establish a perspective for the solid state approach. It is not intended to be a comparative assessment.

DC-RF CONVERTERS AND FILTERS

The solid state amplifiers in particular and the transmit active elements in general are at the conceptual level of development.

The currently known leading contender for the specific technology for the devices has been established as Gallium Arsenide MESFET with aluminum gate in the flip chip configuration. Whether this will continue to be the leading contender in the projected time period of deployment is not known, however it has taken many years to reach a significant state of maturity for this technology and it is not likely to be supplanted in the near term.

If it is supplanted it will be by a device that has the requisite performance characteristics and is more efficient, with higher temperature, less expensive, more reliable, or some subset of these. In any event, the actual circuits, devices and processes have not yet reached laboratory proof of principal status.

The above considerations in combination with the critical aspects of high reliability for long life at necessarily high temperatures presents a technology development problem of major magnitude. In addition, the radiation hardening technology is intimately involved with the details of the yet-to-be-defined specific fabrication processes.

In order to achieve the requisite goals of performance and low cost, the amplifier devices, circuits and processes as well as the waste heat dissipation techniques must be the subject of SPS related Advanced Technology Development.

Current programs in the above technology area will be supportive, however the specific high power density, long life and exceedingly low cost goals require a dedicated program. Such a program is in the multiple millions of dollars per year, multiple years and multiple contractor category. To answer the question of whether or not it is worth undertaking requires (a) further system level concept definition studies, (b) design integration investigations addressing the thermal control issues in concert with the DC power transfer and RF performance, and (c) a first step toward demonstration of the device efficiency projected to requisite power levels and gain.

MATERIALS

The high conductivity waste heat conductors and associated thermal control coatings have not been demonstrated for this type of application. These areas of technology and the technology for maximization of waste heat dissipation form factor are intimately tied to the problem of achieving low temperature gradients between the ground plane and the most critical junctions. Maintenance of thermal control coating performance has been alluded to as a refurbishment item for maintenance. This is not considered to be a straightforward surface recoating function, rather a carefully developed process that (a) does not degrade electrical and RF performance of the microwave system and (b) does not contaminate equipment such as open electronics. In particular, this may be a most significant factor against the hybrid concept of high power tube amplifiers and lower power solid state amplifiers in the same spacetenna. Long life coating performance should be a major goal.

PHASE CONTROL SUBSYSTEMS

Except for the unique packaging requirement, the phase control functions are projected to be implementable with evolving technology from other programs such as that of the Advanced Onboard Signal Processor. Small sizes and weights have been established as goals and the technology development is progressing favorably. The unique packaging requirement for the solid state microwave power system is to distribute the elements of such equipment over an area of a subarray interleaved between power transmission amplifiers. This must be done without creating undue shielding or blockage of waste heat dissipation paths.

Provisions have been made for wideband pilot receiver elements, however the detail technology of (a) retrodirective ground based systems and (b) onboard control systems have not been addressed in this investigation. The potential near field operations may be such as to change the general phase control concept to control and shape the beam to economic advantage.

IONOSPHERE

The ionospheric modeling uncertainties with respect to phase control have been discussed at length in other reports and most recently by Raytheon in Appendix A. These uncertainties apply to solid state systems as well as tube systems, however the potential of far field control from onboard may be shown to be advantageous for the larger aperture of the low power density solid state concepts.

BIOLOGICAL

The single step power taper concept optimized for maximum sidelobe margin as discussed in Section 2 and in Appendix C offers a potential for lower sidelobes compared to the peak of the beam than the uniform power taper case. There is a penalty for this; however, if significantly higher power density in the ionosphere can be shown to be acceptable from environmental and beam control points of view, there is significant margin in sidelobe levels to take economic advantage of the resulting smaller rectenna. On the other hand, if biological limits are reduced below the 0.1 mW/cm^2 level, such potential margins would be reduced. It would be advantageous to increase the biological allowable limits as well as the ionospheric limits. Understanding both of these areas remains a critical item in the progressive advancement of the SPS concept.

POWER TRANSFER

The autonomous concept inceed makes power transfer a non-issue with the possible exception of the thermal load paths that are inherent in short DC power conductors. This, however, is considered to be resolvable in a relatively standard design integration activity.

The potential specific power advantages of non-autonomous concepts and of semi-autonomous concepts establishes the need for in-depth investigation of DC power transfer with attendant implications of converting from high voltage to low voltage to the minimization of weight and waste heat radiation blockage.

SWITCH GEAR

In the autonomous concepts the switching issues are relatively minimal, however from the equipment safety point of view multiple switches at the subarray level may be required. They may also not be required if the RF control system can be shown to provide adequate protection by control of power at the central amplifier, drive amplifier, or transmit element amplifier levels.

RADIO FREQUENCY

Amplifier efficiency may continue to be a significant function of frequency, however this is assumed to be addressed in the advanced technology development program. Similarly, noise generation and filtering concepts are assumed to be included in the same program. Harmonic generation and the ability to attenuate the harmonics must be a significant part of waveform and spread spectrum investigations as well as active suppression investigations. The generation of harmonics by the rectenna as well as by the spacetenna continues to be an issue to be resolved in appropriate technology development programs or by establishing appropriate frequency allocations.

RELIABILITY

Reliability as discussed in Section 6 and as assessed in Section 8 is considered to be essentially a junction temperature and associated probability of survival problem. Criteria and designs that result in progressively higher temperatures require a more complete data base than is currently available for completely rational determination of limits. While Section 8 addresses the concept of increasing junction temperature to maximize total energy over time periods like 20 to 30 years, it is based on a minimal data base and a major projection from that data base. Nevertheless it will be necessary to explore such concepts to their limit in order to establish technically viable and economically attractive approaches for comparative assessments.

OTHER ITEMS FROM NASA CR-134886

The other items from Section 11 of the subject report are not considered to be significantly different for the solid state concepts, however such items as structure, manufacturing modules, remote manipulators, support modules and orbital assembly operations have not been investigated in any depth. It should be noted, however, that the several elements of the system that were of concern for the open

tube approach due to their generation of potential contaminants do not appear to be so critical to the solid state concept in part due to the low voltages involved.

Appendix D presents in vugraph format the following issues and considerations that have more clearly characterized the solid state approach:

- Low Voltage Distribution
- Harmonic and Noise Suppression
- Subarray Size
- Monolithic Technology
- Lifetime
- Mutual Coupling
- Input to Output Isolation
- Charged Particle Radiation Effects
- Topological Considerations
- Sidelobe Suppression

The resolution/status summarized in Appendix D for each of these items is primarily for the autonomous case, i.e., high voltage distribution only becomes an issue or consideration in semi-autonomous or segregated concepts where DC power is to be transported over large distances. The overall assessment at this time indicates that such DC power transport cases should be investigated in depth.

2.3.8 Recommendations for Further Investigations

It is recommended that solid state concepts continue to be investigated at the following levels.

A. Further Concept Definition Studies -- These should include not only the classes of approaches familiar to the community involved with SPS but approaches used in other programs such as space-fed active and/or passive lens arrays.

B. Limited but specific technology investigations into the following to support concepts definition:
   - Active element concepts and performance;
   - Phase and other central control electronics packaging for distribution to achieve minimal interference with microwave, photovoltaic and thermal control functions;
   - Thermal isolation techniques to maintain large temperature gradients between (a) regions of stepped power density for semi-autonomous concepts and (b) layers of an autonomous sandwich subarray;
   - Efficient and effective DC power transport technology that permits the potential of single step and multiple step taper semi-autonomous concepts as well as segregated uniform power distribution concepts to be achieved;
   - Others that may be identified in the course of concepts definition to evolve a most effective approach.

C. A specific investigation of the single step taper concepts in the hybrid configuration using tubes in the central high power density region and solid state in the outboard low power density region.

D. A specific investigation into total system concepts that provide near optimum illumination of the spacetenna/photovoltaics to achieve maximum utilization of deployed areas.

It is recommended that the above investigations be performed in an environment that encourages individuals and teams to participate in depth. Such individuals and teams must have the requisite interest, talent and experience to conceive imaginative approaches and to establish viable concepts. The goal should be to

ferret out the approach that, with a fundable plan, can realize the near-full potential of the SPS concept. The fundable plan is not the least of the outputs. It must be progressive and begin with adequate funding to support rational definition of subsequent milestones. It is to be expected that at any milestone the assessment may be favorable and support funding for subsequent efforts or may be unfavorable and modify or cancel the effort.

SECTION 3
PRELIMINARY PARAMETRIC STUDIES

Preliminary parametric studies began with establishing ranges of interest for microwave power system parameters. Table 3-1 summarizes the primary solid state MPTS parameters and constraints. In performing the antenna analyses the fixed parameters and assumptions of Table 3-2 were employed.

The key formulas for the spacetenna diameter and for the rectenna diameter are given in Table 3-3.

The spacetenna diameter as it relates to peak power density and edge taper is depicted in Figure 3-1. The cross-plot shown in Figure 3-2 illustrates how D_T must decrease as P_O increases to maintain the P_{DI} at 23 mW/cm^2 and the first sidelobe at 0.1 mW/cm^2.

For the uniform case the relationship of spacetenna diameter D_T to power density is depicted in Figure 3-3.

The ratio of synchronous orbit range to far field range is shown in Figure 3.4. The beam geometry of Figure 3-5 then illustrates the nature of the field in the vicinity of the earth for the tapered illumination case as being in the transition region. Similarly for the uniform case, Figure 3-6 indicates that the earth is in the far field for the uniform illumination.

The pattern level and beam efficiency for the tapered illumination is illustrated in Figure 3-7. The rectenna and site radii are both within the first sidelobe.

The pattern level and beam efficiencies in the uniform illumination case are shown in Figure 3-8. The rectenna is about 10% larger in radius than for the tapered illumination and the fence line moves out beyond the peak of the first sidelobe. The second sidelobe free space pattern level is maintained within the 0.1 mW/cm^2 limit.

The advantage of uniform over tapered illumination lies in the smaller diameter on orbit, i.e., only 78% in diameter and all the advantages that go with uniformity in the satellite equipment.

Table 3-1

Solid State MPTS Parameters and Constraints

FREQUENCY (TRANSMIT)	= 2.450 GHz
FREQUENCIES (PILOT)	= 2.301 GHz 2.550 2.799
SYNCHRONOUS ORBIT RANGE	= 37×10^3 kM
POWER DENSITY LIMITS	
AT IONOSPHERE	23 mW/sq cm
AT EDGE OF RECTENNA	1 mW/sq cm
PEOPLE SAFETY	0.1 mW/sq cm

ELECTROMAGNETIC INTERFERENCE - 154 $dBW/m^2/4$ kHz

SOLAR FLUX	
NOMINAL	1350 W/m^2
USEFUL	820 W/m^2

Table 3-2

Solar Power Satellite Antenna Analysis

FIXED PARAMETERS:

FREQUENCY (f_o) = 2.45 GHz

SYNCHRONOUS ORBIT RANGE (R_o) = 37×10^3 KM

ASSUMPTIONS:

POWER DENSITY AT IONOSPHERE (P_D) = 23 mW/SQ CM

ATMOSPHERIC EFFICIENCY (η_{AT}) = 0.98

ARRAY EFFICIENCY (η_{AR}) = 0.98

ELEMENT SPACING (a/λ) = 0.80

Table 3-3

Key Formulas (Assumes Far Field Analysis)

SPACETENNA DIAMETER:

$$D_T = 2\left(\frac{P_D}{P_o\ \eta_{AR}\ \eta_{AT}}\right)^{.25} \sqrt{\lambda_o\ R_o}\ \sqrt{\frac{.115\ B}{\pi\ (1 - 10^{-B/20})}}$$

GAUSSIAN ILLUMINATION

EDGE TAPER B (DB)

RADIATED POWER DENSITY AT CENTER OF ARRAY P_o (W/SQ M)

RECTENNA DIAMETER (UNIFORM ILLUMINATION):

$$D_R = 1.96\ \frac{\lambda_o}{D_T}\ R_o \quad \text{(AT 1 mW/SQ CM)}$$

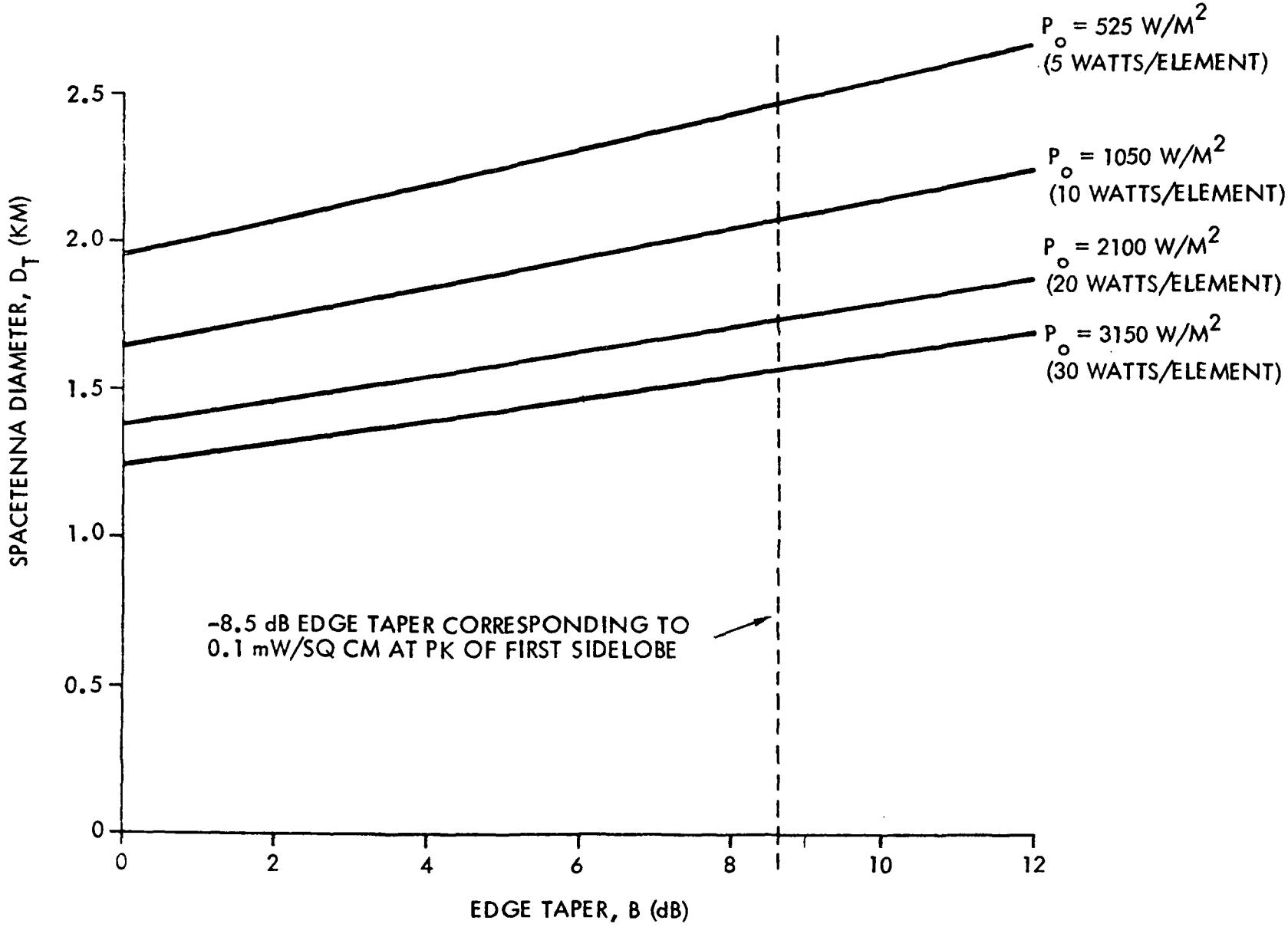

Figure 3-1 Spacetenna Diameter and Power Density Versus Edge Taper

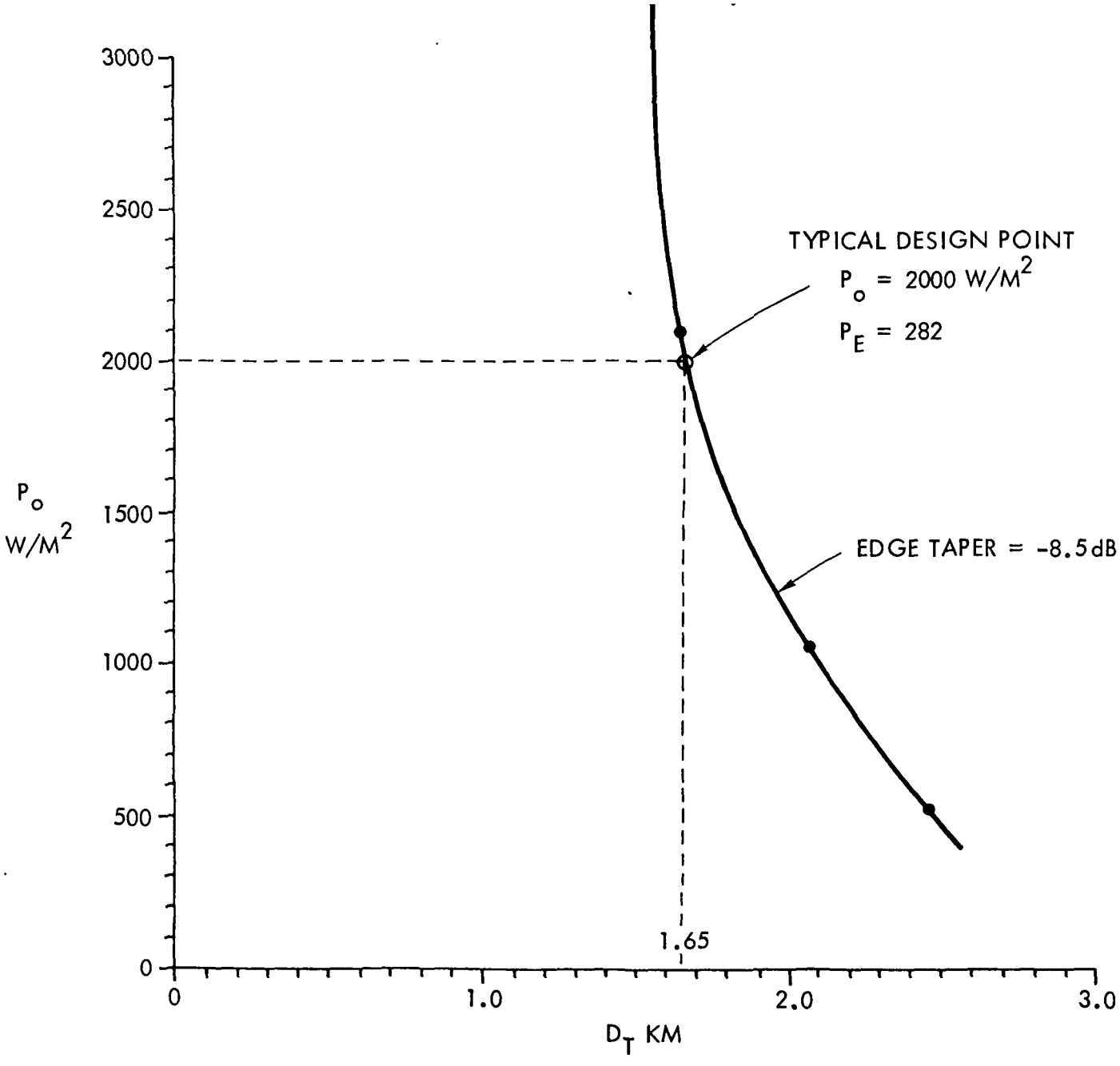

Figure 3-2 Cross Plot from Figure 3-1

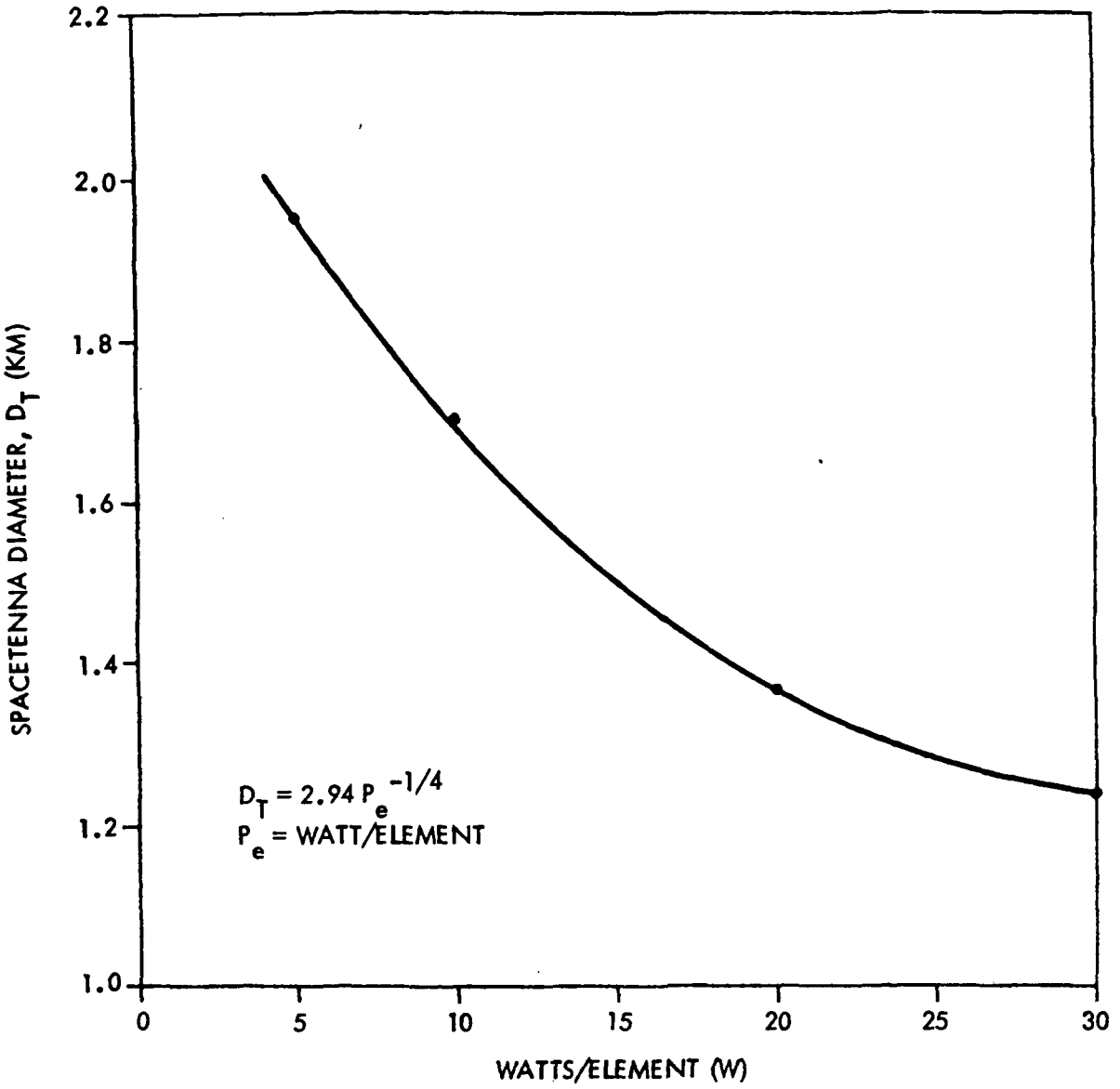

Figure 3-3 Spacetenna Diameter Versus Active Element Power Output For Uniform Illumination

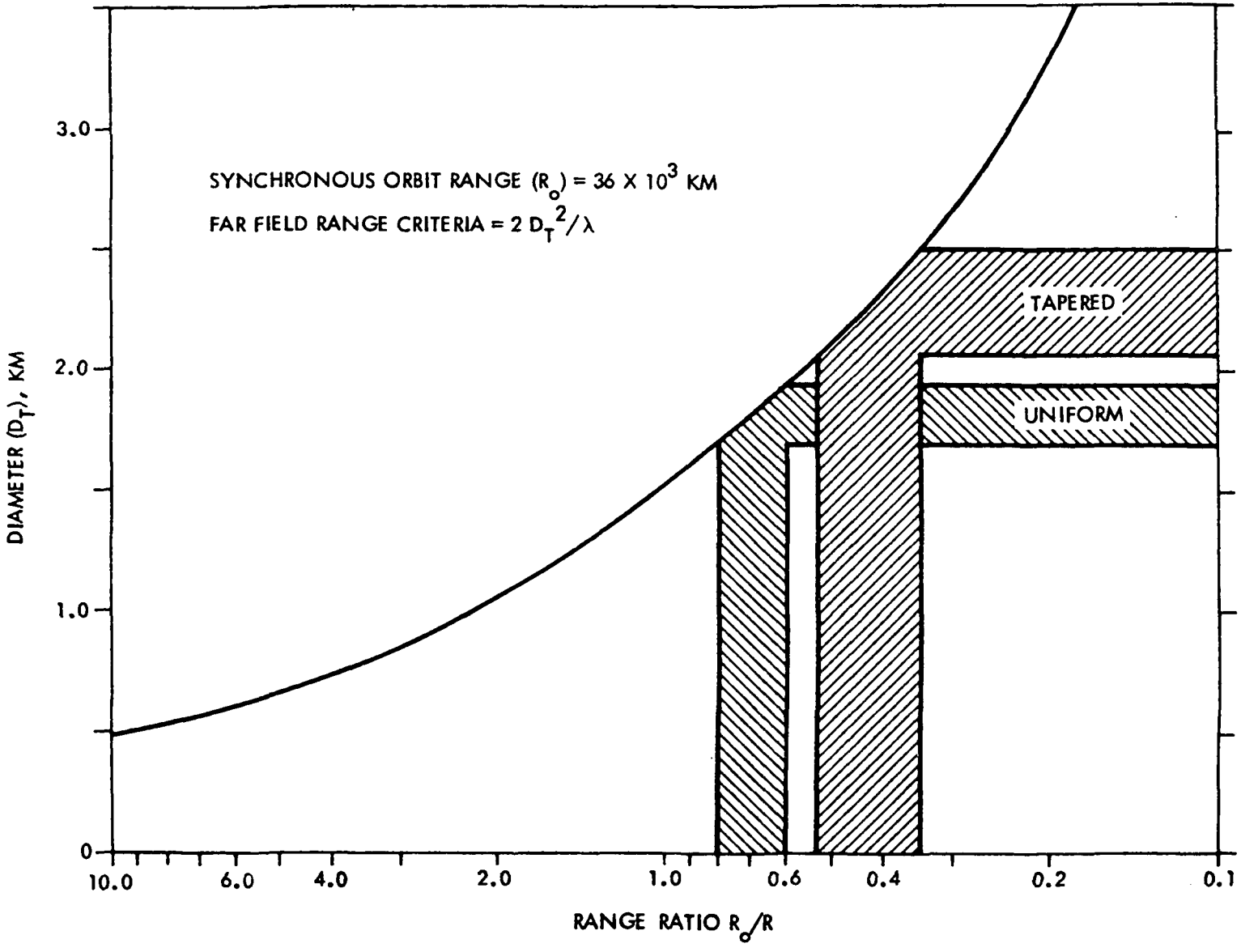

Figure 3-4 Ratio of Synchronous Orbit Range to $2D_T^2/\lambda$

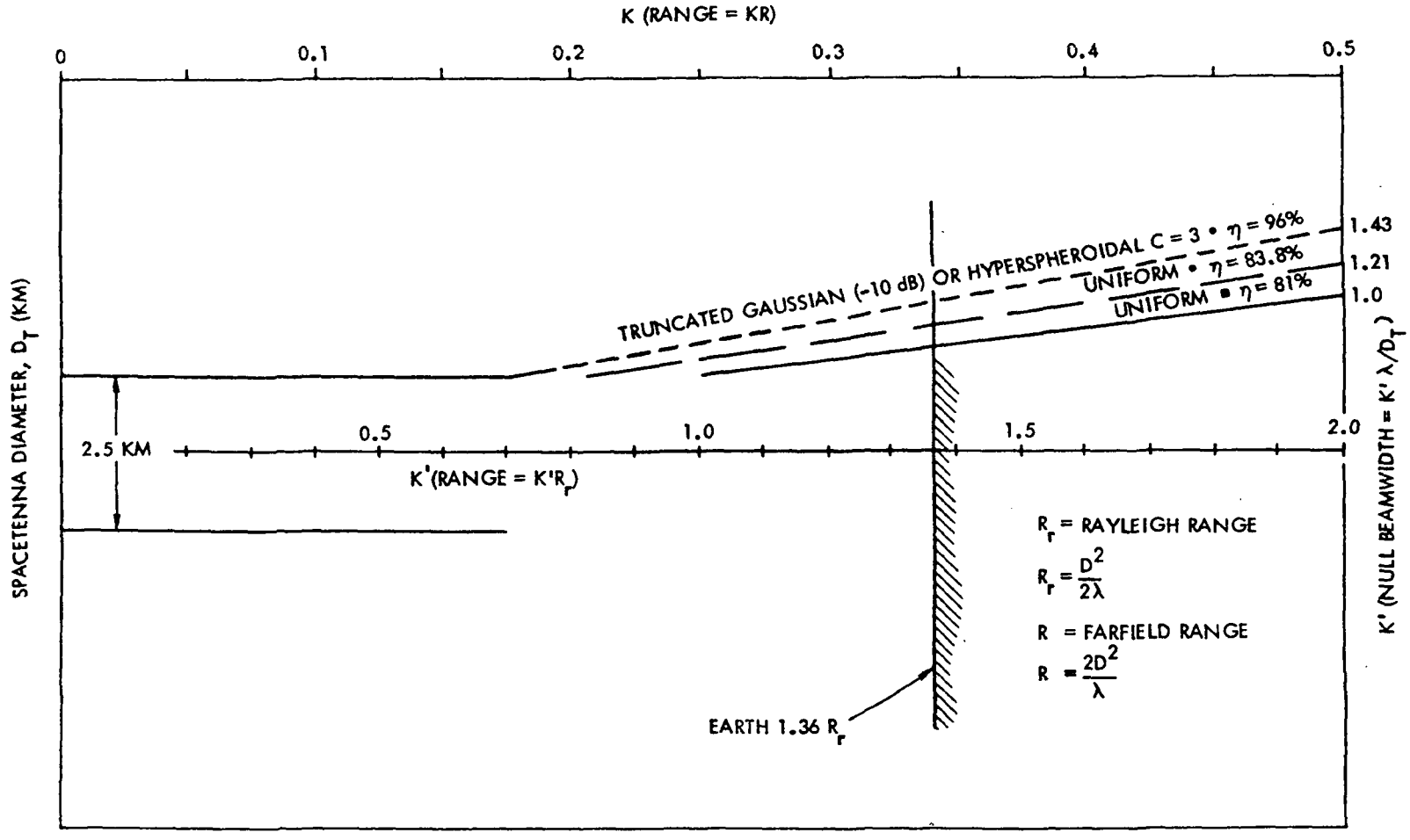

Figure 3-5 SPS Beam Geometry, Tapered Illumination (5W/Element)

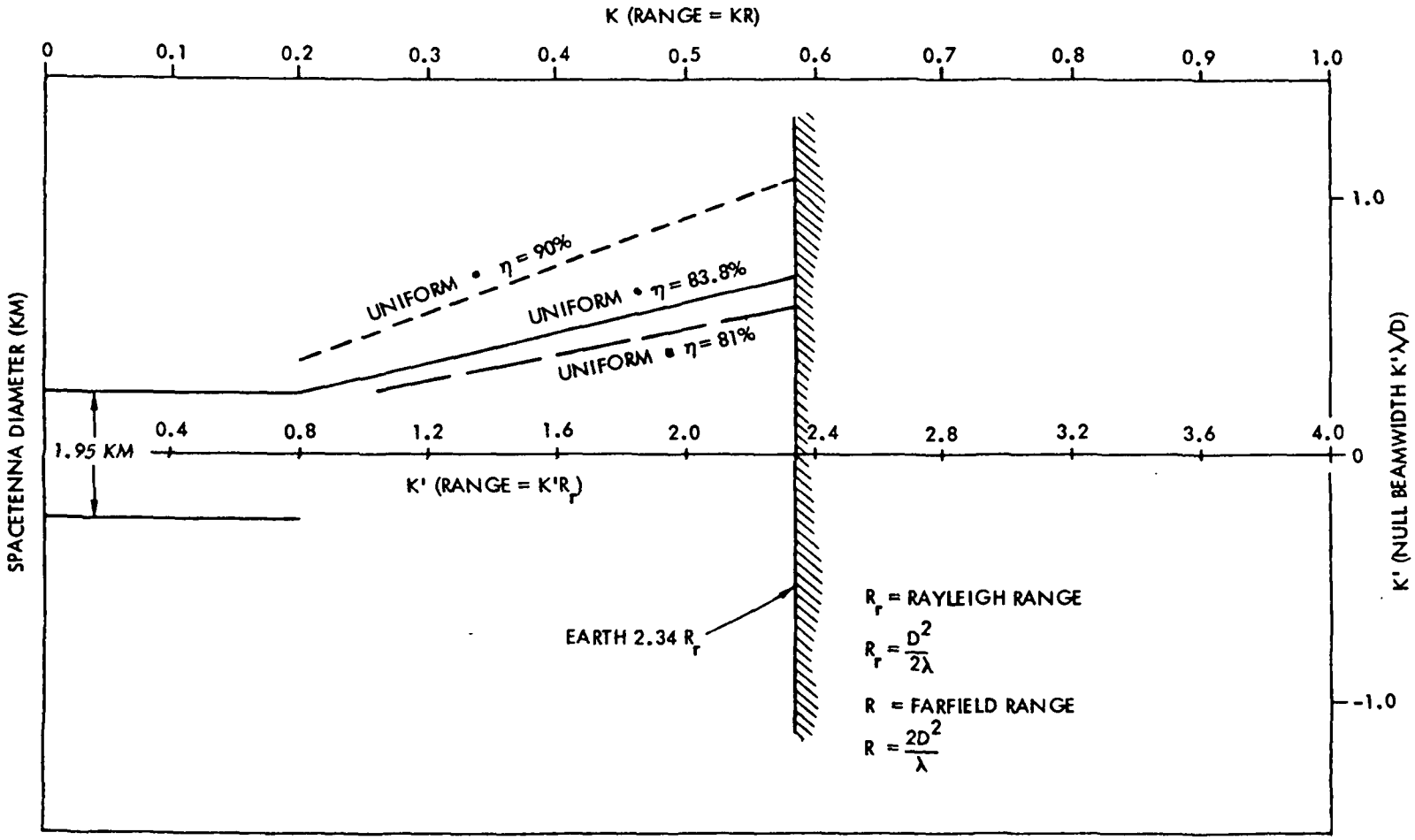

Figure 3-6 SPS Beam Geometry, Uniform Illumination (5W/Element)

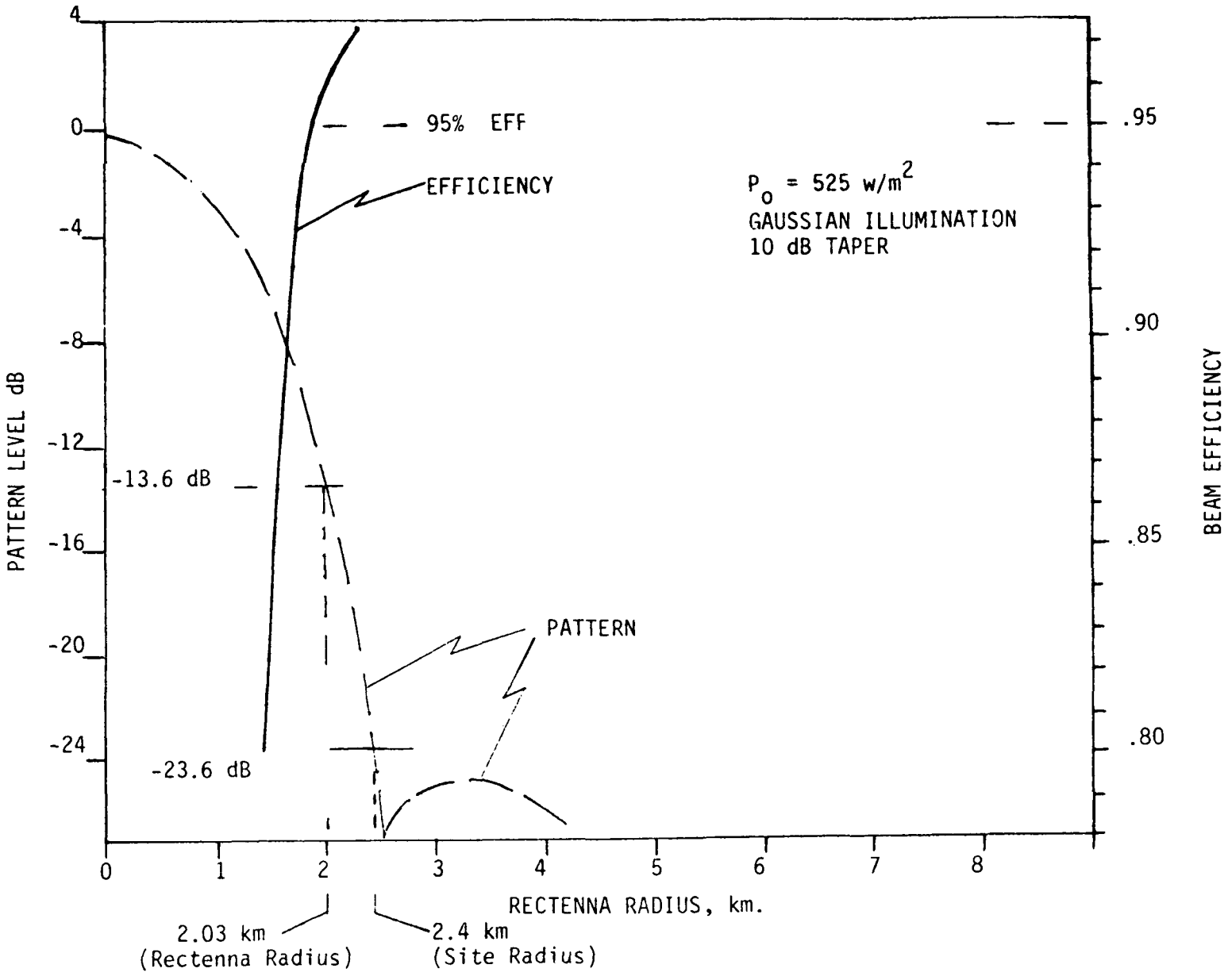

Figure 3-7 Rectenna Size Versus Beam Efficiency - Tapered Illumination

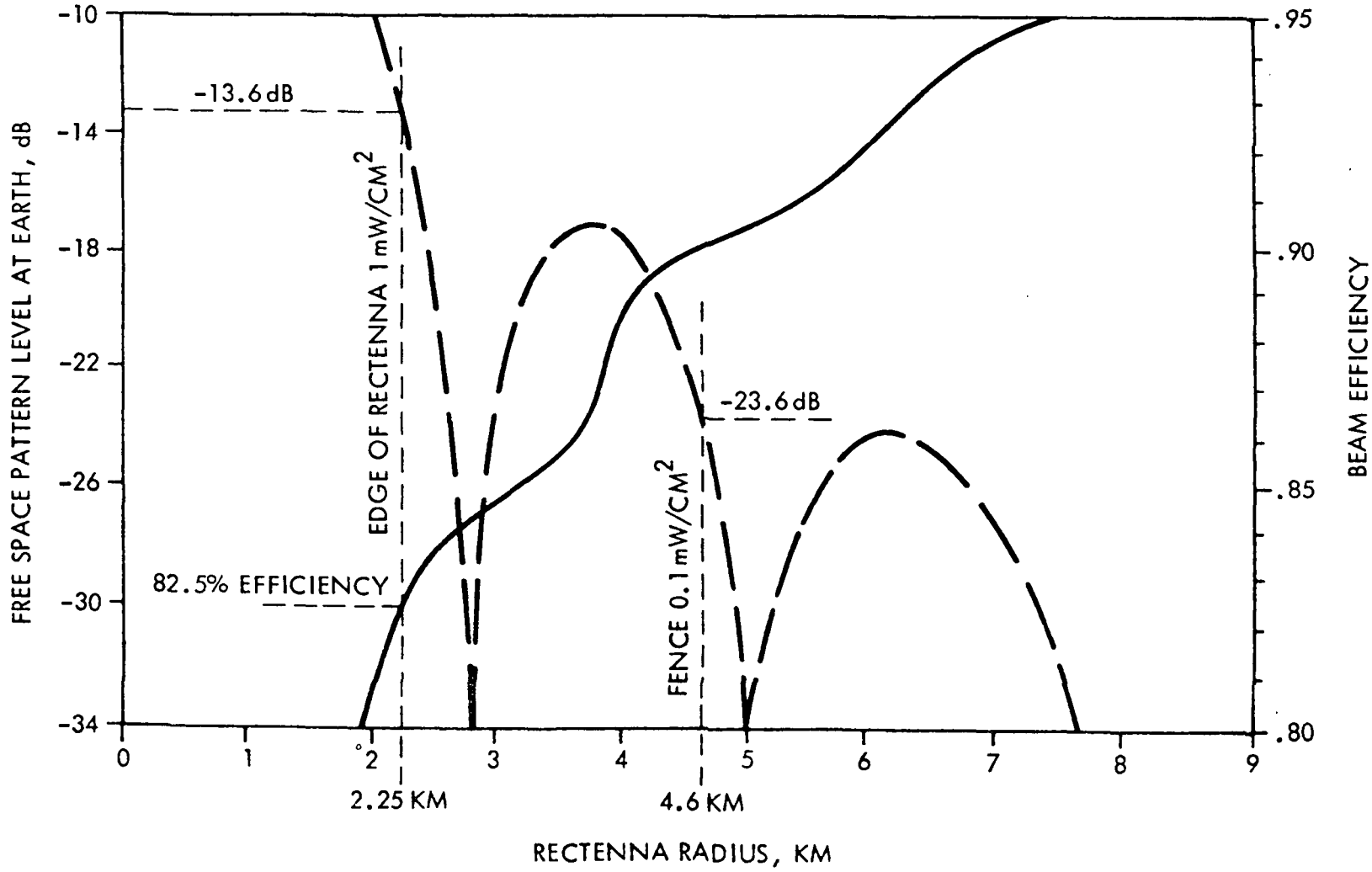

Figure 3-8 Rectenna Size Versus Beam Efficiency - Uniform Illumination

The number of elements versus aperture diameter to element spacing ratio increases as the square of diameter and inversely with the square of the spacing as illustrated in Figure 3-9. For both the tapered and uniform cases the spacing would be the same. The large diameter for the tapered case means many more elements and attendant higher cost, i.e. (2.5/1.95) = 1.64 times as many elements. This will be a major factor against the tapered case.

The uniform illumination case was selected for the baseline because of its relative simplicity and significant potential. As will be discussed later, investigations have been pursued to a lesser degree on single and multiple step edge tapers as well to provide the flexibilities in terms of options for future consideration.

The following sections discuss the pertinent points in more detail.

3.1 FREQUENCY CONSIDERATIONS

The specific values for frequency of power transmission f_0 = 2.45 GHz and the spacetenna to rectenna range R_0 = 37,000 km were selected and established as basic system parameters and the results of the study have not indicated significant sensitivities for small ranges about these values.

Frequencies and, more importantly, bandwidth for the receive elements are areas under investigation by others. Raytheon has indicated that significant bandwidth may be required for the pilot beam of the retrodirective system to compensate for ionospheric effects. This has been reported in Reference [1] and Appendix A of this report includes a more detailed discussion of this issue. For the purposes of the present study, the receive elements have been considered to be in the wide bandwidth class.* This impacts the form factor F at the cell level and at the subarray level.** For this and other reasons the pattern of receive elements is minimized, requiring higher power aperture produce levels for the pilot transmitters than previous studies had indicated. Reference [1] covered the pilot beam sizing considerations.

---

*Element selection is discussed further in Section 4.

**Form factor F is discussed as a critical waste heat dissipation parameter in Sections 3.4 and 8.

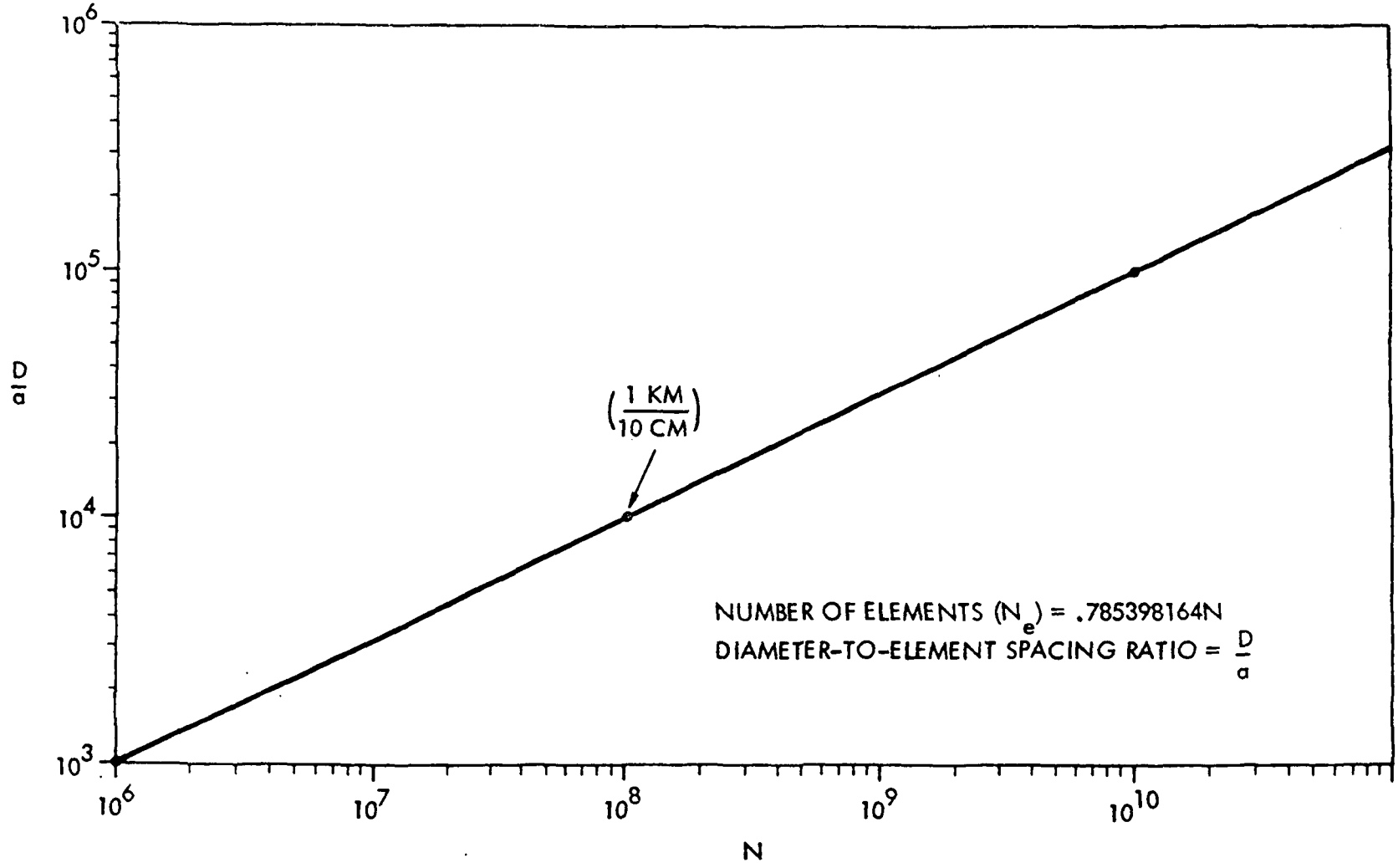

Figure 3-9 SPS Number of Elements Versus D/a Ratio

3.2 IONOSPHERIC AND SIDELOBE POWER DENSITY CONSIDERATIONS

Assumptions with respect to power density limits at the ionosphere P_{DI} = 23 mW/cm^2 continued to be applied throughout the investigation. It is, however, recognized from earlier work reported in Reference [2] (among others) that economic advantages increase with increases in P_{DI}, however uncertainties in both general and MPTS control related environmental impact also increase with increases in P_{DI}. For purposes of assessments of MPTS concepts, within the solid state family, the 23 mW/cm^2 continues to be valid.

The power density at the edge of the rectenna was considered to be 1 mW/cm^2 as a cost effective limit which continues to be valid for the solid state systems employing retrodirective concepts as the primary approach to phase and pattern control. Further investigations of pattern control, as discussed under Spacetenna and Rectenna Size Considerations, Section 3.6, may lead to changes in the rectenna edge power density near-optimum value.

The value of 0.1 mW/cm^2, as a limit, for power densities outside the rectenna and within the protected region is an uncertainty that is under investigation by others. It is recognized that this value may increase or decrease as a "requirement." This solid state MPTS concept study has indicated that power density taper is the primary means of controlling the parameter, however, as will be discussed further under Sidelobe Control Considerations, the larger spacetenna aperture decreases beamwidth to the point where including the first sidelobe in the protected region of the rectenna site becomes worthy of consideration so that the above limit is considered to apply to second and subsequent sidelobes primarily. This makes uniform distribution of RF power density for transmission potentially viable. Single step tapers and multiple step tapers, although initially believed to be penalties, have been shown to be possibly advantageous from other points of view and should be investigated further.

Assumptions with respect to atmospheric efficiency η_{AR} = 0.98 continue to be valid.

3.3 ARRAY EFFICIENCY CONSIDERATIONS

Assumptions with respect to array efficiency $\eta_{AR} = 0.98$ are considered to continue to be valid, however further study of dipole and stripline concepts for antenna elements and subarrays are required. Further investigations of these concepts must include the interactive nature of coupling between transmit and receive elements as well as the effects of other material and phenomenological aspects. Such items include (a) protuberances in the ground plane, (b) conductive thermal control coatings, variations of configuration across the subarray, (c) potential discontinuities across subarray boundaries that may derive from more detailed implementation investigations, and (d) potential thermal and other distortions in both radial and normal directions across the subarrays that may derive from more detailed investigations.

3.4 WASTE HEAT DISSIPATION FORM FACTOR CONSIDERATIONS

The importance of achieving high values of the form factor F for the waste heat radiator system at the 10 x 10 cm cell level and at higher levels has been brought out in other phases of the investigation. Maximizing microwave power transmission density P_{RF} in the autonomous sandwich concept in general minimizes cost and it may be shown in more detailed investigations that η_{AR} vs F tradeoffs may result in a different near-optimum value for η_{AR}.

3.5 ELEMENT SPACING CONSIDERATIONS

Element spacing a/λ - 0.80 may be shown to have a nearer-to-optimum value in more detailed investigations for similar reasons to those discussed above, however the RF subarray size which has resulted, primarily from topological considerations, is only 3.2 x 3.2 m. Transmit element spacing increases are not conceived to go beyond one wavelength due to grating lobe considerations and associated loss considerations. In this event, the RF subarray size would increase to about 4 x 4 m, which is not believed to be a problem. Tradeoffs of element spacing and associated losses with respect to form factor F from the waste heat dissipation point of view should be investigated further.

3.6 SPACETENNA AND RECTENNA SIZE CONSIDERATIONS

Spacetenna and rectenna size relationships are not impacted significantly (with respect to earlier tube system studies) for the solid state concepts investigated, except that the lower transmit power density P_D for the solid state concept results in a larger spacetenna aperture and smaller rectenna aperture. This is more pronounced for the tapered illumination case. The transmit aperture is sufficiently large and would increase further with increases in allowable ionospheric power density, to bring the earth into the transition region between Rayleigh and far field ranges. In view of the issues relating to retrodirective concept uncertainties and the general desirability of more cost effective systems, operating in the near field may be shown to be advantageous. Onboard control of transmit phase and power distributions in conjunction with ground command and supplemental control may result in receive patterns which permit more effective utilization of rectenna real estate without exceeding ionospheric limits.

Transmit antenna patterns which result in low power densities in the relatively small central area of the rectenna and high power densities over the mid-radii of the rectenna should be investigated further. Sidelobe uncertainties and power taper on transmit for sidelobe control continues to be of concern.

3.7 SIDELOBE CONTROL

For uniform RF power distribution at the transmitting antenna, initially adopted as the baseline approach, the second sidelobes were estimated to be at or below the 0.1 mW/cm^2 limit, as shown in Figure 3-8 . The first sidelobe out to about 4.6 km radius is well above 0.1 mW/cm^2, but a 4.6 km radius fenced region for protection is reasonable if the land has a sufficiently small value.

In order to provide, in the concept and in the parametric data, for the options to (a) suppress the second and subsequent sidelobes still further, as may become a requirement, and (b) to include the second sidelobe suppression as a possible requirement, the following investigations were conducted.

3.7.1 Single Step Edge Tapers

For Item (a) above, a range of single step edge tapers were investigated and compared to uniform as well as 10 dB Gaussian illumination.

As indicated in Table 3.7-1, the advantages and disadvantages for uniform as compared to 10 dB Gaussian include (a) spacetenna diameter reduction but more land required to fence the rectenna region and higher sidelobes, (b) commonality of amplifier modules, and (c) short conductor lengths for simple implementation of the low voltage power transfer requirements while the approximation to the Gaussian illumination becomes complex, largely in terms of DC power distribution.

Similarly, the advantages and disadvantages for step tapers, with constant power level at each step, compared to uniform include (a) lower sidelobes but less power available on transmit, (b) all amplifiers continue to operate at the same power level by feeding more dipoles with a single amplifier in the low power density region, and (c) the spacetenna size increased by as much as 30%.

Section 3.9 discusses how some of the disadvantages of the single step taper may be overcome and Section 9.3 discusses how multiple step tapers may be implemented. The multiple step taper approach taken to its limit requires several different amplifiers to be developed, however if other system level and economic advantage is demonstrated, the numbers of amplifiers are so large that several sizes become of less importance.

3.8 BASELINE FOR PRELIMINARY ANALYSIS

The baseline selected for preliminary analysis features a 1.95 km diameter spacetenna having uniform power distribution of P_{RF} = 500 watts/m^2.

The rectenna diameter is 4.5 km, the site diameter is 9.2 km and the total power delivered to the grid is approximately 1 GW for a total efficiency of 51%. In the course of preliminary analyses, the efficiency chain of Figure 3.8-1 was evolved and additional parameters were selected as shown in Table 3.8-1.

The spacetenna subarray circuit diagram of Figure 3.8-2, as defined early in the study, included the concept of combining DC and RF power distribution at the subarray into one network. This was found to constitute a risk and complexity and the subsequent analyses treated the negative DC side of the distribution system integrated into the ground plane with a separate positive DC power plane.

Table 3.7-1 Sidelobe Suppression Considerations

- UNIFORM VERSUS 10 DB GAUSSIAN ILLUMINATION AT SPACETENNA RESULTS IN THE FOLLOWING:

ADVANTAGES FOR UNIFORM

- SMALLEST TRANSMIT ANTENNA
- ALL AMPLIFIER MODULES OPERATE AT SAME POWER LEVEL
- EASY TRANSFER OF DC VOLTAGES FROM SOLAR ARRAY (IF DENSITY TAPERING IS EMPLOYED TO APPROXIMATE GAUSSIAN ILLUMINATION THEN DC DISTRIBUTION AND SOLAR ARRAY ARCHITECTURE BECOMES COMPLEX AND HEAVIER)

DISADVANTAGES FOR UNIFORM

- LOWER POWER BEAM EFFICIENCY
- HIGHER SIDELOBES (-17 DB, -24 DB, -28 DB BELOW 23 MW/CM^2 AND MORE LAND REQUIRED TO FENCE RECTENNA

- SINGLE STEP TAPER VERSUS UNIFORM (CONSTANT POWER DENSITY AT EACH LEVEL)

ADVANTAGES FOR STEP

- LOWER SIDELOBES (-28 DB BELOW 23 MW/CM^2)
- ALL AMPLIFIERS OPERATED AT SAME POWER LEVEL

DISADVANTAGES FOR STEP

- LESS POWER AVAILABLE
- LARGER SPACETENNA

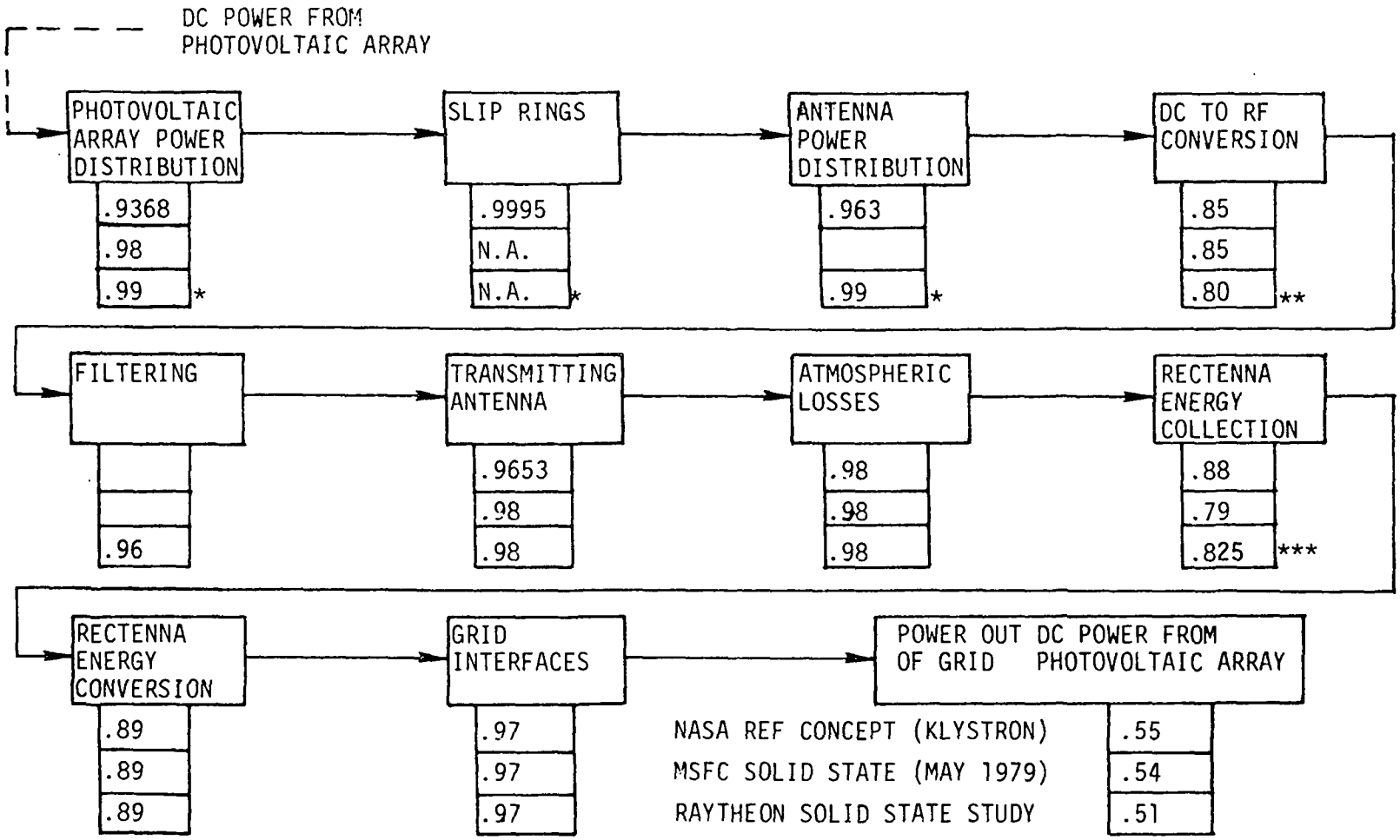

*For autonomous sandwich cases with no radial DC power transport.

**For solid state amplifier (nominal unit).

***For uniform power distribution at spacetenna.

NOTE: For considerations different from those of the lower line, assumptions are to be identified and discussed in the appropriate system.

Figure 3.8-1 Preliminary Estimates of Power Transmission and Conversion Efficiency Chain

Table 3.8-1 Solid State MPTS Baseline

SPACETENNA

Illumination - Uniform

Diameter - 1.95 km

Area Gain - 94 dB

Beamwidth - 0.128 Milliradians (.0073°)

Element Spacing - 0.1 m

Number of Elements $\simeq 3 \times 10^8$

Elements Per Subarray $\simeq 10^3$

Number of Subarrays $\simeq 3 \times 10^5$

RECTENNA

Diameter - 4.5 km

Site Diameter - 9.2 km

SYSTEM

Efficiency - 51%

Power Delivered To Grid - 1 GW

Cost (ROM) - 4G$

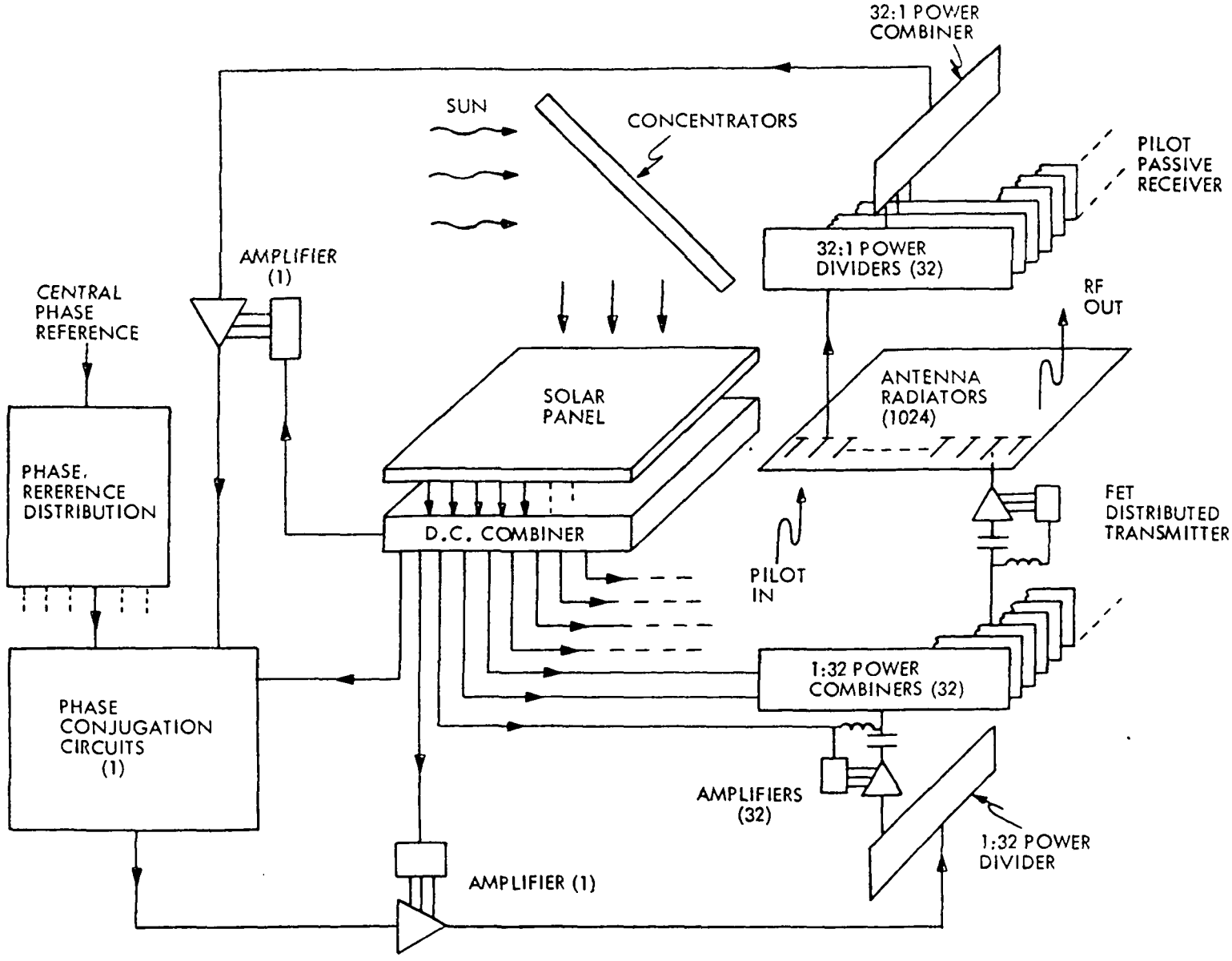

Figure 3.8-2 Solid State MPTS Spacetenna Subarray Circuit Diagram

The dipole concept, Figure 3.8-3, included narrow-band dipoles for transmit with orthogonal wideband dipoles for receive. RF element selection is discussed further in Section 4; however, the following is summarized for baseline purposes. The need to have (a) receive as well as transmit elements in a common aperture at the subarray level and (b) the isolation of transmit noise from the receive element was a major factor in the orthogonal dipole selection. Other less well understood element concepts shoudl be investigated, keeping in mind that the waste heat radiation from amplifiers is the primary limitation on power density and that the waste heat radiator form factor is key to maximizing P_{RF} allowable. Element-mounted amplifiers that may provide for waste heat dissipation form factor enhancement should be included in further investigations, however this study has continued with the orthogonal dipole approach.

3.9 SELECTED SYSTEM CONCEPT ASSESSMENT WITH RESPECT TO SIDELOBE CONTROL AND MAXIMUM POWER DENSITY POTENTIAL

From a preliminary analysis for a uniform distribution of P_{RF} = 5 watts/element in a .01 m^2 cell, it was determined that a spacetenna diameter of 1.95 km would yield 23 mW/cm^2 (max) at the ground. The spacetenna area = $\pi 1950^2/4$ = 2.986 x 10^6 m^2. The total transmitted power 2.986 x 10^6 x $\frac{5}{.01}$ = 1.493 x 10^9 W.

Similarly, a single step power taper where the power level per element = $\frac{1}{4}$ x 5 = 1.25 watts in the outboard ring was investigated for third and subsequent sidelobe suppression purposes. In that analysis, as depicted in Figure 3.9-1, the spacetenna diameter = 1.1303 x 1.95 = 2.204 km and the diameter of the central region over which 5 watts/element applied was 0.85 x 1.95 = 1.658 km. This reduced the second sidelobe to more than 30 dB below the main lobe. This was thought to constitute a penalty that may have to paid as we come to understand more clearly (a) how the sidelobes will behave in an actual implementation and (b) what the limits on sidelobes must be for a totally acceptable system. The purpose of the following paragraphs is to investigate the nature of this assumed penalty as a preliminary assessment. More specific and optimized example cases are included in Section 2.3.6.2.

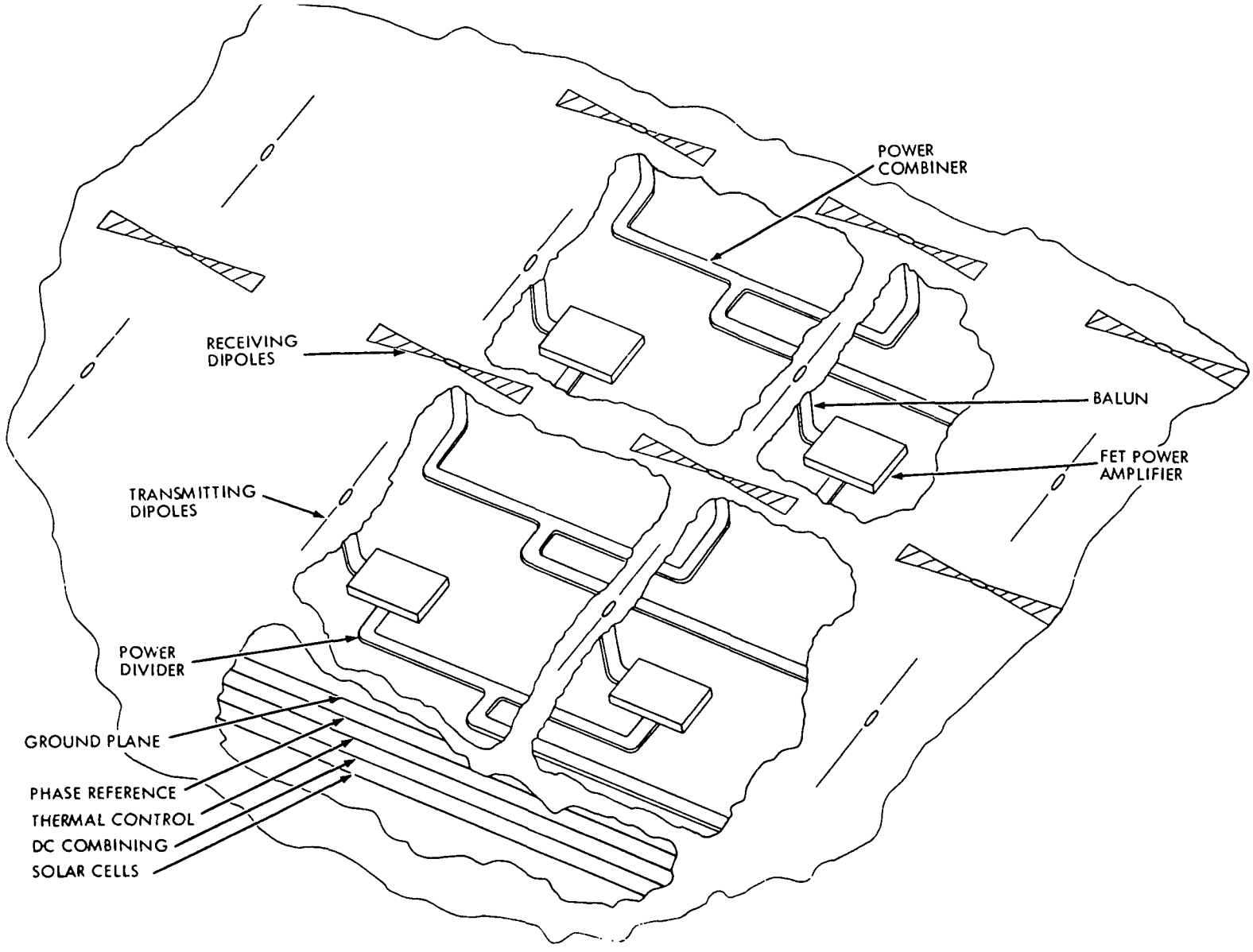

Figure 3.8-3 Spacetenna - Dipole Concept

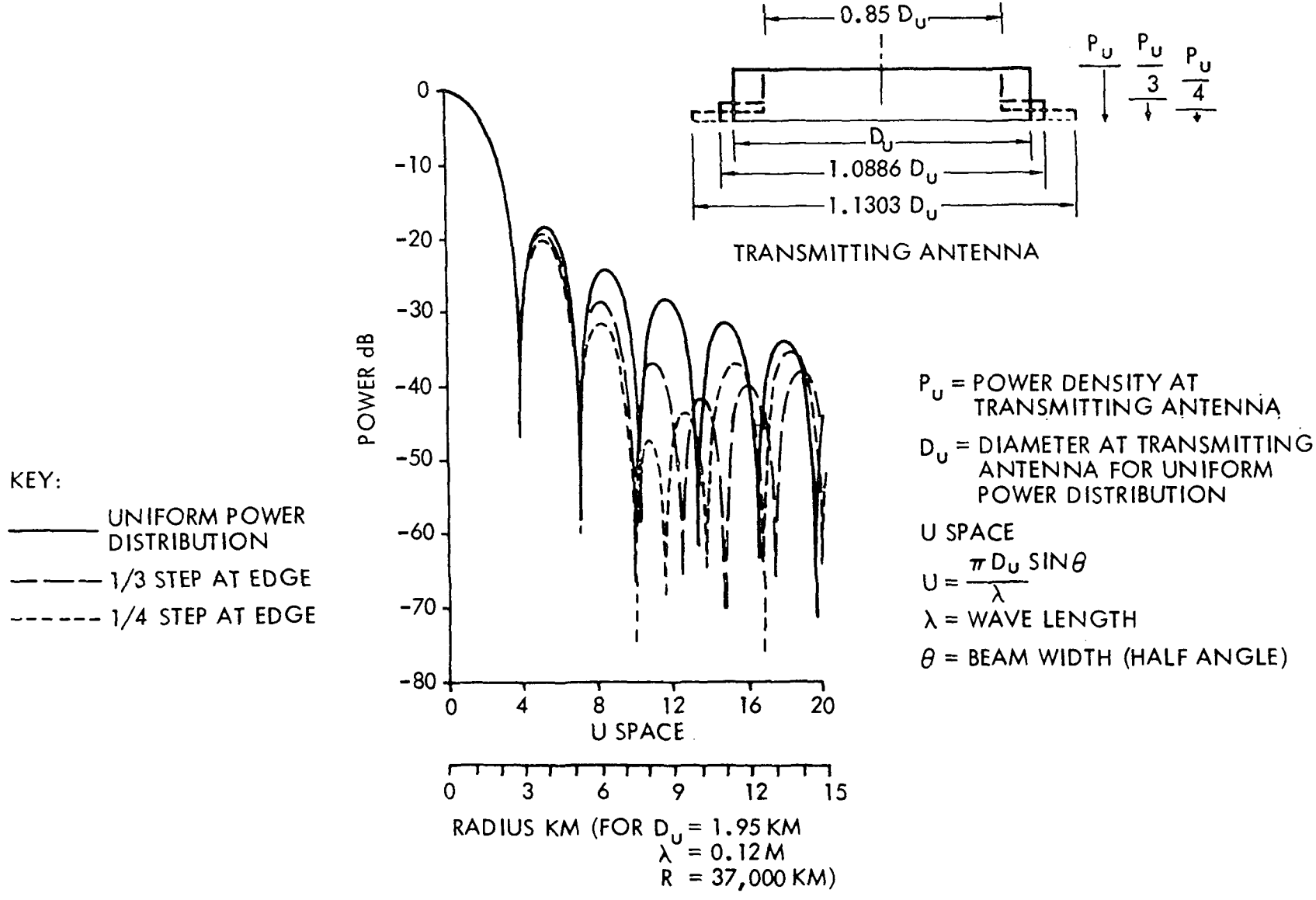

Figure 3.9-1 Sidelobe Comparison of Uniform Power Distribution With Two Examples of Single Step Edge Taper

The area of the outboard ring = $\frac{\pi}{4}$ (2204^2 - 1658^2) = 1.656×10^6 m^2. The area of the central region = $\frac{\pi}{4}$ 1658^2 = 2.159×10^6 m^2. The total area = π $2204^2/4$ = 3.815×10^6 m^2. The transmitted power would be $\frac{1.656 \times 10^6 \times 5}{4 \times .01}$ = $.207 \times 10^9$ W from the outboard ring and $2.159 \times 10^6 \times \frac{5}{.01}$ = 1.079×10^9 W from the central region for a total of 1.286×10^9 W, which is only 1.286/1.493 = 86.1% of the above totally uniform case. Not only is there less transmitted power but there is also an increase in spacetenna area of 3.815/2.986 = 1.278. In terms of transmitted power/m^2, the factor would be .861/1.278 = .674, which is a significant penalty.

The penalty is not quite so bad in terms of kg/watt or $/watt because the solar cells on the outboard ring would be reduced in numbers or the concentration ratio would be reduced. The number of elements would, however, increase by a factor of 1.43.

If we increased the solar cells in the outboard ring and/or the concentration ratio in the outboard ring up to the thermal limits of both the microwave and photovoltaic equipment (assumed to be 114°C for amplifiers and 200°C for photovoltaics) while keeping the $P_{RF} = \frac{5}{4 \times .01}$ = 125 W/m^2, the following would result.

The DC power available would be ≃ 900 W/m^2 of which 125/.7377 = 169 W/m^2 would be used for microwave power transmission on the adjacent face of the sandwich and 731 W/m^2 would be available for transfer to the central region, i.e., a total of $731 \times 1.656 \times 10^6 = 1.211 \times 10^9$ W would be available for export.

If we now reduced the DC power developed over the central region by this amount, we would have $1.286 \times 10^9 - 1.211 \times 10^9 = .075 \times 10^9$ watts being supplied in the central region from immediately adjacent photovoltaics. This is a reduction to ≃ .075/1.079 x 5/.01 = 34.7 watts/m^2 or .347 watts/cell which could be supplied without approaching the thermal limits while P_{RF} is as high as 14 W/cell for no waste heat transfer from the photovoltaic side. The local power available assuming this no heat transfer constraint would be 640 W/m^2 or $640 \times 2.159 \times 10^{-6}$ = $.382 \times 10^9$ W. Approaching the thermal limits more closely, with waste heat P_{SM} ≃ 300 W/m^2, the P_{DC} = 720 W/m^2 and P_{RF} would go up to 920 W/m^2 at the 114°C junction temperature limit. This would give $720 \times 2.159 \times 10^6 = 1.554 \times 10^9$ W as locally available DC power.

The autonomous P_{RF} would have increased by 5.88/5 = 1.176, which would effectively reduce the factor to 1.46/1.176 = 1.24.

The local DC power available and the imported power total (1.554 + 1.211) x 10^9 = 2.765 x 10^9 W. If this available power is distributed through the central region, the DC power density would be 2.765 x 10^9/2.159 x 10^6 = 1280 W/m^2 or 12.8 watts/cell. This would result in a P_{RF} = 9.6 watts/cell or 960 watts/m^2 at the 114°C junction temperature limit. The 920 watts/m^2 is therefore slightly conservative.

Note: Further optimization of taper step sizing could lead to even higher RF power densities over the central region, possibly as high as 1400 W/m^2. However, staying with the 920 W/m^2 in this preliminary assessment, the following total transmitted power would result. From the outboard ring there would be .207 x 10^9 W and from the central region there would be 920 x 2.159 x 10^6 = 1.986 x 10^9 W, for a total of 2.193 x 10^9 W. This is higher than the original uniform 5 W/element case by 2.19/1.493 = 1.46. The spacetenna area ratio increased by 3.815/2.986 = 1.28, which is the theoretical limit to be expected.

The effective concentration ratio would increase from about 3.7 to 5 over the outboard region and to about the 4.0 level over the central region. How this concentration ratio variation would be accomplished should be the subject of further system level investigations.

The transfer of power from the outboard ring to the central region should also be the subject of further system level investigations.

The apparent improvement factor for change of transmitted power density would be 1.24/1.28 = 0.97 for the inboard flow of DC power concept rather than the penalty of .674 for the autonomous subarray (no radial power transport) concept appears to be real.

The maximum power density at the rectenna will be higher than the 23 mW/cm^2 when the total transmitted power is increased so that the total spacetenna diameter and transmitted power would be less than those indicated if this constraint is maintained.

It should be noted that the above analysis was conducted to more clearly understand what was thought to be a penalty for reducing sidelobes and the mitigating approach has not been optimized. Further investigations should include optimization of the architecture for both the single step taper approach and multiple step taper approaches. Such investigations have been initiated and reported upon in the example calculations of Section 2.3.6.

3.10 POWER DELIVERY AND ASSOCIATED COST ESTIMATION

Beginning with power delivered to the grid as a function of power per element, Figure 3.10-1, it is noted that a factor of 2 in power delivery is associated with a factor of 4 in power per element. Increasing power per element in a practical scheme has been the goal of the study from the outset, however P_{RF} in the 4 to 6 watts/element range dominated the allowable values derived in the investigation of power source characteristics which interact with the microwave side of the sandwich. Section 9, however, begins to indicate that higher values of P_{RF} allowable and indeed higher values of total transmitted power come about primarily by (a) partitioning the RF portion from the DC supply portion and (b) by conceiving approaches that yield high waste heat dissipation system form factors (F).

Through utilization of the cost estimating relationships of Tables 3.10-1a through 3.10-1c, the ROM costs of Table 3.10-2 and the normalized values of Table 3.10-3 indicate that cost reductions, \$/W, better than 50% characterize the high power density cases.

Figures 3.10-2 and 3.10-3 indicate that the total cost reduces as power per element increases to 20 and since the total power increases, the power per watt (figure of merit) continues to reduce with higher power density levels.

3.11 CONCLUSION AND RECOMMENDATIONS FROM THE PRELIMINARY DESIGN INVESTIGATION

The three basic conclusions (Table 3.11-1) from this phase are clarified in the following paragraphs.

Solid state microwave power transmission for the SPS application has in the past been viewed with considerable skepticism, largely associated with the fact that solid state amplifiers are not inherently high power devices and the SPS is a high power system. This study has begun to show that a solid state approach may, after more in-depth investigation, be shown to be a viable contender. Imaginative approaches such as the sandwich concept have stimulated considerable interest and as the study progressed the skepticism began to be put in a more proper perspective. The preliminary assessment has brought the expected power density up to 0.5 kW/m^2, which is greater than was anticipated at the outset, although it is well below the 24 kW/m^2 associated with tubes. A perspective assessment conducted subsequent to the preliminary design phase indicates that the RF potential for solid state may be

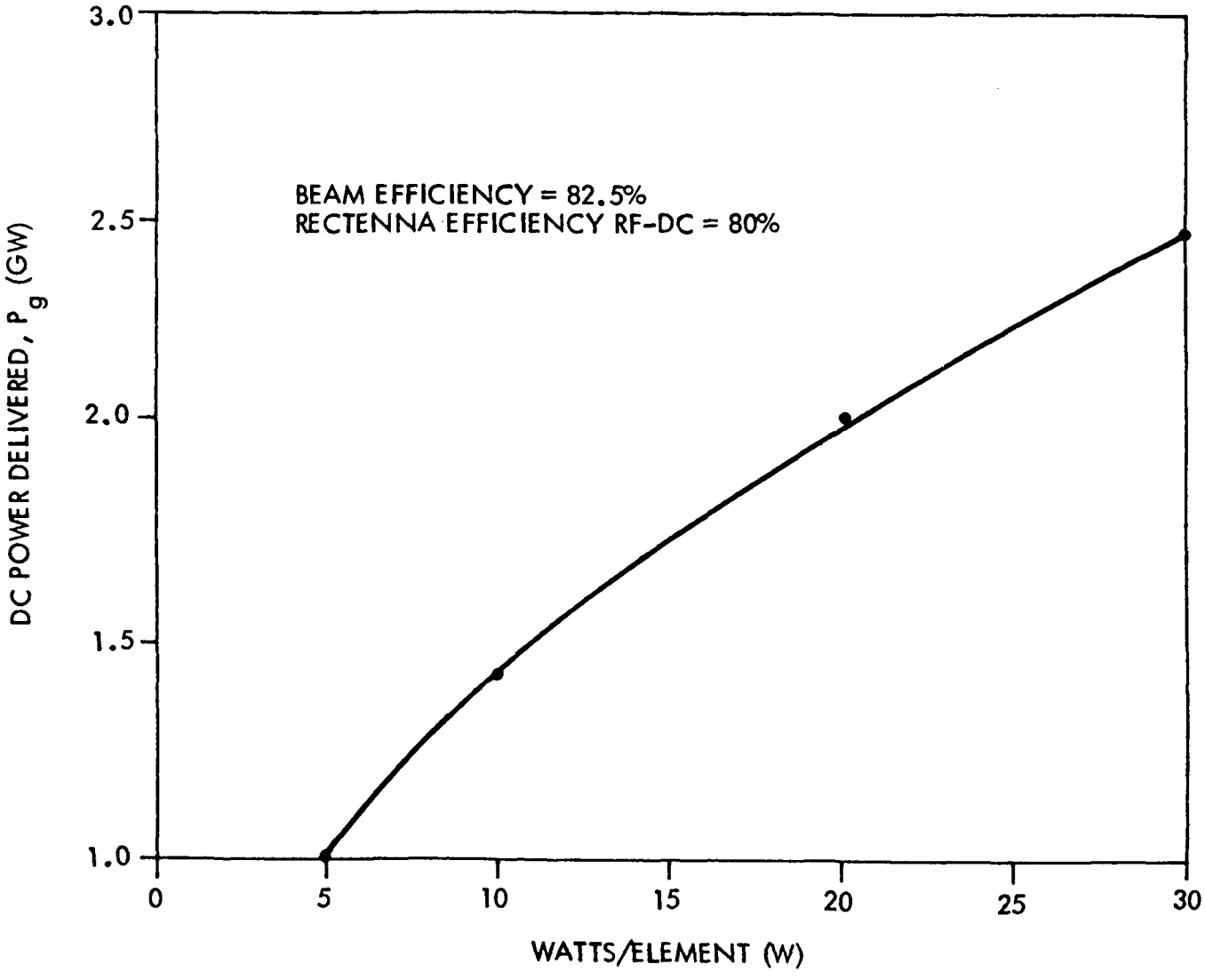

Figure 3.10-1 DC Power Delivered to Grid Versus Module Power Per Element

Table 3.10-1a

SPS Solid State MPTS Cost Estimating Relationships

C_S = Solar Cell Cost ($/m^2) = $67/m^2 (ADL)

C_M = RF Amplifier Module Cost ($/Watt) = $.1/W, $10/m^2/W (ROC)

C_E = RF Radiator Element Cost ($/Element) = $25/Element (RAY)

C_C = RF Power Combiner Cost ($/m^2) = $25/m^2 (RAY)

C_P = RF Phase Control Cost ($/Circuit) = $400/Circuit (RAY)

C_R = Rectenna Cost ($/m^2) = $40/m^2 (ROC); $44/m^2 (MSFC)

C_L = Land Cost ($/m^2) = $.25/m^2 (MSFC)

C_W = Launch Weight Cost ($/kg) = $70/kg (MSFC)

ADL: Arthur D. Little
RAY: Raytheon
MSFC: Marshall Space Flight Center
ROC: Rockwell

Table 3.10-1b SPS Solid State MPTS Cost Estimating Relationships -- Continued

$$\text{COST} = \underbrace{\frac{C_R \ 61.47 \times 10^6}{D_T^2}}_{\text{RECT.}} + \underbrace{C_S \ \frac{\pi}{4} \ D_T^2}_{\text{SOLAR}} + \underbrace{C_M \ 25 \ \pi \ W \ D_T^2}_{\text{MODULE}}$$

$$+ \underbrace{C_E \ 25 \ \pi \ D_T^2}_{\text{ELEMENT}} + \underbrace{C_c \ \frac{\pi}{4} \ D_T^2}_{\text{STRIPLINE}} + \underbrace{C_P \ \frac{\pi}{4} \ \frac{D_T^2}{A_{S.A}}}_{\text{ELECTRONICS}}$$

$$+ \underbrace{\frac{C_L \ 255.9 \times 10^6}{D_T^2}}_{\text{Land Cost}} + \underbrace{C_W \ 10 \ D_T^2}_{\text{Transportation Cost}}$$

Table 3.10-1c SPS Solid State MPTS Cost Estimating Relationships -- Continued

$$C = \frac{2.705 \times 10^9}{D_T^2} + 52.62\ D_T^2 + 39.27\ D_T^2 + 39.27\ D_T^2$$

RECT | SOLAR | MODULE | ELEMENT & COMBINER

$$30.68\ D_T^2 + \frac{.064 \times 10^9}{D_T^2} + 700\ D_T^2$$

ELECTRONICS | Land | Transportation

Table 3.10-2 SPS Solid State MPTS Costs (ROM)

M$

WATTS/ELEMENT	5	10	20	30
SPACETENNA DIAMETER (KM)	1.965	1.652	1.389	1.255
1 RECTENNA	700	991	1420	1717
2 SOLAR ARRAY	203	144	102	83
3 MODULES	152	214	303	371
4a ELEMENTS 4b STRIPLINE	152	107	76	62
5 ELECTRONICS	118	84	59	48
6 LAND	17	23	33	41
7 TRANSPORTATION	2702	1910	1350	1102
TOTAL	4042	3473	3343	1878

Table 3.10-3 SPS Solid State MPTS Costs (Normalized ROM)

	M$			
WATTS/ELEMENT	5	10	20	30
SPACETENNA DIAMETER (KM)	1.965	1.652	1.389	1.255
RECTENNA AND LAND	716	1015	1453	1758
SPACETENNA	624	548	540	564
SUBTOTAL	1340	1563	1993	2322
TRANSPORTATION	2702	1910	1350	1102
TOTAL	4042	3473	3343	3424
PG (GW)	1	1.42	2.05	2.43
$/W	4.04	2.44	1.62	1.41

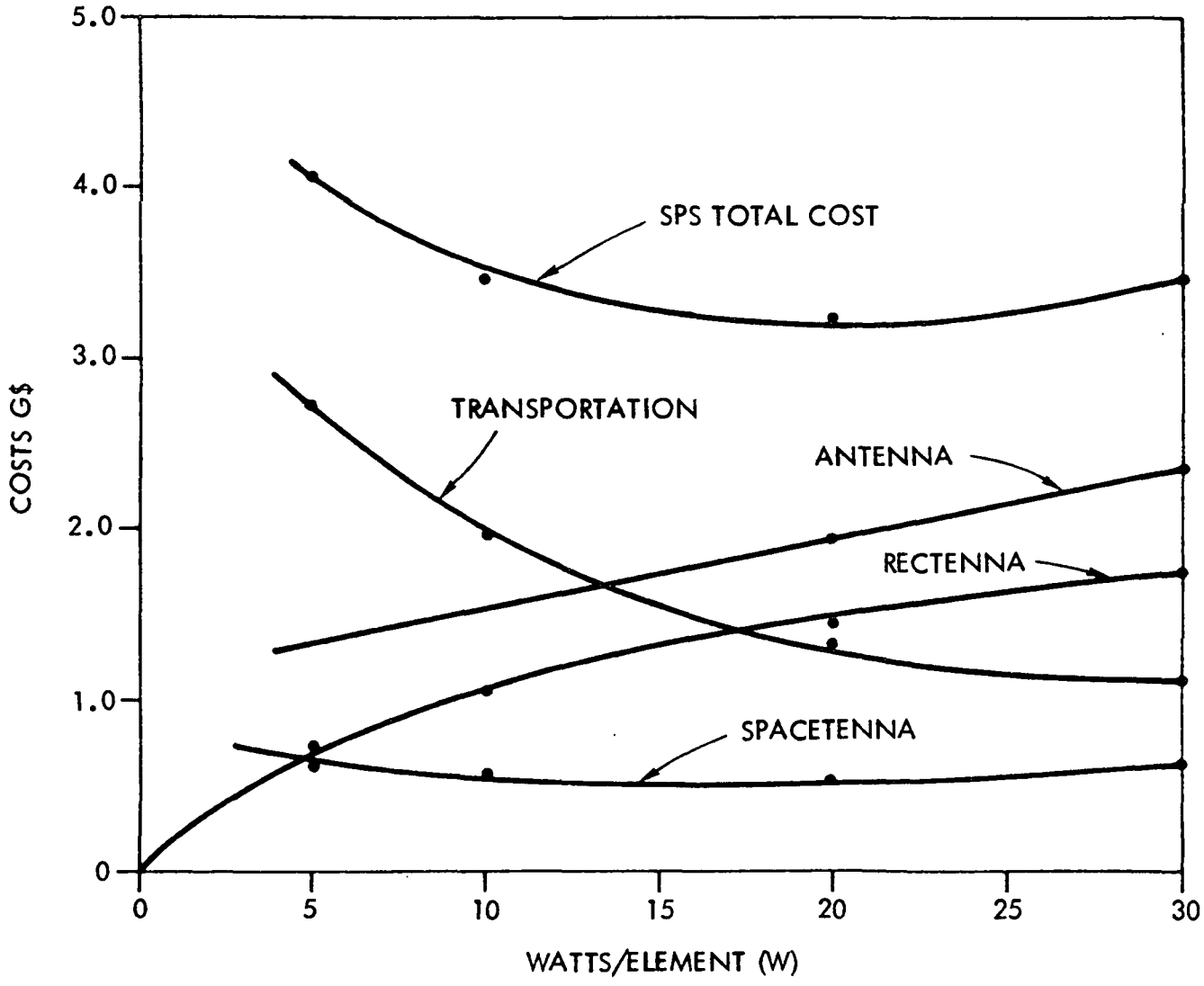

Figure 3.10-2 Solar Power Satellite System and Subsystem Costs

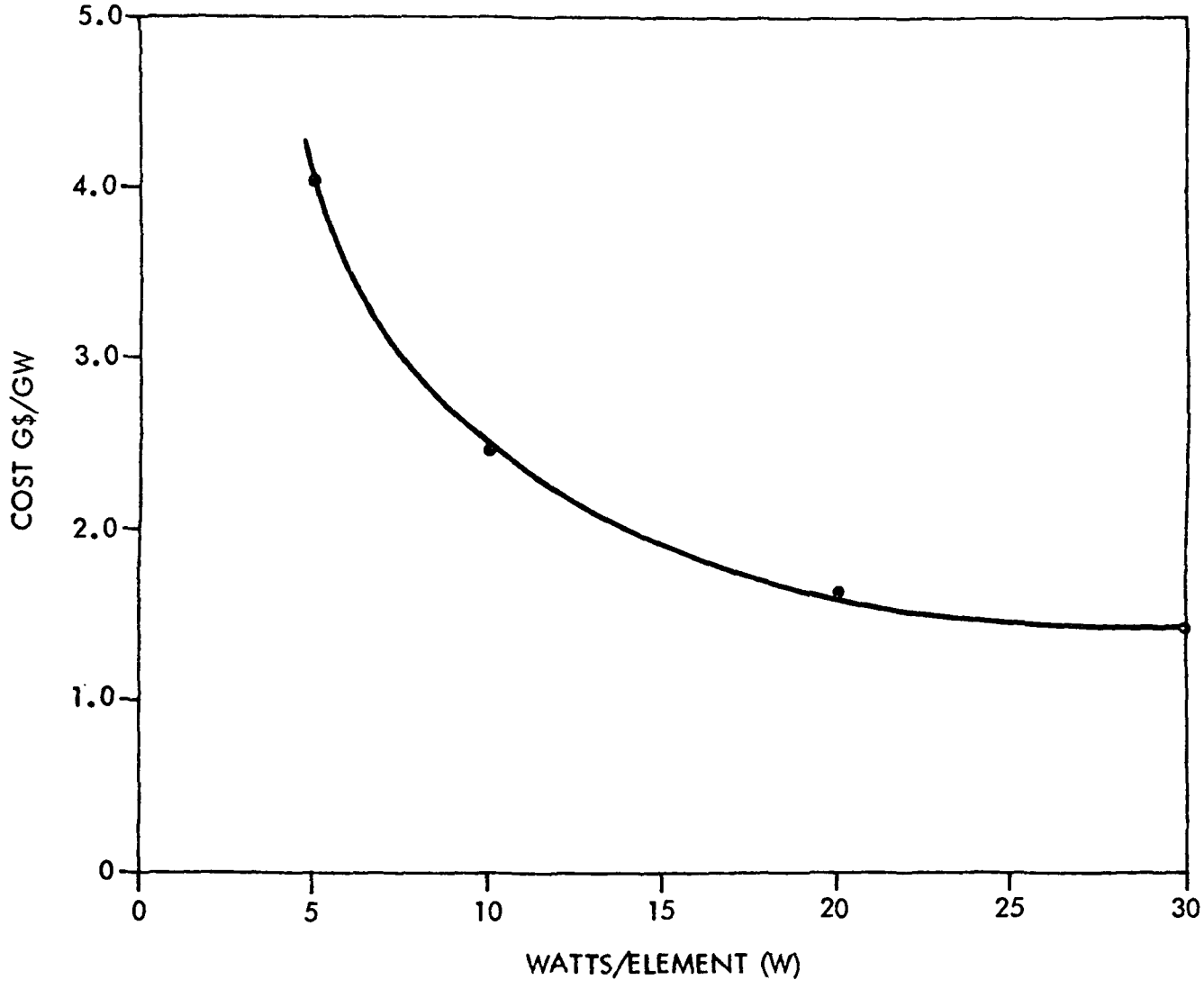

Figure 3.10-3 Solar Power Satellite Cost Figure of Merit

Table 3.11-1
Conclusions

1. Select Uniform Illumination
   - Minimizes Spacetenna Diameter
   - Simplifies Active Element and RF Feed

2. Select Dipole Radiator Implementation
   - Lightweight
   - Low Impedance For Best FET Operation
   - Most Room for RF and DC Feeds

3. Select Goal of Between 10 and 15 Watts RF Output Per Active Element
   - Minimizes Cost Per Watt

4. Continue to Investigate, With Imaginative Thinking In All Areas, and Do Not Incorporate The Above Conclusions As Constraints On Such Investigations
   - The Potential Is Only Beginning To Become More Clear

2 kW/m^2 or higher. This, having happened in a relatively short period, tends to confirm the optimistic view that "solid state is the answer because of the great strides that have been made over the years and because there are many imaginative people working to advance solid state concepts, technologies and associated applications."

It does remain to be shown, however, that (a) the relatively high efficiency of ≈80% can indeed be achieved, (b) the life of the system can indeed be as high as 30 years, and (c) costs can indeed be at a low $/amplifier level while maintaining stringent space flight performance, including reliability at high power, requirements.

A specific advanced technology development program for the amplifiers tailored to the SPS application is required to resolve these issues. This is a several million dollar undertaking, however it should be given serious consideration. Similar programs, primarily for lower power applications but in other senses having more stringent requirements, have advanced the technology significantly and they have a spin-off to this application. The exceptionally high power, particularly long life, exceedingly low cost and high not-yet-attained efficiency goals are the drivers necessitating a dedicated advanced technology development program.

The first phase of such a program must include further MPTS studies to formulate the specific goals and further SPS system investigations to refine the imaginative approaches already conceived, as well as conceptual investigations of yet more imaginative approaches primarily to reduce cost and to permit a properly progressive development program.

It should be noted that such solid state investigations and technology developments have a place in the high power tube approach as well. Independent of the decision as to solid state versus tubes for primary power transmission, the solid state technology must be developed.

With the above perspective, the conclusions of Table 3.11-1 continue to apply. The selection of uniform illumination is good and proper for limited breadth and depth investigations but should not be construed as "the answer" to limit further imaginative thinking. Similarly, the dipole radiator has its proper place as a

leading contender, but should not be taken as clearly the optimum implementation. Again the 10-15 watt RF output per active element should not be so constrained, however it is a tough but reasonable goal for the autonomous sandwich approach.

The fourth conclusion is not a disclaimer rather an endorsement of the imaginative thinking that has brought the overall SPS and solid state MPTS, in particular, this far.

SECTION 4
RF ELEMENT SELECTION

The solid state sandwich concept is represented by the subarray schematic diagram of Figure 4-1. Here incident solar energy concentrates on the solar cells on the back of the solid state sandwich panel. Here conversion to DC takes place and the DC powers all the amplifiers and phase conjugation electronics. Also incident on the sandwich is an RF pilot signal from the ground. This pilot signal is picked up by a high bandwidth set of antenna elements, combined, amplified, phase conjugated, amplified, divided, amplified again and divided to provide the RF drive power for each of the narrow-band high power transmit dipole amplifiers. The narrow-band transmit dipoles are orthogonal to the pilot signal receive dipoles.

Several candidate implementations were investigated for the radiators and power division/combining networks as follows:

- Electric dipoles above a ground plane
- Slot radiators on a ground plane
- Patch radiators on a dielectric slab

The ratings of these candidates are listed in Table 4-1. The electric dipole concept, as shown in Figure 4-2, is comprised of printed transmit and receive dipoles on a kapton sheet. The transmit dipole is very thin for filtered operation over a narrow bandwidth at 2.45 GHz, the receive dipole is in the shape of a bow tie for good impedance match to the pilot beam at 2.55 and 2.30 GHz; it is also orthogonal to the transmit dipole for good transmit/receive isolation. A quarter wave section transforms the high dipole impedance to match the low module output impedance and provide balun action. The power dividers and combiners can be laid directly on the ground plane surface or in stripline layers below or a combination thereof. The kapton sheet on which the elements are mounted and supported is otherwise open to provide a clear thermal radiation path for the rejection of the FET amplifier junction and other waste heat. The DC voltages can also be brought in along the top of the ground plane via feedthroughs from the DC combining networks.

The slot or magnetic dipole concept is shown in Figure 4-3. The transmitting slot is thin, having a narrower bandwidth than the receiving slot. There is essentially no room on the ground plane for transmission lines. Also the slots require dielectrically loaded cavities to obtain an efficient radiation resistance;

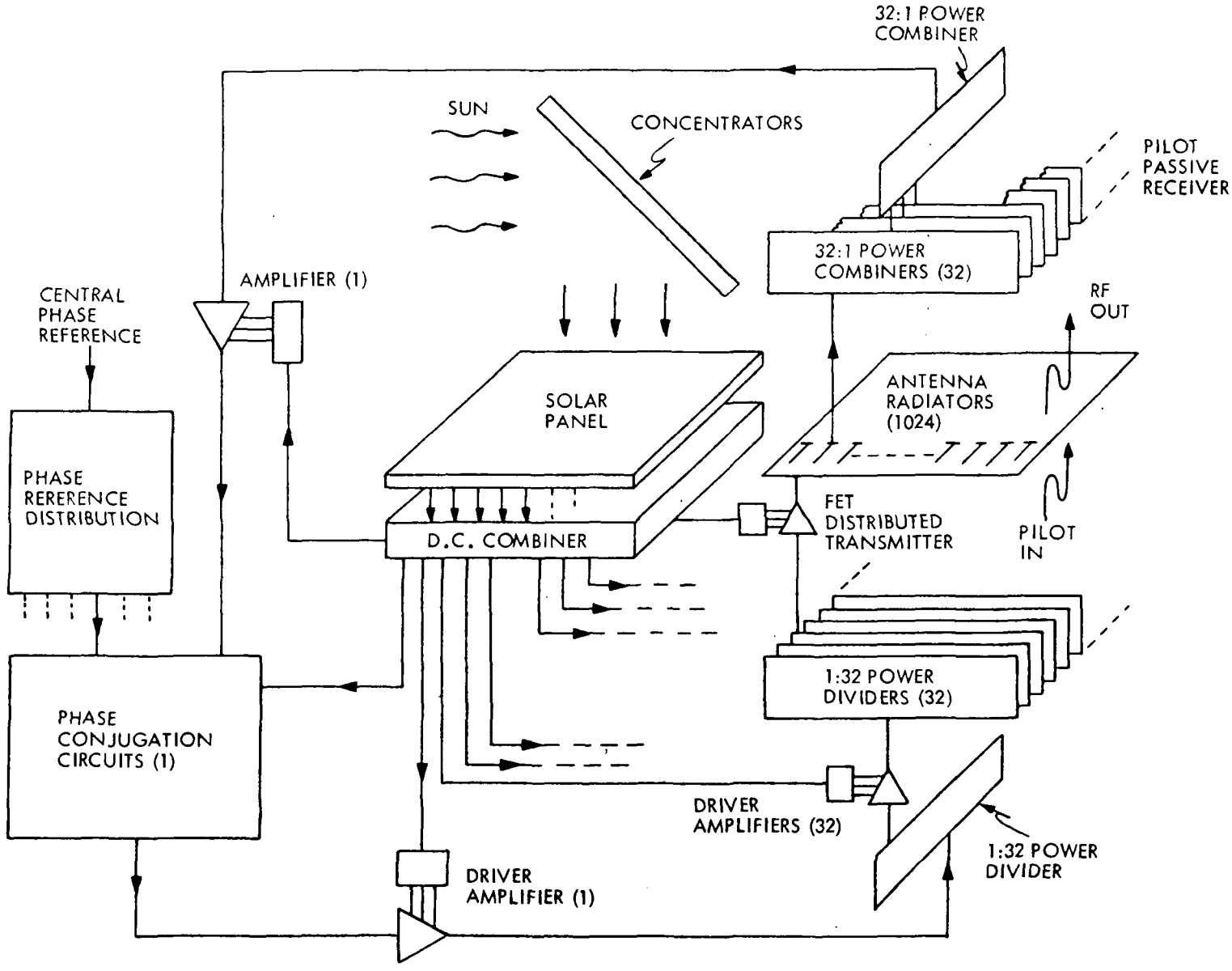

Figure 4-1 Solid State MPTS Spacetenna Subarray Circuit Diagram

Table 4-1 Radiator Implementation Comparison

DESIGN FEATURE	PERFORMANCE RATING		
	ELECTRIC DIPOLE	SLOT	MICROSTRIP PATCH
Overall Design Simplicity	E	F	P
Weight	E	F	F
Transmit Match	G	G	G
Pilot Wideband Match	G	F	F
Transmit - Pilot Isolation	E	F	F
Thermal Radiation Window	G	E	G
Transmission Line Space Availability	E	F	P
Module RF Interface	G	G	F
Module Equipotential (Ground)	E	F	P
Module DC Interface	E	F	P

E - Excellent
G - Good
F - Fair
P - Poor

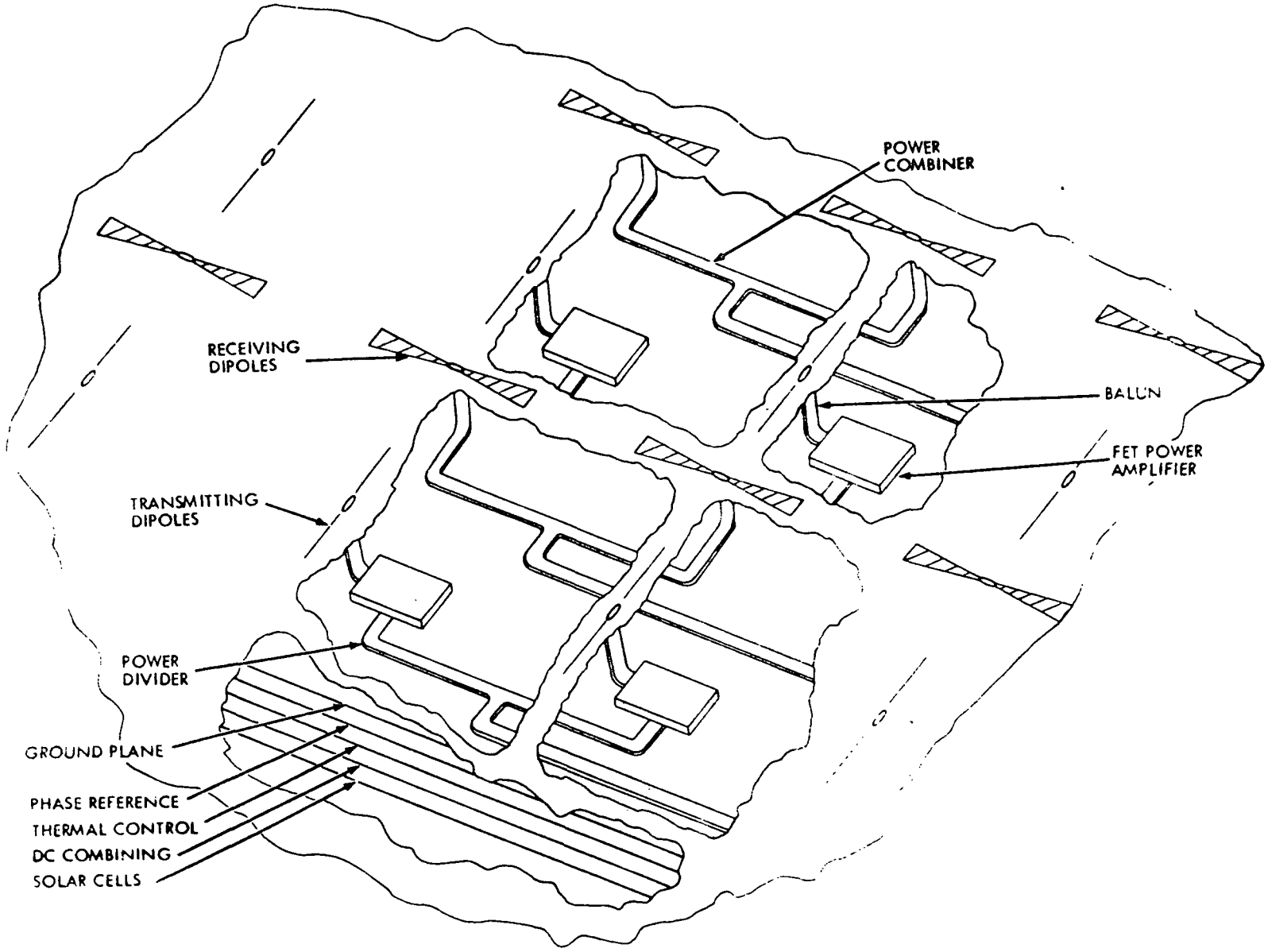

Figure 4-2 Spacetenna - Dipole Concept

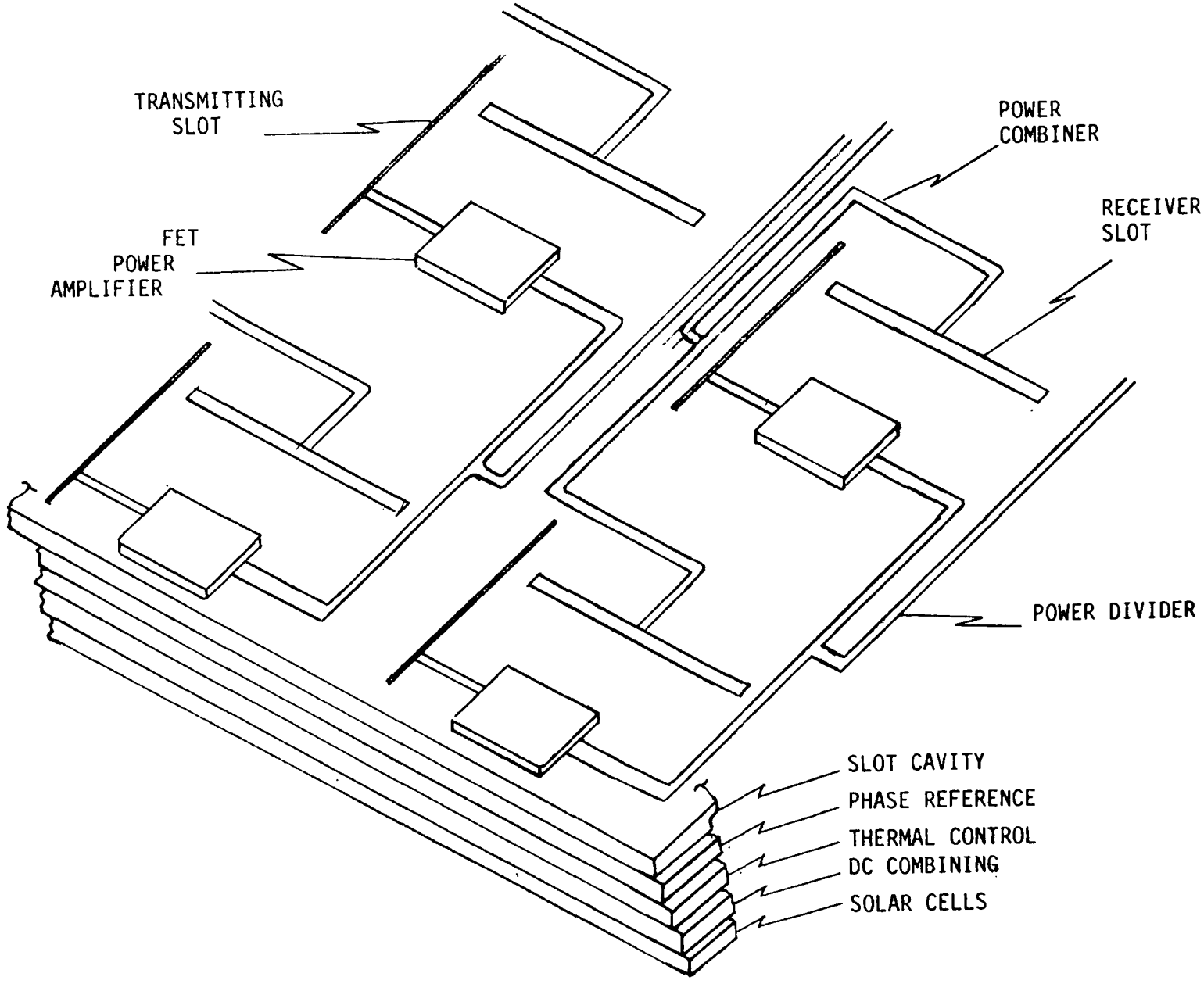

Figure 4-3 Solid State MPTS Spacetenna - Slot Concept

therefore a dielectric layer is needed. Since the power division and combining must be in stripline below the cavities, feedthroughs are necessary to excite the slots. The amplifier modules are mounted directly on the ground plane which provides a good surface for efficient heat radiation and module ground. The thin slot is offset fed for a lower input impedance. Although the slots are mounted orthogonally, they are not oriented symmetrically, therefore a degradation in isolation cannot be avoided.

The patch radiator concept is shown in Figure 4-4. The patch is a conductor etched on a dielectric disc which is mounted on a ground plane or on a dielectric slab. The patch can be excited by parallel probes with 90° (quadrant) translation with respect to each other. The amplifier module is mounted on the conducting patch with a DC return provided by a central coaxial feedthrough. This is an integrated approach and as such it is difficult to approach optimum designs for any of the three functions, RF, DC and thermal dissipation. The amplifier module is mounted above the RF ground plane and above the DC equipotential surface. Although a clear heat transfer path from the module to free space is provided, the waste heat radiation is limited by the patch size and the thermal flow from the solar cells is constrained by the dielectric slab material. The input exciting probes will tend to couple; also higher mode generation is possible.

The latter two approaches are heavier than the dipole concept since they require dielectric loading to obtain efficient radiation. They also require the feed transmission lines to be located below the ground plane adding stripline layers for power division and combining.

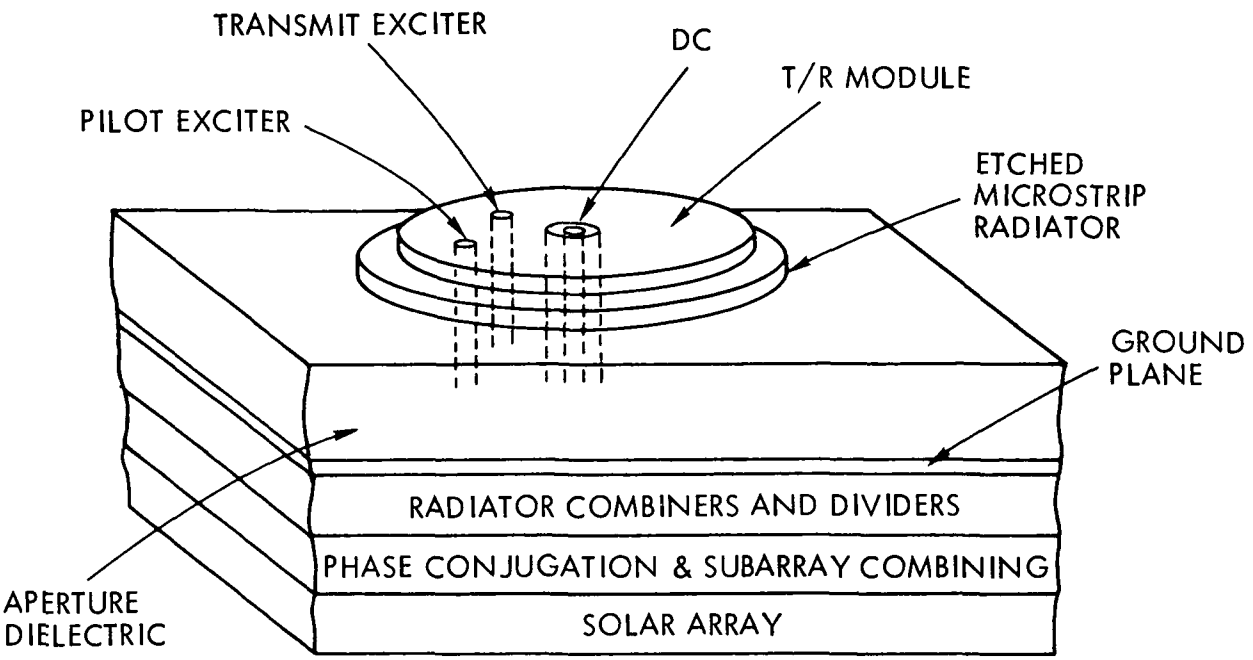

Figure 4-4 Microstrip Patch Radiator

SECTION 5
MICROWAVE DEVICES AND CIRCUITS

This section presents the results of concept definition and preliminary design investigations into:

(a) Microwave Device Performance
(b) Simplified Amplifier Circuit Considerations
(c) Active Element Transmitter
(d) Harmonic Noise Generation, Suppression and Transmission Characteristics
(e) Active Element Pilot Receiver
(f) Present State of the Art Versus SPS Amplifiers.

5.1 MICROWAVE DEVICE PERFORMANCE

The microwave active element provides the high-power microwave amplification of the microwave drive signal and this amplified power is the vehicle for the transmission of electrical power from the SPS. With an operating frequency of 2.45 GHz the candidate technologies for the microwave device can be narrowed to those given in Table 5.1-1.

Table 5.1-1 Candidate Device Technologies

- Silicon Bipolar Transistors
- Gallium Arsenide Bipolar Transistors
- Silicon MESFET Devices
- Gallium Arsenide MESFET Devices

Of this group of technologies, the silicon bipolar and GaAs MESFET devices are the most prominent. The silicon technology is well adapted to operating frequencies up to 3 GHz, while GaAs devices are well suited to applications above 2 GHz. Silicon device processing is well established as a manufacturing technology and the raw materials are relatively easy to acquire. GaAs technology, on the other hand, is still in development and the wafer materials have limited availability.

The technology selection criteria, however, must be based on the operational performance of the microwave devices. In an SPS application the criteria of device

performance as an amplifier are high amplification gain, high power added efficiency and high power density. Based on these criteria, it would appear that the optimum device technology would be the GaAs MESFET devices because of the inherent advantage of the higher electron mobility of GaAs versus that of silicon. The choice of MESFET rather than bipolar is based on two factors. The processing involved in the manufacture of an FET device is simpler than that of bipolar devices because the FET structure is surface defined while the bipolar structure is dependent on vertical diffusion technology which is difficult with GaAs materials. The second factor is that a MESFET is a majority carrier device which is an advantage under high power operation. Imbalances in device heat dissipation are self-limiting and so prevent localized hot spots that would degrade reliability. Bipolar transistors which are minority carrier devices tend to develop hot spots that can degrade or eventually destroy the device.

In an SPS application the microwave amplifier must have a high power-added efficiency, which is the ratio of the RF output power divided by the sum of the DC amplifier bias power and RF input drive power. With a high RF gain, the input drive power does not have a large effect on overall efficiency. The other factor, the DC bias power, is dependent on the class of operation of the microwave device in the amplifier. The criteria for judging amplifier performance and their relationship to the amplifier class of operation are given in Table 5.1-2. Notice that these criteria are very similar to those of the device.

The three common classes of operation are Classes A, C and E. The gain figures are relative to Class A small signal operation for any given device. The efficiency factors are theoretical limits and the output power capabilities are normalized to a device limited power factor called P_{MAX}. This factor and other terms used in later paragraphs are summarized in Table 5.1-3. Note that Class A operation has the best gain and power output capabilities but is severely suffering in efficiency. Class C operation has much better efficiency performance but has a lower gain because its inherent non-linear operation does not use the full input signal swing. Class E operation is similar to Class C but it shows the most efficient operation because it minimizes dissipation in the active device by controlling the voltage and current waveforms. It appears that some form of a Class E operation is required for the microwave amplifier in SPS.

Table 5.1-2 Microwave Power Amplifier Circuit

Basic Amplifier Requirements

- High Gain
- High Efficiency
- High Output Power

Circuit Operational Mode: Theoretical

Class	A	C	E
Gain (Relative)	0 dB	-6 dB	-6 dB
Efficiency	50%	90%	100%
P_{Out}/P_{Max}	0.125	0.098	0.098

Table 5.1-3 Definition of Microwave Terms

F_{MAX}	Frequency Where Power Gain Reduced to 1 (0 dB)
BV_{CB}	Breakdown Voltage, Collector-Base
I_{CMAX}	Maximum Saturated Collector Current
R_{SAT}	Effective Collector-Emitter Saturation Resistance
BV_{GD}	Breakdown Voltage, Gate-Drain
I_{DSS}	Saturated Drain Current
$R_{CHANNEL}$	Effective Channel Resistance
EFFICIENCY	Power-Added Efficiency
P_{MAX}	(Max Voltage) x (Max Current)
Q	Component Q
Q_M	(Component Q)/(Impedance Transform Q)

The relationship of device performance to amplifier performance is given in Table 5.1-4. The amplifier circuit uses the device in a mode that can be modeled by a switch that has operational limits. These limits are determined by the device characteristics which are in turn a function of the physical parameters of the device. The amplifier performance can be directly determined by the device structure and processing or, put in another way, the performance can be optimized by the proper design of the active device. However, in general the electrical parameters can be optimized in the design independently because each physical parameter affects the electrical parameters differently.

Table 5.1-4 Microwave Device Characteristics

SWITCH MODEL	BIPOLAR	MESFET
Electrical Parameters:		
High Gain at Operating Frequency	F_{MAX}	F_{MAX}
High "Off" Voltage	BV_{CB}	BV_{GD}
High "On" Current	I_{CMAX}	I_{DSS}
Low "On" Voltage	R_{SAT}	$R_{CHANNEL}$
Physical Parameters:		
	Base Width	Gate Length
	Base Doping	Channel Depth
	Emitter Periphery	Channel Doping
	Base Area	Mobility/Saturated Velocity
	Collector Doping	Gate Width
	Collector Thickness	

5.2 SIMPLIFIED AMPLIFIER CIRCUIT

The design of the amplifier for a Class E operational mode can be based on a simplified circuit model as shown in Figure 5.2-1. The device is modeled as a switch with some loss and is terminated at its output with real and reactive loads at the fundamental frequency and all its harmonics. These terminations determine the magnitude and phase of each frequency component of the voltage and current waveforms across the device and the terminations. These waveforms can be used to calculate the circuit losses due to power dissipation in the active device and in the non-ideal dissipative components that make up the actual circuit. This circuit model was the basis for a simulation of the voltage and current waveforms for a pseudo Class E operation shown in Figure 5.2-2. This simulation uses the Class E principles to minimize transistor dissipation during the switching intervals, but efficiency is ultimately limited by the loss characteristics of the actual device and the impedance matching components of the circuit. Simulations such as this can be used to determine which elements and parameters have the greatest effect on the overall efficiency.

With this general technique, an effective efficiency budget distribution for the circuit can be generated to determine an estimate of the overall circuit, as shown in Table 5.2-1. Based on projected realizable components, but not necessarily on today's available state of the art, it should be possible to realize a net efficiency of about 80%. Note that no factor has been shown for load mismatch effects because it should be possible to match the antenna loading impedance to that required by the amplifier. However, in actual experience mismatches usually result because of tolerances and possible antenna steering when the antenna array is viewed as a phased array.

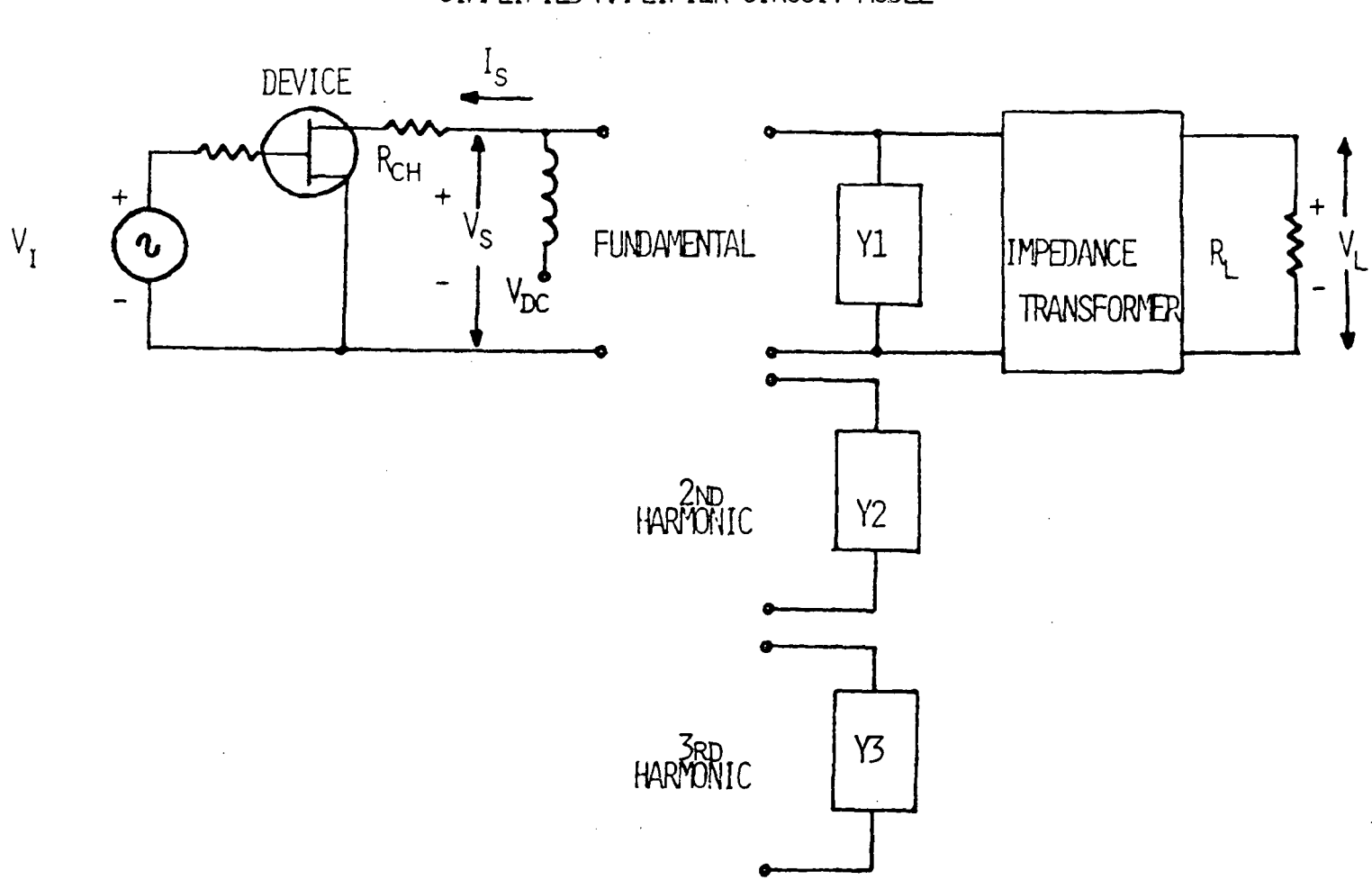

Figure 5.2-1 Simplified Amplifier Circuit Model

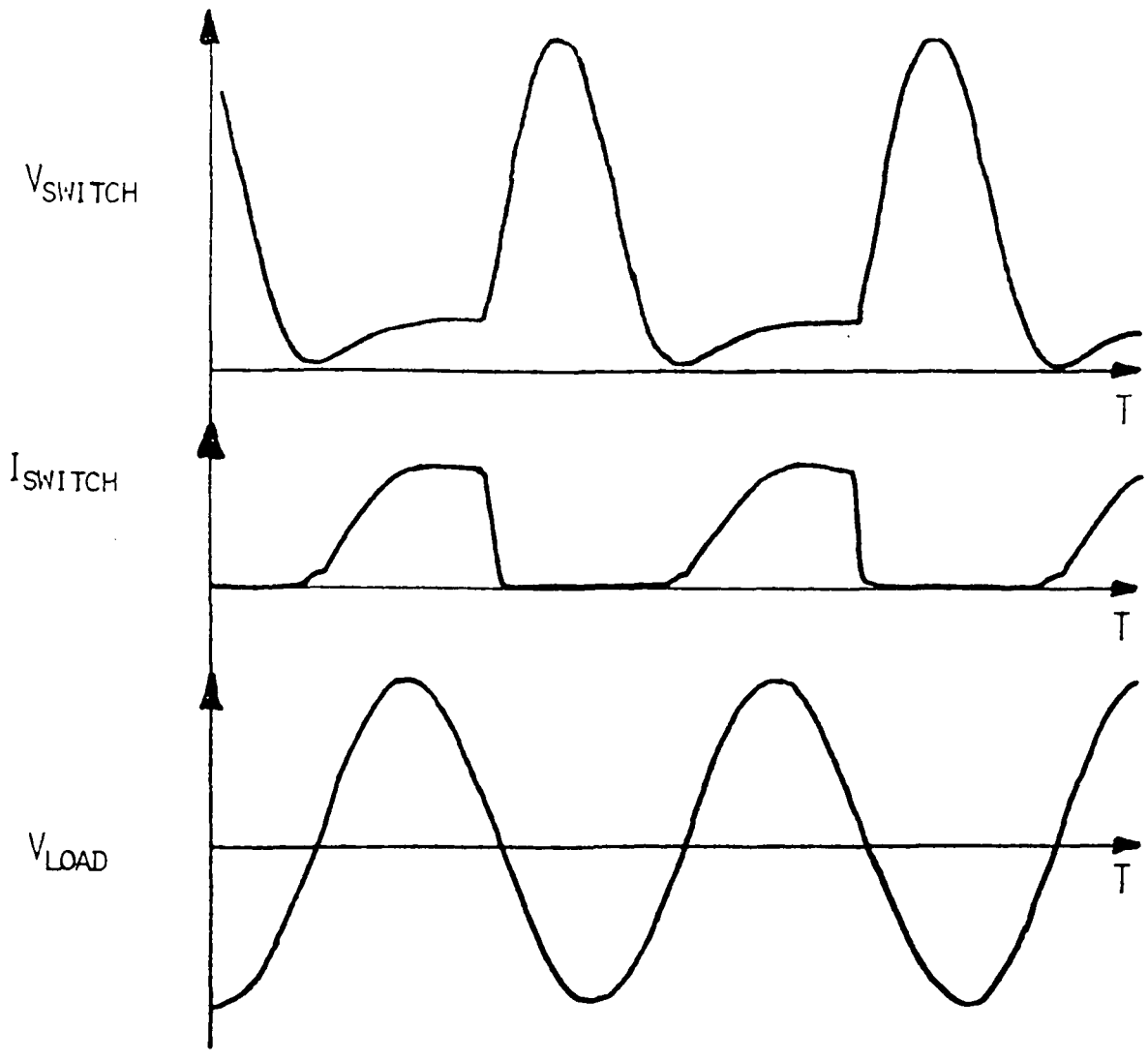

Figure 5.2-2 Simulated Microwave Power Amplifier Waveforms

Table 5.2-1 Microwave Power Amplifier

Degradation of Power-Added Efficiency	Typical	Efficiency Factor
• Finite Gain	15 dB	.97
• Switch Resistance	$(36/P_{MAX})$ Ohms	.90
• Circuit Loss		
Fundamental	Q = 50	.98
Harmonics	Q = 70	.99
• Load Transformer	Q_M = 30	.94
• Load Mismatch	--	--
• Efficiency Factor Product		.80
Net Efficiency About 80%		

5.3 ACTIVE ELEMENT TRANSMITTER

The block diagram in Figure 5.3-1 indicates the function requirements and how they interact for the active element transmitter. It is only prudent at this point in concept definition to include both harmonic and noise filtering as requirements to begin to understand their impact on the system. For this purpose, their being necessarily in series with the matched power from the amplifier will contribute to the efficiency chain. Again for the purposes of subsequent assessment, a value of 96% for the filters has been selected as a preliminary design value.

5.4 HARMONIC NOISE GENERATION, SUPPRESSION AND TRANSMISSION CHARACTERISTICS

The transmitter noise density requirement as seen at the earth is estimated, as shown in Table 5.4-1, to be -181 dBW/m^2/4 kHz for 2 GW total transmitted power. For multiple systems of 2 GW each the noise density on earth for points in line of sight would increase and for 500 systems it would be -154 dBW/m^2/K khz.

The amplifier noise requirement is therefore established as -156 dBW/Hz noncoherent between subarrays as a goal. Achieving this goal must be a primary objective for the advanced technology development program.

ACTIVE ELEMENT TRANSMITTER

REQUIREMENTS

- o GAIN
- o EFFICIENCY
- o HARMONIC SUPPRESSION
- o NOISE FILTERING

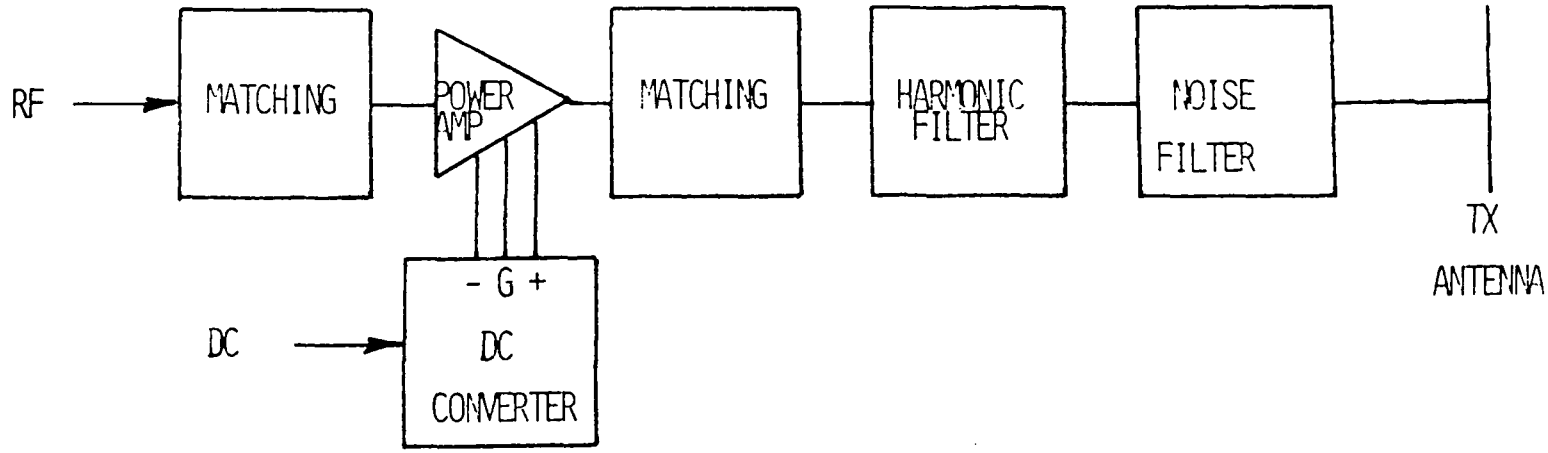

Figure 5.3-1 Transmitter Active Element Block Diagram and Requirements

Table 5.4-1 Transmitter Noise Goals

Total Transmitter Power (2 GW)	+ 93 dBW
Amplifier Noise Relative to Carrier	-156 dBW/Hz
$G_T = (4 \pi A_T)/(\lambda)^2$ $A_T = (0.1m)^2$, $\lambda = 0.12m$	+ 9 dB
$G_R = (4 \pi A_R/(\lambda)^2$ $A_R = (1m)^2$	+ 29 dB
$L_P = (4 \pi D/\lambda)^2$ $D = 3.71 \times 10^7$ m	-192 dB
Noise Density At Earth	-217 dBW/m^2/Hz
CCIR Requirement (-154 dBw/m^2/4 kHz	-181 dBW/m^2/4 kHz

Noise filters are, in the interim, to be provided and accounted for at the element module level on transmit and at the subarray conjugating electronics level on receive.

The residual harmonic power density that may be coherent over the total transmitting array periodically as estimated at the earth is -66 dBW/m^2 at the third and less at higher harmonics. Table 5.4-2 summarizes the estimate for the transmitter harmonics. Since grating lobes for the second harmonics do not intersect the earth, it is not considered a fundamental requirement to contend with.

Table 5.4-2 Transmitter Harmonics

Harmonic Output Correlated Element to Element	
Mainbeam at Earth (23 mW/cm^2)	+ 24 dBW/m^2
Grating Lobe Suppression	- 10 dB
Harmonic Level Relative To Carrier	- 80 dB
Grating Lobe At Earth	- 66 dBW/m^2

This may be difficult to achieve as a goal and it may lead to a requirement for frequency allocation at third and higher harmonics. Spread spectrum as well as active suppression should be investigated as possible mitigating approaches.

5.5 ACTIVE ELEMENT PILOT RECEIVER

The block diagram in Figure 5.5-1 indicates the functional requirements and how they interact for the active element except that there is the limiter function as well as a bandpass notch filter and the polarization is orthogonal to that of the transmitter for isolation purposes. The amplifier in this case is a low noise amplifier.

5.6 PRESENT STATE OF THE ART VERSUS SPS AMPLIFIERS

Virtually all electronic functions of the SPS solid state amplifier can be done using today's technology. However, the requirement for small size, low weight, high power, long life, very high efficiency, and low cost for the SPS application dictates the technology development program requirements. Specifically the amplifier must be small compared to a 10 x 10 cm cell, i.e., as a package it must be in the region of 3 cm^2 x .5 cm thick and weigh about 3 grams. At this size the weight goal will be about 3.32 grams per amplifier (an order of magnitude less than that available from present technology). It must produce power in a range of RF power levels of about 2 to 20 watts or higher per amplifier (several amplifiers at several specific power levels; two or more may be required). The life expectancy for 20 to 30 years must be at a high probability with a goal of 80% or higher at a most critical junction temperature of 140°C and 98% or higher at a most critical junction temperature of 114°C (assuming the total amplifier life is driven by the life of only one junction) without the complexities of switchable redundancy. The efficiency must be in the vicinity of 80% with a goal of 85% or higher (75% is the lower limit of interest).

Going along with the small size, low weight, high power and long life goals and assuming that the very high efficiency goals may be achieved, the low cost requirement will consume a major segment of an advanced development program for the SPS application.

Present L-band modules have similar but admittedly more complex functions to perform at a cost in excess of a thousand dollars each. Advanced technology programs, in the frequency region of interest to SPS, have adopted an order of magnitude reduction in cost as a goal.

ACTIVE ELEMENT PILOT RECEIVER

REQUIREMENTS

- o SENSITIVITY (NOISE FIGURE)
- o ISOLATION FROM TRANSMITTER
  - o CARRIER AND HARMONICS
  - o NOISE
- o GAIN
- o DAMAGE LEVEL LIMITING

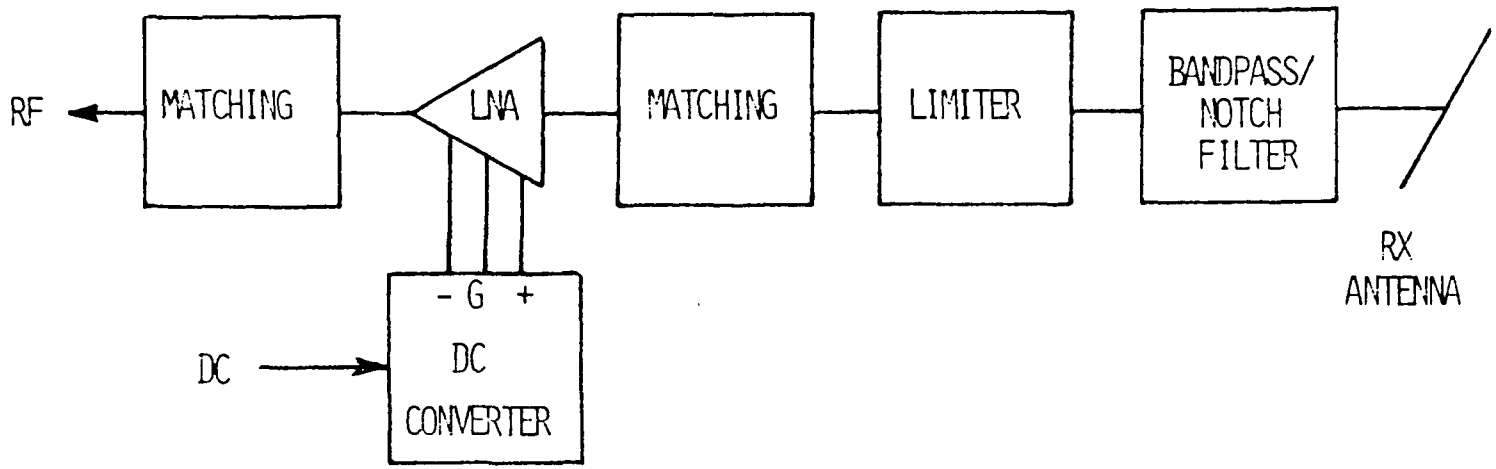

Figure 5.5-1 Pilot Receiver Active Element Block Diagram and Requirements

The key to achieving both low cost and light weight in such amplifiers is to innovate effective batch processing or monolithic techniques. By doing batch processing, that is many units in one photolithographically delineated substrate or wafer, the cost for SPS amplifier applications may be lowered. This lowering of cost occurs because the price to fabricate a wafer using photolithograhic and implantation techniques is insensitive to batch size. Therefore, the more amplifier assemblies that can be made in one batch the lower the unit cost will be. Obviously by putting more amplifiers on one substrate, a size reduction that can be translated directly to weight is also achieved.

Techniques to be investigated for making SPS power amplifiers or functional subassemblies should include lumped element, matching elements with discrete semiconductor chips or possibly full monolithic techniques.

The possibility for full monolithic techniques is a strong function of the yield which is a strong function of the magnitude of the power output required since the area of the device associated with the junction is at least proportional to power and imperfections in the necessary semiconductor area therefore increase with power.

The preliminary goals for weight and cost of SPS amplifiers should be set at about 3 grams and less than 10 dollars. How much less than 10 dollars per amplifier as well as whether or not it can be achieved and whether or not the industry could or would find it viable are questions that could only be answered progressively as an advanced development program is initiated and progresses.

SECTION 6
POWER BALANCE, THERMAL MODELING AND EXPECTED LIFE

This section presents the results of concept definition and preliminary design investigations into:

(a) Power Balance and Partitioning

(b) Amplifier Thermal Model

(c) Amplifier Expected Life Relationships Due to Thermal Considerations.

These are the key inputs to Section 8 (Basic Parametric Relationships and The Derivation of Resulting Data) pertaining to the achievement of maximum performance in terms of RF power density at the spacetenna with long life and compatibility with the DC power supply and distribution options.

Terms such as T_J, P_{SM}, P_{SE}, etc. are more completely defined in Section 8.

6.1 POWER BALANCE AND PARTITIONING

The concept of partitioning the microwave array surface into sections dedicated to dissipation of solar array waste heat in one region at high temperature (compatible with photovoltaic temperature limits) and microwave waste heat in another region at lower temperature (compatible with amplifier junction temperature limits) has been addressed at the antenna cell size of 10 x 10 cm and in large scale across the aperture.

Figure 6.1-1 depicts the thermal power balance associated with the total system. For the Raytheon antenna concept and the concept of distribution of amplifiers relatively uniformly over the subarray, partitioning below the subarray level is not recommended. This is because of the complexities of heat transport within the fundamental 10 cm x 10 cm cell, as will be discussed further in the section on basic parametric relationships and resulting data. The question that could not be resolved satisfactorily was how to assure transport of P_{SM} to a dedicated region operating at high relative temperature without undue thermo-mechanical complexities and at the same time preclude unwanted heat leak to lower temperature regions associated with the critical amplifier junctions.

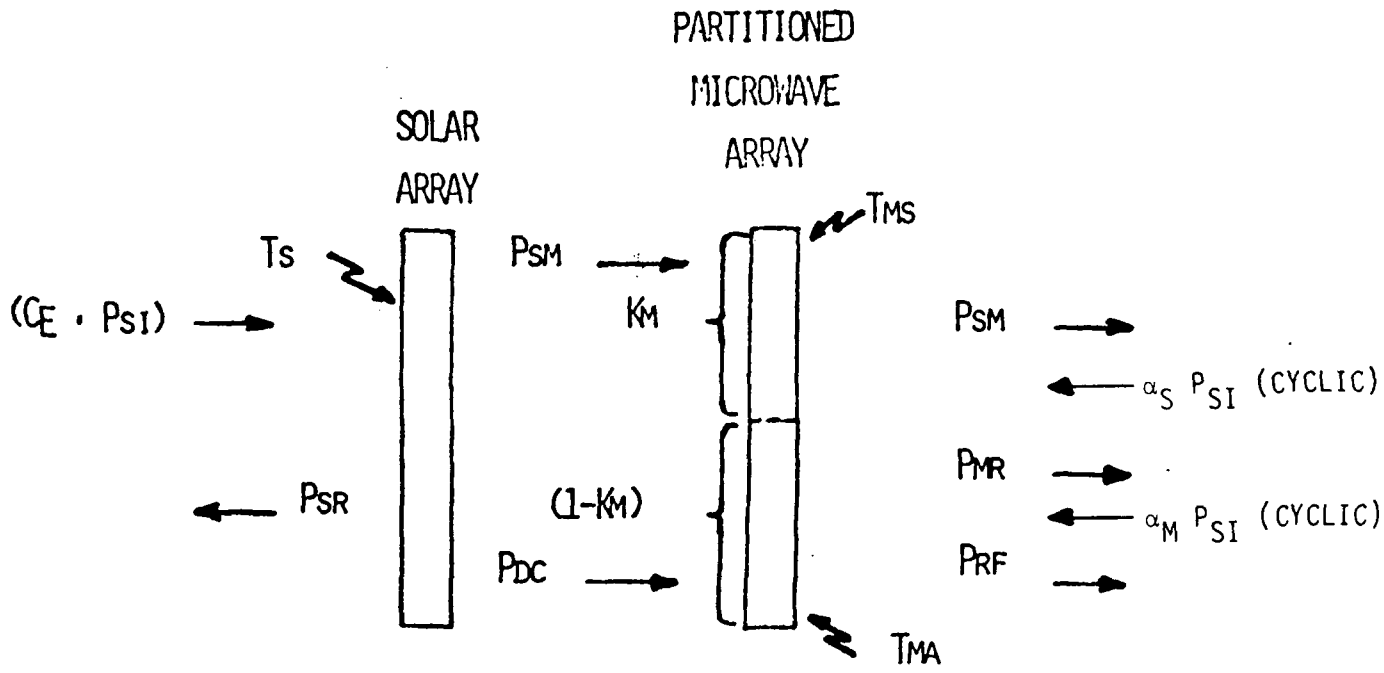

THERMAL POWER BALANCE ON SOLAR ARRAY AND K_M PARTITION OF MICROWAVE ARRAY SURFACE

$$P_{SW} = P_{SR} + P_{SM}$$

WHERE

$$P_{SW} = (\alpha_S - N_S)\, C_E P_{SI}$$

$$P_{SR} = \epsilon_S\, \sigma\, (T_S + 273)^4$$

$$P_{SM} = K_M \epsilon_M \sigma (T_{MS} + 273)^4$$

Figure 6.1-1 Preliminary Thermal Power Balance

Table 6.1-1 defines the thermally related terms and although K_M is termed the "effective" fraction of microwave surface. "Effectiveness" is intimately related to temperatures of the ground plane and to the waste heat associated with RF power generation. It was considered most relevant to treat K_M locally as being either 1, 0, effectively negative, or resolved as a simultaneous equation relating the solar array portion to the microwave portion with P_{DC} and P_{SM} as relatively uniformly distributed elements of the system. As will be seen in the parametric relationships and resulting data section, for the maximization of total energy transmitted over time, it may be desirable to transport P_{DC} surpluses from the solar array side to regions of the aperture where higher RF power density is required.

Table 6.1-1 Definition of Thermally Related Terms

C_E	Effective Concentration Ratio
P_{SI}	Incident Solar Power: 1353 W/m^2
P_{DC}	DC Electrical Power From Solar Array
P_{RF}	Radiated Microwave Power
P_{SR}	Thermal Power Reradiated from Solar Cells
P_{SM}	Thermal Power From Solar Cells Radiated From Microwave Array
P_{SW}	Total Waste Thermal Power From Solar Cells
P_{MR}	Thermal Power From Microwave Circuits Radiated From Microwave Array
K_M	Effective Fraction of Microwave Surface Available for Solar Cell Waste Heat Radiation
T_S	Temperature of Solar Cells
T_{MS}	Temperature of Microwave Surface Available For Solar Cell Heat (km)
T_{MA}	Temperature of Microwave Surface Available For Microwave Amplifier Heat (K-1)
T_E	Temperature of Surface Available Simultaneously For Solar Cell and Microwave Heat ($T_E = T_{MS} = T_{MA}$)
N_S	Solar Cell Efficiency
N_M	Total DC to RF Efficiency of Microwave Array
N_D	Power-Added Efficiency of Microwave Active Device
α_S	Solar Cell Absorptivity (0.61)
ε_S	Solar Cell Emissivity (0.82)
ε_M	Microwave Surface Emissivity (0.82)
σ	Radiation Constant (5.67×10^{-8})
T_J	Junction Temperature of Microwave Active Device
MTTF	Mean Time To Failure

6.2 AMPLIFIER THERMAL MODEL

The amplifiers providing RF power to the transmitting dipoles and the amplifiers which drive the transmission grid are considered to be critical in that the thermal limitations for RF power transmission are at the junctions of those amplifiers.

The GaAs, Flip Chip approach to the FET device was selected as the best approach to minimize the temperature gradient between the junction and the heat sink. An 18 node representation of the device mounted at the center of a circular waste heat thermal conductor and radiator was employed to analyze the heat flows and temperature gradients associated with the device in the presence of the following; (a) its own waste heat to be dissipated P_A watts/element, (b) other waste heat from the microwave system ΔP_B associated with an element cell of 10 x 10 cm, (c) incident solar heat load P_S, (d) waste heat from the photovoltaic side of the sandwich and, (e) deep space temperature of absolute zero in one direction.

The thermal conductor geometry was that of a 10 cm diameter disc, 1 mm thick at the center, where the device makes thermal contact, tapered linearly to 0.1 mm at the edge. Three materials for the thermal conductor were investigated to introduce the effects of a range of conductivities and to provide a basis for weight estimates. (a) Heat Treated Pyrographite with a thermal conductivity of 12.5 W/cm ^{o}C and a density of 2.25 gm/cm^3. (b) Copper with a thermal conductivity of 3.5 W/cm ^{o}C and a density of 8.9 gm/cm^3. And (c) Aluminum with a thermal conductivity of 1.8 W/cm ^{o}C and a density of 2.7 gm/cm^3.

Analyses of computerized printouts of temperature at the several nodes indicated that the system could be represented by a simplified model, as indicated on Figure 6.2-1. This figure shows typical data from the computer printouts and the following relationsips were found to approximate the temperature to within 1 C^{o} over a broad range of the parameter values.

$$T_J \simeq T_E + \frac{\Delta T}{P_A} P_A$$

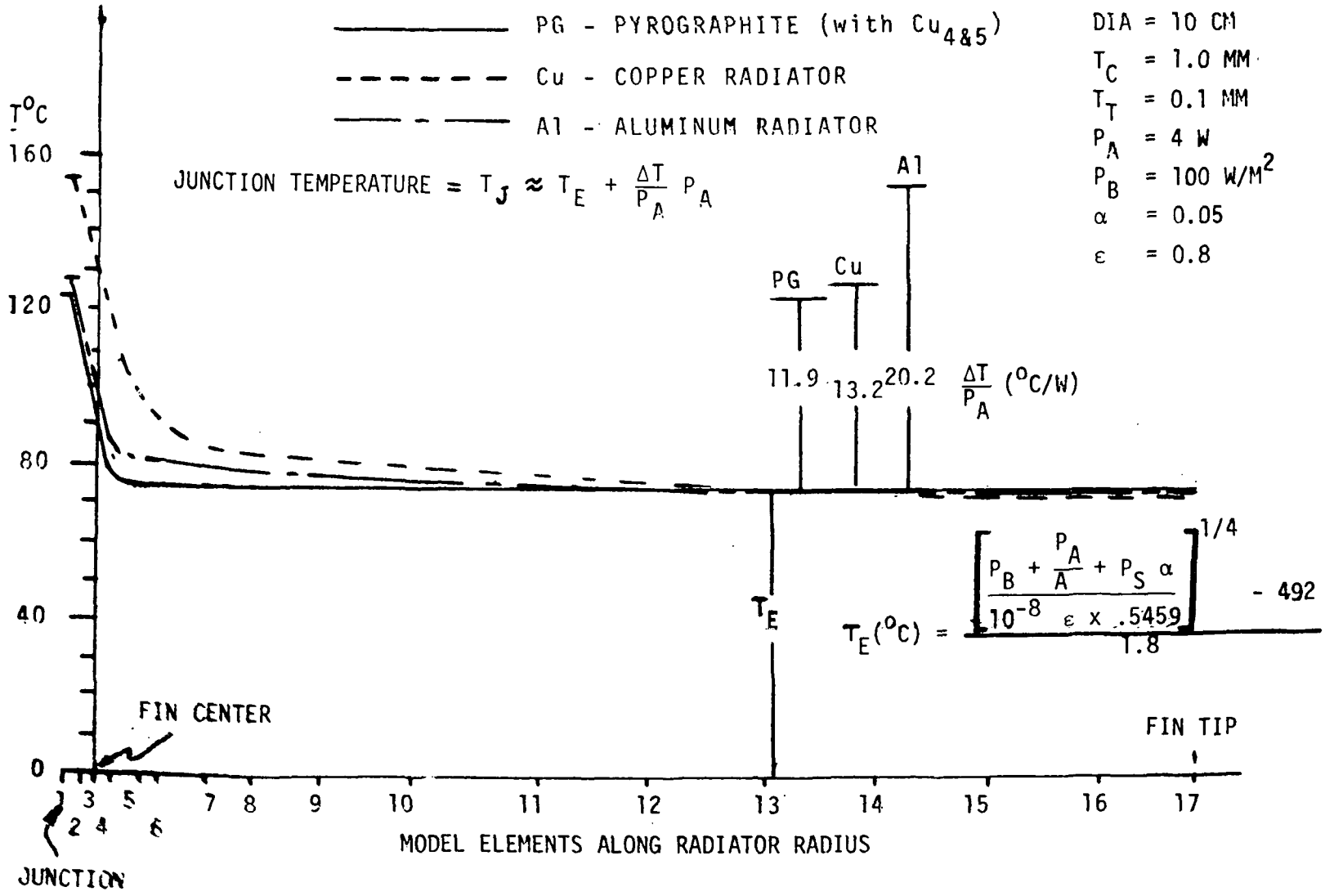

Figure 6.2-1 Amplifier Thermal Model

For the purposes of correlating this model with other parameters introduced as the study progresses the following relationships are defined:

P_B = Waste heat introduced to the thermal conductor network at points remote from the junction on the average are equivalent to a uniform heat load in terms of W/m^2. This includes (a) ΔP_B watts/m^2 from the non amplifier junction sources of the microwave and dc power transmission portions of the sandwich within a 10 x 10 cm cell and (b) P_{sm} watts/m^2 from the photovoltaic portion of the sandwich.

P_A = Waste heat (watts/cell) generated at the critical junction having temperature T_J (^oC).

A = Estimated area of the cell from the temperature gradient point of view.

P_S = Incident solar load W/m^2.

α = Absorptivity for P_S of the thermal control coating applied to the thermal conductor on the deep space side.

ϵ = Emissivity of the thermal control coating applied to the thermal conductor on the deep space side.

As may be seen, from subsequent design analyses, the waste heat radiator equilibrium temperature ranges between 70^o C and 120^o C while the system is operating. Similarly, the amplifier junction temperatures range between 110^oC and 140^oC.

The temperatures for non-operating conditions, particularly while in the shadow of the earth, are not included in these design analyses. They will be a function of the mass of the entire spacetenna/photovoltaic sandwich and they are not anticipated to be particularly low. It may however be important to control the lower limit for certain equipment including certain parts of the solid state system.

The basic concept is for passive control of the upper limits by control of heat leak paths as well as by selection and maintenance of the thermal control coatings. The concept for control of the lower temperature limits is

considered to be "active" which may include heaters with power from associated energy storage as required. Analyses for (a) the active control requirement and (b) the implementation should be the subject of further study.

Figure 6.2-2 indicates the absorptivity and emissivity values from presently available technology approaches to thermal control coatings. The projected life requirement is in a 30 year time period; the waste heat rejection goals are toward high emissivity simultaneously with low absorptivity; low cost and RF compatibility without degrading the microwave system are essential. The approaches to be taken must also recognize the need to achieve electrical conduction performance to preclude excessive local charge buildup. Compatibility must be developed to permit long life at the interface between the thermal conductors and other materials such as those that may be employed for thermal control coatings.

These taken together constitute a formidable set of requirements to be considered in the thermal control advanced development program.

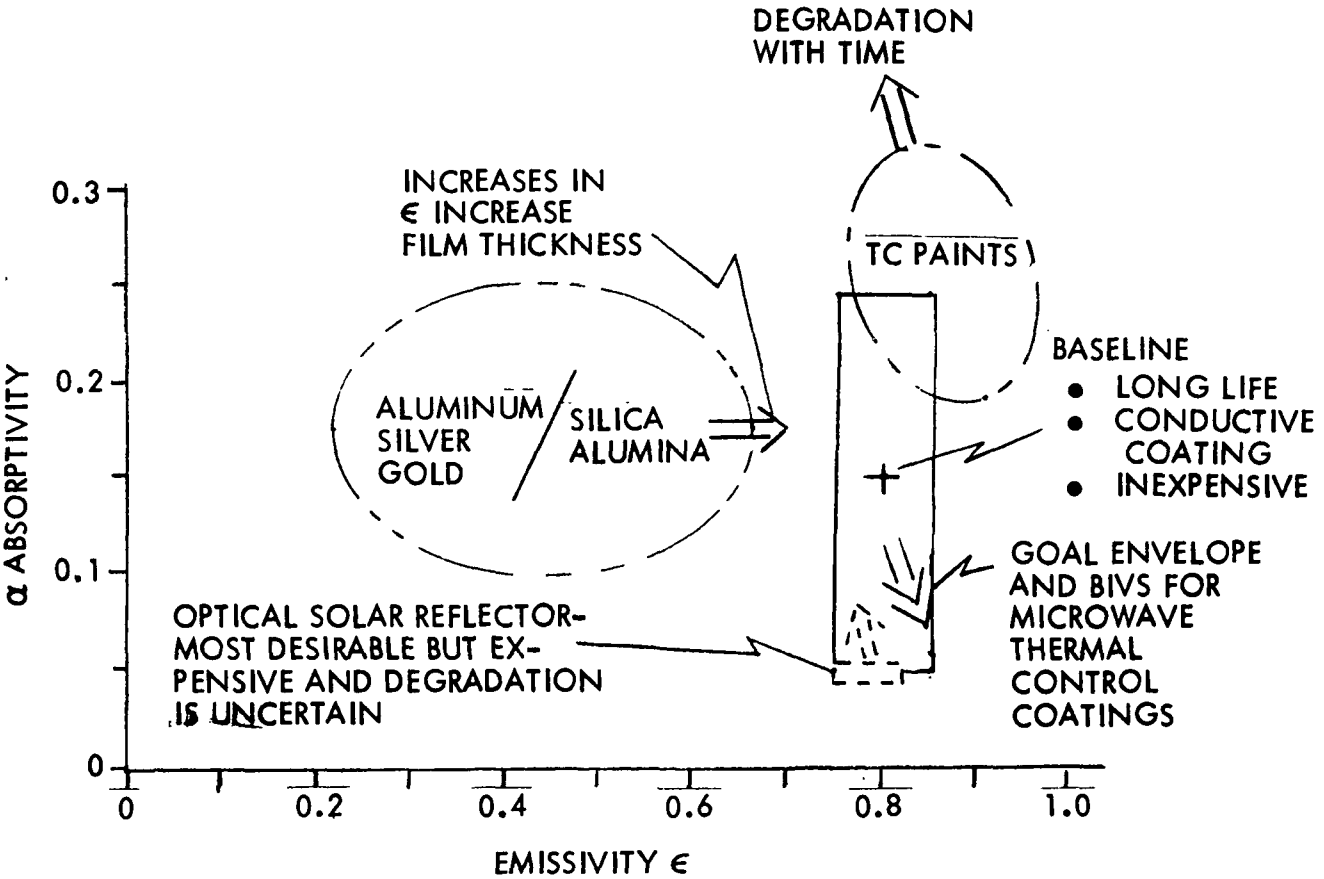

Figure 6.2-2 Current and Projected Technology and Goals for Absorptivity and Emissivity

6.3 AMPLIFIER EXPECTED LIFE RELATIONSHIPS DUE TO THERMAL CONSIDERATIONS

6.3.1 Background

There are approximately 300 x 10^6 amplifiers in the 1.95 km diameter fully filled uniform power density high power spacetenna.

The replaceable unit, a 3.2 x 3.2 m subarray, has 1024 non-redundant amplifiers, one for each transmitting element. Thirty-two drive amplifiers and centra electronics amplifiers will be switchably redundant. Failure of the non-redundan amplifiers causes (a) a loss of power and (b) a loss of aperture. A 1% random loss of amplifiers gives effectively about a 2% loss of useful power. There are about 293,000 subarrays and a single subarray loss results in about a 10^{-7}% loss of power.

Maintenance strategy must be the subject of subsequent investigations, however it is clear that a low probability of failure is a worthy goal.

The design goal is here assumed to be (a) <2% random loss of amplifiers over a 30 year period, (b) provide access for in situ preventive maintenance such as may be required for thermal control coatings in order to maintain high ε and low (c) provide for removal and replacement at a level larger than a 3.2 x 3.2 m subarray, i.e., 100 or more RF subarrays, (d) provide for maintenance, refurbishment and repair, but do not unduly compromise the random failure limit by creation of additional blockage to waste heat dissipation, hot spots or causing failures in neighboring regions while attempting to replace or maintain a known-to-be-degrade region, (e) provide for isolation at about the 100 or fewer subarray level such a to preclude failure propagation, e.g., shorts across bus bars from one region to another, and (f) provide for space charge paths across and among the surfaces to preclude undue arcing.

6.3.2 Amplifier Reliability

Random failure rates for the 300 x 10^6 non-redundant amplifiers are directly related to the junction temperature time produce as shown in Figure 6.3-1. The data base is minimal, however these specific projected relationships applied in a consistent fashion serve to assess several approaches and form the bases for further investigations.

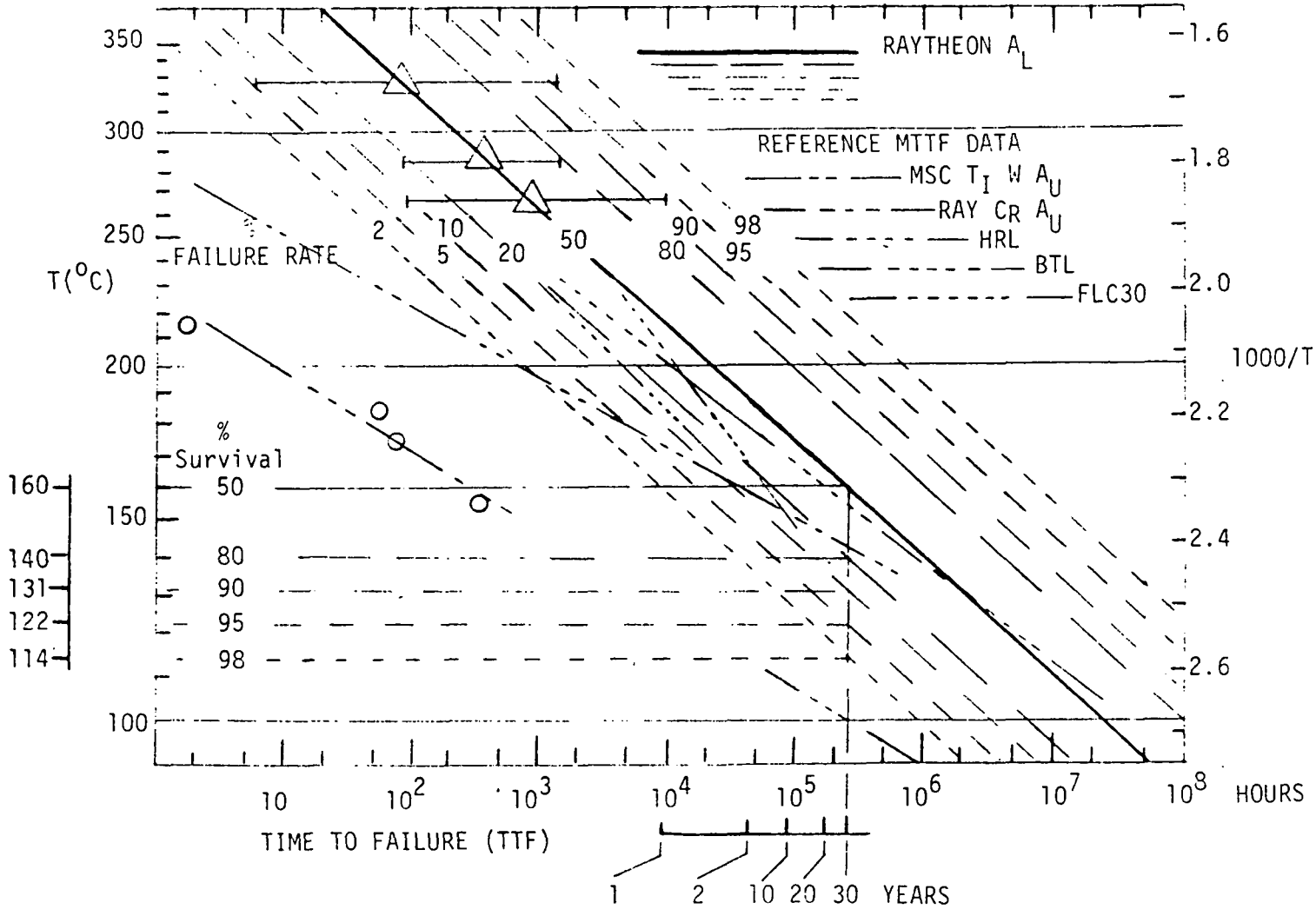

Figure 6.3-1 Accelerated Life Data and Projections for Solid State SPS MPTS Study

6.3.3 Failure Rate Versus Junction Temperature

Figure 6.3-2 is a plot of failure rate versus junction temperature which presents a different perspective from that of the standard format. Failure rates below 2% become of major interest for the SPS application where the 30-year life goal is important.

Previous MPTS investigations by Raytheon have sought approaches where there are no known modes of failure because the on-orbit maintenance and repair of such a vast system was not considered "routine" by any means. For the solid state amplifier approach, however, we must address the random failure rate question with a more open mind.

Preliminary investigations assumed that the operational system junction temperatures would be close to the maximum that will result from the worst-case environment, i.e., the waste heat radiators will have the solar load P_S on them continuously for 30 years. This was considered to be properly conservative, however it now appears to be unduly conservative.

T_J changes in a daily cycle are as much as 25C°. Recognizing that 25C° is equivalent to 25/.119 = 210 W/m^2 of RF or more than the 151 W/m^2 for the baseline indicates the need to reformulate the baseline.

The daily cycle of P_{SI} is shown in Figure 6.3-3 and indicates that for a singl sided radiator half the time P_{SI} will be zero and may be assumed to build up in one-hour steps (182, 468, 822, 1093, 1249 and 1353 W/m^2), the total time at each step being 2 hours.

Junction temperatures were estimated for each step and they were found to be 101°C to 122°C. These were plotted on Figure 6.3-4 and the cumulative failure rate was found to be 1.6% or ≈2% for 15 years at 101°C and 2.5 years at each of the other temperatures up to 122°C. The effective P_{SI} was therefore found to be less than the maximum of 1353 W/m^2 and 822 W/m^2 for a design yielding T_J = 114°C gave effectively the same 2% failure rate. This then is the basis for P_{SE} = 822 W/m^2 in subsequent analyses.

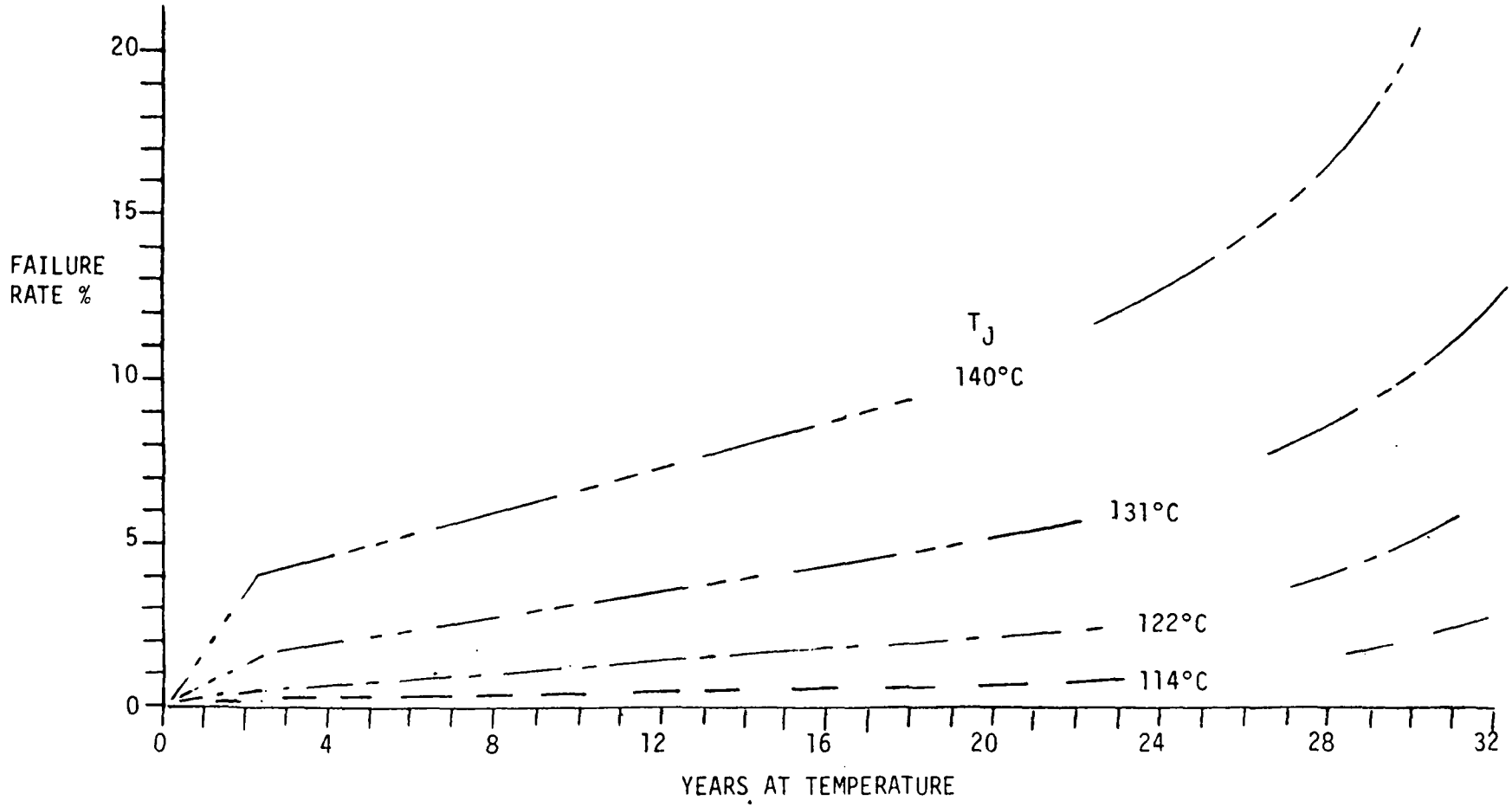

Figure 6.3-2 Failure Rate Vs Years at Temperature Based on Raytheon A_L Gate Projections

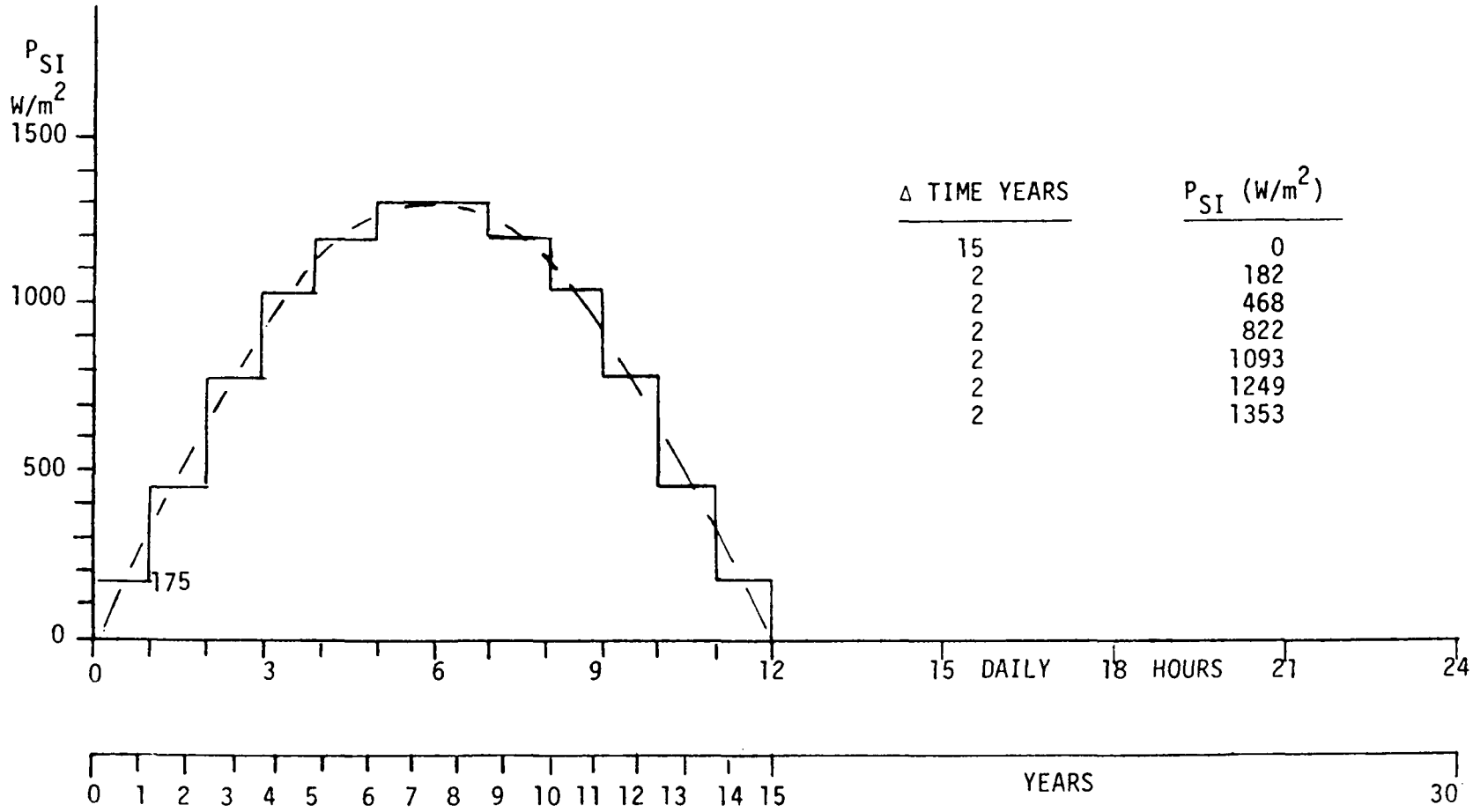

Figure 6.3-3 Daily Cycle of Normally Incident Solar Flux on Microwave Side of Sandwich

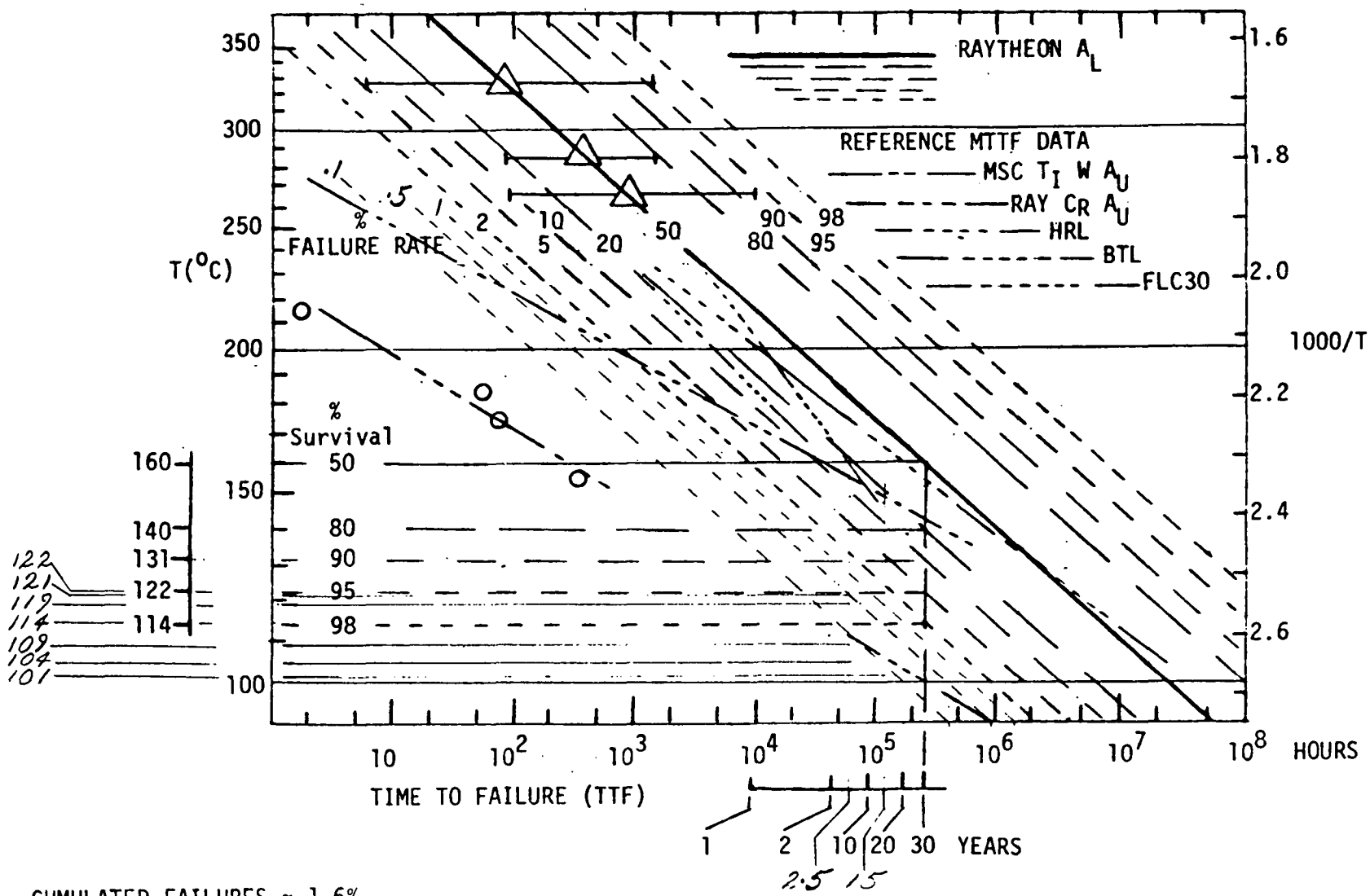

CUMULATED FAILURES ≈ 1.6%
(15 YRS AT 101°C & 2.5 YRS AT EACH:
104, 109, 114, 119, 121 & 122°C)
APPROXIMATELY EQUIVALENT TO 114°C FOR 30 YEARS, I.E., ≈ 2% FAILURES.

Figure 6.3-4 Accelerated Life Data and Projections for Solid State SPS MPTS Study

6.3.4 Form Factor and Negative Values of P_{SM}

P_{RF} allowable will improve beyond the limit for P_{SM} approaching zero from the positive side if P_{SM} is allowed to go negative. Architectures where P_{DC} is imported from outboard regions have been considered to have as their lower limit $P_{SM} = 0$.

Extending the above to the limit case where all DC power is imported, as may be the case for highly tapered RF power distributions, P_{SM} may indeed be zero. However, where the side of the microwave ground plane remote from the earth is not used for solar cells, the question arises as to whether or not it could be used as an additional waste heat radiating surface.

A review of the equations of Section 8 leading up to Equation (8-16) reveals the following:

(a) From Equation (8-15) we note that P_{SM} can go to zero and we note that P_{SE} will apply to both sides of A_C but not at the same time. Where P_{SE} was assumed to be zero 50% of the time in the case of the autonomous sandwich, however, it will now take on the form of two buildups and decays to and from the maximum value.

This may be represented by having two components $P_{SE(Front)}\ A_{C(Front)} + P_{SE(Back)}\ A_{C(Back)}$. $A_{C(Back)}$ may be less than $A_{C(Front)}$ due to partial population by solar cells with controlled heat leakage, however configurations can be conceived where $A_{C(Front)} = A_{C(Back)} = A_C$.

When $P_{SE(Front)}$ is positive, $P_{SE(Back)}$ is zero or it may have a value that is a function of the concentrator system. Configurations of concentrators may be conceived where the concentration ratio is varied over the back of the solar array so that at the most central region a concentration ratio of 1.0 may be feasible. For the purposes of this preliminary analysis, P_{SE} will be taken to have the same value on both sides.

Variations of P_{SI} with time, however, will be such as to increase the average value P_{SE} as it relates to total failure rate. Since the failure rate contribution at zero, P_S, is associated with a $T_J \simeq 100°C$, it is essentially zero and the 1.6% (≈2%) estimated for the other steps would be doubled or ≈ 4% (conservatively). A countering strategy would be to decrease T_J by ≈ 4 C° or design for an associated increase in P_{SE}. The associated P_{SE} is estimated by noting that $\Delta T = 122 - 114 = 8 C°$

when P_{SE} changes from 822 to 1353, so that a weighted average would be conservatively P_{SE} = 1200 for preliminary assessment purposes.

(b) In the denominator of Equation (8-14) it is noted that AF is a simple product and a factor of 2 applied to either one would be equivalent. For the purposes of preliminary assessment, doubling the values of F will represent a form factor as high as 2.

SECTION 7
CHARGED PARTICLE RADIATION EFFECTS

The GaAs FET (MESFET) with Al gate has been selected as the best present approach to achieve the life at the junction temperatures expected.

Effects of charged particle radiation depend on the level. High proton fluences have been reported* to have caused detectable change in saturation drain current, transconductance and noise figure. At higher levels the devices are reported to have not functioned.

The level of proton and other particles depends on natural and man-made environments to be experienced over the time period of operation. This is not clearly known.

Attenuation by mass shielding (aluminum, brass, beryllium copper or others as may be dictated by the rigors of the environment) is the best known protection approach, however effects that may take place over extended time periods require further investigation to determine the proper combination of device and shielding technologies.

Channel doping and other processes are expected to be advanced and more will be learned about the design of harder circuits.

The nature of the ultimate environment and the general device technology advances that will be ultimately developed may change the simplified assumptions employed here.

Weight estimates will be based on an average 0.1" aluminum shadow shield as part of the amplifier case which may be tailored for local thickness variations or local addition of other materials.

---

*Proton Irradiation Effects on GaAs FETs, Ken'ichi Ching, Yoshinori Wada and Masamitsu, Suzuki Musashino Electrical Communication Laboratory, Nipon Telegraph and Telephone Public Corporation.

In summary, (a) charged particle radiation environments must be determined, (b) technology advances, both supported by other programs and by SPS, must be considered as a part of the amplifier advanced technology development effort, and (c) the assumption of an average 0.1" aluminum shadow shield for the amplifier case must be assessed as progress is made in the above areas.

SECTION 8
BASIC PARAMETRIC RELATIONSHIPS AND RESULTING DATA

This section formulates (a) the basic power source characteristics which interact with parameters on the microwave side of the sandwich, (b) microwave and DC power demand characteristics which interact with waste heat dissipation and with other power supply parameters of the photovoltaic array, and (c) calculations of waste heat (ΔP_B and P_B) as a function of the efficiency chain and the DC power (P_{DC}) requirements as they relate to RF power (P_{RF}) and amplifier junction waste heat (P_A) as well as other microwave parameters.

Work sheets for the resulting relationships both on the microwave and photovoltaic side are included for ready reference.

The resulting parametric data are presented in the last part of the section using a standard format that relates supply and demand interactions with waste heat transfer between the two portions of the sandwich as the common constraint. P_{DC} demand and P_{DC} supply are indicated on a common scale, however it should be noted that only where the supply and demand curves intersect is P_{DC} supply $\equiv$ P_{DC} demand.

8.1 POWER SOURCE CHARACTERISTICS WHICH INTERACT WITH PARAMETERS ON THE MICROWAVE SIDE OF THE SANDWICH

From the photovoltaic array the delivered DC power per m^2 (as a function of solar array temperature T_S and photovoltaic waste heat P_{SM} radiated from the microwave side of the sandwich) is estimated as follows:

$$P_{DC} = \eta_S \, C_E \, P_{SI} = \eta_S(T_S) \quad C_E(T_S, P_{SM}) \quad P_{SI} \tag{8-1}$$

$$\eta_S(T_S) = 0.2095 - 0.00038 \, T_S \, (°C)^{(*)} \tag{8-2}$$

$$= (551 - T_S) \times 0.00038$$

$$C_E = \frac{P_{SW}}{(\alpha_S - \eta_S)P_{SI}} \tag{8-3}$$

$$P_{SW} = P_{SR} + P_{SM} \tag{8-4}$$

$$= (\alpha_S - \eta_S) \, C_E \, P_{SI}$$

$$\therefore \quad C_E = \frac{P_{SR} + P_{SM}}{(\alpha_S - \eta_S)P_{SI}}$$

$$P_{SR} = \varepsilon_S \, \sigma(T_S + 273)^4 \tag{8-5}$$

$\sigma = 5.67 \times 10^{-8}$ $W/m^2 \, °K^4$ Boltzmann's Constant in the Metric System

$$\therefore \quad C_E = \frac{\varepsilon_S \, \sigma(T_S + 273)^4 + P_{SM}}{(\alpha_S - \eta_S(T)) \, P_{SI}}$$

(*) Rockwell International "Satellite Power System (SPS) Concept Definition Study" (Exhibit D), October 10, 1979, page 195.

$$\therefore \quad P_{DC} = \eta_S(T_S) \left[\frac{[\varepsilon_S \sigma(T_S + 273)^4 + P_{SM}]}{(\alpha_S - \eta_S(T_S))\, P_{SI}} \right] P_{SI}$$

$$P_{DC} = \left[\frac{\varepsilon_S \sigma(T_S + 273)^4 + P_{SM}}{\frac{\alpha_S}{\eta_S(T_S)} - 1} \right]$$

For $\varepsilon_S = 0.82$ and $\alpha_S = 0.61$, $P_{SI} = 1353\ W/m^2$

$$P_{DC} = \left[\frac{0.82 \times 5.67 \times 10^{-8} (T_S + 273)^4 + P_{SM}}{\frac{0.61}{0.2095 - 0.00038T_S} - 1} \right]$$

$$P_{DC} = \left[\frac{4.6494 \times 10^{-8}(T_S + 273)^4 + P_{SM}}{\frac{0.61}{0.2095 - 0.00038T_S} - 1} \right] \qquad (8\text{-}6)$$

Related effective concentration ratio

$$C_E = \frac{P_{DC}}{\eta_S P_{SI}} = \frac{P_{DC}}{(0.2095 - 0.00038T_S)P_{SI}}$$

$$C_E = \left[\frac{4.6494 \times 10^{-8}(T_S + 273)^4 + P_{SM}}{0.4005 + 0.00038T_S} \right] \frac{1}{P_{SI}} \qquad (8\text{-}7)$$

$$P_{SM} = P_{SI}C_E(0.4005 - 0.00038T_S) - 4.6494 \times 10^{-8}(T_S + 273)^4 \qquad (8\text{-}8)$$

8.2 MICROWAVE AND DC POWER DEMAND CHARACTERISTICS WHICH INTERACT WITH WASTE HEAT DISSIPATION AND OTHER POWER SUPPLY PARAMETERS OF THE PHOTOVOLTAIC ARRAY

From the microwave side of the sandwich, the required and allowable DC power per m^2 [as a function of waste heat dissipation at (a) the transmit dipole amplifiers P_A (one every .01 m^2), (b) the rest of the DC power distribution and microwave equipments ΔP_B (assumed to be uniformly distributed over the subarray) and (c) the photovoltaic waste heat P_{SM} radiated from the microwave side of the sandwich (assumed to be uniformly distributed) is estimated as follows:

$$P_{RF} = \eta_{-DC} \times \eta_{+DC} \times \eta_{AMP} \times \eta_{FILT} \times \eta_{ANT} P_{DC} \qquad (8\text{-}9)$$

$$= .99 \times .99 \times \eta_{AMP} \times .96 \times .98 P_{DC} \quad \text{(from preliminary efficiency chain and treating } \eta_{AMP} \text{ parametrically)}$$

$$= .922\ \eta_{AMP} P_{DC}(T_J)$$

P_{DC}, allowable, is a function of junction temperature T_J, which itself is a function of time at temperature which results in junction failures on a probability basis. For preliminary design definition and analysis purposes, it is assumed that the rate of failure R_F is limited to 2% failures at the end of 30 years of life or survivability R_S is 98%. Sensitivities to R_F will be estimated for the purposes of assessing the needs for maintenance.

The term T_{JE}, effective junction temperature, will be used in the primary analysis. Preliminary analyses have indicated that T_J will vary over a 24-hour period due to the variations in P_{SI}, incident solar load on the microwave side of the sandwich. T_{JE} is that temperature which gives a failure rate equivalent to the accumulated failure rates at the several T_J values over the 30-year life cycle. Since P_{SI} causes the variation, a relationship between T_{JE} and P_{SI} becomes of interest. Preliminary analyses have indicated that for a realistic range of values for α, solar absorbance of amplifier waste heat radiators, T_{JE} can be approximated by

$$T_{JE} = \frac{T_J(P_{SI} = 0) + T_J(P_{ST} = 1353)}{1.95} \qquad (8\text{-}10)$$

which can be further approximated by $T_{JE} \simeq T_J(P_{SI} = 822)$. See Figures 8.2-1 and 8.2-2 for confirming data.

$$P_{SE} = 822 \text{ W/m}^2 \tag{8-11}$$

will be used as the "design" solar power density incident on the microwave side of the sandwich.

T_E = Equilibrium temperature of the microwave system which is calculated based on no thermal gradients in thermal conductors or in waste heat radiation. The major gradient from the amplifier junction to the waste heat radiator is taken into account in the estimation of T_J.

T_J = Amplifier junction temperature is increased above that of the immediate vicinity of the radiator by the thermal resistance essentially within the device and by the gradients within the waste heat radiator due to finite values of thermal conductivity.

$T_J = \Delta T + T_E$, where ΔT is a function of waste heat P_A dissipated at the amplifier junction and the thermal conductivity of the waste heat radiator. Preliminary analyses and computer simulations indicate that for GaAs flip chip devices mounted on copper heat sink brazed to the high conductivity surface of a heat treated pyrographite thermal conductor with appropriate thermal control coatings, $\Delta T \simeq 11.9\ P_A$ and somewhat higher for copper and higher still for aluminum conductors.

Therefore, for the purpose of estimating DC power limitations:

$$T_J(°C) = T_E(°C) + 11.9\ P_A \tag{8-12}$$

for GaAs devices and P.G. thermal conductors.

$$\therefore\ P_A = 0.084(T_J - T_E)(°C) \text{ watts per cell} \tag{8-13}$$

with cell area being $A_C = 0.01 \text{ m}^2$.

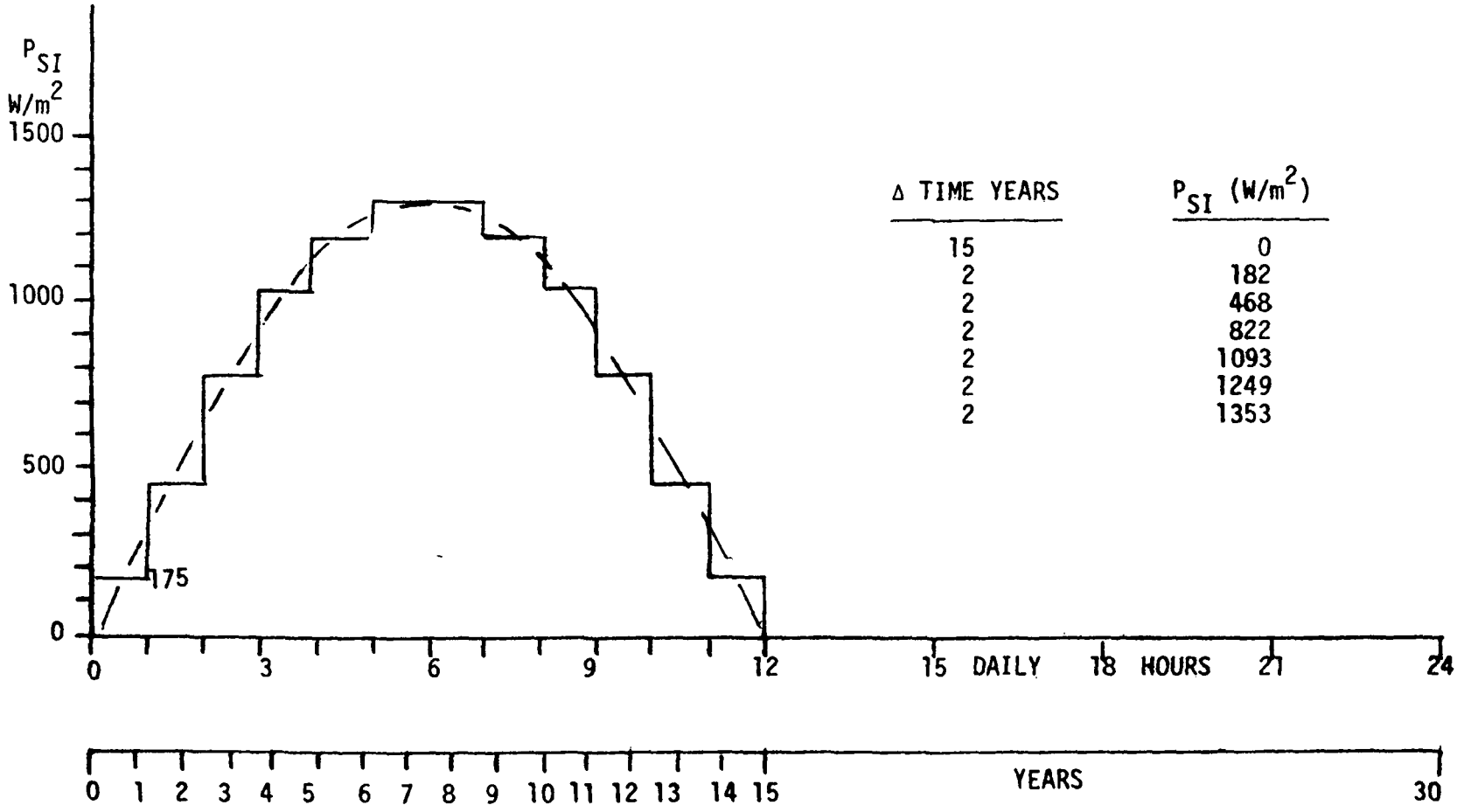

Figure 8.2-1 Daily Cycle of Normally Incident Solar Flux on Microwave Side of Sandwich

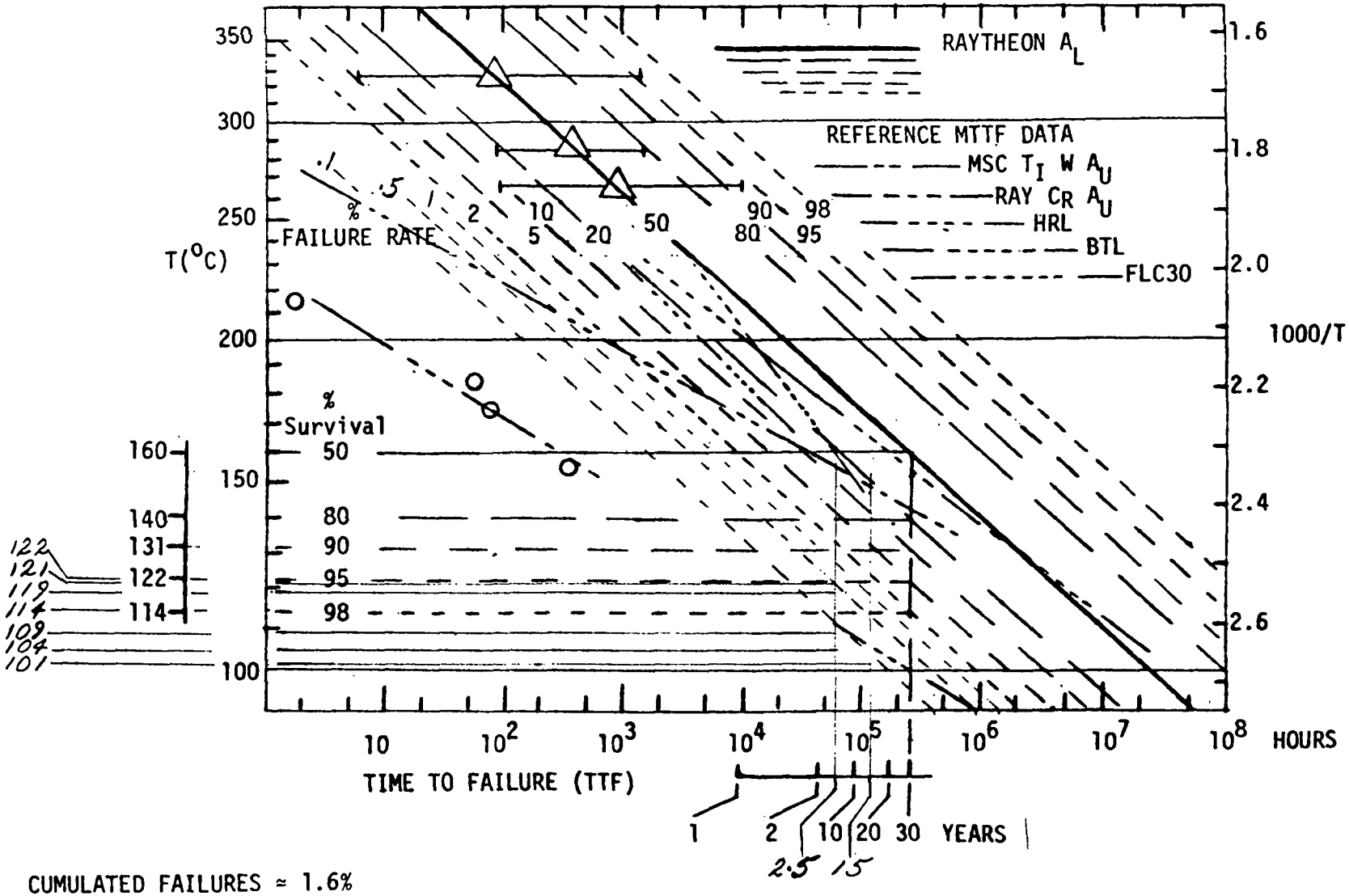

CUMULATED FAILURES ≈ 1.6%
(15 YRS AT 101°C & 2.5 YRS AT EACH:
104, 109, 114, 119, 121 & 122°C)
APPROXIMATELY EQUIVALENT TO 114°C FOR 30 YEARS, I.E., ≈ 2% FAILURES.

Figure 8.2-2 Accelerated Life Data and Projections for Solid State SPS MPTS Study

$$T_E = \left(\frac{q}{\sigma \varepsilon A \, 10.759 \, F} \right)^{1/4} {}^\circ R \qquad (8\text{-}14)$$

where $\sigma = 0.173 \times 10^{-8}$ (Boltzmann's constant in English system).

$$q = (P_{SM}A_S + \Delta P_B A_B + P_A + P_{SE}A_C\alpha)\ 3.40955 \quad BTU/hr/cell$$

P_B (W/m^2), P_A (watts/cell), P_{SE} (W/m^2), ΔP_B (W/m^2)

A_S = m^2/cell through which waste heat from the solar array is propagated and radiated

A_B = m^2/cell over which microwave waste heat other than from the amplifiers is distributed and radiated

A_C = m^2/cell which sees incident solar heat load and has an absorptivity α

A = m^2/cell area of waste heat radiator having emittance ε

F = (dimensionless) form factor of waste heat radiation configuration. $F = 1$ is for normal radiation over the entire area A without blockage and without enhancement. Configurations have been limited to those where no region on the microwave side will be at a temperature higher than the amplifier junction temperature because there are several thermally conducting paths from which heat could flow directly into the amplifier package. For the configuration investigated by Raytheon in the preliminary design activity, F is assumed to be in the range of .7 to 1.0. This is estimated by assuming equivalence to the ratio of unblocked to total area of a cell (.765-.875 range) degraded by configuration dependent imperfections in the radiator. Such degradations are assumed to be as much as 8%, giving a lower bound for F of .70. Limiting the maximum temperature of the tapes to the same as the ground plane radiator and achieving that temperature consistently would raise the upper bound to 1.0 as a maximum.

Configurational considerations of simplicity and low complexity, primarily to facilitate low cost production, preclude partitioning of areas for dedication to waste heat radiation for each of the contributors, therefore the waste heat radiator effective area is considered to be FA_C. Partitioning of areas to permit more efficient waste heat radiation at higher temperatures, such as may be allowable for waste heat from the photovoltaic array, has been investigated to a limited extent. The materials and configurations conceived in these investigations indicated that such concepts were feasible, however they were heavy and complex, so much so that they cannot be made clearly understandable without detailed simulation and technology development and testing. The potential for such approaches is indicated by noting the ratio of T^4 for temperatures associated with solar cells ≈ 200°C, i.e., 473°K, and those associated with microwave amplifiers 120°C, i.e., 393°K, T^4 ratio is ≈ 2, which could improve the ability of the photovoltaic array to produce power above that indicated by the analyses of this report. Such improvements, taking into account the effect of reducing areas dedicated to the microwave portion of the sandwich, may not approach a factor of 2, however they may approach a factor of $\sim 3^{1/4} = 1.3$ as a rough approximation.

Because of the above considerations, it is most appropriate to formulate a design based on the concept of distributing all waste heat as uniformly as possible. This should be implemented with a single waste heat conducting and radiating ground plane that will integrate well as a single structural plane of a sandwich subarray. Intimately attached to this plane is the most critical amplifier junction whose temperatures are to be limited by minimizing the waste heat at any one point. As an example of how far this should go, $\Delta T \approx 11.9\ P_A$ would be 12C° for $P_A = 1$ and $\Delta T = 23.8$C° for $P_A = 2$. Based on a $T_J = 114$°C these would result in a T_E of 102°C (375°K) and 90.2°C (363.2°K) respectively. The T^4 ratio would be 1.14. If one were to halve the power per amplifier and double the number of amplifiers, there may be an improvement in power density by a factor of about 1.14, however the additional cost of devices, the complexity of interconnections and the degradation of waste heat radiator effectiveness may easily result in low cost effectiveness.

It is necessary to have RF connections to each of the transmitting dipoles and it is possible for them to come from either a dedicated amplifier or one that feeds several dipoles. Steps in power taper across the transmitting antenna for

sidelobe control may be as high as 10 dB in ten steps. These steps could be operated at 80 to 90% of the central power level for the first step down to 10 to 20% for the last one. For the high power inboard regions of cells, the portion of the solar array behind the cells could be deleted and the DC power could be transported in from the regions where such amplifier cells were less populous. The DC power would flow radially inboard with the ground plane/waste heat radiator as the negative electrical conductor and a positive power grid of bus bars could be employed for the other half of the circuit. This approach may result in about a factor of 2 increase in RF power density at the center of the array. The distance over which the DC power would be transported would be in the 100 to 400 meter range. The optimum way of transporting power over this distance should be the subject of further investigation if this approach is otherwise worthy of consideration. Section 9 discusses the power distribution system concepts in more detail.

Because of the above possibilities, parametric data on the RF side of the sandwich will be developed for a configuration which (a) operates as an autonomous sandwich where DC power is generated directly behind the using microwave elements, and (b) operates such that no heat load from the photovoltaic array is required to be dissipated on the microwave side and temperatures for dissipation of photovoltaic waste heat are not constrained by the relatively low junction temperatures of the microwave amplifiers.

Furthermore, provisions for multiple steps to approximate an efficiently tapered RF power distribution would possibly require several power levels for amplifiers that are not multiples of 2, as may be implemented by power splitting. Two to three such power levels per device may be required. Parametric data then should cover a continuous range of combinations.

By way of summary, the parameters to be the subject of parametric analyses are as follows:

(a) Transmitting dipoles will be on a leg of a 10 x 10 cm grid.

(b) Receiving dipoles will be orthogonal to the transmitting dipoles and will be centered at the grid intersection points of the same 10 x 10 cm grid. They will be fewer in number to leave room for drive amplifiers and other electronics.

(c) The area of a cell housing an amplifier for a transmit dipole is $A_C = .01\ m^2$.

(d) The ground plane will be treated as a waste heat radiator as a continuous sheet over a subarray 3.2 x 3.2 m.

(e) A subarray waste heat radiator will be designed with a T_E less than T_{JE} such that amplifier junction life goals are met.

(f) Provisions will be made for transport of DC power inboard from low RF power density subarrays with higher DC power densities to high RF power power density subarrays with lower, down to zero, DC power densities.

(g) Values of form factor at the $.01\ m^2$ cell level will be assumed to be .70, .875 and 1.0 for parametric purposes.

(h) Values of amplifier efficiencies will be assumed to be .75, .80 and .85 for parametric purposes.

(i) The rest of the efficiency chain will be held constant.

(j) ε for the waste heat radiator on the microwave side will be 0.75, .80 and .85. α will be assumed to be 0.05, 0.15 and 0.25. The nominal set will be $\varepsilon = 0.8$ and $\alpha = 0.15$.

(k) The design value for P_{SE} on the microwave side will be fixed at 822 W/m^2, however provisions will be made for sensitivity analyses at a range of values.

$$T_E = \left[\frac{(P_{SM} A_C + \Delta P_B A_C + P_A + P_{SE} A_C \alpha)\ 3.40955}{0.173 \times 10^{-8}\ \varepsilon\ A_C \times 10.759\ F} \right]^{1/4} \ ^\circ R$$

$$= \left[\frac{P_{SM} + \Delta P_B + \frac{P_A}{A_C} + P_{SE}\ \alpha}{0.5459\ \varepsilon\ F \times 10^{-8}} \right]^{1/4}$$

and for $A_C = 0.01\ m^2$,

$$T_E = \left[\frac{P_{SM} + \Delta P_B + 100\ P_A + P_{SE}\ \alpha}{0.5459\ \varepsilon\ F \times 10^{-8}} \right]^{1/4} \ ^\circ R$$

$$T_E(^\circ C) = \frac{\left[\frac{P_{SM} + \Delta P_B + 100\ P_A + P_{SE}\ \alpha}{0.5459\ \varepsilon\ F \times 10^{-8}} \right]^{1/4} - 492}{1.8} \qquad (8\text{-}15)$$

$$\frac{P_A}{A_C} = [(1.8\ T_E(^\circ C) + 492)^4 \times 0.5459 \times 10^{-8}\ \varepsilon\ F - P_{SM} - \Delta P_B - P_{SE}\ \alpha] \qquad (8\text{-}16)$$

8.3 CALCULATION OF ΔP_B and P_A AS A FUNCTION OF THE EFFICIENCY CHAIN, P_{DC} SUPPLY, P_{DC} DEMAND AND OTHER MICROWAVE SYSTEM PARAMETERS

Based on the preliminary estimates for the efficiency chain, the conserved and waste heat power levels are shown in the following table:

CONSERVED POWER	WASTE HEAT P_{DC}		CONTRIBUTOR
	Σ	Δ	
$1.0 \times P_{DC} = 1.0\ P_{DC}$		0.01	Negative DC Power Distribution
$1 \times .99\ P_{DC} = .99\ P_{DC}$	0.01	0.0099	Positive Power Distribution
$1 \times .99 \times .99\ P_{DC} = .9801\ P_{DC}$	.0199	.9801-9801 η_{AMP}	Amplifier
$1 \times .99 \times .99 e_{AMP}\ P_{DC} = .9801\ \eta_{AMP}\ P_{DC}$	$1-.9801\ \eta_{AMP}$	.0392 η_{AMP}	Filter
$1 \times .99 \times .99 e_{AMP} \times .96\ P_{DC} = .9409\ \eta_{AMP}\ P_{DC}$	$1-.9409\ \eta_{AMP}$	.0188 η_{AMP}	Transmitting Antenna
$1 \times .99 \times .99 e_{AMP} \times .96 \times .98\ P_{DC} = .9221\ \eta_{AMP}\ P_{DC}$	$1-.9221\ \eta_{AMP}$	$\Sigma = 1 - .9221\ \eta_{AMP}$	DC Distribution Through Microwave Transmitting Antenna

DC and Microwave Waste Heat = $[1 - (\eta_{-DC} \times \eta_{+DC} \times \eta_{AMP} \times \eta_{FILT} \times \eta_{ANT})]\ P_{DC}$

$$\Delta P_B = P_{DC}\ [1 - \eta_{-DC} \times \eta_{+DC} \times \eta_{AMP} \times \eta_{FILT} \times \eta_{ANT} - \eta_{-DC} \times \eta_{+DC}(1 - \eta_{AMP})]$$

$$= P_{DC} \left\{ 1 - \eta_{-DC}\ \eta_{+DC}\ [1 - \eta_{AMP}(1 - \eta_{FILT}\ \eta_{ANT})] \right\}$$

$$= P_{DC}\ [1 - \eta_{-DC}\ \eta_{-DC}(1 - \eta_{AMP} + \eta_{AMP}\ \eta_{FILT}\ \eta_{ANT})]$$

For configurations where DC power is transferred from one area of the aperture to another, there will be an additional ΔP_B that will be applied over those subarrays through which this remote sourced DC power is transported. The near optimum η for such power transmission would be less than the .99 x .99 of the efficiency chain. If such configurations are to be investigated further, the exact value and routing of this ΔP_B related equipment would have to be taken into account. For the present analysis, that portion of P_B associated with a subarray under investigation will be taken as the value shown, whether the power source is local P_{DCL} or remote P_{DCR}.

For values in the preliminary efficiency chain and to treat η_{AMP} parametrically,

$$P_{RF} = 0.9221\ \eta_{AMP}\ P_{DC} \tag{8-17}$$

$$\Delta P_B = P_{DC}\ [1 - .99 \times .99(1 - \eta_{AMP} + \eta_{AMP} \times .96 \times .98)]$$

$$= (0.0199 + 0.0580\ \eta_{AMP})\ P_{DC} \tag{8-18}$$

$$\frac{P_A}{A_C} = 0.9801\ (1 - \eta_{AMP})\ P_{DC} \tag{8-19}$$

$$P_{DC} = \frac{P_A/A_C}{0.9801\ (1 - \eta_{AMP})} \tag{8-20}$$

$$P_{RF} = .9408\ \frac{\eta_{AMP}}{(1 - \eta_{AMP})}\ \frac{P_A}{A_C} \tag{8-21}$$

$$\Delta P_B = \frac{(.0199 + .0580\ \eta_{AMP})}{0.9801(1 - \eta_{AMP})}\ \frac{P_A}{A_C} \tag{8-22}$$

Substituting the efficiency chain relationships for ΔP_B into the thermal equilibrium equations,

$$\frac{P_A}{A_C} = [(1.8T_E(°C) + 492)^4 \times 10^{-8} \times \epsilon \times .5459F - P_{SM} - (.0199 + .058\eta_{AMP})P_{DC} - P_{SE}{}^{\alpha}] \tag{8-23}$$

Similarly, substituting for P_A/A_C,

$$P_{DC}\,[.9801(1 - \eta_{AMP}) + 0.0199 + 0.058\,\eta_{AMP}] =$$

$$[(1.8\,T_E(°C) + 492)^4 \times 10^{-8} \times \varepsilon \times .5459\,F - P_{SE}\alpha - P_{SM}]$$

$$P_{DC} = \frac{[1.8\,T_E(°C) + 492]^4 \times 10^{-8} \times \varepsilon \times .5459\,F - P_{SE}\alpha - P_{SM}}{.9801\,(1 - \eta_{AMP}) + 0.0199 + 0.058\,\eta_{AMP}} \qquad (8\text{-}24)$$

$$\frac{P_A}{A_C} = (1.8\,T_E(°C) + 492)^4 \times 0.5459 \times 10^{-8}\,\varepsilon F - P_{SM} - P_{SE}\alpha$$

$$- \frac{(0.0199 + .0580\,\eta_{AMP})}{0.9801\,(1 - \eta_{AMP})}\,\frac{P_A}{A_C}$$

$$\frac{P_A}{A_C} = \frac{(1.8\,T_E(°C) + 492)^4 \times 0.5459 \times 10^{-8}\,\varepsilon\,F - P_{SM} - P_{SE}\alpha}{1 + \frac{.05918\,(.3431 + \eta_{AMP})}{(1 - \eta_{AMP})}} \qquad (8\text{-}25)$$

For subarrays that receive their total DC power from remote sources, P_{SM} will be zero, however the photovoltaic areay would have to be replaced with a thermal reflector or thermal control coating that would preclude heat leak through to the microwave side. For further investigations in this area the goal should be to (a) minimize P_{SM} and (b) achieve the capability to dissipate some of the microwave waste heat on the "photovoltaic" side of the sandwich, i.e., let P_{SM} be a negative value.

Worksheets for the more specific cases which form the basic parametric data are included to facilitate further parametric data development as may be required. The specific data used in conjunction with data for the microwave side of the sandwich are shown in Table 8.3-1.

POWER SUPPLY WORK SHEET FROM EQUATIONS (8-6) AND (8-7)

For T_S = 200°C:

$$P_{DC} = \frac{4.6494 \times 10^{-8}(200 + 273)^4 + P_{SM}}{\frac{0.61}{0.2095 - 0.00038 \times 200} - 1} = \frac{2327 + P_{SM}}{3.569288}$$

$$= 651.95 + 0.280\ P_{SM}\ W/m^2$$

$$C_E = \frac{P_{DC}}{(.2095 - 0.00038 \times 200)\ P_{SI}} = \frac{P_{DC}}{.1335 \times 1353} = \frac{P_{DC}}{180.6255} = 3.6094 +$$

$$+ .00155\ P_{SM}$$

For T_S = 150°C:

$$P_{DC} = \frac{4.6494 \times 10^{-8}(150 + 273)^4 + P_{SM}}{\frac{0.61}{0.2095 - 0.00038 \times 150} - 1} = \frac{1488.533 + P_{SM}}{3.0}$$

$$= 496.18 + 0.3333\ P_{SM}$$

$$C_E = \frac{P_{DC}}{(.2095 - 0.00038 \times 150)\ P_{SI}} = \frac{P_{DC}}{.1525 \times 1353} = \frac{P_{DC}}{206.33} = 2.4048 +$$

$$+ .001616\ P_{SM}$$

For T_S = 250°C:

$$P_{DC} = \frac{4.6494 \times 10^{-8}(250 + 273)^4 + P_{SM}}{\frac{0.61}{0.2095 - 0.00038 \times 250} - 1} = \frac{3478.593 + P_{SM}}{4.3275}$$

$$= 803.83 + 0.2311\ P_{SM}$$

$$C_E = \frac{P_{DC}}{(0.2095 - 0.00038 \times 250)\ P_{SI}} = \frac{P_{DC}}{0.1145 \times 1353} = \frac{P_{DC}}{154.9185}$$

$$= 5.1888 + .0014917\ P_{SM}$$

Power Supply Worksheet Summary Data

P_{SM}	T_S = 150°C	T_S = 200°C	T_S = 250°C
	$P_{DC} = 496.18 + 0.333\ P_{SM}$	$P_{DC} = 651.95 + 0.280\ P_{SM}$	$P_{DC} = 803.83 + 0.2311\ P_{SM}$
	$C_E = 2.4048 + 0.001616\ P_{SM}$	$C_E = 3.6094 + 0.00155\ P_{SM}$	$C_E = 5.1888 + 0.0014917\ P_{SM}$
0	$P_{DC} = 496$	$P_{DC} = 652$	$P_{DC} = 803$
	$C_E = 2.405$	$C_E = 3.609$	$C_E = 5.189$
400	$P_{DC} = 630$	$P_{DC} = 764$	$P_{DC} = 896$
	$C_E = 3.051$	$C_E = 4.229$	$C_E = 5.7855$
800	$P_{DC} = 763$	$P_{DC} = 876$	$P_{DC} = 989$
	$C_E = 3.698$	$C_E = 4.8494$	$C_E = 6.382$
956		$P_{DC} = 919.63$	
		$C_E = 5.0912$	
527.8		$P_{DC} = 799.7$	
		$C_E = 4.427$	
520		$P_{DC} = 797.5$	
		$C_E = 4.4154$	
178.5		$P_{DC} = 701.93$	
		$C_E = 3.886$	

Table 8.3-1 Microwave and Associated Thermal Related Parameters - Worksheet (values not shown are taken to be those above)

PARAMETRIC / RELATIONSHIPS / CASE	① $T_E(°C)$	② E	③ F	④ EF	⑤ P_{SE}	⑥ α	⑦ $P_{SE\alpha}$	⑧ P_{SM}	⑨ η_{MMP}	⑩ $1-\eta_{MMP}$	⑪ $.3H+\eta_{MP}$	⑫ $.0578\,⑪/⑩$	⑬ $1+⑫$	⑭ $⑧(①+172)=⑭/.5459\times10^{-8}$	⑮ $⑭\times0.5459\times10^{-8}=⑭+⑦+⑧$	⑯ $⑮-⑧-⑦=⑰\times⑬$	⑰ P_A/A_C	⑱ ΔP_B	⑲ .8801×⑩	⑳ P_{DC}	㉑ .9408×⑨/⑩	㉒ P_{RF}	㉓ $\Delta T(°C)$ For R.C.A.	㉔ $T_J(°C)$	㉕ $P_{RF}/.562$	㉖ $P_{DC}/.772$
	⑭−492/1.8 = ㉔−㉓			②×③	WATTS/M²		⑤×⑥	⑧−⑦ WATTS/M²		1−⑨	.3H+⑨	.0578 ⑪/⑩	1+⑫	⑭/.5459 ×10⁸ (⑭+172)	⑭×.5459×10⁻⁸	⑮−⑧−⑦ WATTS/M² = ⑰×⑬	⑯/㉔ WATTS/CELL	⑰×⑱ WATTS/M²		⑳/⑱ WATTS/M²	.9408×⑨/⑩	㉑×⑰ WATTS/M²	$1.112\,⑰$ °C	①+㉓ °C	㉕.562	㉖/.772
DESIGN BASELINE	96.	0.8	1.0	0.80	822.	0.15	123.3	527.8	0.80	0.20	1.1431	0.3382	1.3382	664.8	853.6	202.5	151.3	51.	0.176	772.	3.763	562.	18.	114.	1.0	1.0
FORM FACTOR SENSITIVITIES	110.93		.875	.70				706.7						620.8	870.1	40.1	30.0	10.		153.		113.	3.57	114.	.20	.20
	78.6		"	"				70.6						633.5	615.4	401.5	300.	102.		1531.		1129.	35.4	114.	1.99	1.98
	110.		.700	.56				527.8						690.	692.2	41.8	31.3	10.6		160.		118.	3.75	114.	.21	.21
	98.2		"	"				237.						654.4	560.5	274.4	200.	67.6		1020.		753.	23.8	114.	1.32	1.32
SOLAR HEAT LEAKAGE FROM PHOTOVOLTAIC ARRAY SENSITIVITIES	78.6		1.0	0.80				178.5						633.5	703.3	401.5	300.	102.		1531.		1122.	35.4	114.	1.98	1.98
	110.4							831.						690.8	774.4	40.1	30.	10.		153.		113.	3.57	114.	.20	.20
VARIATIONS IN P_{SE} ON MICROWAVE SIDE (DAILY MAX & MIN)	103.9				1313.		203.	527.8						670.	733.3	202.5	151.3	51.		772.		562.	18.	122.	1.0	1.0
	88.2				"		"	178.5						650.7	783.	401.5	300.	102.		1531.		1129.	35.4	124.	1.98	1.98
	117.8				"		"	831.						704.2	1074.	40.1	30.	10.		153.		113.	3.57	121.4	.20	.20
	81.6				0.		0.	527.8						637.	730.3	202.5	151.3	51.		772.		562.	18.	99.6	1.0	1.0
	62.2				"		"	178.5						604.	580.	401.5	300.	102.		1531.		1129.	35.4	77.6	1.98	1.98
	97.8				"		"	831.						668.	871.1	40.1	30.	10.		153.		113.	3.57	101.4	.20	.20
EMISSIVITY SENSITIVITIES.	90.5	.85		.85	822.		123.3	527.8						654.9	853.6	202.5	151.3	51.		772.		562.	18.	108.5	1.0	1.0
	78.3							219.9						632.9	744.7	401.5	300.	101.5		1531.		1129.	35.7	114.	1.98	1.98
	108.85							840.3						686.5	1031.	66.9	50.	16.9		255.		188.	5.95	114.	.33	.33
	93.42							527.0						660.2	881.3	231.0	173.	58.5		882.		651.	20.58	114.	1.14	1.14
	102.1	.75		.75				527.8						675.7	853.6	202.5	151.3	51.2		772.		569.	18.	120.1	1.0	1.0
	78.3							132.3						632.9	657.1	401.5	300.	101.5		1530.		1129.	35.7	114.	1.98	1.98
	108.0							718.6						686.4	908.8	66.9	50.	16.9		255.		188.	5.95	114.	.33	.33
	93.4							922.6						660.1	777.4	231.5	173.	58.5		883.		651.	20.58	114.	1.14	1.14
ABSORPTIVITY SENSITIVITIES.	48.8	.80		.80		.05	41.	527.8						579.8	771.3	202.5	151.3	51.		772.		562.	18.	66.8	1.0	1.0
	78.3							258.3						632.9	700.9	401.5	300.	101.5		1531.		1129.	35.7	114.	1.98	1.98
	108.05							862.						686.5	969.9	66.9	50.	16.9		255.		188.	5.95	114.	.33	.33
	93.42							556.9						660.2	829.4	231.5	173.	58.5		882.		651.	20.58	114.	1.14	1.14
	104.6					.25	205.5	527.8						680.4	935.8	202.5	151.3	51.		772		569.	18.	122.6	1.0	1.0
	78.3							93.9						632.9	700.9	401.5	300.	101.5		1530		1129	35.7	114.	1.98	1.98
	108.0							697.0						686.4	962.4	66.9	50.	16.9		255		198.	5.95	114.	.33	.33
	93.4							372.3						660.1	829.3	231.5	173.	58.5		883		651.	20.58	114.	1.14	1.14
AMPLIFIER EFFICIENCY SENSITIVITIES.	98.2					.15	123.3	527.8	.85	0.15	1.1731	.4707	1.4707	668.8	873.6	222.5	151.3	71.2	0.197	1029.	5.3312	807.	18.	116.2	1.42	1.33
	78.3							136.4						632.9	700.9	441.2	300.	141.2		2041.		1579.	35.7	114.	2.81	2.64
	108.05							773.1						686.5	969.9	73.5	50.	23.5		340.		267.	5.95	114.	.47	.44
	93.42							451.7						660.2	829.4	254.4	173.	81.4		1177		922.	20.58	114	1.62	1.52
	94.76							527.8	.75	0.25	1.0931	.2588	1.2588	662.6	841.6	190.5	151.3	190.5	0.245	618.	2.8224	427.0	18.	112.7	.75	.800
	78.3							200.0						632.9	700.9	377.6	300.	377.6		1224.		847.	35.7	114.	1.49	1.58
	108.05							783.7						686.5	969.9	62.9	50.	61.9		204.		141.	5.95	114.	.25	.26
	93.42							988.3						660.2	829.4	217.8	173.	217.7		706		488.	20.58	114.	.86	.91
COPPER																							$\Delta T C°$ FOR ξ_{Cu} = .1121 ①				
	96.1	.80	1.0	0.80	822	0.15	123.3	527.8	0.80	0.20	1.1431	0.3382	1.3382	664.8	853.6	202.5	151.3	51.	0.196	772.	3.763	562.	20.0	116.1	1.0	1.0
	74.4							145.4						625.9	670.2	401.5	300.	101.5		1531.		1129.	32.6	114.	1.98	1.98
	107.4							773.1						685.3	963.3	66.9	50	16.9		255.		188.	6.6	114.	.33	.33
SENSITIVITY TO MAT'L FOR THERMAL CONDUCTOR ALUMINUM	91.2							454.7						656.2	809.5	231.5	173	58.5		883.		651.	22.8	114.	1.14	1.14
																							$\Delta T C°$ FOR ξ_{Al} = .2021 ②			
	96.1							527.8						664.9	853.6	202.5	151.3	51.		772.		562.	30.6	126.7	1.0	1.0
	53.4							−2.4						588.1	523.5	401.5	100.	101.5		1531.		1122.	60.6	114.	1.98	1.98
	103.9							738.2						677.0	928.4	66.9	50.	16.9		255.		188.	10.1	114.	.33	.33
	79.1							352.5						634.4	707.3	231.5	173.	58.5		883.		651.	34.2	114	1.14	1.14
																							.1121 ①			
BASELINE (98	96.							527.8						664.8	853.6	202.5	151.3	51.2	0.196	772.	3.763	562	18.8	114	1.0	1.0
SENSITIVITY (953	100													672.	890.5	237.5	177.0	60.5		913.		674.	21.3	121.3	1.18	1.18
TO JUNCTION (91.3	104													679.2	929.4	278.2	208.0	70.3		1061.		783.	24.8	128.75	1.38	1.37
TEMPERATURE (77.6	110													690.	1006.2	355.1	265.4	89.8		1384.		999.	31.6	141.6	1.76	1.75
% initial (50.6	120.													708.	1027.3	446.2	333.5	112.8		1702.		1255.	39.6	159.6	2.20	2.20
AT 30 HRS >99.	70.							200.0						618.	637.0	313.7	234.4	79.3		1196.		882.	27.9	97.8	1.55	1.55
>99.	74													625.2	672.2	343.9	257.0	86.9		1311.		967.	30.6	104.6	1.70	1.70
97.7	80													636.	714.5	391.2	292.4	98.9		1492		1100.	34.8	114.8	1.93	1.53
84.	92													657.6	816.7	493.4	368.7	124.7		1881		1387.	43.9	135.9	2.44	2.44
53.2	109.													679.2	929.4	606.1	452.9	153.1		2311		1704.	53.9	157.9	2.99	2.99
SUPPLY = DEMAND AT T_J = 160°C (50% Failure)	138.63	For P_{DC} = 651.95 + 0.280 P_{RF} from Solar Array at 200°C (T_J) : For P_{DC} = 919.63, P_{RF} = 956.0						956.0						741.5	1320.5	241.2	180.24	60.36		919.63		678.2	21.45	160.98	1.19	1.19
SUPPLY = DEMAND AT T_J = 114°C (27% Failure)	96.25	For P_{DC} = above relationship : For P_{DC} = 800, P_{RF} = 528.25						528.25						666.5	861.2	209.18	156.8	53.03		800.0		590.0	19.06	115.8	1.037	1.036
	97.14	" = 722.86, P_{RF} = 253.25						550.72						666.85	863.6	189.60	141.68	47.92		722.86		533.1	16.86	114.0	.236	.736
	95.91	" = 793.55, P_{RF} = 520.0						520.0						663.74	859.46	209.20	156.3	52.86		797.55		588.2	18.60	114.12	1.039	1.033
DOUBLE SIDED RADIATOR (Double E)	45.47	.8	2.0	1.6	1800.	0.15	180.	0.						573.85	847.2	767.2	573.3	193.89		2925.		2157.	66.2	113.62	3.75	3.79
	51.31		1.75	1.4	"	"	"	0.						584.37	891.34	711.34	531.5	179.75		2712.		2000	63.24	114.35	3.51	3.51
	59.70		1.40	1.12	"	"	"	0.						599.45	789.5	609.50	455.4	154.00		2323.		1714	54.2	113.90	3.01	3.01

PARAMETRIC RELATIONSHIPS — DIMENSIONS — COPPER — ALUMINUM — PYROLYTIC GRAPHITE RADIATOR THERMAL CONDUCTOR

8.4 PARAMETRIC DATA SUMMARY

8.4.1 Introduction and Data Format

Figure 8.4-1 shows the interactive parameters of the selected baseline system where the "supply" and "demand" curves intersect. This is what is referred to as the autonomous subarray design point. Subsequent figures, showing different combinations of parameters at curve intersections, indicate the sensitivity to the basic parameters.

The DC DEMAND curve is plotted from the microwave data sheet for the Design Baseline parameters shown in the top row. The actual value of P_{SM} for Supply = Demand at $T_J = 114^{o}$ C comes from the lower row near the bottom of the work sheet.

The Supply curve is plotted from the power supply work sheet for $T_S = 200^{o}$ C.

The basic parameters for the microwave portion are shown in the top center, i.e., for Figure 8.4-1; amplifier efficiency = 0.8, DC to RF efficiency = 0.7377, $\epsilon = 0.8$, $\alpha = 0.15$, Form factor F = 1.0, Pyrographite waste heat thermal conductor conductivity is assumed, probability of survival for amplifier junction is 98% and the junction temperature relating to that for GaAs/AL devices is 114^{o} at a weighted average value of $P_{SE} = 822$ W/m^2. Three cases shown in Figure 8.4-1 are discussed which explain the data relationships and applicability. The third case is for the autonomous subarray.

Case [1] shows typically that for low values of $P_{SM} \simeq 178.5$ W/m^2 (waste heat load common to the microwave and solar cell portions of the sandwich), P_A, (waste heat for the amplifier), can be typically 3 watts per element cell (10 cm x 10 cm). The radiated RF power that can be transmitted, consistent with the efficiency assumptions, is $P_{RF} = 11.29$ watts per element cell, i.e. $P_{RF} = 1129$ W/m^2. In order to generate this much P_{RF} the DC power demand, consistent with the efficiency assumptions, is P_{DC} (Demand) = 1.531 watts per cell or P_{DC} (Demand) = 1531 W/m^2. Operating with the same value of P_{SM} (178.5 W/m^2), the photovoltaic array will generate 7.02 watts per cell or P_{DC} (Supply) = 702 W/m^2 while operating at $T_S = 200^{o}$ C and an associated effective concentration ratio $C_E = 3.89$. We note that the demand for DC power is in excess of the supply locally available by 1531 - 702 = 829 W/m^2 of DC

POWER PER ELEMENT CELL (10 CM x 10 CM) RELATIONSHIPS

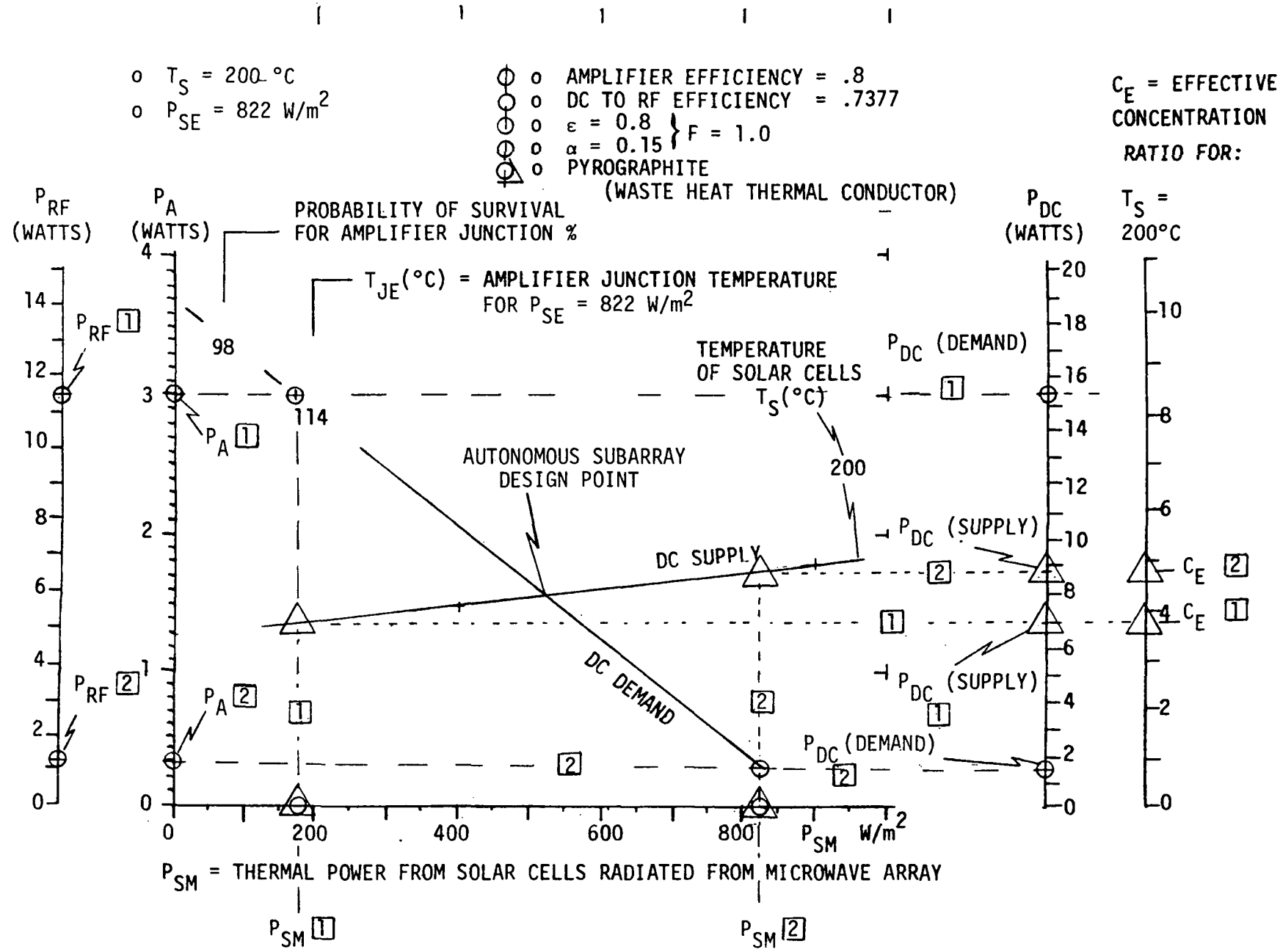

power which would have to be supplied from a remote source that did not increase P_{SM}.

Case [2] shows typically that, for a high value of $P_{SM} \simeq 800$ W/m^2, P_{RF} is $\simeq$ 1.5 W/Cell = 150 W/m^2 and the P_{DC} (Demand) = < 2 W/Cell or 200 W/m^2; while the P_{DC} (Supply) is about 9 W/Cell or 900 W/m^2 and CE is < 1. It should be noted that the specific values can be scaled from the chart however the work sheets should be used to establish the specific numbers where high precision is essential.

Case [3] (Autonomous Subarray) for the power supply, the following values are taken from the work sheet: P_{SM} = 520 W/m^2, P_{DC} (Supply) = 797.5, C_E = 3.886. Similarly, the microwave work sheet gives: P_{SM} = 520 W/m^2, P_{DC} (Demand) = 797.5 W/m^2, P_{RF} - 588.2 W/m^2, P_A/A_C = 156.3 W/m^2 or P_A = 1.563 watts per element, T_J = 114.02^o C, and T_E = 95.41^o C. These are slightly different from the design baseline for the RF system where P_{RF} was 569 W/m^2, while P_{SM} was 527.8 as measured from a data plot. Figure 8.4-2 is a simplified summary of the format which illustrates its applicability to a range of concepts which are not necessarily autonomous throughout the array with regard to DC power demand and supply.

8.4.2 Baseline Sensitivity to Daily Variations in Incident Solar Heat Load on the Microwave Side

On the demand curve of Figure 8.4-3 the range of junction temperature and equilibrium temperatures are shown at three points, for three values of incident heat load. The 822 W/m^2 set of temperatures shows that as junction temperature decreases, equilibrium or average temperature over the waste heat radiator increases, (31 C^o), for the range shown. For high thermal conductivity materials, the gradient across a 10 x 10 cm cell is high in the region of the amplifier junction, but low on the average. The waste heat radiators for the cells form a continuous ground plane and the equilibrium temperature is in general referred to as the ground plane temperature. The 31 C^o temperature range could only be tolerated if it occured over a large distance like 10 to 15 meters, otherwise the junction temperature would rise 2 to 3 centigrade degrees which could begin to affect life. Even in the 10 to 15 meter range the heat load P_{SM} would have to be applied relatively uniformly.

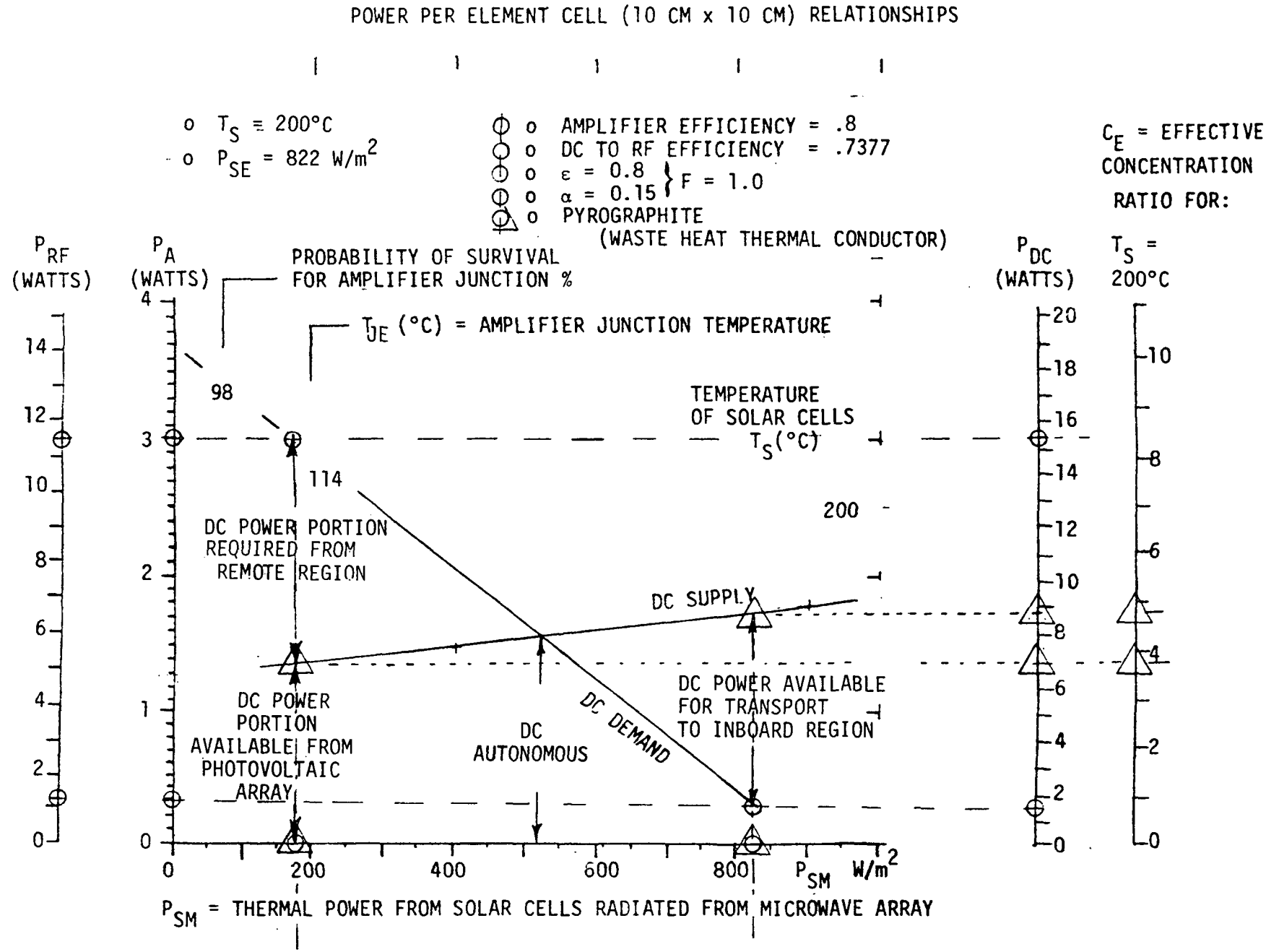
POWER PER ELEMENT CELL (10 CM x 10 CM) RELATIONSHIPS
o T_S = 200°C
o P_{SE} = 822 W/m²
o AMPLIFIER EFFICIENCY = .8
o DC TO RF EFFICIENCY = .7377
o ε = 0.8 } F = 1.0
o α = 0.15
o PYROGRAPHITE
(WASTE HEAT THERMAL CONDUCTOR)
C_E = EFFECTIVE CONCENTRATION RATIO FOR:
P_{RF} (WATTS)
P_A (WATTS)
PROBABILITY OF SURVIVAL FOR AMPLIFIER JUNCTION %
T_{JE} (°C) = AMPLIFIER JUNCTION TEMPERATURE
98
114
200
TEMPERATURE OF SOLAR CELLS T_S(°C)
DC POWER PORTION REQUIRED FROM REMOTE REGION
DC SUPPLY
DC POWER PORTION AVAILABLE FROM PHOTOVOLTAIC ARRAY
DC AUTONOMOUS
DC DEMAND
DC POWER AVAILABLE FOR TRANSPORT TO INBOARD REGION
P_{DC} (WATTS)
T_S = 200°C
P_{SM} W/m²
P_{SM} = THERMAL POWER FROM SOLAR CELLS RADIATED FROM MICROWAVE ARRAY

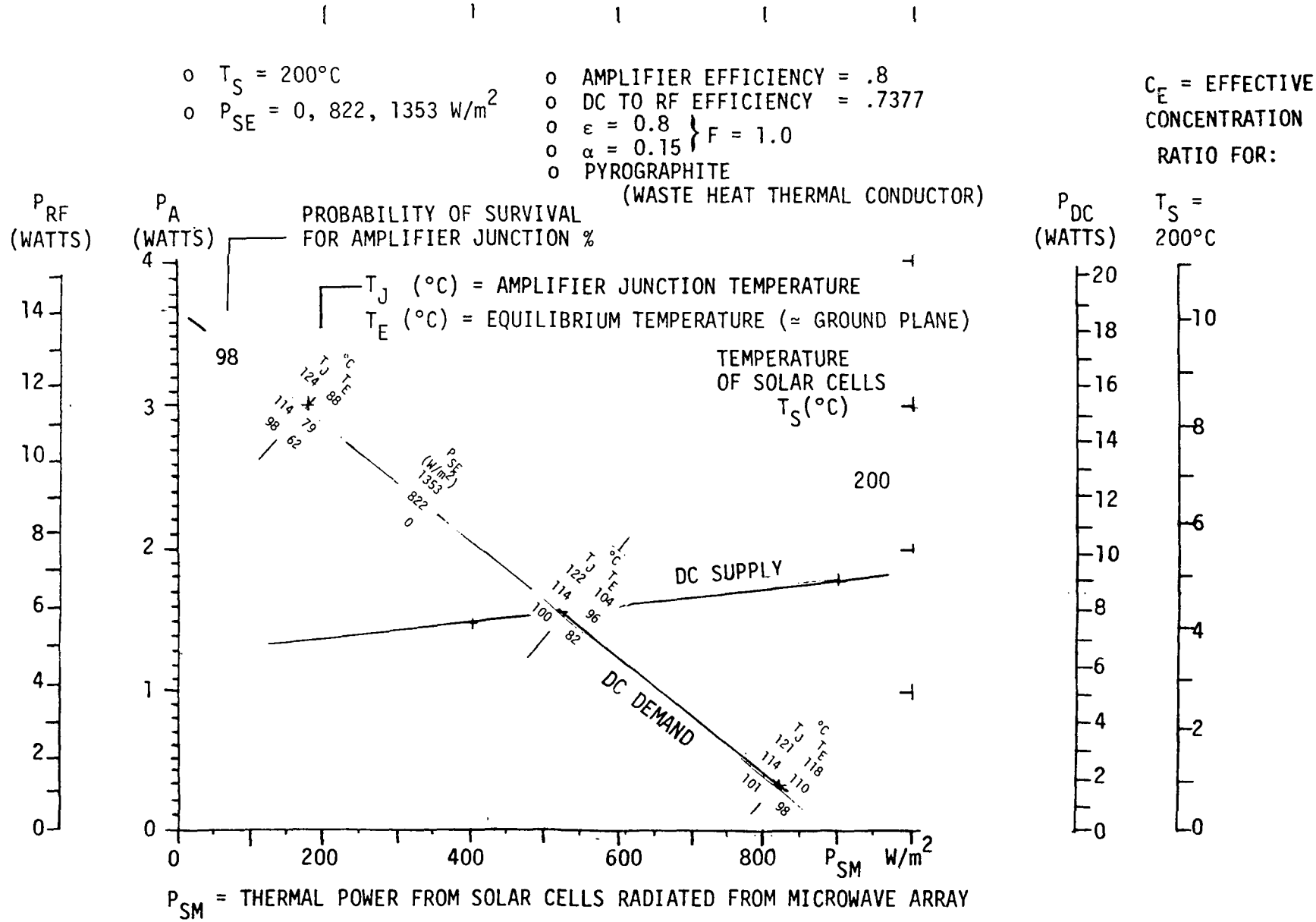

Figure 8.4-3 Baseline Sensitivity to Daily Variations of P_{SE}

For the autonomous case, it is noted that the ground plane temperature goes through a daily range of 22 C^{o} as does the junction temperature. This would make the DC supply value increase and decrease considerably unless P_{SM} is controlled. When the sun is loading the microwave side, the photovoltaic side is loaded only by the reflector system. It is not difficult to conceive of the situation where, when the sun is not radiating the microwave side, it is increasing the P_{SI} on the photovoltaic side. This would increase the DC power available. The amplifiers tend to act as resistive loads and the power demand would not change significantly unless the voltage changed significantly. Voltage/current characteristics of both the Demand or Load and Supply must be considered further in future investigations. The value of P_{SM} cannot increase as T_E decreases if the integrated average effects of T_J on probability of survival are to remain as indicated. Letting T_E stay at 104°C would raise the minimum value of the junction temperature by ≃ 22C°, which would in thirty years give a probability of failure of 5% as compared to the design value of 2%. Inherent in the assumption that an equivalent failure rate approach be employed is an assumption that P_{SM} be controlled or accept the possible life degradation. Future investigations should address that area in more detail and perhaps the assumption for this study will be shown to be unduly optimistic. In any case, mechanization for P_{SM} heat transfer must be approached with great care.

Temperature gradients with time are essentially the same on the DC Command curve over a large range of values of P_{RF}, however T_J maximum does increase with P_{RF}.

8.4.3 Baseline Sensitivity to Waste Heat Radiator Form Factor

As shown in Figure 8.4-4, P_{RF} increases with form factor at a high rate for large values of P_{RF} and at a still higher rate for small values of P_{RF}. The form factor has perhaps the most powerful influence on P_{RF} and, as indicated in other sections, very considerable emphasis should be placed on tradeoffs and on technology development in this area.

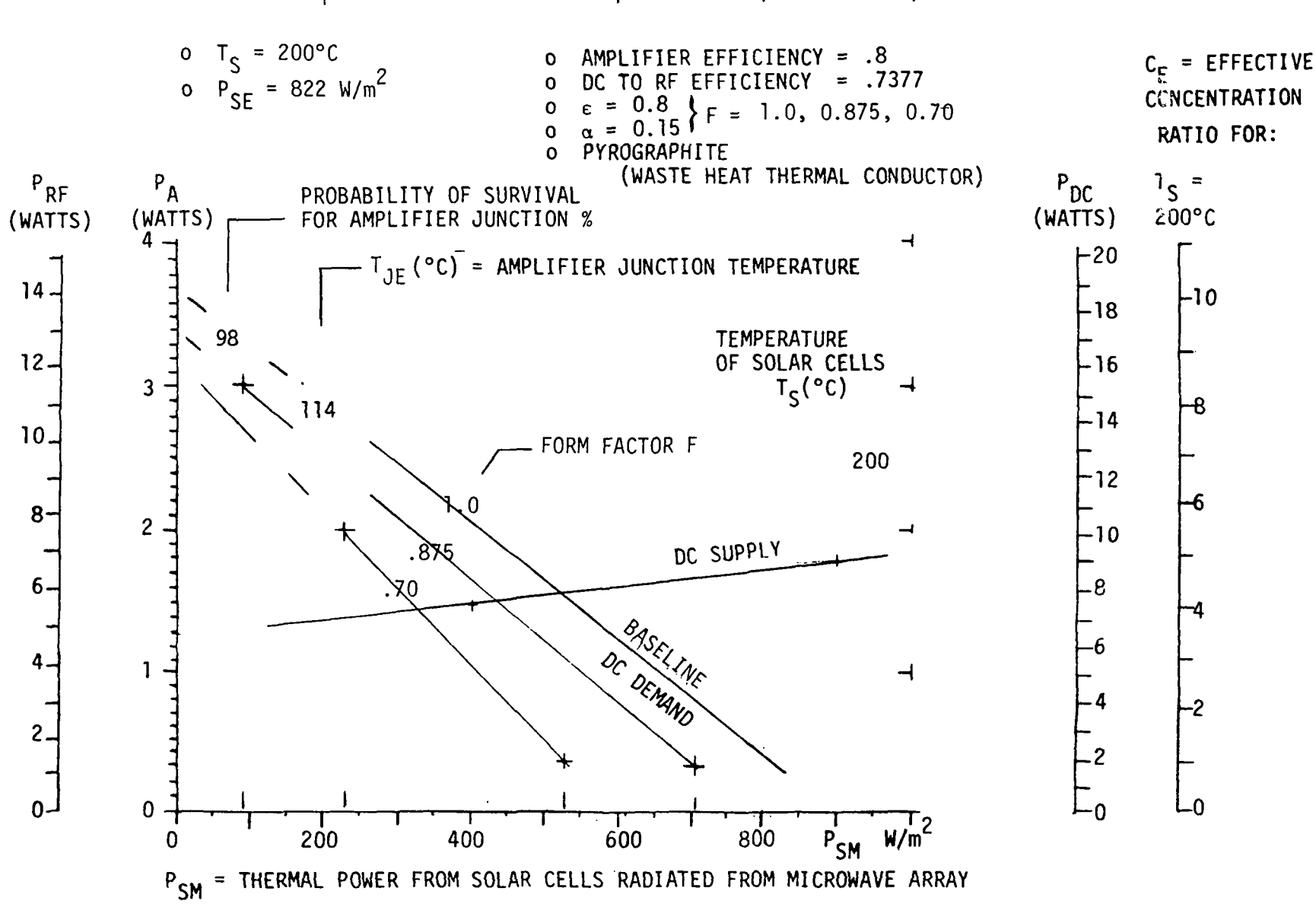

Figure 8.4-4 Baseline Sensitivity to Waste Heat Radiator Form Factor

The assumption of F = 1. for the baseline is possibly optimistic for the antenna element dipole technique where the dipole is mounted above the ground plane $\simeq 5$ cm laterally from the amplifier junction which is mounted on the ground plane.

Values of F = 0.7 and above have a high probability of being demonstrated. However, the effects of the basic form factor in conjunction with both external and internal thermal control coating performance over time compounds the problem and its resolution.

8.4.4 Baseline Sensitivity to Emissivity and Absorptivity

P_{RF} increases significantly as emissivity increases to 0.85 and decreases a similar amount as emissivity decreases to 0.75. Figure 8.4-5 shows that for a constant $T_J = 114^{o}$ C and a probability of survival of 98% the absolute value of change in P_{RF} is not much different over a large range of values for P_{RF}. The percentage of change is very high at low values and is not so significant at high values however.

Temperatures at the autonomous point decrease as ϵ increases. Emissivities of thermal control coatings have degraded with time; in which case temperatures would increase. There may then be an excess of DC power available, however life of the amplifier junctions would degrade.

As Figure 8.4-6 indicates, P_{RF} decreases markedly as absorptivity, α, increases for constant junction temperature. At the autonomous point, the available power decreases.

From a design point of view, RF equipment could be developed to operate over a range of power levels. However this will impact the already difficult technology development significantly.

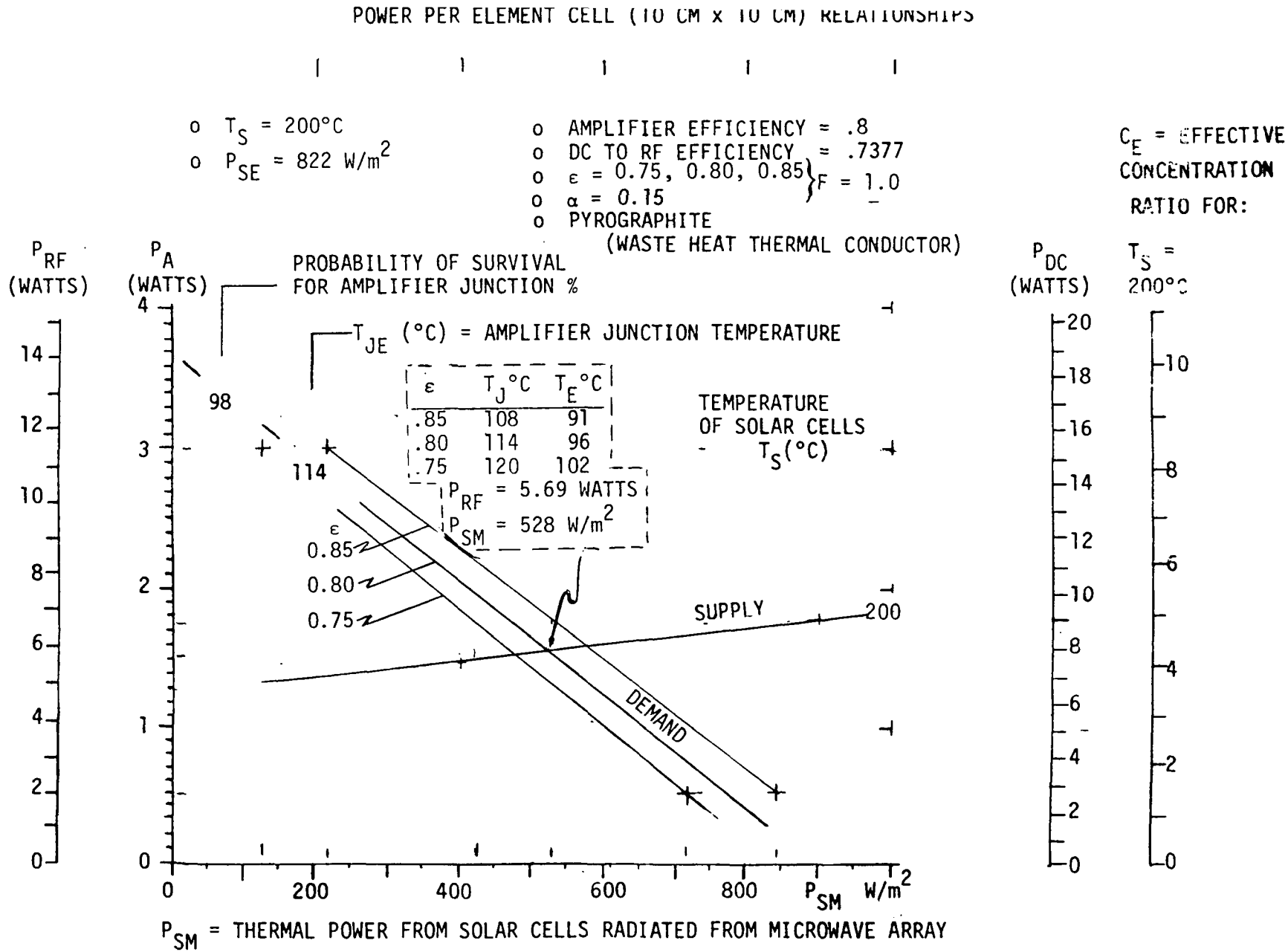

Figure 8.4-5 Baseline Sensitivity to Emissivity

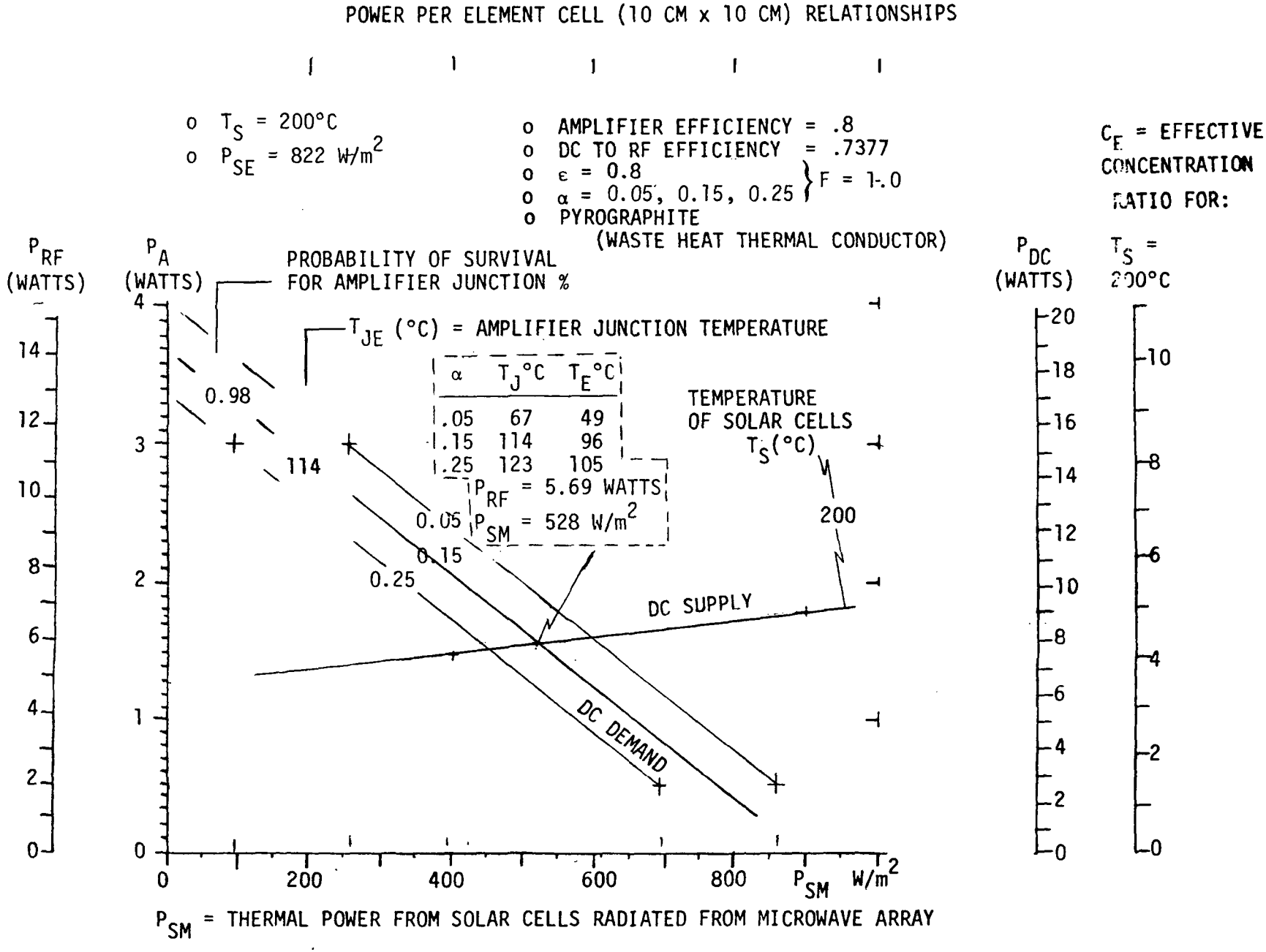

Figure 8.4-6 Baseline Sensitivity to Absorptivity

8.4.5 Baseline Sensitivity to Amplifier Efficiency

The efficiency of the amplifier, η_{AMP}, is assumed to be 0.80 for the baseline. It is recognized that this is yet to be demonstrated, however it is considered to be a rational goal. The lower value, $\eta_{AMP} = 0.75$, has not been demonstrated either, however it is considered to have a higher probability. Advances in the technology may result in η_{AMP} as high as 0.85. Taking these values as representative of nominal, low and high probabilities of performance, the interactive data for the microwave power transmission system in the sandwich concept has been developed. The rest of the values in the efficiency chain have been left fixed. The nature of the data presented in Figure 8.4-7 shows that $(1 - \eta_{AMP})$ is more indicative of the importance of the parameter. This is the "inefficiency" which causes the losses which in turn cause the junction temperature increase above that of the ground plane. For a given set of parameters (upper left on the figure) held constant and plotting the data from the worksheets for the two sets of η_{AMP} values about the baseline, the following is observed.

For $\eta_{AMP} = 0.85$, the transmitted power density P_{RF} (at the autonomous point) increases to about 6.2 W/element from the 5.88 for the "supply = demand" case. This is only a factor of 1.05 while the amplifier inefficiency ratio went down to .15/.20 = .75. P_{SM} went from 520 to above 570 W/m^2, which is a factor of > 1.1 to generate the DC power (just above 8 watts) that would have been demanded. The 200°C constraint for the photovoltaics limits P_{SM} to 570 W/m^2 and the P_{DC} supplied is less than 8 W/m^2 rather than greater. This indicates the nature of the constraint of designing for operation at the autonomous point.

Improvements in P_{RF} with increases in η_{AMP} above 0.8 are small (1.05) for the autonomous case, while at $P_{SM} = 0$ the improvement increases to 20.5/14.1 = 1.45. Similarly, if the photovoltaics are not constrained to limit the heat leakage to the microwave side, e.g., for $P_{RF} = 0$ . . $P_{SM} \geq 900$ watts/m^2 which allows the generation of ≥ 8.8 watts per 10 cm^2 cell. This gives reason to believe that since the real problems are to both generate DC and transmit RF power at high power density for low cost an approach which segregates the functions may show improvement in overall performance if the on-orbit DC power transmission problem could be resolved cost effectively.

POWER PER ELEMENT CELL (10 CM x 10 CM) RELATIONSHIPS

- T_S = 200°C
- P_{SE} = 822 W/M^2
- ϵ = 0.8, α = 0.15 } F = 1.0
- PYROGRAPHITE (WASTE HEAT THERMAL CONDUCTOR)

AMPLIFIER INEFFICIENCY	$(1-\eta_{AMP})$	.25	.20	.15
AMPLIFIER EFFICIENCY	η_{AMP}	.75	.80	.85
DC TO RF INEFFICIENCY	$(1-\eta_{DCtoRF})$	.308	.2623	.216
DC TO RF EFFICIENCY	η_{DCtoRF}	.692	.7377	.784
			BASELINE	

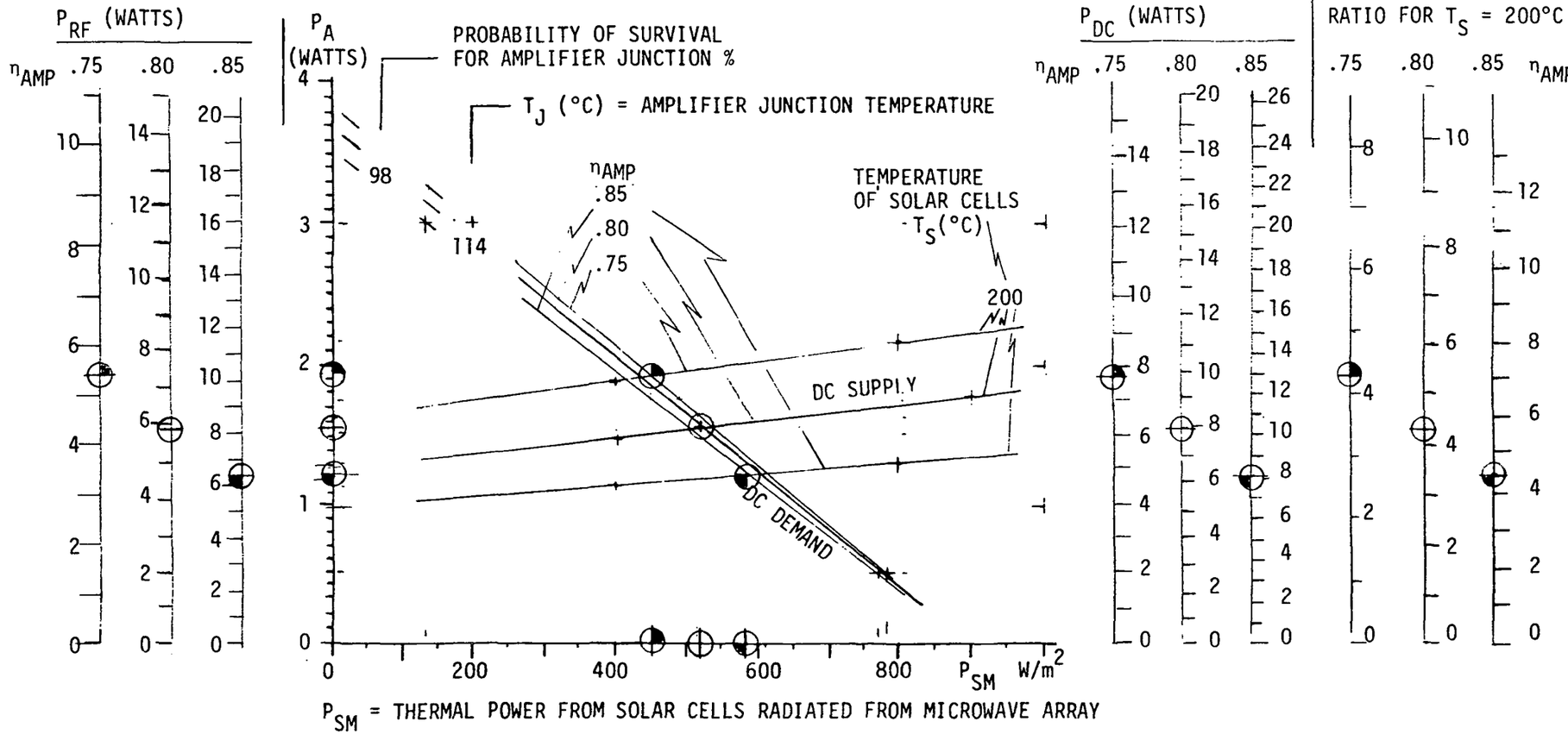

P_{SM} = THERMAL POWER FROM SOLAR CELLS RADIATED FROM MICROWAVE ARRAY

Figure 8.4-7 Baseline Sensitivity to Amplifier Efficiency

For η_{AMP} = 0.75, the transmitted power density, P_{RF} (at the autonomous point), decreases to about 5.4 W/element from the 5.88 for the supply = demand case. This is a factor of only .92, while the amplifier inefficiency ratio went up to .25/.2 = 1.25.

Degradation in P_{RF} with decreases in η_{AMP} below 0.8 to η_{AMP} = 0.75 are small (.92) for the autonomous case, while at P_{SM} = 0 the degradation changes to 9.9/14.1 = 0.70. Comparing this 0.7 to the 1.45 (two paragraphs earlier) reveals that there is ≈30% degradation in performance for 1 - η_{AMP} = .25, while there is a 45% enhancement in performance for 1 -η_{AMP} = .15, both compared to performance at 1 - η_{AMP} = .2.

The achieving of maximum potential performance for both the microwave and photovoltaic portions of the sy-tem is significantly constrained by requiring P_{DC}(Demand) to be satisfied by P_{DC}(Supply) along with the heat transfer and associated temperature constraints.

Operating at the microwave baseline condition, P_{SM} = 520 W/m^2 and T_J = 114°C for η_{AMP} = 0.8.

Operating at the microwave baseline design point where P_{SM} = 527.8, T_E = 96°C and T_J = 114°C, the P_{RF} = 569 when η_{AMP} = 0.8. If η_{AMP} is simply increased to 0.85, as a design value and keeping P_{SM} = 527.8, P_{RF} increases to 1029 (81% increase) and T_J increases to 116.2, while T_E only increased to 98.2 (only 2C° increase each). The P_{DC} demand increased from 7.72 watts per cell to 10.3 (33% increase). Again, the desire for DC power from a remote region appears a worthy objective.

8.4.6 Baseline Sensitivity to Material for Thermal Conductor

The key to achieving low junction temperature for a given inefficiency is to first spread the junction out in area. Length is constrained by other performance requirements and increase in RF power is developed by increase in width of the junction, which makes heat generation proportional; $P_{DC} \times (1 - \eta_{AMP})$ and $P_A/A_C = P_{RF}(1 - \eta_{AMP})/.94081\ \eta_{AMP}$. We need to get P_A out of the junction area at a high rate to preclude temperature increase. The flip chip approach is the best known method for achieving this so that the very small area of the junction makes thermal contact with a heat sink. This very local heat sink in turn must make low thermal resistance contact with a yet larger region and the conductivity of that region should be high. This is indeed the critical part of the thermal chain. It will be an essential part of the amplifier advanced development program to include these considerations in the technology for performance and low cost production.

The next link of the chain has to do with getting this heat into a material that will transport it to an area where it can be radiated. The optimum passive approach is to provide thick material in close to the junction that has high conductivity to let the heat flow out radially.

If the heat flow radially for small temperature gradients can be high, then the heat sink locally can be cooler and the junction temperature will stabilize at a lower value.

It may be optimum from the thermal point of view to distribute junctions even a few millimeters from each other, however combining is undesirable. This should, however, be considered further in the amplifier advanced technology development program.

For the purposes of this investigation, the thermal conductivity of copper, aluminum and heat-treated pyrographite were employed in a fixed geometry such that the relative weights are proportional to their densities. The copper thermal conductor for the amplifier would therefore be 3.3 times as heavy as the pyrographite version. The aluminum conductor would be 1.2 times as heavy as aluminum.

From Figure 8.4-8, the P_{RF} allowable decreases by about 1% for copper and 4% for aluminum and the weight increases for copper by a factor of 1.2. If the

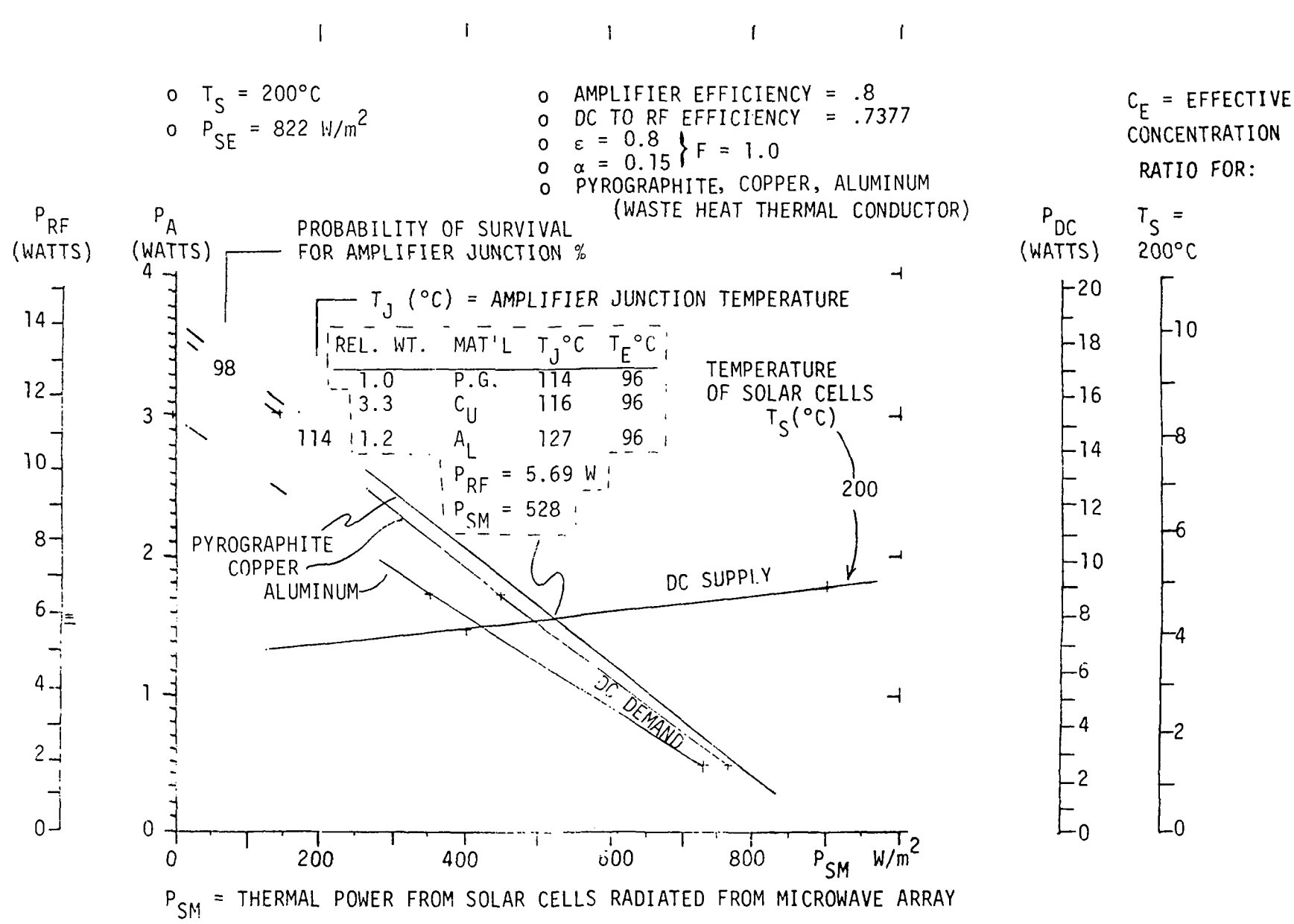

Figure 8.4-8 Baseline Sensitivity To Waste Heat Conductor Material

aluminum conductor weight were increased to that of copper by increasing average thickness, its thermal performance would approach that of copper. In the most critical region of the heat sink at the junction the performance would be degraded for aluminum. If copper is used in this region and a high thermal performance bond is made with the aluminum and appropriate filleting is employed, the hybrid aluminum/copper conductor could achieve a performance similar to that of pyrographite.

For the pyrographite case, it is presently inconceivable to achieve the transition function of the very local heat sink and achieve the benefit of the high conductivity of pyrographite. A copper "slug" under the junction was assumed to be employed for the pyrographite case and copper conductivity was used in this region. This is similar to the concept discussed for aluminum, however this was not taken into account in the computer program for aluminum. This transition region properly filleted for both pyrographite and aluminum must be investigated further.

When results of such investigations are taken into account, it is conceivable that the total cost of the pyrographite/copper hybrid approach will exceed that of copper certainly and may be close to that for the aluminum/copper hybrid approach. It is clear that the pyrographite/copper approach would be significantly lighter and the final tradeoff would have to include transportation penalties that may or may not exist, depending on the pre-launch packing density and associated on-orbit deployment strategy.

This material question is a design and development problem, while other parameter questions may relate to both design and operations, i.e., thermal control coatings as an example may degrade with time and alter the interactions with the photovoltaics, while the thermal conductor performance will be fixed. Incompatabilities between the several materials of the thermal conductor, as well as between the thermal conductor surfaces and the thermal control coatings, must be resolved in the thermal control technology development program.

Degradation of performance in these areas can affect the interactive parameters of the sandwich concept.

8.4.7 Baseline Sensitivity to Junction Temperature

The section on Amplifier Expected Life Relationships discusses failure rate and its integrated effect over time versus junction temperature.

From Figure 8.4-9 it is noted that P_{RF} at the autonomous point increases from about 5.882 W/element at T_J = 114°C to 6.782 W/element at T_J = 160°C in a progressive fashion. As energy far as energy is concerned, for no failures, there would be more energy deliverable over the 30-year period if the design point were on the 160°C line compared to the 114°C line (6.782/5.882 = 1.153); i.e., 15.3% more. Similarly, if the design point were on the 122°C line, there would be 2.37% more energy, at 131°C there would be 5.1% more, and at 140°C there would be 8.5% more.

The 114°C is associated with a failure rate of 2% at 30 years, while T_J = 160°C is associated with a 50% failure rate at 30 years. For failure rate histories following the projections of Figure 8.4-10, the time integral effect at 114°C is to lose the "% junction years" indicated in Table 8.4-1. The effect of losing a junction is to lose -ransmit RF power for a cell and the effect at the ground is about equivalent to losing the same percentage of aperture as well, i.e., the energy loss in % watt years will be about twice the % failure years.

Table 8.4-1 Device and Energy Loss Relationship to Junction Temperature

T_J (°C)	% Failure Years By The End Of Year:				Energy Loss in % Watt Years (Average % Loss) By End of Year:			
	2.5	20	25	30	2.5	20	25	30
140	5.0	134.5	192.5	272.2	10.0 (4.0)	269.0 (13.45)	385.0 (15.4)	544.0 (18.13)
131	2.0	63.1	92.6	133.5	4.0 (1.6)	126.0 (6.3)	185.0 (7.4)	267.0 (8.9)
122	0.65	24.70	36.95	56.2	1.3 (0.52)	49.4 (2.41)	73.9 (2.96)	112.4 (3.75)
114	0.125	7.062	11.438	18.688	0.25 (0.10)	14.1 (0.705)	22.9 (0.916)	37.4 (1.247)

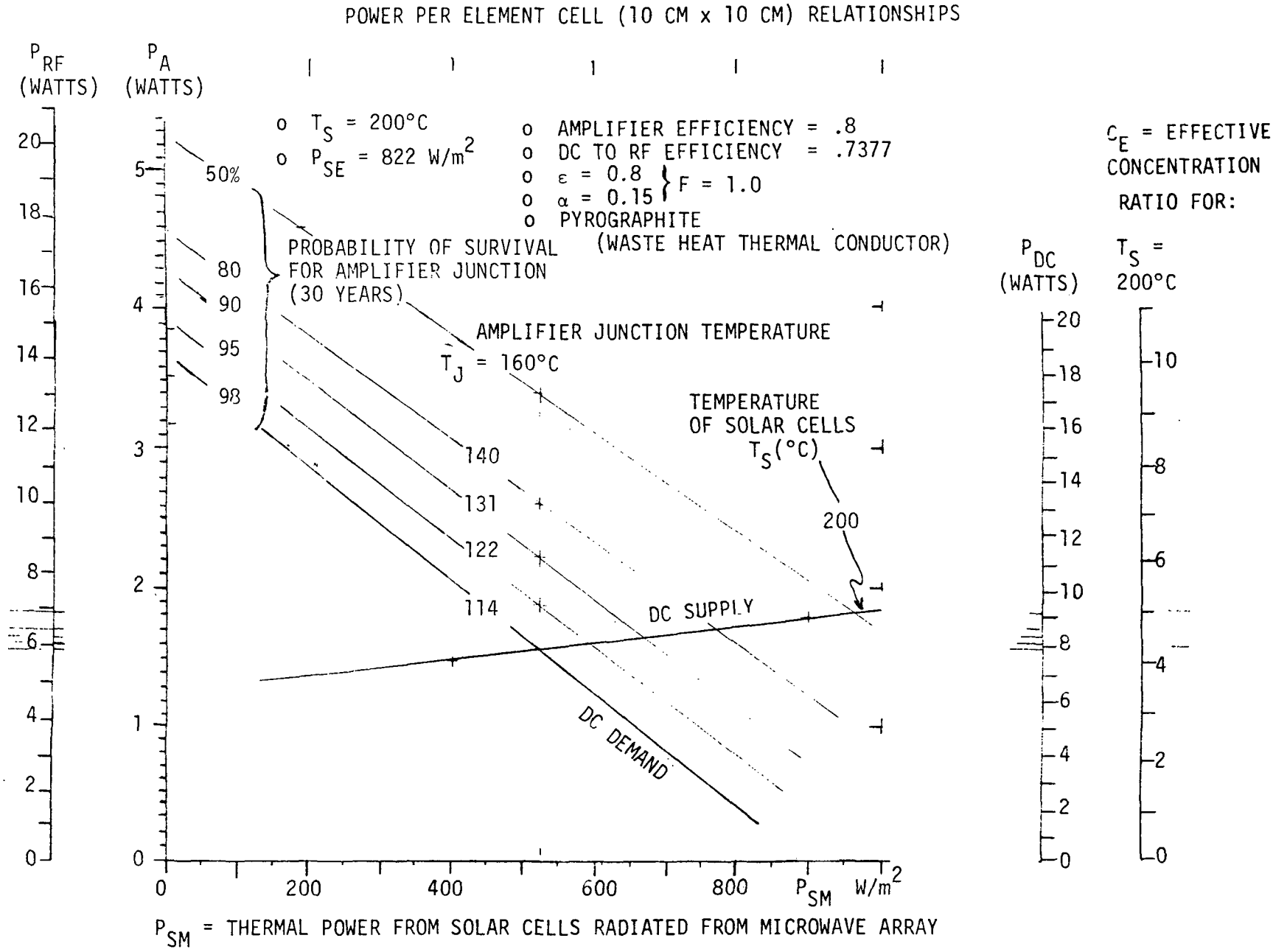

Figure 8.4-9 Baseline Sensitivity to Junction Temperatur

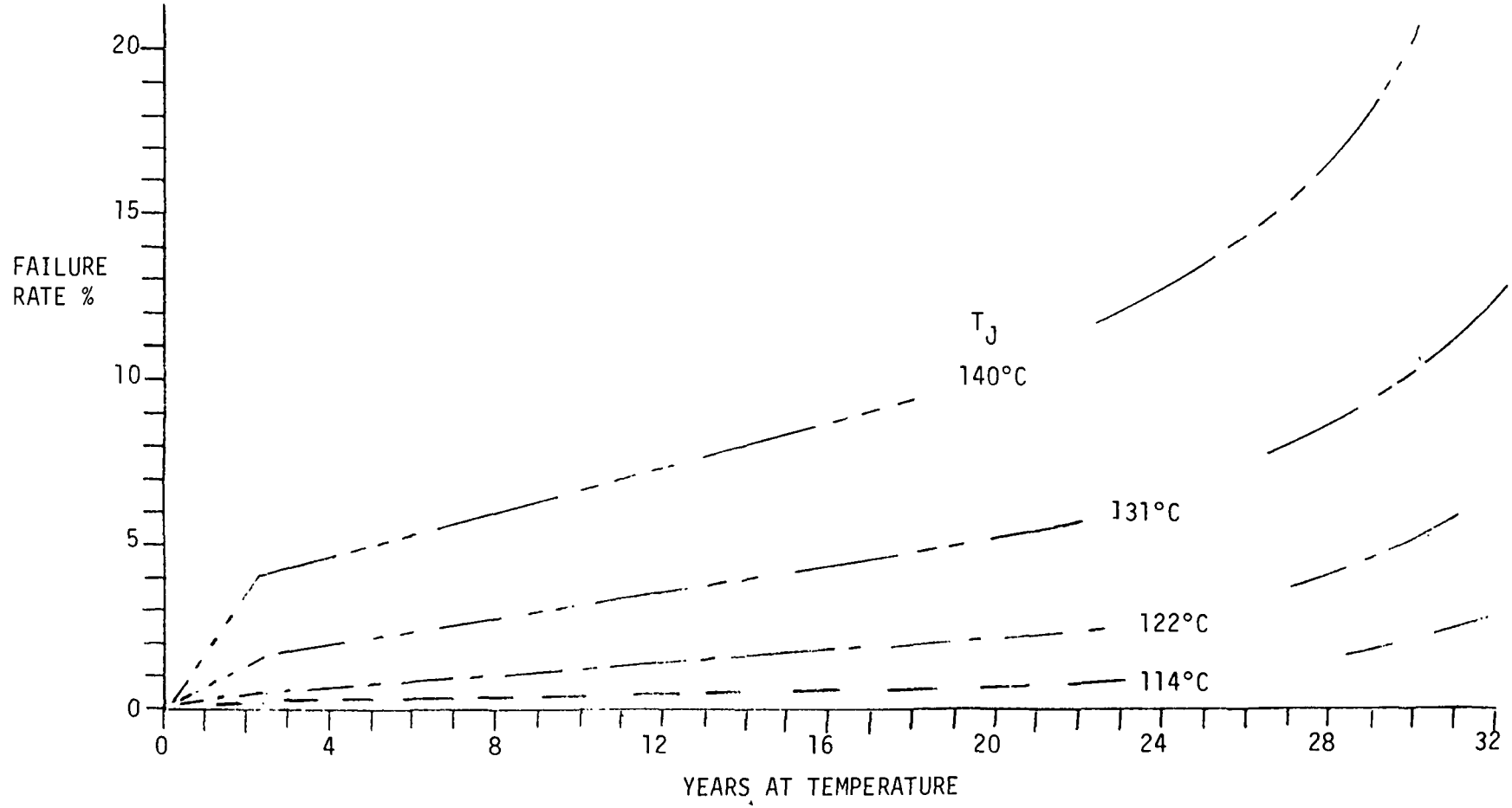

Figure 8.4-10 Failure Rate Vs Years at Temperature Based on Raytheon A_L Gate Projections

8.4.7.1 Design Performance For the Autonomous Case

By designing for the higher junction temperatures, again for the autonomous case, the allowable power density would be as shown in Table 8.4-2 and the resulting average energy per element is shown for comparison.

Table 8.4-2 Average Energy Per Element Related to Junction Temperature and Autonomous P_{RF}

T_J (°C)	P_{RF} Design (Watts/Element)	Average Energy Per Element, I.E., Watt Years Without Failures (With Failures) By The End Of Year:			
		2.5	20	25	30
140	6.382	15.96 (15.32)	127.6 (110.4)	159.6 (135.0)	191.5 (156.8)
131	6.182	15.46 (15.22)	123.6 (115.8)	154.5 (143.1	185.5 (169.0)
122	6.022	15.06 (14.98)	120.4 (117.4)	150.6 (146.1)	180.7 (173.9)
114	5.882	14.71 (14.70)	117.6 (116.7)	147.1 (145.8)	174.3 (174.3)

From this table it is evident that the maximum performance in terms of energy is a function of design temperature and the design life in terms of years.

These data, as shown in Table 8.4-3 and on Figure 8.4-11, indicate that effective energy performance can improve depending upon at which end time the integrated performance is measured. Although for T_J = 140°C performance is high, compared to T_J = 114°C, up to about 10 years of integration, it then degrades at a continuing high rate. Similarly, T_J = 131°C crosses over at about 17 years and T_J = 122°C crosses over at about 27 years. The time values of investment and of energy have not been included nor have the effects of maintenance and repair.

These data indicate that reliability projections and demonstrations for the amplifier junctions must play an important role in the associated advanced technology development program.

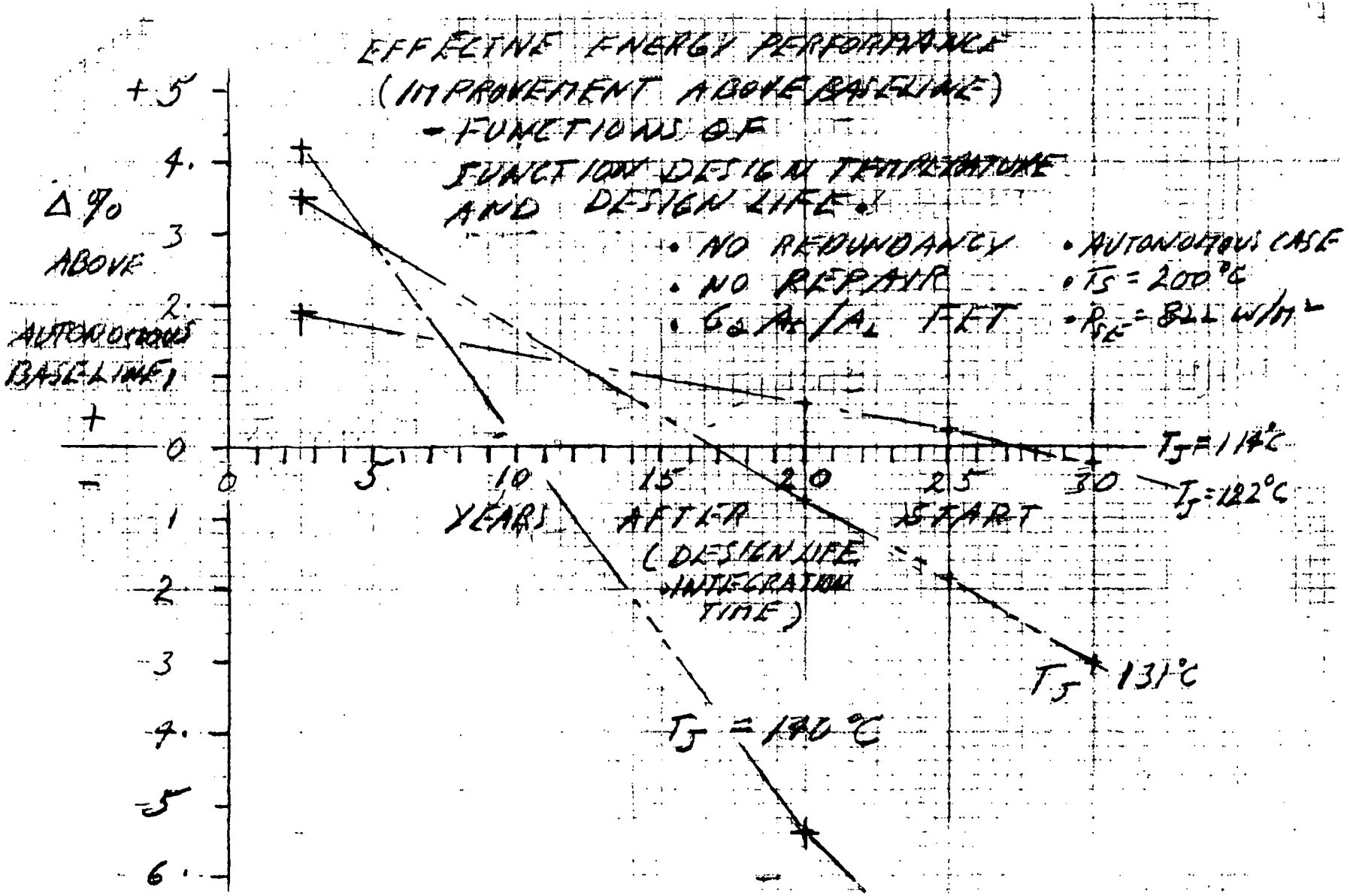

Figure 8.4-11 Effective Energy Performance Improvement Above Autonomous Baseline

Table 8.4-3 Effective Energy Performance Improvement Percentage Above Baseline (Autonomous Case)

T_J (°C)	Effective Energy Performance Improvement Percentage Above Baseline By The End Of Year:			
	2.5	20	25	30
140	+ 4.2	- 5.4	- 7.4	-10.0
131	+ 3.5	- 0.77	- 1.85	- 3.04
122	+ 1.9	+ 0.60	+ 0.21	- 0.23
114 (Baseline)	0	0	0	0

8.4.7.2 Design Performance For the Non-Autonomous Case ($P_{SM} = 0$)

The above discussion had to do with operation at the autonomous design points For situations where P_{SM} can be small, or even negative, the percentage improvement in performance can increase at a much higher rate. As an example, at $P_{SM} = 0$ and $T_S = 140°C$, a value of $P_{RF} \approx 17.6$ is obtained and comparing that to the value at $T_S = 114°C$, $P_{RF} = 14.2$, there is a factor of 1.24 improvement. Comparing this to the 6.382/5.882 = 1.085 of the autonomous case, we see that the tradeoff to maximize average energy per element over a similar set of design times will move more in favor of the higher junction temperatures. The format of the tables and figures above can be used to develop data for a complete range of design concepts.

The first table remains the same and the second table (Table 8.4-4) is unique for the values of P_{RF}.

Similarly, Table 8.4-5 and Figure 8.4-12 indicate the improvement in effectiv energy performance above the $P_{SM} = 0$ baseline, with temperature and design time. Table 8.4-6 provides data for the $P_{SM} = 0$ case with respect to the autonomous baseline for comparative assessment.

Table 8.4-4 Average Energy Per Element Related To Junction Temperature Non-Autonomous (P_{SM} = 0)

T_J (°C)	P_{RF} Design (Watts/Element)	Average Energy Per Element i.e., Watt Years/Element Without Failures (With Failures) By The End Of Year:			
		2.5	20	25	30
140	17.6	44.0 (42.24)	352.0 (304.55)	440.0 (372.2)	528.0 (432.3)
131	16.5	41.2 (40.56)	330.0 (309.2)	412.0 (381.6)	495.0 (451.0)
122	15.2	38.0 (37.86)	304.0 (296.4)	380.0 (368.6)	456.0 (438.8)
114	14.0	35.0 (34.98)	280.0 (277.6)	350.0 (346.9)	420.0 (414.8)

Table 8.4-5 Effective Energy Performance Improvement Percentage for P_{SM} = 0 Above the P_{SM} = 0 Baseline

T_J (°C)	Effective Energy Performance Improvement Percentage Above P_{SM} = 0 Baseline By The End Of Year:			
	2.5	20	25	30
140	+ 21.0	+ 9.7	+ 7.3	+ 4.2
131	+ 16.0	+11.4	+10.0	+ 8.7
122	+ 8.2	+ 6.7	+ 6.3	+ 5.7
114	0	0	0	0

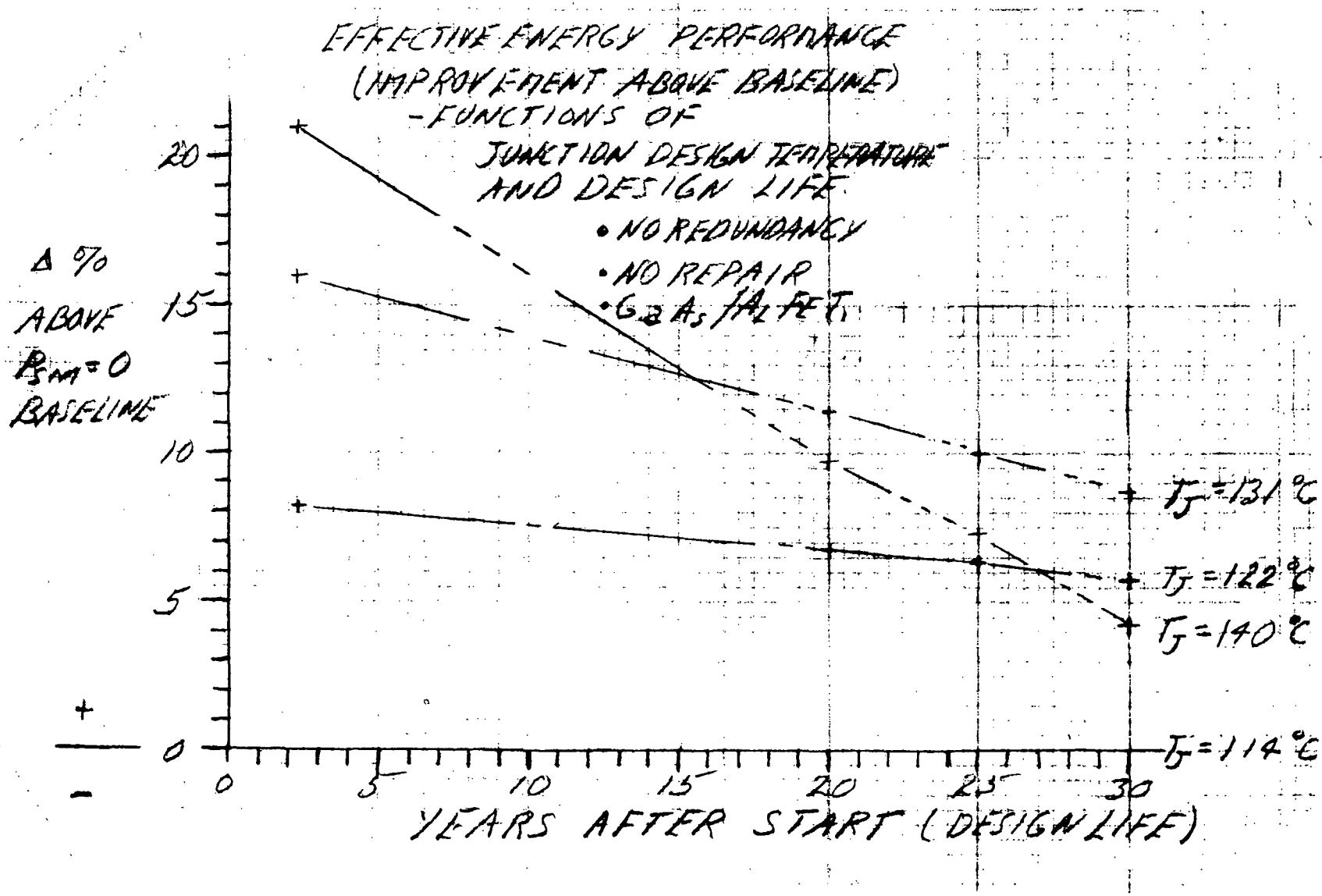

Figure 8.4-12 Effective Energy Performance Improvement Above P_{SM} = 0 Baseline

Table 8.4-6 Effective Energy Performance Improvement Percentage For P_{SM} = 0 Above the Autonomous Baseline

T_J (°C)	Effective Energy Performance Improvement Percentage Above P_{SM} = 0 Baseline By The End Of Year:			
	2.5	20	25	30
140	187.3	161.0	155.3	148.0
131	175.9	165.0	161.7	158.7
122	157.6	154.0	152.8	151.7
114	138.0	137.9	137.9	138.0

8.4.7.3 Summary, Comparison and Assessment

Design constraints, requirements and goals are significantly different for the autonomous as compared to the non-autonomous examples given in Figure 8.4-13.

The near optimum (autonomous) effective integrated average power densities range from 582 to 587 watts/m^2. The near optimum design values for the junction temperatures range from 118°C for a 30 year design life and 120°C for a 25 year design life to 123°C for a 20 year design life. Temperatures above the 121 to 128 range begin to cause an overall degradation of energy delivery performance for the no-maintenance case.

The near optimum (non-autonomous P_{SM_2} = 0) effective integrated average power densities range from 1500 to 1550 watts/m^2. The near optimum design values for the junction temperatures range from 130°C for a 30 year design life and 132°C for a 25 year design life to 134°C for a 20 year design life. The range of temperatures extend above 140°C, for all integration times, before a situation of overall degradation of energy delivery performance takes place.

The above discussion provides the background for the conclusion that the autonomous case is highly constrained and energy performance margins are very small and they are maintained at positive values only over a narrow range of junction temperature. The non-autonomous case has a large performance margin over the autonomous case and is less sensitive to temperature excursions. To capitalize

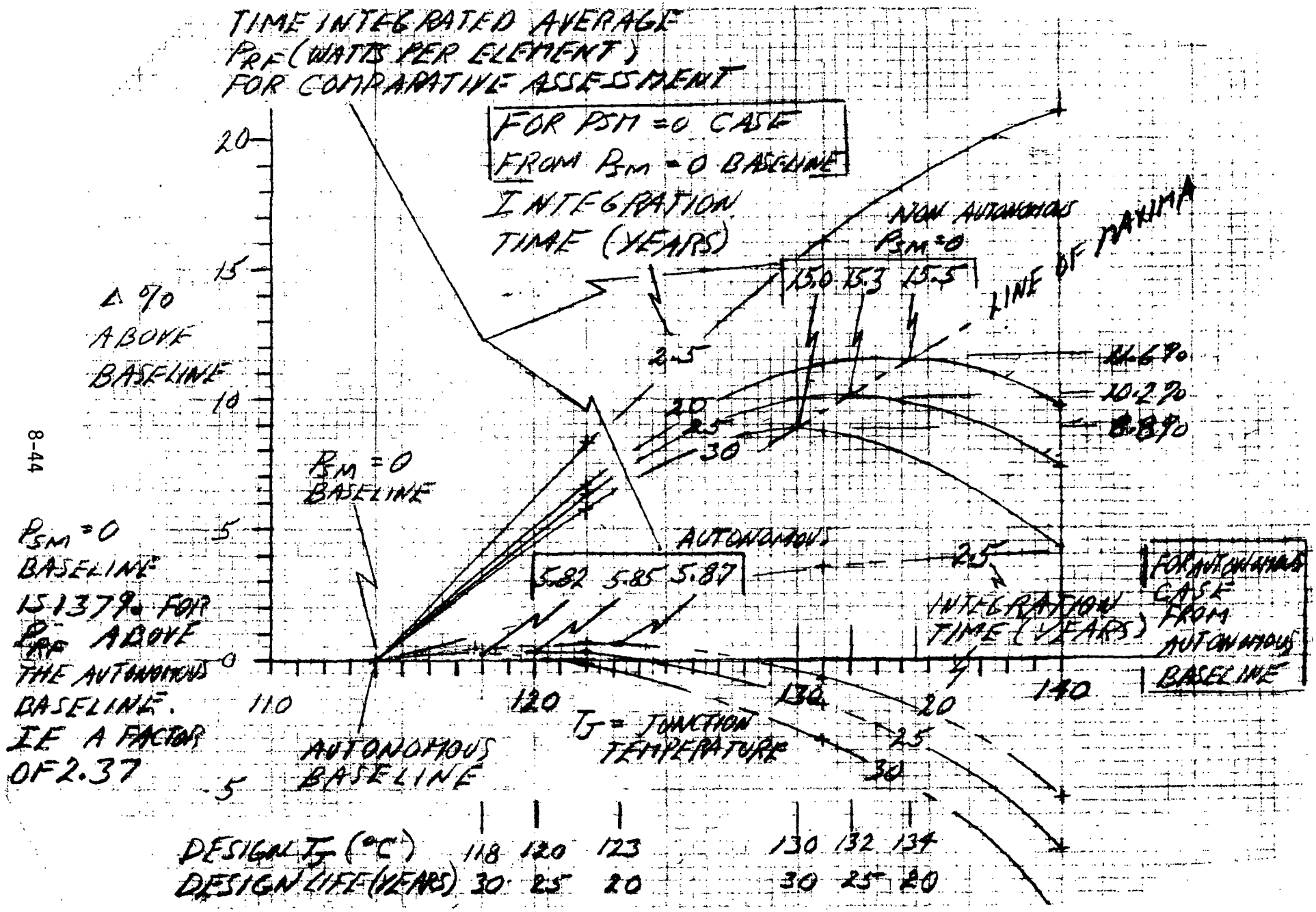

Figure 8.4-13 Effective Energy Performance Improvement Above Baseline Vs Junction Temperature

on this, the non-autonomous approach should be investigated vigorously and its penalties, such as those associated with requirement for large amounts of DC power to be transmitted for use at low voltage, should be included in the investigation with major emphasis.

8.4.8 Baseline Sensitivity to Solar Cell Temperature

The power source characteristics which interact with other parameters on the mi-rowave side are represented by Equations (8-) through (8-). These relationships derive from the work presented by Rockwell International in their Satellite Power Systems Concept Definition Study (Exhibit D), October 10, 1979. The intent of this present investigation, being to provide relevant microwave system data to contribute to overall systems investigations, is not to enter into the photovoltaic technology. There are no doubt other approaches to be pursued in photovoltaics and insofar as they can be related to P_{DC}, P_{SM} and the physical bus bar geometries assumed (not unduly constraining), the parametric relationships should apply.

The actual variations and limits of T_S from the reliability, life, maintenance and repair point of view will be a function of that technology. It is presumed that sensitivity and tradeoff analyses in this area similar to those presented under the section on Baseline Sensitivity to Junction Temperature will be performed. It is further presumed that the integration of the photovoltaic, microwave, DC distribution, mechanical and thermal, will be performed in such a manner as to arrive at a near optimum total concept. As in other multifunction design integration activities, design is usually a "complex compromise." Provisions in the microwave parametric data detail, as well as format, have been formulated in this report to facilitate its application to overall concept definition and design integration. The near-optimum set of compromises are assumed to be in favor of reliably and safely delivered power to the user ground grid at low cost.

In the above context, the data presented in Figure 8.4-14 illustrates some of the microwave system interactive relationships.

A value of T_S = 200°C was chosen as a first approximation to the solar cell limits similar to the 114°C (preliminary baseline) limit. The variations with T_S of the autonomous case data are then as follows.

Solar Array Temperature Sensitivities in the Autonomous Case

When T_S increases by 50°C, P_A will increase from about 1.56 to 1.29 watts per element and P_{SM} will decrease from about 520 to 470 W/m^2 to arrive at a compatible supply = demand situation with T_J constrained to 114°C. If T_J is allowed to

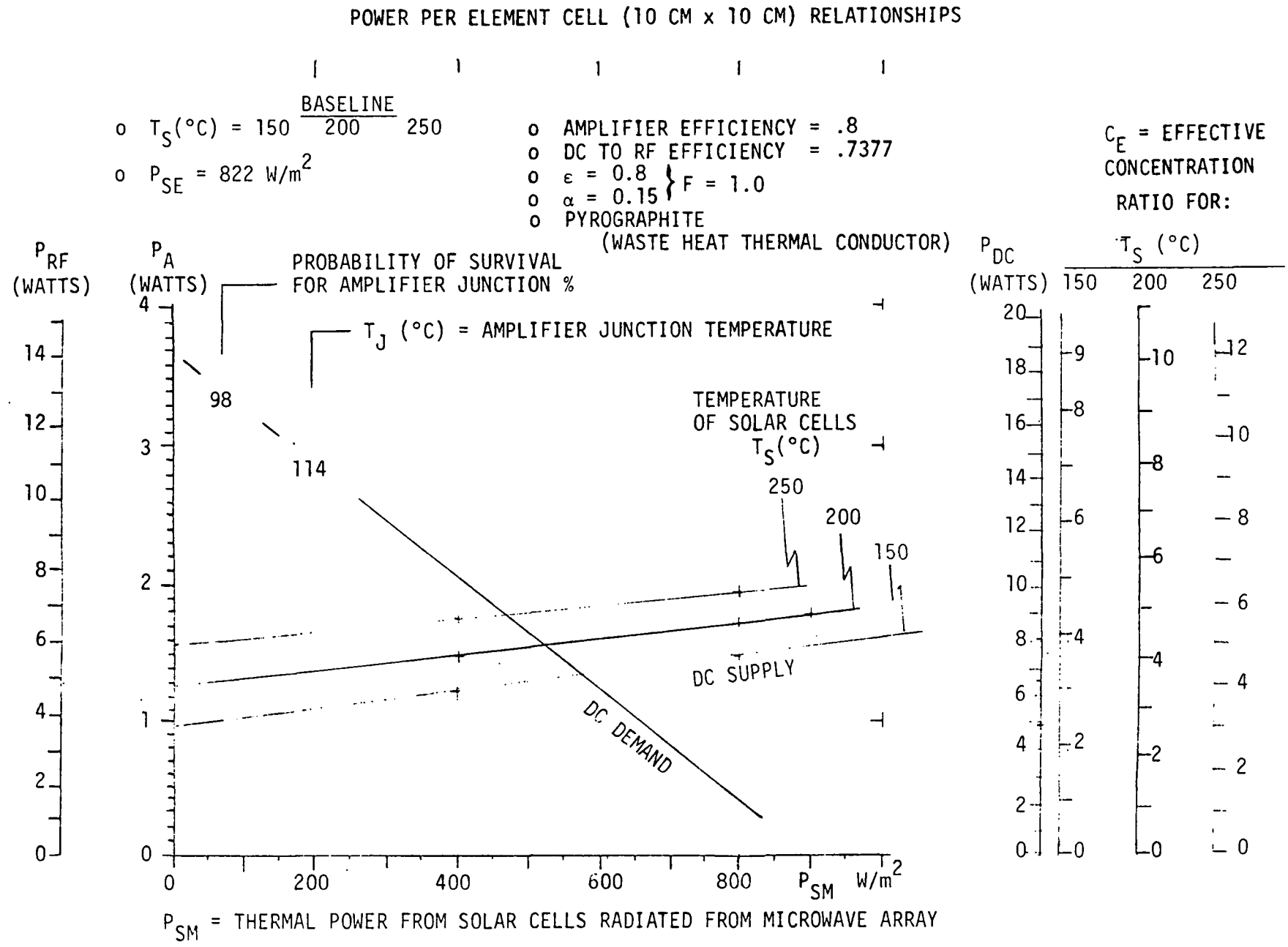

Figure 8.4-14 Baseline Sensitivity to Solar Array Temperature

increase, as it probably will in the optimization process, either P_A will increase or P_{SM} will increase or they both may increase a "compromised to a near optimum" amount that may be determined in an overall model using (a) the equations in Section 8.2 or the microwave worksheets for the microwave or demand side and (b) the equations in Section 8.1 or the power supply worksheets (as they may be reformulated for other photovoltaic considerations) for the power supply side.

Details of the heat transfer paths that dictate the transfer of P_{SM} from the photovoltaic side to the microwave side can be formulated in the design integration process. This will be a non-trivial activity involving heat transfer mechanisms that include both conductive and radiative paths and processes. DC power wires and switches, possible instrumentation interconnections and mechanical connections, as well as possibly special thermally conductive control mechanizations, must be considered in the series of conductive paths. Inherent and specially designed insulation layers, including the fixed and time varying thermal control coating variations, must be considered in the series of radiative paths.

The design problem will be largely one of bias toward minimization of paths that introduce concentrations of heat flow into the ground plane in close proximity to the amplifiers and their most critical junctions. The junction temperature limits are in the 110 to 140°C region (see discussion of Baseline Sensitivity to Junction Temperature) with associated ground plane temperatures lower than these values, i.e., T_E is in the 70 to 120°C region. The difference is a strong function of the transmitted RF power per amplifier junction. The solar cell temperatures are in the 200 to 250°C region. The temperature gradient between the photovoltaic side and the microwave ground plane is in the vicinity of 140°C in the direction causing heat flow toward the microwave side. A high level of detailed design, analysis, simulation and test will be required to formulate the design along with the near-optimum set of compromises to be taken in the heat transfer activities of system integration.

The heat transfer model must be formulated and included as the third part of the problem to be solved simultaneously, i.e., known microwave relationships, power source relationships and interfacing heat transfer relationships are essential to the resolution of an integrated autonomous concept.

Solar Array Temperature Sensitivities in the Non-Autonomous Case

As P_{SM} decreases below the autonomous design point value, the heat transfer design integration problem in fact gets more difficult in terms of precluding concentrations of heat flow in the presence of a high temperature gradient. The curves of DC Supply are not realistic in the low P_{SM} region unless active thermal control techniques or detailed and thermally isolated partitioning of the ground plane are employed.

As T_S increases with the associated increase in temperature gradient between the photovoltaics and the microwave ground plane, the design integration task is progressively more difficult and will lead to yet further compromises.

As P_{SM} increases above the autonomous, the heat transfer design integration problem is made less difficult. This indicates that low P_A and the resulting allowable P_{RF} values may be feasible. Again, the determination of the limits at which a practical design is feasible must be made in the design integration activity previously discussed. It is projected that integrated concepts operating on the right-hand side of the autonomous design point may in the integration process be shown to be feasible.

SECTION 9

ASSESSMENT OF PRELIMINARY DESIGN INVESTIGATIONS AND PARAMETRIC DATA

This section presents an approach to assessment of the concepts and results discussed in previous sections with emphasis at the system level. Technology levels are discussed within the appropriate section.

The interactive nature of the photovoltaic and microwave portions of the sandwich are considered, in some degree, to constrain the potential total performance of the system in terms of maximum power generation and output.

Imaginative approaches may be taken in several areas to improve performance and cost effectiveness. It is the intention here to provide first approximations to approaches that should be investigated in more detail.

By way of overall assessment of results, it should be said that the solid state sandwich concept and its several related options offer potential for performance and cost effectiveness that has only begun to be explored in this investigation. Certain critical technologies are necessarily assumed to be developed, the key ones being the amplifier and its relationships to the waste heat dissipation and antenna concepts. The range of parameters employed in this investigation are believed to envelope the potential of the technology, however advanced development programs must be initiated to narrow the range before practical assessments can be made.

9.1 DC POWER DISTRIBUTION SYSTEMS

The DC power must be delivered to the using equipment at the required (low) voltages. Loss of efficiency and generation of additional waste heat are to be minimized.

Three power distribution networks with conditions for interconnection are postulated:

(a) Direct flow from the photovoltaic buses at the subarray level to the using amplifiers and other equipment on the same subarray. The characteristic of this network is that the conductor lengths are short (< 20 cm) and the weight of the network is minimal (113 gm/subarray) because the power supply is very close to the using equipment. This network has 8 sets of 3.2 m long bus bars 40 cm apart for a 13 V system A negative bus bar from one set is very close to a positive bus bar from another set, however the voltages are small and isolation by material insulation is not an issue. Power from external supply can be added at these bus bars with appropriate switching and isolation protection at 13 V in parallel with the autonomous photovoltaic cells. The 113 gm/subarray would have to increase significantly in this case. The 8 sets of buses feed to a 10 cm grid on the positive side and to the ground plane on the negative side. Switches are provided for two reasons, DC power control for overall safety and possibly thermal leakage control; and both power control and thermal control require further investigation.

Two 3.2 x 3.2 m power planes isolated from each other, an array of switches to the 8 bus bars, and the eight (3.2 m) sets of bus bars constitute the power grid at the 3.2 x 3.2 m subarray level.

(b) One of the power planes, the negative ground plane, could be electrically connected to neighboring subarray planes for electrical power and thermal power radial flow purposes. Again switches for control may be required. The other power plane (the positive grid) could be electrically connected to neighboring subarray planes as well if subsequent investigations can show that power shut-off for safety reasons can be achieved at and by the RF network for transmission control and by special support equipment for installation purposes.

Additional weight must be added to both the power planes, for passthrough power, and to the boundaries for installation and possibly real time switching and control.

This intersubarray power distribution system must operate at the using equipment voltage levels (≈ 13 V) which may thereby optimize at a higher level, possibly as high as 20 V as limited by the constraints of using equipment.

Continuity of one or both of the two power planes with the possible need for switching and control of both DC power and thermal radial flow constitute the inter-subarray power distribution network.

(c) Transfer of DC power from one 3.2 x 3.2 m subarray or a contiguous group of these (example, 16 RF subarrays = 1 power module, 12.8 x 12.8 m) to other inboard groups by a separate power distribution network may be shown to offer weight and cost advantages. It may operate at high voltages AC or DC to minimize weight and size, however power conditioning equipment at the power module level would add complexity, size and weight.

This concept should also be considered in further investigations.

(d) Transfer of DC power from a region dedicated to its generation, such as an outboard ring of photovoltaic arrays, may use an approach similar to that discussed in (c). It may be a separate network that drives central subarrays or it may be integrated with (c).

This concept should also be considered in further investigations.

9.2 SPACETENNA GENERAL ARCHITECTURE (EXAMPLE)

The concepts indicated in Figure 9.2-1, at the spacetenna quadrant level, illustrate the basic architectural partitioning. The RF power densities, as high as 2 kW/m^2, are consistent with junction temperatures of T_J = 114°C, photovoltaic temperatures of T_S = 200°C, η_{AMP} = 0.8, α = 0.15, and ε = 0.8. In this regard the figure shows realistically what may be achieved. The quantitative data shown are not optimized (e.g., RF power levels in the several rings may be shown to be different as sidelobe control requirements may dictate). Optimizations with respect to the several DC power distribution approaches require further investigation. Overall SPS schemes to achieve stepped or otherwise varying photovoltaic power levels that increase with distance from the spacetenna center are worthy of further investigation.

For the example data shown in Figure 9.2-1 the power flow in terms of kW/met of circumference is indicated on Figure 9.2-2. The maximum 430 kW/meter occurrin at the 500 meter radius is indicative of the magnitude of the power distribution issues to be addressed in future investigations. It appears to be the major issu for the concept of the hybrid (combinations of RF dedicated, RF/photovoltaic autonomous and photovoltaic dedicated regions) approach.

The waste heat equilibrium temperatures are higher in the most central regio (T_E = 51.3°C for T_J = 114°C, F = 1.75, P_{SM} = 0 and P_{RF} = 20 watts per element or 2000 $watts/m^2$) than in the next region. The outboard (634 to 813 m radius) regio operates at the highest waste heat radiator temperature while T_J is at 114°C. Th next region inboard (493 to 634 m radius) operates at a lower waste heat radiator temperature while the T_J is at 114°C. If the ground planes are thermally connect there will be an inboard flow of heat at the 634 m radius that will cause the T_J the inboard side of the radius to increase above 114°C. In order to preclude thi either the autonomous DC supply density will have to be reduced or the RF power density in the ≃ 600 to 634 m radius region will have to be reduced. The sharp steps in power density taper are undesirable from at least this point of view in the mid radius regions. Therefore, techniques for graduation of RF power density require further investigation. This will impact on the already difficult technology for power amplifier advanced development, but at least in this region the power densities are small, i.e., 7.5 W/element as compared to 20 in the central

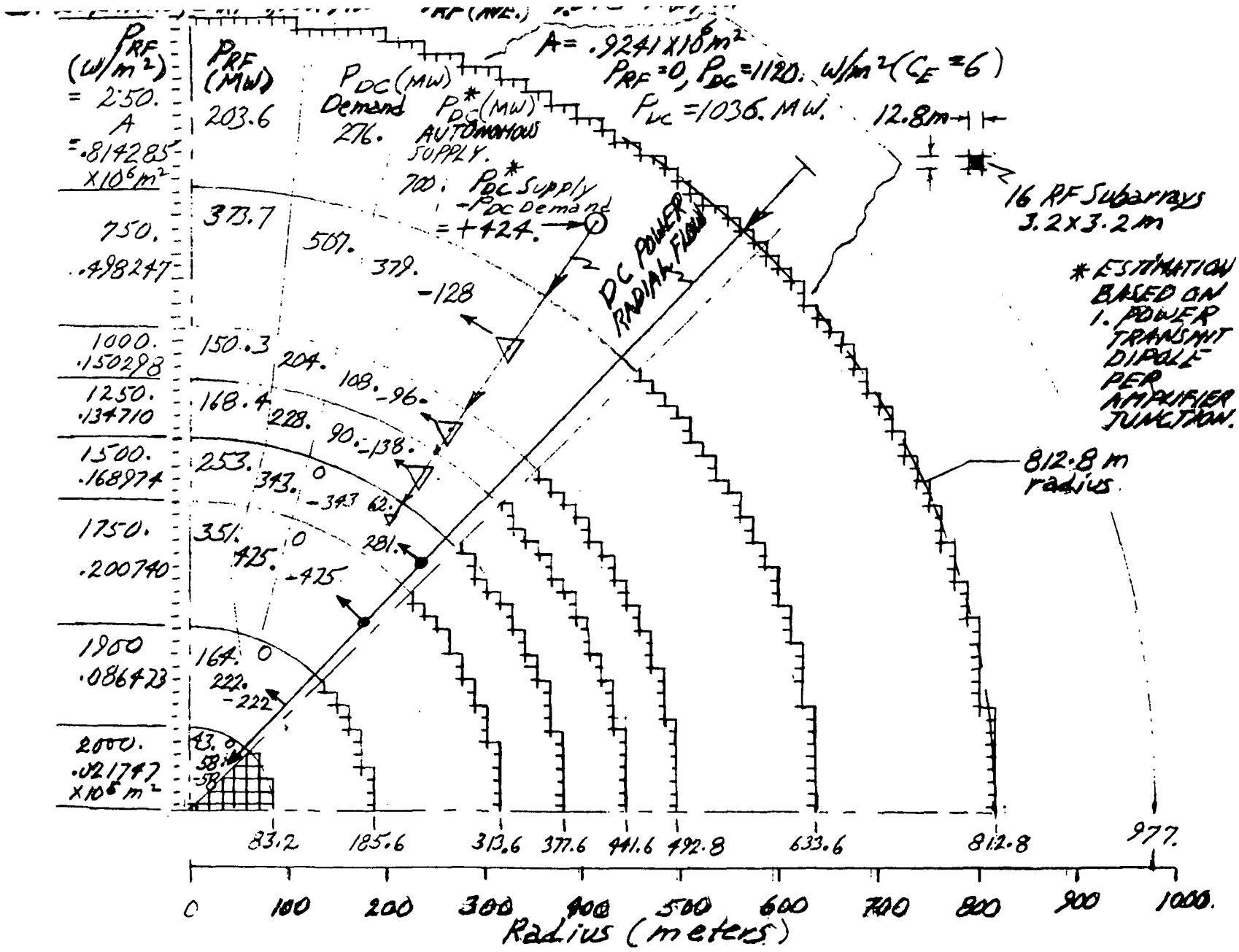

Figure 9.2-1 First Approximation of Multi-Step Taper Architecture

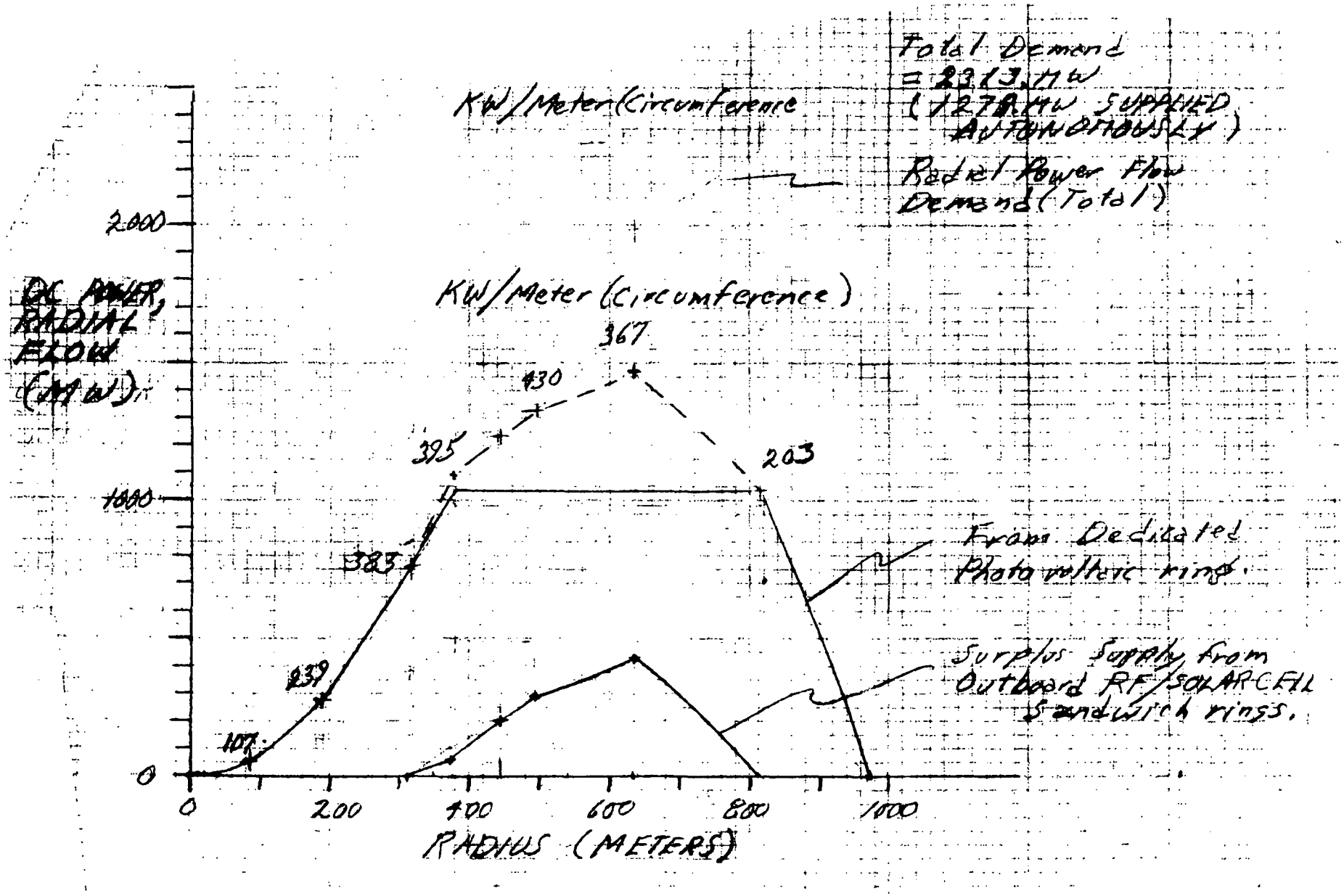

Figure 9.2-2 Power Flow for First Approximation to Multi-Step Taper Concept

region. The same issue does not apply in going from the 20 W/element to 19 W/element at the 83 meter radius. In this case, the temperature of the waste heat radiators is decreasing as radius increases, so interconnecting ground planes thermally will be an advantage between inboard regions.

The radial heat flow will be decreasing from a high outward flow at 83 m to zero at about 300 m and flow inboard at progressively higher values at the 314, 378, 442, 493 and 634 m region interfaces.

9.3 MULTIPLE STEP TAPER

A layout is shown in Figure 9.2-1 of the multiple step taper approach where DC power is transferred from the outboard ring to the central region, thus enabling operation of modules at higher power densities and higher junction temperatures. Profiles of the power density versus radius, both normalized, are shown in Figure 9.3-1. This profile approximates a Gaussian power distribution with a -8.5 dB edge taper, as shown in Figure 9.3-2. The total power available represented by this distribution is:

$$P_T = \frac{P_o \pi}{2K} \left(1 - e^{-2KR_T^2}\right)$$

where

$P_o = 2000\ W/m^2$

$R_T = 812.8\ m$

$K = 1.48 \times 10^{-6}/m^2$

Then the total power available is 1.81 GW. This compares to 1.7 GW from summing the output from rings of amplifiers as shown in Figure 9.2-1.

The power delivered to the grid can be determined from:

$$P_g = P_T\, \eta_{ar}\, \eta_{at}\, \eta_b\, \eta_r\, \eta_{gnd}$$

where values for the various efficiencies are as follows:

η_{ar} = array efficiency = .98

η_{at} = atmospheric efficiency = .98

η_b = beam efficiency = .95

η_r = rectenna efficiency = .89

η_g = grid interface efficiency = .97

Both the available power P_T and the beam efficiency assume a Gaussian power taper with a -8.5 dB edge level. This results in 1.43 GW being delivered to the grid. The step taper case applying the same efficiencies would deliver 1.35 GW. This compares to the baseline uniform illumination system having 1.49 GW available and 1.02 GW delivered.

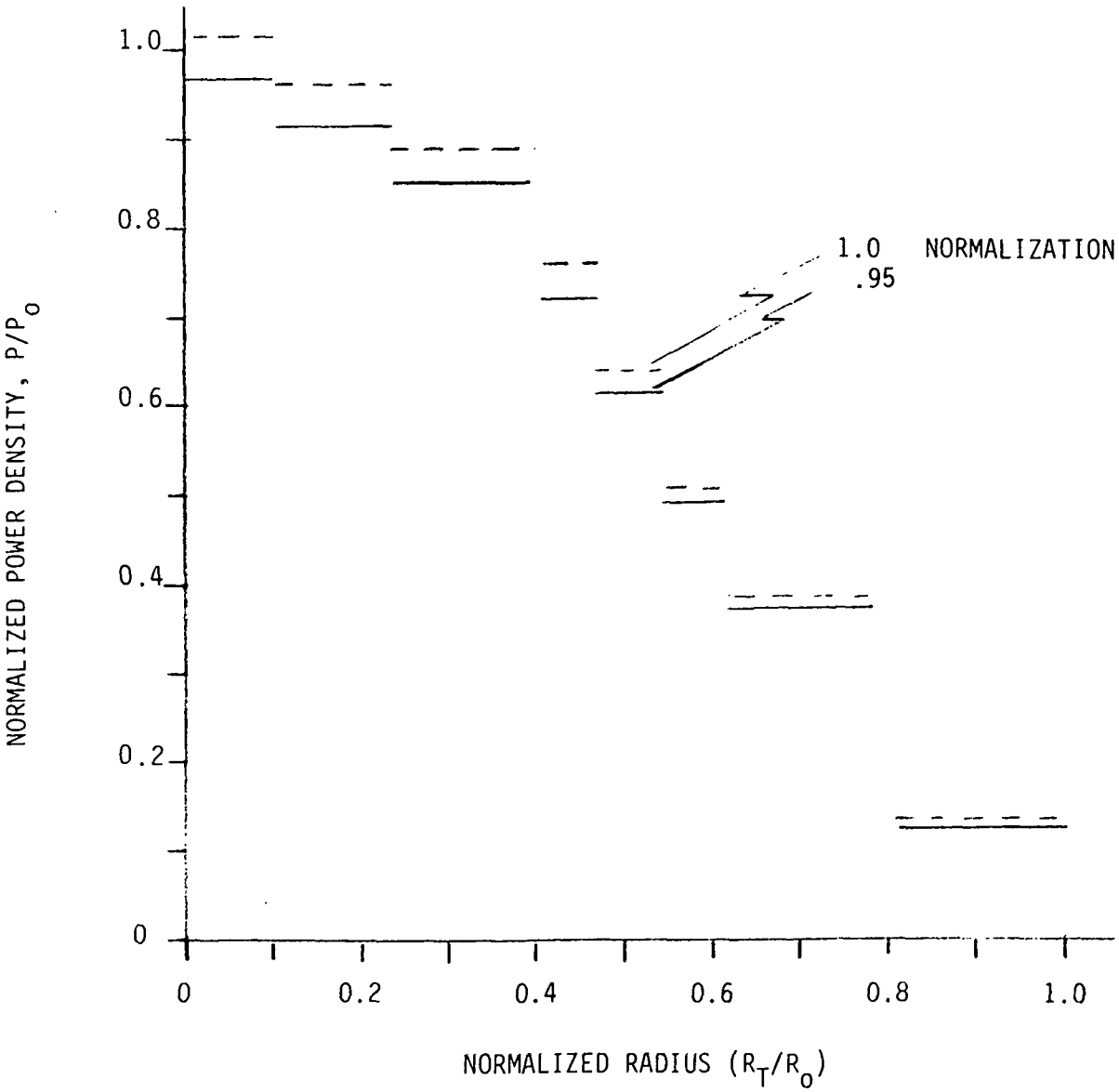

Figure 9.3-1 Transmit Antenna Illumination Multiple Step Taper

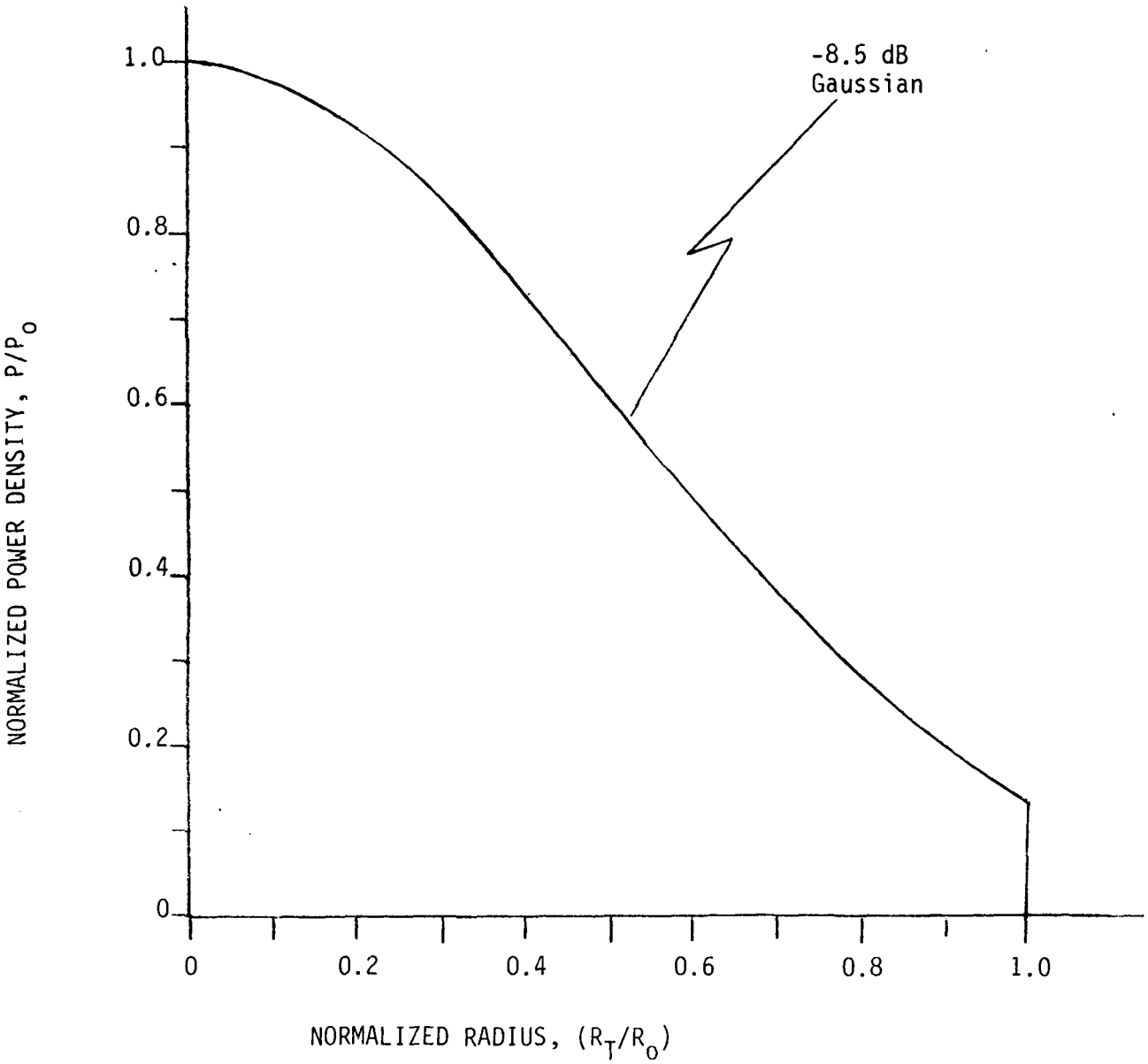

Figure 9.3-2 Transmit Antenna Illumination Taper Smoothed Gaussian

The other important parameter is the power density in the ionosphere (P_{di}). This can be determined from

$$P_{di} = \frac{P_T A_T \eta_t}{(\lambda R)^2} \eta_{AR}$$

where η_t is the taper efficiency,

$$\eta_t = \frac{2\pi \left(1 - e^{-K R_T^2}\right)^2}{K A_t \left(1 - e^{-2K R_T^2}\right)}$$

The taper efficiency equals 1.0 for uniform illumination and .927 for the Gaussian taper. This results in 21.3 mW/cm^2 for the baseline, 16.7 mW/cm^2 for Gaussian and 15.7 mW/cm^2 (extrapolated from Gaussian) for the multiple step taper case.

A summary of the results of the above discussion is presented in Table 9.3-1. From this first approximation analysis it is evident that the multistep taper shows an improvement in power delivered to the ground of more than 30%. The rectenna is reduced in size and the spacetenna is reduced in size, although including the photovoltaics around the edge they are comparable sizes.

Table 9.3-1 Summary of Results

SPS Concept	Performance Parameter					
	P_o (W/m^2)	D_T (km)	D_R (km)	P_{di} (mW/cm^2)	P_T (GW)	P_g (GW)
Baseline (Uniform)	500	1.95	4.5	21.3	1.49	1.02
Gaussian (-8.5 dB)	2000	1.65	4.0	16.7	1.81	1.43
Multiple Step Taper	2000	1.65	4.0	15.7	1.70	1.35

The maximum power density for the step taper is about 74% of that for the baseline uniform case. If the stepped taper for the spacetenna were optimally sized and the aperture was optimized to achieve low sidelobes and comparable maxima for power density at the ground, the stepped taper would clearly hold certain advantages. The ground power would increase and, although the spacetenna aperture

would increase and the rectenna would decrease, it is expected that the multi-step taper would still be advantageous. It would suppress all sidelobes and the penalties would be associated with (a) illumination concepts at the total satellite level and (b) development of the DC power distribution system for the satellite.

This indicates that not only should high power density uniform and single step cases with segregated photovoltaics and DC transport be investigated further, but multiple step tapers should be included.

1. Report No.	2. Government Accession No.	3. Recipient's Catalog No.
NASA CR-3338		

4. Title and Subtitle	5. Report Date
SOLID STATE SPS MICROWAVE GENERATION AND TRANSMISSION STUDY VOLUME I - PHASE II FINAL REPORT	November 1980
	6. Performing Organization Code

7. Author(s)	8. Performing Organization Report No.
Owen E. Maynard	ER80-4074-1
	10. Work Unit No. M-311

9. Performing Organization Name and Address	11. Contract or Grant No.
Raytheon Company Equipment Division Advanced Development Laboratory Wayland, MA 01778	NAS8-33157
	13. Type of Report and Period Covered
12. Sponsoring Agency Name and Address	Contractor Report
National Aeronautics and Space Administration Washington, DC 20546	14. Sponsoring Agency Code

15. Supplementary Notes

NASA Marshall Technical Monitor: Woolsey Sinell, III
Final Report

16. Abstract

The purpose of this investigation was to further define the solid state sandwich concept for SPS. The design effort concentrated on the spacetenna, but did include some system analysis for parametric comparison reasons. The study specifically included definition and math modeling of basic solid state microwave devices, an initial conceptual subsystems and system design, sidelobe control and system selection, an assessment of selected system concept and parametric solid state microwave power transmission system data relevant to the SPS concept. Although device efficiency was not a goal of this study, the sensitivities to design of this efficiency were parametrically treated. Sidelobe control consisted of various single step tapers, multistep tapers and Gaussian tapers. A preliminary assessment of a hybrid concept using tubes and solid state is also included. There is a considerable amount of thermal analysis provided with emphasis on sensitivities to waste heat radiator form factor, emissivity, absorptivity, amplifier efficiency, material and junction temperature.

The document is organized to provide useful design data for future studies, identify issues associated with the solid state sandwich design, and estimate technology requirements.

17. Key Words (Suggested by Author(s))	18. Distribution Statement
SPS Microwave Dipole Subarray Solid State Sandwich Power Balance Tapered Illumination Efficiency Power Density	Unclassified - Unlimited Subject Category 44

19. Security Classif. (of this report)	20. Security Classif. (of this page)	21. No. of Pages	22. Price
Unclassified	Unclassified	230	A11

For sale by the National Technical Information Service, Springfield, Virginia 22161

NASA-Langley, 1980

National Aeronautics and
Space Administration

Washington, D.C.
20546

Official Business
Penalty for Private Use, $300

SPECIAL FOURTH CLASS MAIL
BOOK

Postage and Fees Paid
National Aeronautics and
Space Administration
NASA-451

NASA

POSTMASTER: If Undeliverable (Section 158
Postal Manual) Do Not Return